Novel approaches to targeting

ATM-deficient tumours

Letitia Elizabeth Harris

University College, University of Oxford

Thesis submitted for the degree of Doctor of Philosophy in Oncology

Hilary 2022



MRC Oxford Institute for Radiation Oncology

Department of Oncology, University of Oxford

Medical Research Council Oxford Institute for Radiation Oncology

UNIVERSITY OF OXFORD

UNIV UNIVERSITY COLLEGE OXFORD

Novel approaches to targeting ATM-deficient tumours

Letitia Elizabeth Harris

University College, University of Oxford

Thesis submitted for the degree of Doctor of Philosophy in Oncology

Abstract

Ataxia-telangiectasia mutated (ATM) is an apical kinase involved in the response to DNA damage through the coordination of DNA repair with temporary cell cycle arrest. Germline mutations in ATM give rise to ataxia-telangiectasia (A-T), a genome instability syndrome characterised by progressive neurodegeneration, profound radiosensitivity and susceptibility to cancer.

The role of ATM in the DNA damage response (DDR) to irradiation and irinotecan treatment was evaluated using both ATM-deficient cell lines and mice, and by using pharmacological inhibition of ATM.

This study revealed the frequent loss of ATM protein expression in human tumours, with the greatest extent reported in pancreatic cancers. Through a pharmacological kinase screen, compounds that can preferentially target ATM-deficient cells were identified including insulin-like growth factor 1 receptor (IGF1R) inhibitors. Studies in ATM-deficient cells revealed potentially complex compensatory mechanisms for DDR signalling following irinotecan treatment. The characterisation of the DDR *in vivo* clearly demonstrated ATM-dependent S phase DNA damage signalling in normal tissues as a consequence of irinotecan treatment, with the surprising observation of an S phase-independent DDR in regions of the heart and lung.

Whilst the concept of targeting ATM loss in tumours remains promising, the complexities surrounding compensatory DDR signalling and the inconsistency of synthetic lethality in combination with topoisomerase I inhibition are confounding and will require further study to better understand the potential of irinotecan in the treatment of ATM-deficient tumours. Alternative targets, such as those identified in the compound screen, warrant further investigation.

Acknowledgements

First and foremost, I would like to give tremendous thanks to my supervisor Dr Andy Ryan for the incredible support and guidance over the past four years. Andy, you have been an excellent mentor and I am beyond grateful for all of your dedication to teaching, inspiring, and challenging me. I could not have asked for a better supervisor during my DPhil, and I am the scientist I am today because of you.

I would like to extend my gratitude to the members of the Ryan Group with particular thanks to Dr Steve Stribbling for all of your hard work involved in this project for which I am so grateful. To all of the members of the Department of Oncology, thank you for your support and guidance throughout my DPhil. I would like to specifically express my gratitude to Professor Val Macaulay, Dr Guillaume Rieunier, Dr Daniel Ebner and Dr Stephanie Hatch for imparting their wisdom and expertise through our collaboration. I am extremely grateful to the Medical Research Council (MRC) for funding my DPhil as this would not have been possible without their support.

I am so lucky to have the amazing love, support and understanding of my friends and family. To my amazing friends, thank you for always being there for me and forever willing to celebrate even the tiniest of achievements. Mum and Andy, thank you so much for everything you have done to support me not only for this DPhil, but everything before (and no doubt after too!) I would also like to thank my wonderful family members: Nathan, Lily, Leanne, Grandma, Grandad, Uncle Neil, Auntie Natalie, Uncle Mark, Auntie Danusia, Isaac and Noah for their love and encouragement. Cheryl, Martin, and the family, thank you so much for all of the endless love and support you have given me. I will be forever grateful for everything that you have all done for me.

Finally, Sam – I cannot put into words how grateful I am for your never-ending support and unconditional love. Thank you for always encouraging me and motivating me, I could not have done this without you.

Table of Contents

Abstract I

Acknowledgements II

List of Figures VIII

List of Tables X

List of Abbreviations XI

1 Introduction 1

1.1 Ataxia-telangiectasia (A-T) 1

1.2 Clinical presentation of A-T 1

1.2.1 Neurodegeneration 2

1.2.2 Telangiectasia 2

1.2.3 Immune deficiency 2

1.2.4 Cancer susceptibility 3

1.2.5 Sensitivity to IR 3

1.2.6 Endocrine abnormalities 4

1.2.7 Diagnosis and management of A-T 4

1.2.8 Aetiology of A-T 5

1.3 ATM 5

1.4 ATM and the DNA damage response 6

1.4.1 NHEJ-mediated repair of DNA DSBs 7

1.4.2 HR-mediated repair of DNA DSBs 8

1.5 ATM and the cell cycle 12

1.5.1 The G1/S cell cycle checkpoint 13

1.5.2 The intra-S phase checkpoint 13
1.5.3 The G2/M cell cycle checkpoint 13
1.6 ATM and oxidative stress 14
1.7 ATM and cancer 15
1.8 PIKK family of protein kinases 16
1.9 Cellular phenotype of ATM loss 17
1.10 Targeting the ATM signalling pathway 18
1.11 Genomic instability syndromes 20
1.12 Aims of this study 21
2 Materials and Methods 22
2.1 Buffers and solutions 22
2.2 Cell culture 25
2.2.1 Cryopreservation and thawing of cell lines 28
2.2.2 Mycoplasma testing of cell lines 28
2.3 Sequencing ATM isogenic cell pair 29
2.4 Mice 30
2.4.1 Generation of $ATM^{-/-}$ mice 31
2.5 Administration of drug and irradiation *in vivo* 33
2.5.1 Formulation of compounds 33
2.5.2 Irradiation 34
2.5.3 Experimental design for *in vivo* study 35
2.6 Formalin fixation and paraffin embedding (FFPE) 35
2.7 Immunohistochemistry (IHC) 36
2.8 Compound treatments and irradiation *in vitro* 39
2.9 Cell viability assay 42

2.10 Clonogenic survival assay 43
2.10.1 Irradiation 43
2.10.2 Drug treatment 43
2.11 Western blotting 44
2.11.1 Protein extraction and quantification 44
2.11.2 SDS-polyacrylamide gel electrophoresis (PAGE) 45
2.11.3 Immunoblotting 45
2.12 Immunofluorescence 49
2.13 Cell viability screen 50
2.14 Data analysis 52
3 ATM protein expression in human normal and tumour tissues 53
3.1 ATM protein is highly expressed in normal human tissue 55
3.2 IHC reveals frequent tumoural loss of ATM protein expression 58
3.3 Loss of tumoural ATM may be associated with an immune phenotype 61
3.4 Discussion 64
4 ATM-dependent DNA damage responses in normal tissues 72
4.1 Expression of ATM protein in normal murine tissues 74
4.2 DDR following whole body irradiation 76
4.3 Treatment with the ATM kinase inhibitor AZ31 suppresses DDR signalling following whole-body IR 85
4.4 Genetic loss of functional ATM suppresses DDR signalling following whole-body IR 87
4.5 DDR responses in normal tissues following irinotecan treatment 92

4.6 Treatment with the ATM kinase inhibitor AZ31 suppresses irinotecan-induced DDR signalling 96
4.7 Genetic loss of ATM function suppresses DDR signalling in response to irinotecan treatment 99
4.8 ATM heterozygosity does not significantly affect DDR in response to IR or irinotecan 103
4.9 Discussion 104
5 The effect and consequences of ATM inhibition versus ATM loss 109
5.1 Sensitivity of human non-tumour lung fibroblasts to radiation and cytotoxic compounds 112
5.1.1 Loss of ATM confers radiosensitivity in lung fibroblasts 112
5.1.2 ATM plays a role in the response of lung fibroblasts to chemotherapeutic compounds 114
5.2 Sensitivity of human lung isogenic tumour cells to radiation and cytotoxic compounds 121
5.2.1 Loss of ATM confers radiosensitivity in lung tumours 121
5.2.2 ATM plays a role in the response of lung tumour cells to chemotherapeutic compounds 123
5.2.3 Loss of ATM function in tumour cells is associated with sensitivity to certain chemotherapeutic drugs 126
5.3 Role of ATM independent phosphorylation of KAP1 129
5.3.1 Loss of ATM confers delayed induction of DDR in tumour cells but not fibroblasts 129
5.3.2 SN-38 targeting is predominantly restricted to S phase cells 132
5.3.3 Contributions of DNA-PK to compensate for loss of ATM 135

5.4 Screening-based identification of compounds that confer synthetic lethality with loss of ATM 138

6 General Discussion and Conclusion 155

7 References 160

8 Supplementary 206

Word count: 28417

List of Figures

Figure 1.1 | Overview of the NHEJ pathway 8

Figure 1.2 | Overview of the HR pathway 11

Figure 1.3 | Overview of DNA damage induced cell cycle checkpoint activation 12

Figure 2.1 | Schedule for administration of radiation and drug compounds *in vivo* 35

Figure 3.1 | Normal human tissues express high total levels of ATM protein 57

Figure 3.2 | ATM is frequently lost in human tumours 60

Figure 3.3 | Tumour ATM protein loss may be associated with an immune phenotype 63

Figure 4.1 | Normal murine tissues express high total levels of ATM protein 76

Figure 4.2 | Whole-body IR-induced DDR in murine tissues 83

Figure 4.3 | Inhibition of IR-induced ATM signalling with AZ31 87

Figure 4.4 | Genetic loss of ATM suppresses IR-induced DDR signalling 91

Figure 4.5 | Irinotecan-induced DDR in murine tissues 96

Figure 4.6 | Inhibition of irinotecan-induced ATM signalling with AZ31 98

Figure 4.7 | Genetic loss of ATM suppresses irinotecan-induced DDR signalling 102

Figure 4.8 | ATM heterozygosity does not significantly affect DDR responses 104

Figure 5.1 | ATM loss confers radiosensitisation in lung fibroblasts 113

Figure 5.2 | ATM has a role in the fibroblast response to chemotherapeutic drugs.....118

Figure 5.3 | ATM loss confers radiosensitisation in isogenic lung tumour pair 122

Figure 5.4 | ATM has a role in the tumour response to chemotherapeutic drugs 124

Figure 5.5 | Loss of ATM in tumour cell lines confers differential sensitivities to chemotherapeutic agents 128

Figure 5.6 | Induction of ATM pathway activation in response to SN-38 131

Figure 5.7 | SN-38 targeting of S phase cells 134

Figure 5.8 | Compensation of ATM loss by DNA-PK in response to SN-38 138

Figure 5.9 | Kinase screen reveals compounds that confer synthetic lethality with loss of ATM 140

Figure 8.1 | ATM protein is not detected in normal murine tissues from $ATM^{-/-}$ mice..207

List of Tables

Table 1.1 | Overview of ATM inhibitors.....19

Table 2.1 | Composition of buffers.....22

Table 2.2 | Overview of cell lines 26

Table 2.3 | Overview of compounds used for *in vivo* studies 33

Table 2.4 | Antibodies used for IHC 37

Table 2.5 | Overview of compounds used for *in vitro* studies.....40

Table 2.6 | Antibodies used for Western blotting.....46

Table 2.7 | Statistical measures from cell viability screen 51

Table 4.1 | Percentage of BrdU positive cells in vehicle and IR-treated tissues.....84

Table 5.1 | Overview of chemotherapeutic drugs 115

Table 5.2 | Sensitivity of ATM wildtype, ATM inhibited and ATM mutant lung fibroblasts to paclitaxel, etoposide, gemcitabine, cisplatin, irinotecan, and SN-38 119

Table 5.3 | Sensitivity of ATM wildtype, ATM inhibited and ATM deficient lung tumour cells to paclitaxel, etoposide, gemcitabine, cisplatin, irinotecan, and SN-38 125

Table 5.4 | Screening hits from lung fibroblast cell pair.....141

Table 5.5 | Screening hits from lung tumour cell pair.....144

Table 8.1 | Sample comparison for RNAscope technology 206

List of Abbreviations

53BP1	tumour suppressor p53 binding protein 1
A-T	Ataxia-telangiectasia
alt-NHEJ	alternative non-homologous end joining
APC	antigen presenting cell
ATLD	Ataxia-telangiectasia-like disorder
ATM	Ataxia-telangiectasia mutated
ATR	Ataxia-telangiectasia and Rad3-related
ATRIP	Ataxia-telangiectasia and Rad3-related interacting protein
BRCA1	breast cancer type 1 susceptibility protein
BRCA2	breast cancer type 2 susceptibility protein
BrdU	bromodeoxyuridine
BSA	bovine serum albumin
CD	cluster of differentiation
CDC25	cell division cycle 25
CDK	cyclin dependent kinase
cGAS	cyclic GMP-AMP synthase
CHK1	checkpoint kinase 1
CHK2	checkpoint kinase 2
CNS	central nervous system
CPT	camptothecin
CRISPR	clustered regularly interspaced short palindromic repeats
CtIP	CTBP interacting protein
DAB	diaminobenzidine
DDR	DNA damage response
DMEM	Dulbecco's Modified Eagle Medium
DMSO	dimethyl sulphate
DNA	deoxyribonucleic acid
DNAPKcs	DNA-dependent protein kinase catalytic subunit

DSB	double strand break
EDTA	ethylenediaminetetraacetic acid
EdU	5-ethynyl-2'-deoxyuridine
EGFR	epidermal growth factor receptor
FAT	FRAP-ATM-TRRAP
FATC	FAT C terminal
FBS	foetal bovine serum
FFPE	formalin-fixed paraffin-embedded
FRB	FKBP-rapamycin binding
GI	gastrointestinal
HEAT	Huntingtin, elongation factor 3, protein phosphatase 2A and TOR1
HIF-1	hypoxia-inducible factor 1
HPA	hypothalamic-pituitary-adrenal
HR	homologous recombination
i.p.	intraperitoneal
IC_{50}	half-maximal inhibitory concentration
IGF1R	insulin-like growth factor 1 receptor
IHC	immunohistochemistry
iPSC	induced pluripotent stem cells
IR	ionising radiation
KAP1	KRAB-associated protein 1
KCGS	kinase chemogenomic set
MCL	mantle cell lymphoma
MDC1	mediator of DNA damage checkpoint protein 1
MDM2	murine double minute 2
MHC	major histocompatibility complex
MICA	MHC class I chain-related protein A
MMEJ	microhomology-mediated end joining
MRN	MRE11-RAD50-NBS1
mRNA	messenger RNA
mtDNA	mitochondrial DNA

mTOR	mammalian target of rapamycin
NBF	neutral buffered formalin
NHEJ	non-homologous end joining
NBS	Nijmegen breakage syndrome
NK	natural killer
NSCLC	non-small cell lung cancer
p.o.	per os
PARP	poly (ADP-ribose)-polymerase
PBMC	peripheral blood mononuclear cells
PBS	phosphate buffered saline
PCR	polymerase chain reaction
PD-L1	programmed death-ligand 1
PDAC	pancreatic ductal adenocarcinoma
PI3K	phosphatidylinositol 3-kinase
PIKK	phosphatidylinositol 3-kinase-related kinase
PRD	PIKK regulatory domain
Rb	Retinoblastoma
RNA	ribonucleic acid
ROS	reactive oxygen species
RPA	replication protein A
SCID	severe combined immunodeficiency
SDS	sodium dodecyl sulphate
SEM	standard error of the mean
sgRNA	single guide RNA
SMG1	suppressor with morphological effect on genitalia family member
SSB	single strand break
ssDNA	single strand DNA
STING	stimulator of interferon genes
SV40	simian virus 40
TBE	Tris-borate EDTA
TBS	Tris-buffered saline

TCGA	The Cancer Genome Atlas
TCR	T cell receptor
TMA	tissue microarray
TNF-α	tumour necrosis factor α
TRRAP	transformation/transcription domain-associated protein
UV	ultraviolet
V(D)J	variable (diversity) joining
VEGF	vascular endothelial growth factor
wt	wildtype

1 Introduction

1.1 Ataxia-telangiectasia (A-T)

Ataxia-telangiectasia (A-T) is an autosomal recessive disorder that has been described as a genome and chromosomal instability syndrome. This complex disorder affects multiple body systems which correspond to a range of clinical manifestations spanning neurological, immune, and pulmonary function. Both disease presentation and progression vary across individuals whereby "classic" or "typical" A-T denotes a form that is more severe and/or associated with early age onset. Milder forms of A-T are associated with slower disease progression and greater life expectancy. Worldwide prevalence is estimated at 1 in 40,000 – 300,000 individuals and affects all racial and ethnic backgrounds equally, excluding consanguineous populations[1,2].

1.2 Clinical presentation of A-T

A-T is characterised by progressive cerebellar degeneration, telangiectasia, immunodeficiency, susceptibilities to cancer, genomic instability, and a profound sensitivity to ionising radiation (IR). The complexity of A-T is evident by the variation in clinical presentation, disease severity and cellular phenotype[2]. To date, there is no cure or effective treatment available for A-T patients and current interventions are focused on the management of symptoms. Individuals with A-T have a reduced life expectancy and the most common causes of death are chronic respiratory disease and cancer[1,3].

1.2.1 Neurodegeneration

Neuropathological changes in A-T patients are most prominent within the cerebellar cortex, specifically atrophy and the depletion of Purkinje and granule cell populations. This cerebellar dysfunction manifests as ataxia which first presents as lack of coordination and gradually progresses towards severe motor dysfunction[4,5]. Interestingly, it is the cerebellar cortex that is most severely affected compared to other brain regions however the aetiology of the progressive neurodegeneration observed in A-T patients is not fully understood. Currently there are no treatments available that have successfully slowed the progression of the neurological degeneration seen in A-T[2,6].

1.2.2 Telangiectasia

The occurrence of ocular and cutaneous telangiectasia is a result of blood vessel dilation of the skin and mucous membranes. Telangiectasia in A-T patients are primarily located in the sclera of the eyes and on sun-exposed skin areas. Despite individuals with A-T experiencing impaired visual fixation and control of eye movement, telangiectasia itself does not affect vision or visual acuity[2]. The aetiology of telangiectasia has not been fully elucidated however an association with elevated hypoxia-inducible factor 1 (HIF-1) expression has been described. HIF-1 has been reported to upregulate vascular endothelial growth factor (VEGF) therefore promoting angiogenesis. The formation of vascular abnormalities, such as telangiectasia in A-T patients, can potentially be attributed to the potent angiogenic nature of HIF-1 signalling[7].

1.2.3 Immune deficiency

Defective humoral and cellular immunity contribute to the immune defects observed in A-T including a limited immune repertoire and impaired capacities to produce cytotoxic T

cells and respond to mitogens[5,8,9]. These features are associated with an impaired thymic output that has been reported in A-T. Whilst significant deficiencies in naïve CD4 and CD8 T cells are associated with A-T, an increased natural killer (NK) cell population is also evident[9]. In addition, approximately 10% of individuals with A-T are diagnosed with hypogammaglobulinaemia which presents with a hyper immunoglobulin-M (HIGM) phenotype[10]. RNA sequencing (RNAseq) obtained from A-T peripheral blood mononuclear cells (PBMC) revealed abnormal expression of genes associated with immune regulation and inflammation[11]. The elevated production of pro-inflammatory cytokines such as IL-8 and TNF-α contribute to the generation of an aberrant inflammatory environment. Recurrent sinopulmonary infections in A-T contribute to the development of bronchiectasis and chronic lung disease[12,13].

1.2.4 Cancer susceptibility

Haematological malignancies, including leukaemia and lymphoma that span the T and B cell systems, are frequently reported in A-T[14,15]. Individuals with A-T have a reported incidence of neoplasia of over 20% before the age of 16[16]. Defective T cell maturation results in the aberrant rearrangement of T cell receptor (TCR) loci and failure to eradicate such cells has been reported to promote tumour development. Malignancy in A-T has also been associated with the mutational event, chromothripsis[3,16,17]. Whilst the increased risk of haematological cancer is particularly evident during the first two decades, the incidence of solid malignancies, such as breast, gastric and pancreatic, increases in adulthood[1,18].

1.2.5 Sensitivity to IR

The profound radiosensitivity reported in A-T is a major hallmark of the disorder. This was first observed upon exposure to conventional radiotherapeutic doses used in cancer

treatment and the detrimental consequences on individuals with A-T. In response to radiotherapy, the development of severe radiation-associated complications was fatal[19,20]. The treatment strategy for malignancies in A-T has not been standardised and factors associated with the severity of an A-T phenotype may inform treatment. Cells from A-T patients have been shown to recapitulate the radiosensitivity observed and it has been proposed that analysing patient cells may be a useful tool for guiding therapeutic approach and dose adjustment in the context of each A-T individual[10,21–23].

1.2.6 Endocrine abnormalities

Metabolic syndromes, such as diabetes mellitus, have been associated with A-T. In addition, insulin resistance has been frequently reported with the occurrence of liver dysfunction[24]. Impaired growth has been partially attributed to the downregulation of insulin-like growth factor 1 receptor (IGF1R)[25,26]. Reproductive dysfunction conferred by abnormal pubertal development raises fertility complications in A-T[2].

1.2.7 Diagnosis and management of A-T

Clinical evaluation of individuals provides the preliminary diagnosis based on symptom presentation. However, the variability in the constellation of symptoms presented may hinder a timely diagnosis. Confirmation of diagnosis is performed through laboratory tests, such as testing cellular radiosensitivity[2,27]. Whilst there is no cure for A-T, treatment is limited at managing symptoms including the employment of chest physiotherapy and airway clearance exercises, annual lung function consultation and regular administration of pneumococcal vaccines in children[1].

1.2.8 Aetiology of A-T

Ataxia-telangiectasia mutated (ATM) was identified in 1995 as the gene responsible for A-T[28]. Germline mutations in ATM can be homozygous or compound heterozygous and give rise to A-T by autosomal recessive inheritance. Genotyping of A-T has revealed over 700 mutations which can be found across the entire length of the ATM gene with no apparent hotspots[5,29–31]. In approximately 85% of cases, ATM protein is undetectable due to generation of an unstable and truncated protein, whilst the remaining 15% are associated with reduced functional protein[32,33]. Residual expression of full length ATM protein has been correlated with milder phenotypes of A-T[34].

1.3 ATM

ATM is a member of the phosphatidylinositol 3-kinase (PI3K)-related kinase (PIKK) family of serine threonine protein kinases. The ATM gene spans 150 kb of genomic DNA, contains 66 exons corresponding to a 350 kDa protein of 3065 residues and is mapped to chromosome 11q22-23[28,35]. Consistent with the PIKK family members, ATM has a conserved PI3K domain located towards the C-terminus. The kinase domain is located between a N-terminal FRAP-ATM-TRRAP (FAT) domain and a C-terminal FAT carboxy terminus (FATC) domain. This latter domain consists of Huntingtin, elongation factor 3, protein phosphatase 2A and TOR1 (HEAT) repeats which are also found throughout the N-terminus. In addition, there is a small PIKK-regulatory domain (PRD) adjacent to the kinase and FATC domains[36,37].

ATM is an apical kinase with a well-reported function in the response to DNA double strand breaks (DSBs) to coordinate lesion repair and temporary cell cycle arrest. The orchestration of this response requires the complex recruitment and activation of various

substrates[38]. In addition to a nuclear role of ATM, a cytoplasmic function has also been documented regarding the cellular response to oxidative stress[39,40]. These functions will be discussed in further detail throughout this report.

1.4 ATM and the DNA damage response

In every cell, approximately 70,000 DNA lesions are generated per day which threaten to compromise genome integrity. DNA single-strand breaks (SSBs) account for the vast majority however DSBs are considered to be the most harmful[41,42]. Failure to repair a DSB can induce apoptotic signalling whilst misrepair can lead to mutation and neoplastic transformation[43]. Endogenous factors such as replication stress, metabolic reactions and chemical modifications, and exogenous factors such as genotoxic compounds, ultraviolet (UV) and IR can cause genomic lesions[44].

To maintain genome integrity, cells have evolved a complex network of signalling pathways that respond to DNA insult, collectively termed the DNA damage response (DDR). This extensive network is comprised of 450 genes that encode integral proteins involved in the DDR[45,46]. Depending on the type of damage induced, cells are able to activate particular repair pathways to efficiently deal with the damage and maintain genome stability. The formation of DNA DSBs can occur as a result of several factors including the collapse of stalled replication forks, generation of reactive oxygen species (ROS) and exposure to genotoxic modalities, such as IR. The induction of DNA DSBs can also be during normal physiological processes such as meiotic recombination and V(D)J recombination[5,47–49]. The cell has two predominant, but mechanistically distinct, pathways to orchestrate the repair of DNA DSBs. These are non-homologous end-joining (NHEJ) and homologous recombination (HR)[50–52].

1.4.1 NHEJ-mediated repair of DNA DSBs

NHEJ involves the direct ligation of broken DNA ends and is active throughout all phases of the cell cycle. This direct ligation can be performed on blunt DNA ends or ends with very short overhangs. This process is considered error-prone due to the potential for loss of nucleotides and repair is performed in the absence of a template strand[53]. Initiation of NHEJ follows the binding of the Ku heterodimer, consisting of Ku70 and Ku80 subunits, at the site of damage. The recruitment of DNA-protein kinase catalytic subunit (DNA-PKcs) is triggered by the DNA end-heterodimer interactions which results in the formation of the DNA-PK holoenzyme[54–56]. End bridging occurs to stabilise the broken DNA ends whilst the activity of several NHEJ factors, such as DNA polymerases μ and λ, DNA ligase IV and XRCC4 facilitate gap filling and ligation[57–59]. A schematic of NHEJ-mediated repair of DSBs is shown in Figure 1.1.

Alternative NHEJ (alt-NHEJ), or micro-homology mediated end-joining (MMEJ), is an additional repair pathway that can respond to DNA DSBs. Unlike the classical NHEJ pathway, there is a requirement for microhomology of 4-20 base pairs in order to facilitate lesion repair. In addition, Ku70/80 is not required for this process and further relies on alternative enzymes to mediate resection[60–62].

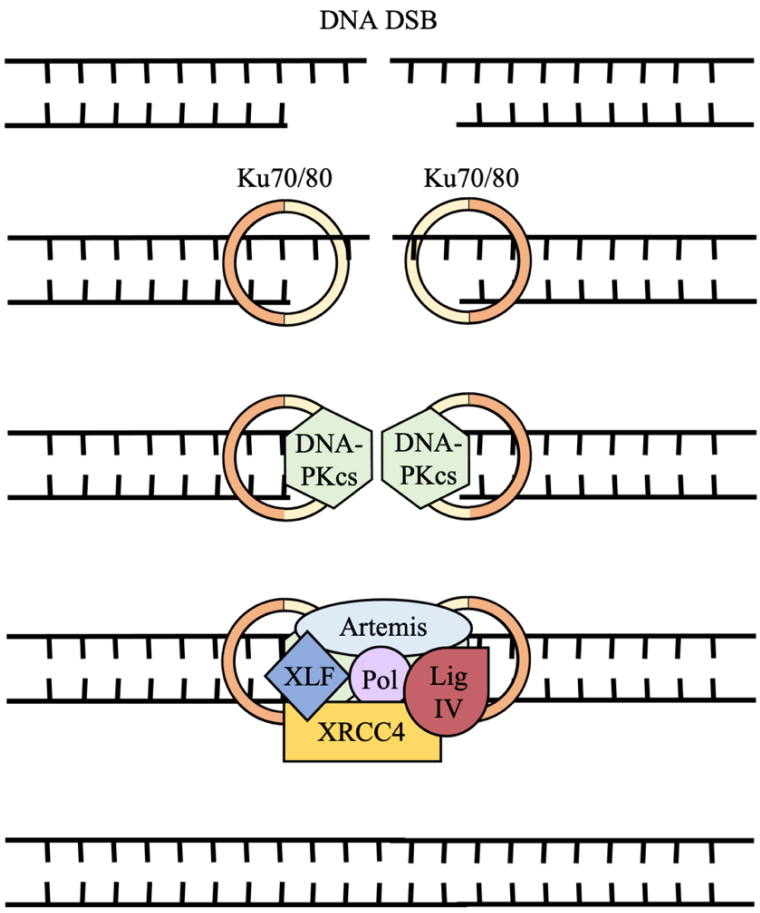


Figure 1.1 | Overview of the NHEJ pathway

Schematic representation of the NHEJ pathway in response to DNA DSBs. The Ku70/80 heterodimer recognises DNA DSB and recruits DNA-PKcs and subsequent formation of the DNA-PK holoenzyme. DNA ends are stabilised, processed by enzymes such as polymerases (Pol; μ, λ) and Artemis followed by ligation with the NHEJ factors XLF, XRCC4 and DNA ligase IV (Lig IV). Figure adapted from Velic *et al*, 2015[63].

1.4.2 HR-mediated repair of DNA DSBs

HR relies on the presence of a sister chromatid to act as a template for repair and therefore this pathway is restricted to the S and G2 phases of the cell cycle. The requirement of a sister chromatid ensures the faithful restoration of genetic information from the damaged chromosome[50,64,65]. The process of HR is initiated by the recruitment of the MRE-11-RAD50-NBS1 (MRN) complex at the lesion site. The subunits of the MRN complex have specific roles during the process of HR. For example, MRE11 initiates end resection

through its nuclease activity, RAD50 provides structural support by tethering the complex using its extended coiled coil tail domain and NBS1 acts as an adaptor protein[66].

The MRN complex promotes the recruitment of inactive ATM dimers to the DSB site which triggers ATM monomerisation[67]. In undamaged cells, ATM predominantly exists as an inactive dimer or higher order multimers through binding of FAT domains. Dissociation from the dimer conformation is associated with ATM activation in which monomeric ATM can perform extensive kinase function[68,69]. Autophosphorylation of ATM at serine 1981 has been reported to mediate dimer dissociation, ATM retention at the lesion site and sustaining DNA damage signalling[3,70]. However, the importance and requirement of this ATM autophosphorylation has been contentious. For example, the serine to alanine mutation of the equivalent site in mice (serine 1987) does not impact ATM recruitment or activation of the downstream signalling pathway. Furthermore, additional ATM autophosphorylation sites have shown to be expendable for adequate DDR *in vivo*[71–73].

Whilst ATM lacks strong DNA binding capacity, it is tethered at DSBs and performs kinase activity to phosphorylate a number of downstream targets to initiate a DDR signalling cascade[74]. An initial event in this pathway is the ATM-dependent phosphorylation of the histone variant H2AX at serine 139 (γH2AX) which leads to the recruitment of mediator of damage checkpoint 1 (MDC1). Following recruitment and binding to γH2AX, MDC1 is recognized and bound by the ubiquitin ligase RNF8 which exerts its enzyme activity on local histones. Together with the ubiquitin ligase RNF168, they facilitate the recruitment of the mediator proteins breast cancer gene 1 (BRCA1) and tumour suppressor p53-binding protein 1 (53BP1)[75–77]. As part of the response to DSB, ATM phosphorylates multiple substrates including BRCA1, checkpoint kinase 2 (CHK2),

p53, C-terminal-binding protein (Ct-BP) interacting protein (CtIP) and Krüppel-associated box (KRAB)-associated protein 1 (KAP1)[78,79]. Retention of ATM at the DSB site supports the phosphorylation of H2AX at sites increasingly distal to the DSB, which stimulates further recruitment of MDC1. Signal amplification corresponds to the distinct γH2AX foci that can be visualised following IR[80–82]. Self-reinforcement of the DDR is implicated from the ATM-mediated phosphorylation of the MRN subunits[83,84].

DSB repair commences with MRN and CtIP-mediated DNA end resection. Generation of 3' single-stranded DNA (ssDNA) overhangs are rapidly bound and coated by replication protein A (RPA)[66]. A BRCA2-RAD51 interaction facilitates the replacement of RPA with RAD51 which mediates strand invasion of the sister chromatid and homology search[85,86]. Following identification of the homologous sequence, DNA polymerases synthesise the complimentary DNA. During the process of HR crossover, structures termed Holliday junctions are formed between the invading strand and the template DNA. Enzymatic activity of GEN1, MUS81-EME1 and SLX1-SLX4 are important for structure resolution[87–89]. A schematic of HR-mediated repair of DSBs is shown in Figure 1.2.

In response to IR, the majority of DSBs are repaired by NHEJ compared to HR (10-15%) in G2 phase, where both DDR pathways are available[90]. Repair pathway choice is dictated by the cell cycle phase due to the requirement of a sister chromatid in HR but can also be determined by the compilation of factors at the damage site. For example, 53BP1 promotes NHEJ as the pathway choice however BRCA1, which facilitates 53BP1 removal, promotes end resection to stimulate HR[59,66].

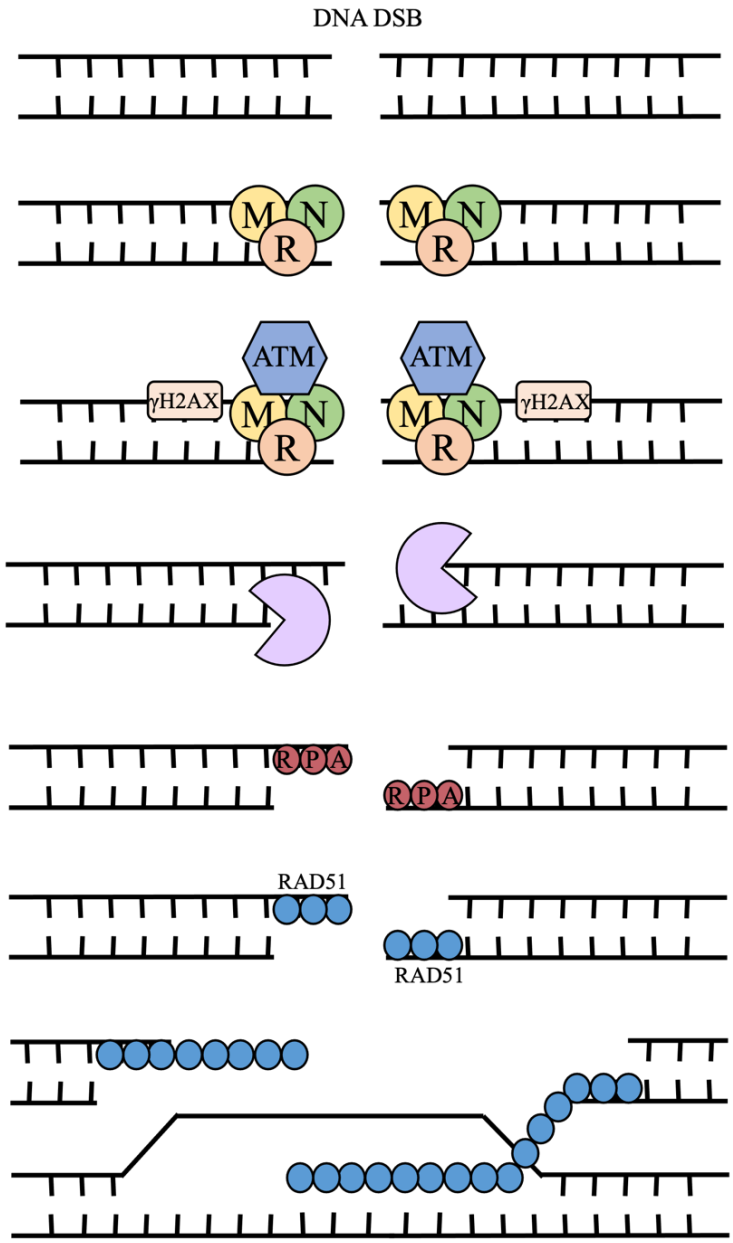


Figure 1.2 | Overview of the HR pathway

Schematic representation of the HR pathway in response to DNA DSBs. MRN detects DNA DSB and facilitates the recruitment and activation of ATM. Following ATM activation is the phosphorylation of H2AX. Nucleases perform DNA end resection prior to RPA coating of single strand DNA ends. RPA is replaced by RAD51 in a BRCA2-mediated mechanism and precedes the strand invasion and structure resolution. Figure adapted from Velic *et al*, 2015[63].

1.5 ATM and the cell cycle

The cellular DDR also functions to induce transient cell cycle arrest to allow for adequate repair. Without this safeguard mechanism, genetic information from cells with unrepaired DNA lesions would be passed down to daughter cells[91]. If the extent of damage exceeds repair capabilities, activation of apoptotic processes may proceed[92,93]. Cell cycle checkpoints exist at the G1/S, intra-S phase, and G2/M transitions. A simplified overview of the DNA damage induced cell cycle checkpoint activation is shown in Figure 1.3.

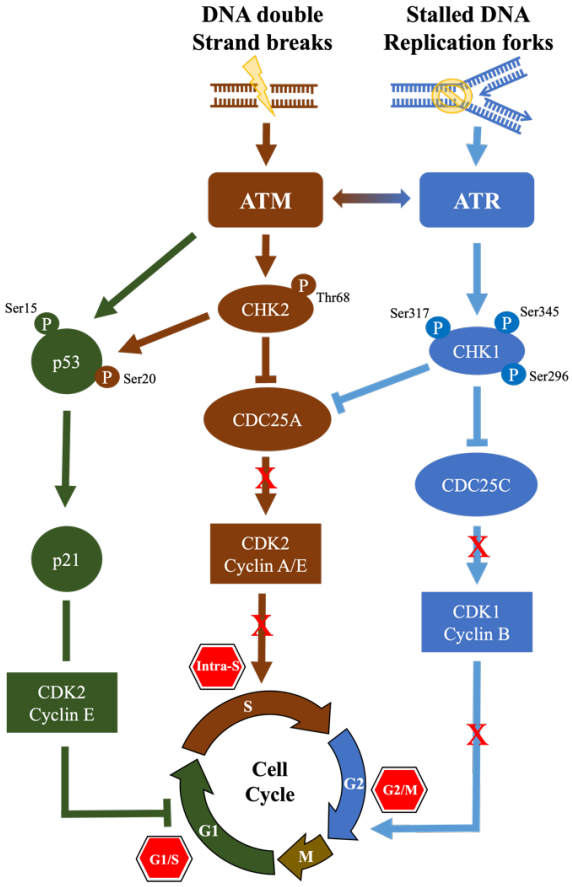


Figure 1.3 | Overview of DNA damage induced cell cycle checkpoint activation

Cell cycle checkpoints are activated in response to DNA damage predominantly through ATM and ATR signalling. G1/S arrest is induced through the p53-mediated increase of the cyclin-dependent kinase inhibitor, p21. The intra-S-phase and G2/M checkpoint is mediated via CHK1/CHK2 activation which inhibit the phosphatase regulation of CDK-Cyclin complexes. Figure adapted from Weber and Ryan, 2015[94].

1.5.1 The G1/S cell cycle checkpoint

Activation of the G1/S cell cycle checkpoint primarily involves the accumulation and stabilisation of p53. Through phosphorylation of p53 at serine 15 and serine 20 by ATM and CHK2 respectively, MDM2-mediated degradation of p53 is prevented. In addition, ATM indirectly contributes to increased p53 through phosphorylation of MDM2 at serine 395[95]. Accumulation of p53 in the nucleus promotes the expression of cell cycle checkpoint and apoptosis-related genes, such as p21[94]. Stabilisation of p53 results in the increased activity of the cyclin-dependent kinase (CDK) inhibitor, p21. Inhibition of CDK2 avoids the release of the transcription factor E2F by preventing retinoblastoma (Rb) phosphorylation[96,97].

1.5.2 The intra-S phase checkpoint

In response to replication stress and the presence of RPA-coated ssDNA, ataxia-telangiectasia and Rad3-related (ATR) interacting protein (ATRIP) binds to RPA-ssDNA and interacts with ATR. The downstream target, CHK1, is phosphorylated by ATR which leads to CDC25A-mediated degradation. When active, the phosphatase CDC25A is responsible for removing inhibitory phosphate groups from CDK2. Due to inactivation of CDK2-Cyclin complexes, the intra-S phase checkpoint is activated[98,99]. The activation of this checkpoint enables time for DNA damage repair and the restart of stalled replication forks by suppressing late origin firing[100].

1.5.3 The G2/M cell cycle checkpoint

The G2/M cell cycle is responsible for preventing the inappropriate entry of cells into mitosis. This checkpoint is primarily regulated by ATR through phosphorylation of CHK1. As previously mentioned, the CHK1-dependent inhibition of CDC25 phosphatase, in this

case CDC25C, prevents CDK-Cyclin B promotion of cell cycle progression[101,102]. Maintaining inhibitory phosphorylation of CDKs is promoted through mediating WEE1 activity. The CHK1-dependent phosphorylation of WEE1 at serine 549 promotes WEE1 and 14-3-3 protein interactions to enhance CDK inhibition[103].

1.6 ATM and oxidative stress

Endogenous ROS are generated during cellular processes such as oxidative phosphorylation in the mitochondria. Sources of exogenously produced ROS include alcohol, radiation and drugs including paracetamol, doxorubicin, and bleomycin[104]. Cellular antioxidant defence mechanisms are responsible for neutralising ROS activity. A metabolic imbalance between these protective mechanisms and the generation of ROS results in oxidative stress. As the antioxidant mechanisms are overwhelmed, cellular components including nucleic acids, proteins, and lipids are damaged[105].

In response to increased cellular ROS, ATM has been reported to mediate the restoration of redox homeostasis through formation of disulphide-linked ATM dimers, specifically between cysteine (C2991) residues[39]. Unlike the requirement for monomeric ATM for the DDR, ATM is active as a covalent dimer in the context of responding to oxidative stress[106]. Through detection of elevated ROS, ATM promotes autophagy and subsequently minimises protein aggregation[107].

Using an artificial system, ATM activation was observed in response to bleomycin or hydrogen peroxide treatment which, in the case of the latter, was independent of DNA damage. Phosphorylation of KAP1 at serine 824 was observed in response to DNA damage but not oxidative stress alone, indicating differential downstream signalling between these scenarios[39,108,109]. Studies have also reported that supplementation of antioxidants to ATM-

deficient mice delays the onset of T cell lymphoma[110,111]. The consequences of loss of ATM have been attributed to its role in mediating oxidative stress due to the presence of oxidative damage to various tissues in A-T, reduced antioxidant plasma levels and aberrant inflammation[112,113]. In addition, the release and accumulation of mitochondrial DNA (mtDNA) from damaged mitochondria into the cytoplasm has been proposed to be a driver of stimulator of interferon genes (STING) activation which can promote an aberrant inflammatory response[114].

1.7 ATM and cancer

The importance of an efficient DDR in human health is evidenced by the pathological contributions in the context of deregulation. In the absence of an intact DDR, disorders spanning the central nervous system (CNS), cardiovascular (CV), immune, reproductive, and endocrine systems have been reported[115,116]. In addition, the deregulation of the DDR has been associated with the development of genetic disorders and cancer. For example, the acquisition of genomic instability and replication stress can promote mutagenesis and cancer development[117,118].

Targeting the DDR has provided an attractive approach in cancer therapy aiming to exploit intrinsic synthetic lethality. In this instance, cancer cells often rely on a particular DNA repair pathway due to defective signalling in the alternative pathway. Targeting the remaining pathway with small molecule inhibitors renders the cancer cell vulnerable and unable to respond to DNA damage. The functional DDR in normal cells promotes selective targeting of cancer cells[119–122]. An excellent clinical example of this is the use of poly (ADP-ribose)-polymerase (PARP) inhibitors in the context of BRCA1/2 deficiency[123–126]. Alternatively, by using genotoxic approaches to maximise damage during the G1 and S phases of the cell cycle, targeting the DDR repair pathway prevents adequate repair

promoting cells with damaged DNA entering mitosis. This results in a concept known as mitotic catastrophe and consequently cell death[127,128].

Germline mutations in ATM give rise to A-T in which individuals have an increased susceptibility to cancer, predominantly leukaemia and lymphoma in childhood which expands to include solid tumours with age[1,14–16,18]. In addition, an increased risk of breast cancer has been reported in individuals with a heterozygous mutation in ATM[129,130]. Somatic ATM mutations are a frequent occurrence in various solid tumours and haematological malignancies[131,132]. Previous reports have demonstrated that loss of ATM may confer a poorer prognosis in some tumour types[133–135]. Whilst ATM loss in early-stage colorectal cancer is coupled with a worse prognosis, loss of ATM appears to be associated with a favourable prognosis in late-stage disease[136]. In addition, particular ATM variants are considered to be a determinant in breast cancer prognosis whilst a relationship between ATM loss and overall survival in lung adenocarcinoma was not reported[137,138].

1.8 PIKK family of protein kinases

Alongside ATM, there have been five additional members of the PIKK family identified in humans. These include ATR, DNA-PKcs, mammalian target of rapamycin (mTOR), suppressor with morphological effect on genitalia family member (SMG1) and transformation/transcription-associated protein (TRRAP)[139]. The PIKK family share significant homology containing a PI3K signature as well as FAT and FATC domains and HEAT repeats[36,140]. Additional protein-specific domains include the N-terminal ATRIP binding domain on ATR and the FKBP-rapamycin binding (FRB) domain on mTOR adjacent to the FAT domain[139]. None of the PIKK family members are associated with lipid kinase activity whilst all, apart from TRRAP, possess intrinsic protein kinase function[141].

ATM, ATR and DNA-PKcs are considered the three main apical kinases involved in mediating the cellular response to DNA damage. As the largest member of the PIKK family, DNA-PKcs consists of 4128 amino acids corresponding to approximately a 470 kDa protein[142,143]. The roles of ATM and DNA-PKcs in the response to DNA DSBs are discussed in section 1.4.1 and 1.4.2 respectively. ATR has a central role in the response to replication stress which can arise through the generation of SSBs, stalled replication forks and DSB resection[144,145]. Activation of ATR is associated with the protection of stalled forks and promoting cell cycle checkpoint activation as illustrated in Figure 1.3. Whilst the DDR kinases have distinct roles in maintaining genome integrity, there is evidence of crosstalk and substrate overlap[3,94]. This redundancy is emphasised by the common phosphorylation sites of the ATM, ATR and DNA-PK which consist of a serine/threonine residue followed by a glutamine residue[38].

Involvement in the DDR is not considered a primary function of mTOR however oxidative stress-mediated interactions have been reported with ATM suggesting crosstalk also exists between these proteins[3]. The primary roles of mTOR involve regulating cell proliferation, survival, growth, and metabolism[139]. The role of hSMG1 concerns nonsense-mediated messenger RNA (mRNA) and has been associated with the response to UV damage[5].

1.9 Cellular phenotype of ATM loss

Functional loss of ATM confers a range of several detrimental consequences, evidenced by the constellation of symptoms manifested in A-T[1,2]. At a cellular level, chromosomal aberrations including rearrangements, translocations and inversions are reported[6]. Following exposure to IR, A-T cells fail to activate the G1/S checkpoint and are incapable of reducing DNA synthesis rates in response to DNA DSBs, named radioresistant DNA synthesis. This phenotype corresponds to the absence of ATM-dependent activation of p53

to induce checkpoint signalling[146–148]. However, despite the profound radiosensitivity of A-T cells, the repair of DNA DSBs is considered mostly proficient[149]. Radiosensitivity of A-T cells has been attributed to the combination of defective checkpoint activation, persistent heterochromatin-located DNA DSBs, and failed capacity to repair DNA DSBs with damaged or blocked DNA ends. Whilst the majority of IR-induced DNA DSBs are repaired in a primarily ATM-independent manner with fast kinetics, ATM has been proposed to have a key role in facilitating the repair of heterochromatic DNA DSBs which occur via slow kinetics[150–154]. Post-mitotic neuronal death has been attributed to the consequences of high rates of metabolism and transcription inherent to these cells which overwhelms ATM-deficient cells. In addition, ATM deficiency is also associated with defective mitochondrial function and impaired mtDNA integrity[5,155].

1.10 Targeting the ATM signalling pathway

Several ATM kinase inhibitors have been developed which demonstrate the potential for clinical utility. Administration of ATM inhibitors in combination with genotoxic modalities increased anti-tumour activity compared with genotoxic agents alone. Promising pre-clinical evaluation of ATM inhibitors have supported further compound development and inclusion in clinical trials[156,157]. Table 1.1 summarises the ATM selective inhibitors developed.

Table 1.1 | Overview of ATM inhibitors

Compound	IC_{50}	Observations	References
CP466722	0.41 μM	Reversible and non-toxic Sensitises cells to IR *in vitro* with transient inhibition	94,158,159
KU-55933	13 nM	First potent and selective ATM inhibitor ATP-competitive Confers radiosensitivity *in vitro* Unsuitable for *in vivo* studies	94,160,161
KU-60019	6.3 nM	Modified from KU-55933 with improved potency and solubility Confers radiosensitivity *in vitro* but poor availability *in vivo*	94,161–163
KU-59403	3 nM	Modified from KU-55933 Confers radiosensitivity *in vitro* Suitable for *in vivo* studies Demonstrated sensitivity to etoposide and irinotecan *in vivo*	94,164
AZ31	1.2 nM	Developed from 3-quinoline carboxamide core structure Suitable for *in vivo* studies Enhances irinotecan anti-tumour activity	165,166
AZ32	0.31 μM	Blood-brain-barrier permeable Modified from AZ31 Radiosensitises intracranial gliomas *in vivo*	167

AZD0156	0.58 nM	Confers radiosensitivity *in vitro* Enhanced efficacy of olaparib *in vivo* Current phase I clinical trial (NCT02588105)	156
AZD1390	0.78 nM	Confers radiosensitivity *in vitro* and *in vivo* Blood-brain-barrier permeable Current phase I clinical trials (NCT03423628; NCT03215381)	157

1.11 Genomic instability syndromes

Aside from ATM, deficiencies in other DNA damage response proteins can give rise to genomic instability syndromes. Mutations in the MRE11 gene confer A-T-like disorder (ATLD), which, as the name suggests parallels the A-T phenotype. However, the clinical presentation of ATLD is milder and disease progression is slower compared to A-T. In addition, the appearance of telangiectasia is not characteristic of ATLD[5,168]. Nijmegen breakage syndrome (NBS) arises due to mutations in the NBS1 gene. Consistent with A-T, individuals with NBS exhibit neurological defects, immunodeficiency and IR hypersensitivity[168]. ATLD and NBS are caused by hypomorphic mutations and attempts to generate murine knockout models of either MRE11 or NBS1 failed due to embryonic lethality[168]. Seckel syndrome arises due to hypomorphic defects in ATR and is characterised as a developmental disorder. ATR is considered an essential gene as inactivation is not viable and causes embryonically lethality[169,170]. DNA-PKcs deficiency confers severe combined immunodeficiency (SCID) which impairs the generation of B and T cells and individuals are exceptionally vulnerable to infection[171]. Germline mutations in p53 is autosomal dominant and gives rise to Li-Fraumeni syndrome, characterised by

increased risk of multiple malignancies[172,173]. These additional genome instability syndromes highlight the importance of the DDR in humans to maintain genome integrity, but the focus of this report is on ATM.

1.12 Aims of this study

1. Evaluate the expression of ATM protein across normal human tissues and assess the extent of ATM protein loss in human tumours

2. Elucidate the impact of ATM expression and activation in normal tissues in the context of ATM deficiency and identify tissue-dependent responses to DNA damage

3. Investigate the effect and consequences of ATM inhibition versus ATM loss in non-tumour and tumour cells

4. Identify pharmacological compounds that confer synthetic lethality with ATM loss

2 Materials and Methods

2.1 Buffers and solutions

Table 2.1 | Composition of buffers

Buffer	Composition
0.5% TBE	45 mM Tris-borate and 1 mM EDTA (*Sigma-Aldrich*) in dH_2O, pH 8.3
10X PBS	50 PBS tablets (*Sigma-Aldrich*) in 1 litre dH_2O, pH ~7.4
10X TBS	1 pack OmniPur® TBS 20X Ready Pack Powder (*Calbiochem®, Millipore*) in 2 litres dH_2O [1X = NaCl (137 mM), KCl (2.7 mM), Tris/Tris-HCl (2.5 mM), pH ~7.2-7.4]
1X Citrate buffer	10X Citrate buffer (*Sigma-Aldrich*) in dH_2O [10X = sodium citrate dihydrate (0.825 M), citric acid (0.175 M) to pH 6 with HCl]

1X PBS [*Tissue culture*]	10X PBS (*Lonza*) in dH_2O [10X = KH_2PO_4 (0.017 M), Na_2HPO_4 (0.05 M), NaCl (1.5 M), pH 7.4]
1X PBS	10X PBS (as prepared above) in dH_2O [1X = NaH_2PO_4/Na_2HPO_4 (0.01 M), KCl (2.7 mM), NaCl (137 mM), pH 7.4]
1X running buffer [*Western blotting*]	10X Tris/Glycine/SDS running buffer (*Bio-Rad*) in dH_2O [1X = Tris (25 mM), glycine (192 mM), SDS (0.1%), pH 8.3]
1X TBS	10X TBS in dH_2O
1X TBS-T	1X TBS and 0.1% (v/v) Tween-20 (*Sigma-Aldrich*)
1X transfer buffer [*Western blotting*]	10X Tris/Glycine buffer (*Bio-Rad*) in dH_2O with 20% (v/v) methanol (*Sigma-Aldrich*) [10X = Tris (250 mM), glycine (1.92 M), pH 8.3]
Agarose gel	2% (w/v) agarose (*Sigma-Aldrich*) in 0.5X TBE buffer

Antibody incubation buffer [*Immunofluorescence*]	1% (w/v) BSA (*Sigma-Aldrich*) and 1% (v/v) Goat serum (*Sigma-Aldrich*) in 1X PBS
Antibody incubation buffer [*Western blotting]*	1:1 mixture of Odyssey® TBS Blocking Buffer (*LI-COR*) and 1X TBS-T
Blocking buffer [*Immunofluorescence*]	1% (w/v) BSA (*Sigma-Aldrich*), 1% (v/v) goat serum (*Sigma-Aldrich*), 0.1% Triton X-100 (*VWR*) in 1X PBS
Blocking buffer [*Western blotting*]	1:1 mixture of Odyssey® TBS Blocking Buffer (*LI-COR*) and 1X TBS
Crystal violet solution	0.5% (w/v) crystal violet (*Merck*) and 75% (v/v) methanol in dH_2O (*Sigma-Aldrich*)

Lysis buffer	50 mM Tris-HCl (*Promega*) pH 7.6, 137 mM NaCl (*VWR*), 10% (v/v) glycerol (*VWR*), 0.1% (v/v) IGEPAL® (*Sigma-Aldrich*), 0.1% (v/v) SDS (*AppliChem GmbH*), 50 mM sodium fluoride (*Sigma-Aldrich*), 1 mM sodium orthovanadate (*Sigma-Aldrich*), cOmplete™ protease inhibitor (*Roche*) and 2 mM sodium pyrophosphate (*Sigma-Aldrich*) in dH_2O [1]
Resazurin stock solution	12.5 mg/mL resazurin (*Sigma-Aldrich*) in dH_2O
Tris-EDTA buffer	10 mM Tris base (*Sigma-Aldrich*), 1 mM EDTA (*Sigma-Aldrich*), 0.05% (v/v) Tween-20 (*Sigma-Aldrich*) in dH_2O; pH 9

2.2 Cell culture

The human cell lines used in this study are listed in Table 2.2. All cell lines were cultured in Advanced Dulbecco's Modified Eagle Medium/Ham's F12 (DMEM/F12; *Gibco® Thermo Fisher Scientific*) supplemented with 5% (v/v) foetal bovine serum (FBS; *Sigma-Aldrich*), 2 mM GlutaMAX™ (*Gibco® Thermo Fisher Scientific*) and 50 U penicillin / 50 µg/mL streptomycin (*Gibco® Thermo Fisher Scientific*). Cells were incubated at 37°C at 7.5% CO_2 and culture medium was replaced every 48 – 72 hours.

[1] Sodium orthovanadate, protease inhibitors and sodium pyrophosphate were added on the day of use

Sub-confluent cultures were washed with 1X PBS (prepared from 10X stock; *Lonza*) and incubated with 0.25% or 0.025% trypsin (*Gibco® Thermo Fisher Scientific*) to prepare cell suspensions and split cells accordingly for routine passaging. For experimental procedures, 0.4% trypan blue solution (*Invitrogen™ Thermo Fisher Scientific*) was mixed with cell suspension at a 1:1 ratio before transferring to a Countess® Cell Counting Chamber Slide (*Invitrogen™ Thermo Fisher Scientific*). Cells were counted using a Countess® Automated Cell Counter (*Invitrogen™ Thermo Fisher Scientific*) and seeded at the appropriate cell density. All cell culture procedures were conducted under sterile conditions in a Class II Biological Safety Cabinet.

Table 2.2 | Overview of cell lines

Cell line	Origin	Obtained from	Mutation status	
			ATM	p53
A549	Lung carcinoma [not specified]	ATCC® [2] CRL-185	wt	wt
AT5-BIVA (GM05849)	Fibroblast derived from A-T patient	Coriell Institute for Medical Research	c.2284_2285delCT (p.L762VfsTer2) c.7278_7283delCCTTAG (p.L2427_R2428del)	SV-40 transformed

[2] American Type Culture Collection

Calu-6	Lung anaplastic carcinoma	ATCC® HTB-56™	wt	c.586C>T (p.R196*)
NCI-H1395	Lung adenocarcinoma	ATCC® CRL-5868™	c.7996A>G (p.T2666A)	wt
NCI-H23	Lung adenocarcinoma	ATCC® CRL-5800™	c.5756A>C (p.Q1919P)	c.738G>C (p.M246I)
NCI-H322	Lung adenocarcinoma	Dr Sebastian Nijman	wt	c.743G>T (p.R248L)
H322 exon 6 $ATM^{-/-}$	Lung adenocarcinoma	Dr Sebastian Nijman [3]	c.757fs[4]	c.743G>T (p.R248L)
HCC827	Lung adenocarcinoma	ATCC® CRL-2868™	wt	c.646_648GTG[2] c.652_654delGTG (p.V218del)

[3] University of Oxford
[4] Additional information on H322 $ATM^{-/-}$ generation in 2.3

HT-29	Colon adenocarcinoma	ECACC [5] #91072201	wt	c.818G>A (p.R273H)
MRC5-SV2	Lung fibroblast	ECACC #84100401	wt	SV-40 transformed

2.2.1 Cryopreservation and thawing of cell lines

Cell stocks were generated and stored in the vapour phase of a liquid nitrogen tank. In preparation, cells were cultured to approximately 80-90% confluency and harvested using trypsin, as described in 2.2. Cell suspensions were centrifuged for 5 min at 225 x g and the cell pellet was resuspended in complete culture medium containing 10% (v/v) dimethyl sulfoxide (DMSO; *VWR*). Cryogenic tubes (*Corning*®) of 1 mL aliquots were stored overnight at -80°C and transferred to liquid nitrogen.

Recovery of cryopreserved cells involved rapidly thawing cells and diluting in 10 mL of complete media. Following a centrifugation at 225 x g for 5 min, cells were resuspended in complete media and cultured as described in 2.2.

2.2.2 Mycoplasma testing of cell lines

Cells were tested for mycoplasma infection using the MycoStrip™ mycoplasma detection kit (*InvivoGen*) according to manufacturer's instructions. In brief, cell culture supernatant was collected, centrifuged at 16,000 x g before adding sterile 1X PBS. The sample was

[5] European Collection of Authenticated Cell Cultures

incubated at 65°C for 40 minutes with a reaction mix to amplify the 16S rRNA gene for mycoplasma species. Following incubation, a migration buffer was added to the sample and results visualised using an immunochromatographic detection strip. The reagents required for mycoplasma testing were provided as part of the kit.

2.3 Sequencing ATM isogenic cell pair

H322 and H322$^{ATM-/-}$ cell pellets were collected, as described in 2.2. DNA was isolated and purified using the MasterPure™ Complete DNA and RNA purification Kit (*Epicentre, Lucigen*) according to manufacturer's instructions. In brief, cells were lysed using a Proteinase K-containing buffer followed by incubation with RNase A. Using the recovered supernatant, DNA was precipitated using isopropanol followed by ethanol rinsing. DNA was resuspended in Tris-ethylenediaminetetraacetic (EDTA; TE) buffer and stored at -20°C. Quantification of DNA was performed using a NanoDrop™ One/One^{C} Microvolume UV-Vis spectrophotometer (*Thermo Fisher Scientific*).

The region of interest in exon 6 was amplified from H322 and H322$^{ATM-/-}$ DNA samples. The primer (*Sigma*-Aldrich) sequences used were as follows:

ATM exon 6 Forward	CAGCAGTTTATAGTTATTCCTGTC
ATM exon 6 Reverse	TAGTTCTGTTATGATGGATCAATG

The polymerase chain reaction (PCR) amplification was performed in 25 µL reactions of 100 ng genomic DNA, 0.5 µM of forward and reverse primers and Phusion® High-Fidelity PCR Master Mix with HF Buffer (*Promega*) using a thermal cycler (*Applied Biosystems*®). PCR was performed under the following conditions:

Hot start	98°C	30 sec	
Denaturation	98°C	10 sec	30 cycles
Annealing	59.6°C	30 sec	
Extension	72°C	30 sec	
	72°C	10 min	
Final extension	4°C	hold	

PCR product purification was performed using QIAquick® PCR purification kit (*Qiagen*) according to manufacturer's instructions. In short, the PCR product purification includes binding, washing, and eluting of DNA sample to remove impurities. Purified PCR products were sequenced by Source BioScience.

H322 $ATM^{-/-}$ cells were generated by the Nijman group using CRISPR-Cas9 technology with a single guide RNA (sgRNA) directed towards the following sequence[174]:

sgRNA	GGATGCTGTTCTCAGACTGACGG

Successful editing of H322 was confirmed by sequencing showing disruption at exon 6. Loss of WT ATM sequence following CRISPR inactivation around the sgRNA target site corresponds to a complex set of changes within the DNA sequence with evidence of a frameshift mutation due to short and long insertions.

2.4 Mice

Female C57BL/6 (*nomenclature:* C57BL/6JOlaHsd) were purchased from Envigo. A breeding trio of B6.129S6-*Atm*^{tm1Awb}/J (1 male, 2 females) were purchased from The

Jackson Laboratory (JAX; JAX stock #008536). Experiments were performed on 7-8-week-old mice and were euthanised by cervical dislocation. All procedures were approved by an Ethical Review Committee and conducted under a project license (PPL 30/3395) in accordance with the Home Office Animals (Scientific Procedures) Act of 1986. Animal experiments were performed by Dr Stephen Stribbling.

2.4.1 Generation of ATM$^{-/-}$ mice

Breeding of B6.129S6-*Atm*^{tm1Awb}/J mice was conducted in house and pups were ear clipped at 3-weeks old and genotyped for selection to a breeding or experimental protocol. For in house genotyping, amplification of DNA was performed using the Phire Tissue Direct PCR Master Mix (*Thermo Fisher Scientific*) according to manufacturer's instructions. Following the JAX protocol, primer (*Sigma-Aldrich*) sequences were as follows:

Wild type Forward	TGATCTGTCAGGGGAATGAAC
Common	GCTGAGATGCTAACGGTATAAACA
Mutant Forward	AGACTGCCTTGGGAAAAGCG

The PCR reactions were performed using a thermal cycler (*Applied Biosystems*®) under the following conditions:

Hot start	98°C	5 min	
Denaturation	98°C	5 sec	40 cycles
Annealing	62°C	5 sec	
Extension	72°C	20 sec	

	72°C	1 min
Final extension	4°C	hold

Genotyping of the mice was confirmed by gel electrophoresis. Samples, alongside the O'GeneRuler Express DNA ladder (*Thermo Fisher Scientific*) were run at 100 V on a 2% agarose (*Sigma-Aldrich*) gel with peqGreen dye (*VWR*) in 0.5X TBE. The gel was imaged using a Gel Documentation System (*Bio-Rad*) in which mice could be genotyped for ATM according to band size, as listed below:

Wild type	300 bp
Heterozygote	~ 200 bp and 300 bp
Mutant	~ 200 bp

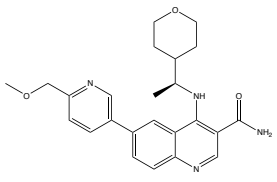
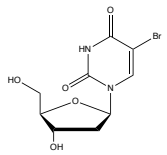
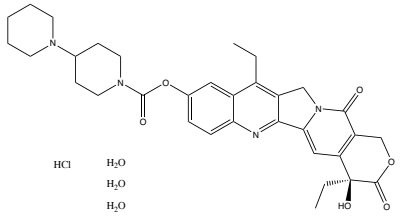
Alternatively, automated genotyping was outsourced and performed by Transnetyx®.

Heterozygous mice ($ATM^{+/-}$) were used to maintain breeding colonies whilst male and/or female mice harbouring a homozygous mutation for ATM, referred to as $ATM^{-/-}$ for the purpose of this study, were selected for experimental purposes. For controls, we also included mice genotyped as homozygous wildtype for ATM ($ATM^{+/+}$) and where appropriate, $ATM^{+/-}$ mice were also included.

2.5 Administration of drug and irradiation *in vivo*

2.5.1 Formulation of compounds

Table 2.3 | Overview of compounds used for in vivo studies

Compound	Dose	Vehicle
AZ31 	50 mg/kg	10% (v/v) DMSO and 90% (v/v) Captisol® solution (Captisol® solution: 30% Captisol® (*Sigma-Aldrich;* (w/v) in dH_2O)
Bromodeoxyuridine (BrdU) 	2 mg (10 mg/mL; 200 µL/mouse)	Saline (*B. Braun*)
Irinotecan hydrochloride trihydrate 	100 mg/kg	Saline (*B. Braun*)

The ATM inhibitor, AZ31 (*Selleck Chemicals*), was prepared in a dosing solution of 10% (v/v) DMSO and 90% (v/v) Captisol® solution. Captisol® solution (30% (w/v)) was prepared by dissolving Captisol® (*Sigma*-Aldrich) in filter-sterilised dH_2O. AZ31 was reconstituted in DMSO followed by dropwise addition of Captisol® solution and diluted to a concentration of 5 mg/mL. AZ31 was administered by oral gavage (per os; p.o.) at a dose of 50 mg/kg.

The thymidine analogue, bromodeoxyuridine (BrdU; *Sigma-Aldrich*), was reconstituted to 10 mg/mL in saline (*B. Braun*) and vortexed and stored at 4°C overnight before use. With regard to dosage, 200 µL of BrdU solution was administered by intraperitoneal (i.p.) injection per mouse.

Irinotecan hydrochloride trihydrate (*Churchill Hospital Pharmacy, Oxford*) was supplied at a stock concentration of 20 mg/mL in saline. A dosing solution of 10 mg/mL was prepared on the day of treatment and mice were dosed at 10 µL/g by i.p. injection. For the remainder of the study, irinotecan hydrochloride trihydrate will be abbreviated to irinotecan.

2.5.2 Irradiation

The inhalational agent, isoflurane (*Teva*), was administered at 2.5-3% to anaesthetise mice prior to whole-body irradiation. Mice were placed inside the Gulmay Medical RS320 X-ray generator (*Gulmay Medical Limited*) and exposed to 3.3 Gy whole-body irradiation (excluding head). Radiation was delivered at a dose rate of 2.02 Gy/min (300 kV and 10 mA; 1 min 39 secs).

2.5.3 Experimental design for *in vivo* study

C57BL/6, $ATM^{+/+}$, $ATM^{+/-}$ and $ATM^{-/-}$ were randomised into groups to receive whole body irradiation (3.3 Gy), irinotecan (100 mg/kg) or vehicle treatment. Where applicable, mice were pre-treated with AZ31 (50 mg/kg) for 1 hour prior to allocated treatment schedule. Mice were sacrificed for tissue collection 2 hours post-treatment with administration of BrdU at 30 minutes prior to sacrifice.

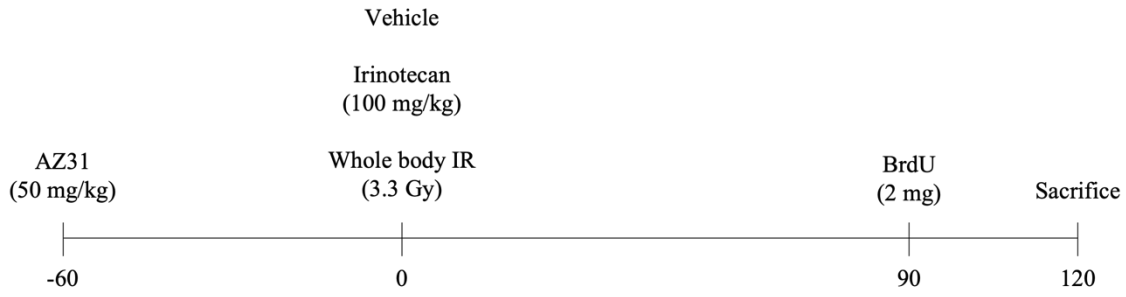


Figure 2.1 | Schedule for administration of radiation and drug compounds in vivo

Mice were treated with irinotecan (100 mg/kg), whole body irradiation (3.3 Gy) or vehicle control, a BrdU injection 90 minutes post-treatment and sacrificed by cervical dislocation at an endpoint of 120 minutes. Where applicable, a pre-treatment of AZ31 (50 mg/kg) was given 60 minutes prior to treatment.

2.6 Formalin fixation and paraffin embedding (FFPE)

Following sacrifice, tissues were collected and fixed in 10% neutral buffered formalin (NBF; *Sigma-Aldrich*) for 24 hours at 4°C and transferred to 70% ethanol (*Sigma-Aldrich*) overnight at 4°C. Tissues collected consisted of the heart, left and right lungs, spleen, gastrointestinal (GI) tract, liver, pancreas, and kidneys. The GI tract was divided into three sections for the duodenum, jejunum and the ileum and colon. The GI tract was opened along its longitudinal axis and rolled upwards according to the 'Swiss roll' technique[175]. Tissue collection from the $ATM^{+/-}$ mice consisted of the left and right lungs, spleen, and

the GI tract. Fixed tissues were transferred to processing/embedding cassettes (*Simport*) in 70% ethanol and stored at 4°C for up to 7 days before processing.

Overnight processing was performed using the STP 120 Spin Tissue Processor (*Thermo Fisher Scientific*). This involved tissue dehydration using a series of increasing concentrations of ethanol followed by tissue clearing in Citroclear (*TCS Biosciences*) and Histoplast PE paraffin wax (*Thermo Fisher Scientific/Epredia*) infiltration. Using the HistoStar™ Embedding Workstation, tissues were removed from cassettes and transferred to metal moulding plates. Paraffin wax was added to the moulds which were then topped with the corresponding cassette lid before setting on the cold plate. Tissue blocks were cut into sections (4 μm thickness) using a Leica RM2125 microtome and mounted onto SuperFrost Ultra Plus™ Adhesion Slides (*Thermo Fisher Scientific*).

2.7 Immunohistochemistry (IHC)

Tissue sections were deparaffinised using Citroclear (*TCS Biosciences*) prior to rehydration with a descending series of ethanol concentrations. Antigen retrieval was performed in either Tris-EDTA buffer (γH2AX Ser139, ATM, BrdU, CD3, p-KAP1 Ser824) or 1X Citrate buffer (p-p53 Ser15) using a pressure cooker to 125°C for 2 minutes (see Table 2.1 for buffer preparation). Samples were cooled on ice prior to washing in dH_2O. Sections were blocked for 1 hour using the Dual Enzyme Block as part of the Dako EnVision®+ Dual Link System-HRP (DAB+) Kit (*Agilent*). Tissues were incubated for 4 hours at room temperature with the target antibody at an appropriate dilution, as specified in Table 2.4. Primary antibodies were diluted in antibody diluent (*Abcam*). Sections were incubated with the Envision+ System-HRP Labelled Polymer anti-rabbit solution (*Dako,*

Agilent) for 45 minutes at room temperature. Following antibody incubation steps, sections were washed in 1X PBS.

For visualisation, sections were incubated for 2 minutes with diaminobenzidine (DAB; *Dako, Agilent*) diluted 50-fold in DAB+ substrate buffer (*Dako, Agilent*) and counterstained with Gill's haematoxylin (*Sigma-Aldrich*). Following visualisation and counterstaining steps, sections were repeatedly washed in tap water. Tissue sections were dehydrated in ascending concentrations of ethanol followed by tissue clearing in xylene (*Thermo Fisher Scientific*) before mounting with dibutylphthalate polystyrene xylene (DPX; *Sigma-Aldrich*). Slides were scanned by an Aperio ScanScope CS digital slide scanner (*Leica Biosystems*) at 20X magnification with a doubler inserted (40X). Digital images were analysed using the Aperio ImageScope or QuPath software platforms.

Table 2.4 | Antibodies used for IHC

Target	Clone	Species	Dilution	Supplier
γH2AX Ser139	20E3	Rabbit	1:500	Cell Signalling Technology #9718
ATM [human tissues]	Y170	Rabbit	1:200	Abcam #ab32420

ATM [murine tissues]	D2E2	Rabbit	1:200	Cell Signalling Technology #2873
BrdU	Polyclonal	Rabbit	1:2000	Abcam #ab152095
CD3	SP7	Rabbit	1:150	Abcam #ab16669
CD8	C8/144B	Mouse	1:100	DAKO, Agilent #M7103
PD-L1	E1L3N®	Rabbit	1:200	Cell Signalling Technology #13684
p-KAP1 Ser824	Polyclonal	Rabbit	1:2000	#A300-767A

p-p53 Ser15	Polyclonal	Rabbit	1:800	Cell Signalling Technology #9284

Colorectal cancer tissue microarrays (TMA) (TMA1 RW, TMA2 DW and TMA3 DW) from the COIN clinical trial were provided by Professor Tim Maughan (University of Oxford) and Professor Richard Adams (Cardiff University)[176]. The melanoma TMA (AVAST-M TA188) from the AVAST-M trial was supplied by Dr Kevin Myers (University of Oxford)[177]. TMAs for bladder (BL1921), breast (BR1141), brain (GL803b), kidney (KD2085), lung (BC041115a and LC2087), oesophageal (ES1921), pancreatic (PA1921) and prostate (PR1921a) tumours and multi-normal TMAs for human tissue (MNO1021) (*Insight Biotechnology/US BioMax Inc.*) were tested for antibodies of interest.

IHC staining of human tissues was carried out as part of a larger project (REC no. 07/H0606/120; P.I. Dr Valentine Macaulay) after ethical review and approval by Oxfordshire REC-C.

ATM expression using the colorectal and lung TMAs and the breast and melanoma TMAs were performed by Dr Anika Weber and Dr John Moore respectively. CD8 and PD-L1 expression of lung tumour tissue was evaluated by M. Mohideen Quwailid and Leticia Campo using a Leica-Bond automated IHC staining system.

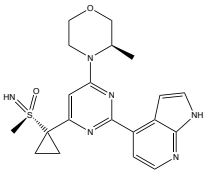
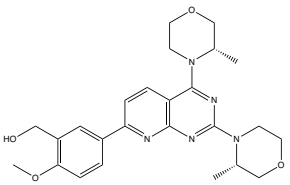
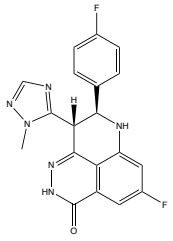
2.8 Compound treatments and irradiation *in vitro*

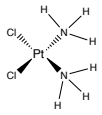
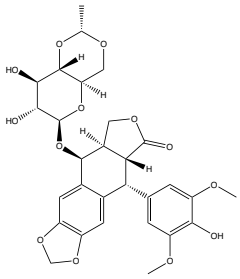
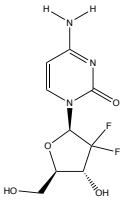
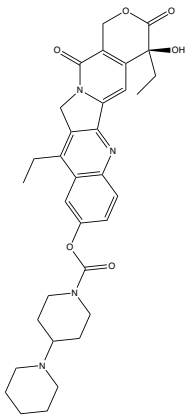
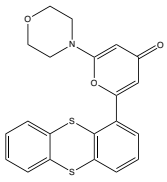
Stock solutions of paclitaxel, etoposide, gemcitabine, irinotecan, SN-38, KU-55933, AZD6738, AZD8055 and BMN673 (*Selleck Chemicals*) were prepared at 10 mM in

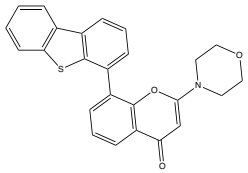
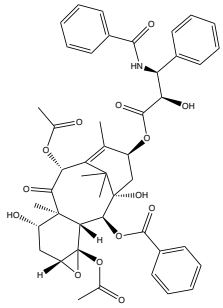
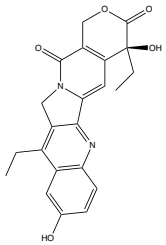
DMSO. NU-7441 (*Selleck Chemicals*) was also prepared in DMSO but to a concentration of 5 mM. Cisplatin (*Sigma-Aldrich*) was prepared in 0.9% sterile saline solution at a concentration of 3.3 mM. Stock solutions were stored as aliquots in -20ºC and were diluted in culture medium for experimental use. Further information on the compounds used in this study can be found in Table 2.5.

Irradiations were performed using a Gamma Service® GSR D1 irradiator (*GammaService Medical GmbH*) containing a caesium-137 (^{137}Cs) source. Radiation was delivered at a dose rate of 1.3 Gy/min.

Table 2.5 | Overview of compounds used for in vitro studies

Drug	Structure	Target
AZD6738		ATR
AZD8055		mTOR
BMN673		PARP1/2

Cisplatin		DNA
Etoposide		Topoisomerase II
Gemcitabine		DNA polymerase
Irinotecan		Topoisomerase I
KU-55933		ATM

NU-7441		DNA-PK
Paclitaxel		Tubulin
SN-38		Topoisomerase I

2.9 Cell viability assay

Cells were plated at a seeding density of 1-1.5x10^3 cells/well in a 96-well plate in triplicate as a minimum. Following overnight incubation, cells were treated with a dilution series of the respective compound or compound combination. Cells were incubated at 37ºC for a further three days. Cell viability was assessed through a resazurin-based assay. The reduction of resazurin to the red-fluorescent product, resorufin, enables quantification of metabolically active, viable cells. Fluorescence intensity was measured following 2-hour incubation with resazurin using a POLARstar Omega plate reader (excitation: 544 nm, emission: 585-595 nm).

Data was blank corrected and normalised as a percentage of vehicle control. For drug combination treatments, data was normalised to the agent added at a fixed concentration. The half-maximal inhibitory concentration (IC_{50}) was calculated from at least three independent experiments using GraphPad Prism. Analysis consisted of log transformation (log10) of the concentration values and normalisation of response to run between 0-100% before fitting a non-linear regression curve fit (Dose response – Inhibition; log[inhibitor] vs. normalised response – Variable slope).

2.10 Clonogenic survival assay

2.10.1 Irradiation

Cells were seeded in duplicate in 6-well plates or 10 cm culture dishes in the presence or absence of 10 μM KU-55933 or vehicle control (DMSO) for one hour. Cells were irradiated with 0, 2, 4, 8 or 10 Gy using a Gamma Service® GSR D1 irradiator containing a caesium-137 (^{137}Cs) source and incubated at 37°C. Once colonies consisted of at least 50 cells, crystal violet was added for fixation and visualisation of colonies.

The number of colonies counted was divided by the number of cells seeded to calculate the plating efficiency for each cell line. The surviving fraction was determined by dividing the number of colonies counted by the number of cells seeded and multiplying by the plating efficiency previously calculated. Data was normalised to either mock-irradiated vehicle control or mock-irradiated inhibitor treated control.

2.10.2 Drug treatment

Cells were seeded in triplicate in 6-well plates and pre-treated with 10 μM KU-55933 for one hour where appropriate. Cells were treated with a dose range of 0-1 μM or 0-0.1 μM

SN-38 for 1 hour or 24 hours respectively. DMSO controls were included for single drug and combination treatments. Following SN-38 incubation, cells were washed with 1X PBS and placed into fresh cell culture medium. Crystal violet was used for fixation and visualisation steps, as described in 2.10.1.

Analysis was performed as described in 2.10.1 where data was normalised to vehicle control for single drug or combination treatment.

2.11 Western blotting

2.11.1 Protein extraction and quantification

Cells were plated in 10 cm cell culture dishes and treated with either vehicle or drug for the indicated time when plates reached 70% confluency. Cells were washed twice with ice cold 1X PBS prior to whole cell protein extraction in lysis buffer which was prepared as described in Table 2.1. Cells were scraped using a sterile, disposable rubber scraper (*Sarstedt*) and transferred to a labelled tube on ice. Lysates were treated with Benzonase® Nuclease (1 µL per 100 µL lysate; *Merck Millipore*), vortexed and incubated at room temperature for 5 minutes. Cell debris was removed by centrifugation at 15,700 x g for 15 minutes at 4°C.

Total protein concentration was determined using the DC™ Protein Assay kit (*Bio-Rad*). Following a 15-minute incubation at room temperature in the dark, absorbance was measured using a POLARstar Omega plate reader at 750 nm.

2.11.2 SDS-polyacrylamide gel electrophoresis (PAGE)

Protein lysates (15-25 μg) were diluted in 4X NuPAGE™ LDS sample buffer (*Invitrogen™, Thermo Fisher Scientific*) and 10X NuPAGE™ sample reducing agent (*Invitrogen™, Thermo Fisher Scientific*). Samples were heated to 95°C for 10 minutes before loading equal protein concentrations onto a 4-20% Mini-PROTEAN® TGX™ or 4-20% Criterion™ TGX™ precast protein gel (*Bio-Rad*) alongside the Precision Plus Protein™ Kaleidoscope™ molecular weight ladder (*Bio-Rad*). Gels were run at 70V in 1X running buffer, as described in Table 2.1.

2.11.3 Immunoblotting

Following SDS-PAGE, proteins were transferred to a nitrocellulose membrane (0.45 μm pore size; *Bio-Rad*) at 150 V for 1 hour in 1X transfer buffer, as described in Table 2.1. Membranes were incubated with blocking buffer (see Table 2.1) for 1 hour at room temperature to prevent non-specific binding before incubation with primary antibodies in antibody incubation buffer (see Table 2.1) overnight at 4°C. PPIB and/or β-actin were used as loading controls. Information on the primary antibodies used is listed in Table 2.6. Following overnight incubation, membranes were incubated with secondary antibodies (see Table 2.1) for 1 hour at room temperature. Between antibody applications, membranes were washed in TBS/TBS-T three times at 5-minute intervals. Protein detection was performed using an Odyssey® Infrared Imaging System (*LI-COR*). Western blots are representative of at least two independent experiments, unless otherwise stated.

Table 2.6 | Antibodies used for Western blotting

Target	Clone	Species	Dilution	Supplier
β-actin	AC-15	Mouse	1:10,000	Sigma-Aldrich #A1978
γH2AX Ser139	20E3	Rabbit	1:1000	Cell Signalling Technology #9718
ATM	Y170	Rabbit	1:500	Abcam #ab32420
CHK2	Polyclonal	Rabbit	1:500	Cell Signalling Technology #2662
KAP1	Polyclonal	Rabbit	1:5000	Bethyl Laboratories #A300-274A

p-AKT Ser473	Polyclonal	Rabbit	1:1000	Cell Signalling Technology #9271
p-ATM Ser1981	EP1890Y	Rabbit	1:10,000	Abcam #ab81292
p-CHK1 Ser345	Polyclonal	Rabbit	1:500	Cell Signalling Technology #2341
p-CHK2 Thr68	Polyclonal	Rabbit	1:1000	Cell Signalling Technology #2661
p-KAP1 Ser824	Polyclonal	Rabbit	1:2000	Bethyl Laboratories #A300-767A
p-NBS1 Ser343	Polyclonal	Rabbit	1:1000	Cell Signalling Technology #3001

p-p53 Ser15	Polyclonal	Rabbit	1:500	Cell Signalling Technology #9284
p-RAD50 Ser635	Polyclonal	Rabbit	1:1000	Cell Signalling Technology #14223
p53	DO-1	Mouse	1:1000	Santa Cruz Biotechnology #sc-126
PPIB	Polyclonal	Rabbit	1:2500	Abcam #ab16045
Mouse IgG (H+L) conjugated to IRDye® 680RD	-	Goat	1:5000	Odyssey® LI-COR Biosciences #926-68070

Rabbit IgG (H+L) conjugated to IRDye® 800CW	-	Goat	1:5000	Odyssey® LI-COR Biosciences #926-32211

2.12 Immunofluorescence

Cells were seeded in 96-well plates and incubated overnight prior to use of the Click-iT™ EdU Cell Proliferation Kit (*Invitrogen™, Thermo Fisher Scientific*) according to manufacturer's instructions. Cells were pre-treated with 10 μM KU-55933 and 10 μM 5-ethynyl-2'-deoxyuridine (EdU) followed by treatment with 1 μM SN-38. All treatments were for 1 hour at 37ºC. Cells were fixed in 10% formalin for 10 minutes and incubated in blocking buffer (Table 2.1) for 1 hour at room temperature. The Click-iT™ reaction cocktail was prepared to contain reaction buffer, copper sulphate ($CuSO_4$), Alexa Fluor® 555 azide and reaction buffer additive and incubated with cells for 30 minutes in the dark at room temperature. Cells were incubated with pKAP1 Ser824 (Table 2.6) at a dilution of 1:800 in antibody incubation buffer (Table 2.1). Following an overnight incubation, cells were incubated with goat anti-rabbit Alexa Fluor® 488 secondary antibody at a dilution of 1:400 and 1X Hoechst 33342 (5 μg/mL) in antibody incubation buffer (Table 2.1). Wash steps in 1X PBS were included between fixation, Click-iT reaction, and antibody incubation steps. Image acquisition was performed on an ImageXpress® Pico Automated Cell Imaging System (*Molecular Devices*) using CellReporterXpress (CRX) Image Acquisition and Analysis software (*Molecular Devices*).

2.13 Cell viability screen

Optimal seeding density for each cell line was determined using the IncuCyte® Live Cell Analysis Imaging System (*Sartorius*). Cells were seeded in 75 µL at a pre-determined density into 384-well plates using the FlexDrop™ Precision Reagent System and Workstation (*PerkinElmer*) and incubated overnight at 37°C. The kinase chemogenomic set (KCGS) small compound library (5 mM stock concentration) contained 187 kinase inhibitors that covered 215 targets[178,179]. Cells were treated with 0.1 µM, 1 µM or 10 µM of compound in addition to the inclusion of DMSO controls and SN-38 treatments (0.1 µM or 1 µM) across duplicate plates Following 72-hour incubation, cell viability was assessed using a resazurin-based proliferation assay, as described previously. Fluorescence intensity was measured using an EnVision® plate reader (*PerkinElmer*).

Collected data was blank adjusted and analysed using Microsoft Excel. Statistical measures of linear correlation (Pearson's correlation coefficient, r) and how close the data fitted the regression line (r^2) for each cell line and respective library concentration are listed in Table 2.7. Data was normalised to vehicle control and z-factors for each plate concentration were calculated as an indicator of quality of screening assay[180].

The z-factor was calculated by:

$$Z = \frac{S}{R}$$

Where:

$S = (\mu_n - 3(\sigma_n)) - (\mu_p + 3(\sigma_p)$ $R = (\mu_n - \mu_p)$

μ = mean of the sample n = negative control (DMSO)

σ = standard deviation of the sample p = positive control (SN-38)

Table 2.7 | Statistical measures from cell viability screen

Cell line	Concentration (μM)	Pearson's correlation coefficient	r^2	z-factor
MRC5-SV2	0.1	0.827	0.684	0.634
	1	0.875	0.765	0.831
	10	0.897	0.804	0.822
AT5 BIVA	0.1	0.853	0.728	0.815
	1	0.879	0.773	0.807
	10	0.724	0.524	0.834
H322	0.1	0.918	0.843	0.610
	1	0.930	0.864	0.701
	10	0.976	0.953	0.686
H322 $ATM^{-/-}$	0.1	0.923	0.852	0.214
	1	0.919	0.845	0.524
	10	0.968	0.937	0.607

To identify differences in effectiveness of the compounds against the paired ATM proficient or deficient lines, the following calculation was used:

$$log_{10}(\frac{relative\ viability\ ATM\ proficient\ cell\ line}{relative\ viability\ ATM\ deficient\ cell\ line})$$

The screen was performed in collaboration with Dr Stephanie Hatch and Dr Daniel Ebner (University of Oxford).

2.14 Data analysis

All data are presented as mean ± SEM and significance visualised as *($p<0.01$), **($p<0.001$) or ***($p<0.0001$). Testing for Gaussian distribution was performed using D'Agostino-Pearson omnibus normality test. If data fit a normal distribution, either ordinary univariate analysis of variance (ANOVA) or Brown-Forsythe and Welch ANOVA was performed depending on the assumption of equal standard deviations. Post-hoc analysis was performed using Dunnett's multiple comparisons test or Dunnett's T3 multiple comparisons test. If data did not fit a normal distribution, the non-parametric Kruskal-Wallis test was performed followed by Dunn's multiple comparisons test. Unpaired two-tailed Student's t-test (parametric) or Mann Whitney test (non-parametric) performed depending on data fit to Gaussian distribution. Graphs and statistical analysis were performed using GraphPad Prism.

3 ATM protein expression in human normal and tumour tissues

ATM has been well-documented to function in the response to DNA damage with a pivotal role in coordinating DNA DSB repair with temporary cell cycle arrest. The signal transduction pathways involved in the DDR utilise a variety of sensors, transducers, and effector molecules to orchestrate a timely repair in a DNA lesion dependent manner. There has been a predominant focus on the nuclear functions of ATM with constant protein level expression reported throughout the cell cycle[38,181]. However, the pathophysiology and clinical manifestation of A-T cannot be entirely attributed to the nuclear role of ATM. In addition to the recognised nuclear function in the response to DNA damage, accumulating evidence supports an important role of ATM in the cytoplasm. ATM has been implicated in mediating the cellular response to oxidative stress as well as regulating metabolism and autophagy processes. ATM protein expression has been reported in cytoplasmic organelles such as the mitochondria and peroxisomes[40,182].

ATM protein is ubiquitously expressed in most human tissue types with observations of noticeably high levels in proliferative tissues as well as across the nervous and reproductive systems. Constitutive expression of ATM is a reasonable notion considering A-T is described as a multi-system disorder whereby the loss of ATM function corresponds to widespread complications. Of note, in the context of both A-T patients and $ATM^{-/-}$ mice, the tissues most affected by the loss of ATM correspond to those reported with higher expression levels[183,184].

Germline mutations in ATM that give rise to A-T are associated with susceptibility to tumorigenesis, in particular tumours of lymphoid origin. A-T patients are reported to have

an increased risk of haematological malignancy that spans both T and B cell systems. In addition, $ATM^{-/-}$ mice display increased incidence of lymphoma[15,185]. The occurrence of solid tumours, such as melanoma, breast, gastric and pancreatic cancers increases in adulthood[1]. Evidence suggests that most A-T patients are compound heterozygotes (two different mutant ATM alleles) in which the majority of mutations (71-86%) confer premature truncation. Missense mutations, as well as short in-frame deletions and insertions have also been reported[14].

A proportion of tumours are ATM deficient due to somatic mutations that arise during tumour development, which identifies a potential molecular subgroup for targeted therapies. However, unlike germline mutations in ATM, sporadic mutation frequency is widely varied across cancer subtypes[186,187]. The occurrence of chromosome loss at 11q22-23, encompassing the ATM locus (11q22.3), has been reported across a range of sporadic neoplasms, with deletion of the long (q) arm of chromosome 11 as one of the most frequent chromosomal aberration events in lymphoid malignancies[185,188]. Pathogenic mutations have been identified spanning the ATM coding region with the consensus of no apparent hot spots recorded. A possible exception has been documented (R377C/H) that was reported to occur in approximately 3% of cancers studied[189]. Heterozygous alterations in ATM have been associated with a predisposition to the development of solid malignancies. For example, carriers for ATM mutations have been linked to increased risk of breast and gastrointestinal cancers[3,14,16].

The occurrence of mutations found in human cancers and the tumour burden associated with loss of ATM function in A-T implies that ATM acts as a tumour suppressor. In addition, the most commonly mutated gene, p53, labelled as the “guardian of the genome” is a tumour suppressor and also a downstream target of ATM[190]. Despite the high mutation

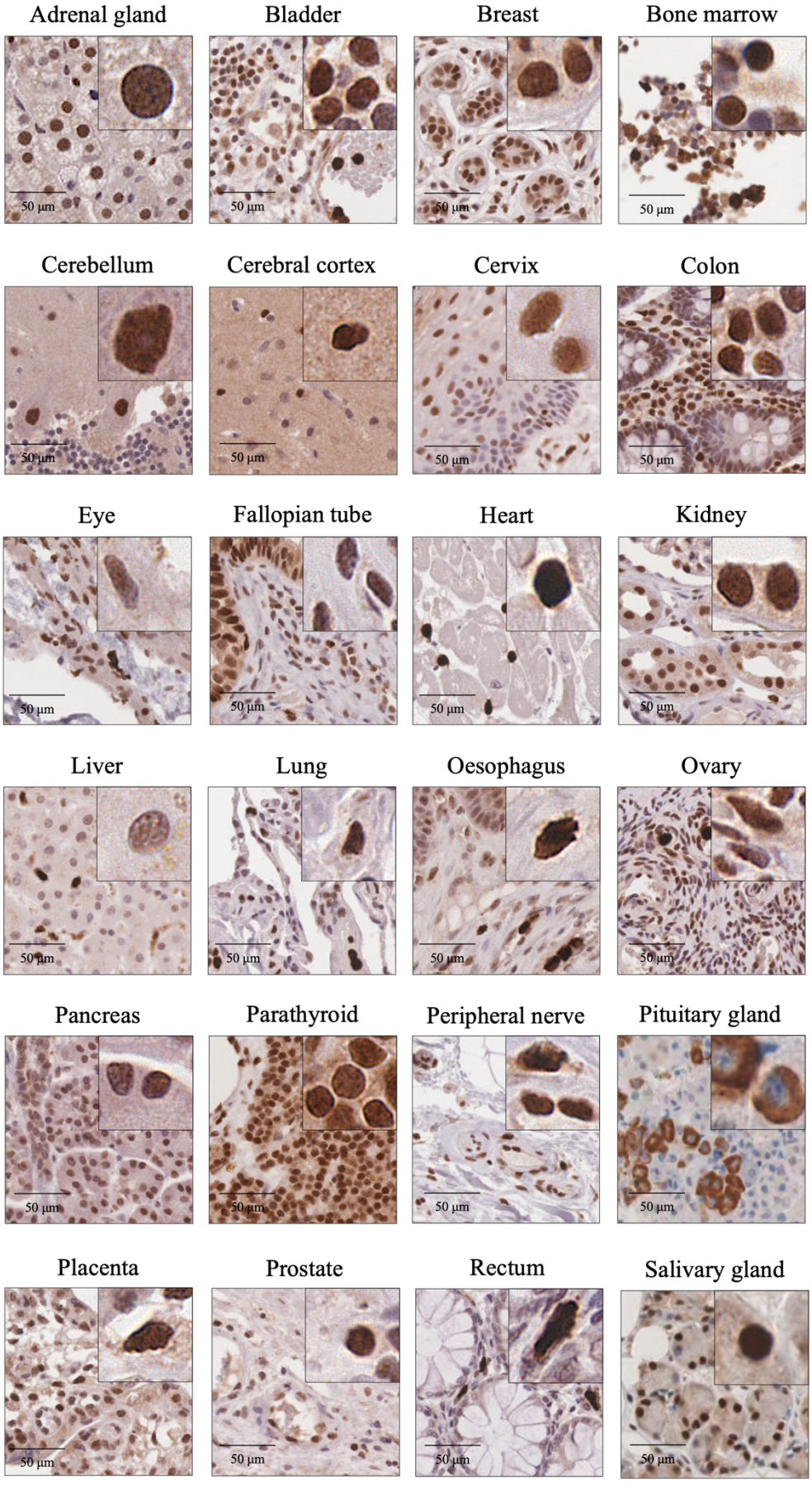
frequency in the TP53 gene, it is not the only cause of p53 dysfunction as demonstrated through the consequences of ATM mutations. Interestingly, ATM and p53 mutations have been reported to show mutual exclusivity suggesting that such alterations may be epistatic[191–193].

The studies described in this chapter aimed to evaluate the expression of ATM protein across normal human tissue types and assess the extent of ATM protein loss in human tumours.

3.1 ATM protein is highly expressed in normal human tissue

Medium-to-high expression of ATM protein has been reported in most normal human tissue types. Exceptions to this have been reported with low expression observed in the glial and neuronal cells of the caudate nuclei, ovarian stromal cells, and the peripheral nerve (The Human Protein Atlas; *proteinatlas.org*)[194–196]. However, this has not been well documented in the literature. To explore this further, a human normal tissue microarray (TMA) was probed for ATM protein expression. An established IHC protocol was conducted using a validated, commercially available antibody directed towards ATM[138]. The human normal TMA (MNO1021) containing 102 cores of 1.5 mm diameter and 4 μm thickness from 35 tissue types was examined with the anti-ATM monoclonal antibody (Clone Y170), with positive signal visualised by brown DAB stain. A nuclear counterstain (haematoxylin) was also included.

The assessment of ATM protein by IHC demonstrated expression across all normal tissues investigated (Figure 3.1). Positive DAB stain, corresponding to ATM protein expression, was predominantly nuclear but evidence of cytoplasmic staining was detected in some tissue sections, as seen in the representative image of a pituitary gland section.


Adrenal gland
Bladder
Breast
Bone marrow
Cerebellum
Cerebral cortex
Cervix
Colon
Eye
Fallopian tube
Heart
Kidney
Liver
Lung
Oesophagus
Ovary
Pancreas
Parathyroid
Peripheral nerve
Pituitary gland
Placenta
Prostate
Rectum
Salivary gland
50 µm

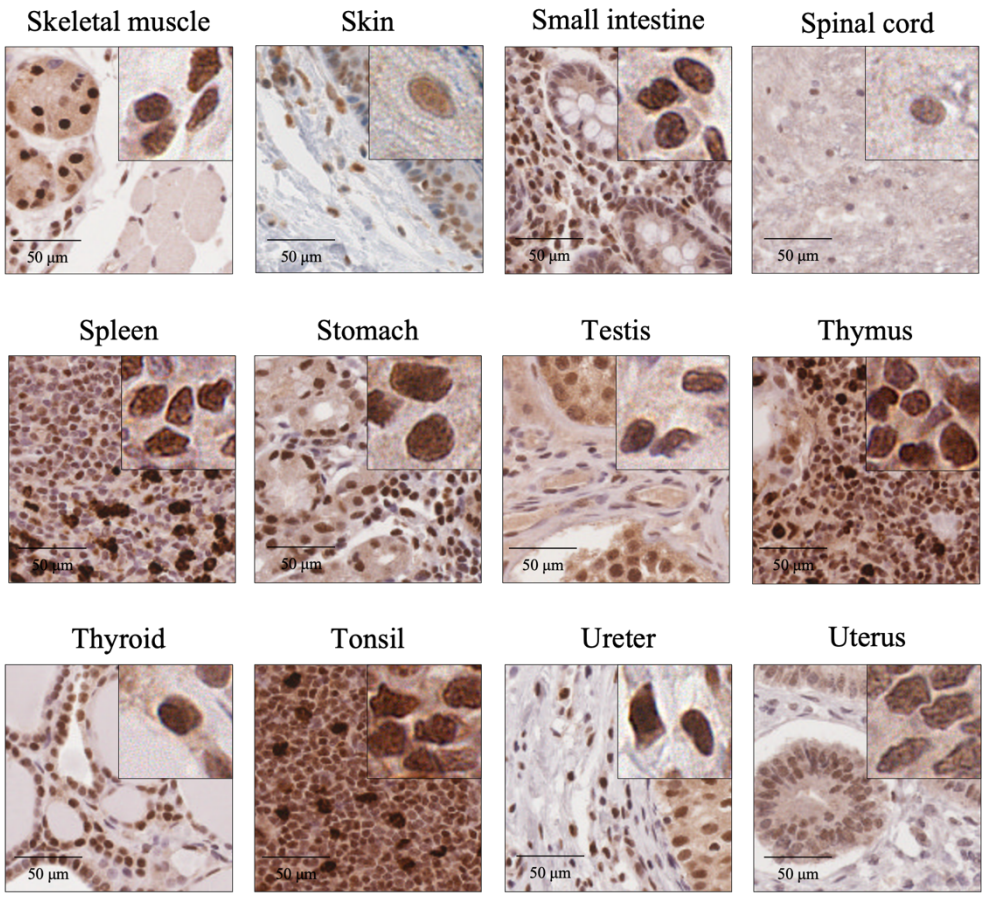


Figure 3.1 | Normal human tissues express high total levels of ATM protein

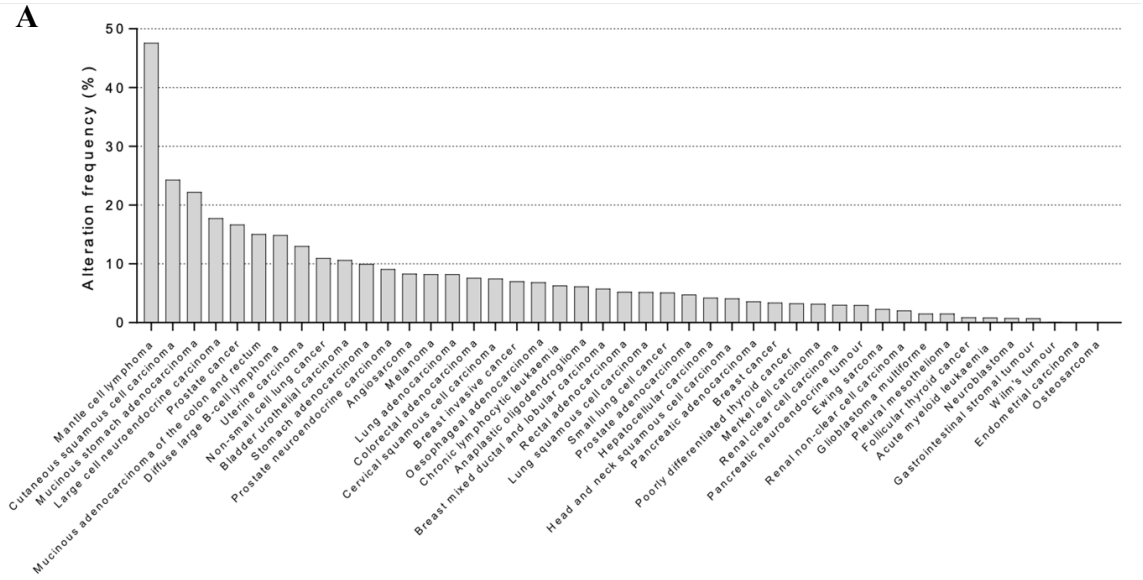
Representative images from multi-normal human TMA (MNO1021) containing 102 cores from 35 tissue types sectioned at a thickness of 4 µm. Each tissue type had 2-3 replicates from different individuals. Positive signal visualised by brown DAB staining that corresponds to ATM (Y170) incubated at 1:200-1:2500. Sections counterstained with haematoxylin. Images shown at 10X and 40X magnification using Aperio ImageScope software. Scale bar = 50 µm.

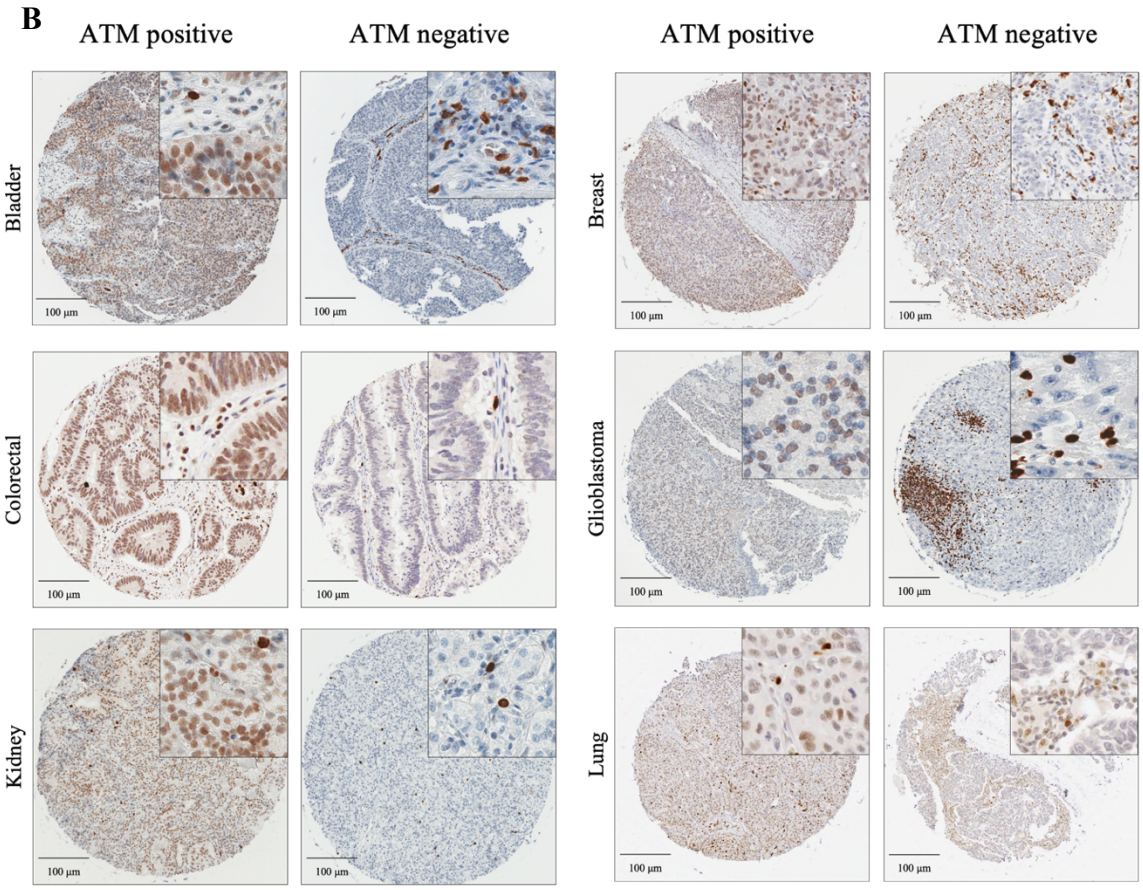
Variability of staining intensity was observed on both a tissue and cell level whereby not every cell was labelled as ATM positive. For example, the Purkinje cells of the cerebellum appear to be those preferentially stained with ATM protein expression evident in both the cytoplasm and the nucleus. An interesting observation was noted, particularly in tissues associated with the immune system such as the tonsil, thymus, and spleen, of a sub-population of cells with high positive stain. Such cells with high intensity staining were also observed in the vascular network. Confirmation of the specificity of the observed

staining patterns of total ATM protein was supported by the inclusion of a no primary antibody control on a serial section of the TMA block (data not shown).

3.2 IHC reveals frequent tumoural loss of ATM protein expression

Somatic mutations across the ATM gene have been identified in various solid and haematological malignancies. Dataset analysis (The Cancer Genome Atlas; TCGA) reveals approximately 5% of tumours possess an ATM mutation. Frequency of mutation incidence varies with reported ~10% in prostate and lung cancers, ~20% in colorectal and uterine cancers and over 40% of mantle cell lymphoma (MCL; Figure 3.2A)[132,186,187,189]. Previous data from the lab demonstrated lack of ATM protein expression in 9.5% non-small cell lung cancer (NSCLC) and 3.9% colorectal cancer[197]. Data identified ATM protein loss in 13% breast cancer and 4% melanoma samples (J. Moore, A. Ryan, unpublished data). This cancer panel was re-evaluated and extended to include additional cancer types to further investigate the extent of ATM protein loss across human cancers. Using the aforementioned IHC protocol, TMAs (1 mm diameter cores, 4 μm thick sections) of bladder (BL1921), brain (GL803b), kidney (KD2085), oesophageal (ES1921), pancreatic (PA1921) and prostate (PR1921a) cancers were evaluated. The brain TMA consisted of different brain cancers including astrocytoma, glioblastoma, oligoastrocytoma, oligodendroglioma, medulloblastoma and ependymoma. To evaluate each section, ATM protein detection had to cover at least 5% of the core where stromal and/or immune infiltrate staining was used as a positive control. A no primary antibody was performed on a serial section of the pancreatic TMA (data not shown).


A
Alteration frequency (%)
50
40
30
20
10
0
Mantle cell lymphoma
Cutaneous squamous cell carcinoma
Mucinous stomach adenocarcinoma
Large cell neuroendocrine carcinoma
Mucinous adenocarcinoma of the colon and rectum
Prostate cancer
Diffuse large B-cell lymphoma
Uterine carcinoma
Non-small cell lung cancer
Bladder urothelial carcinoma
Stomach adenocarcinoma
Prostate neuroendocrine carcinoma
Angiosarcoma
Melanoma
Lung adenocarcinoma
Colorectal adenocarcinoma
Cervical squamous cell carcinoma
Breast invasive cancer
Oesophageal adenocarcinoma
Chronic lymphocytic leukaemia
Anaplastic oligodendroglioma
Breast mixed ductal and lobular carcinoma
Rectal adenocarcinoma
Lung squamous cell carcinoma
Small lung cell cancer
Prostate adenocarcinoma
Hepatocellular carcinoma
Head and neck squamous cell carcinoma
Pancreatic adenocarcinoma
Poorly differentiated thyroid cancer
Merkel cell carcinoma
Breast cancer
Renal clear cell carcinoma
Pancreatic neuroendocrine tumour
Renal non-clear cell carcinoma
Ewing sarcoma
Glioblastoma multiforme
Pleural mesothelioma
Follicular thyroid cancer
Acute myeloid leukaemia
Neuroblastoma
Gastrointestinal stromal tumour
Wilm's tumour
Endometrial carcinoma
Osteosarcoma


B
ATM positive
ATM negative
ATM positive
ATM negative
Bladder
Breast
Colorectal
Glioblastoma
Kidney
Lung
100 µm

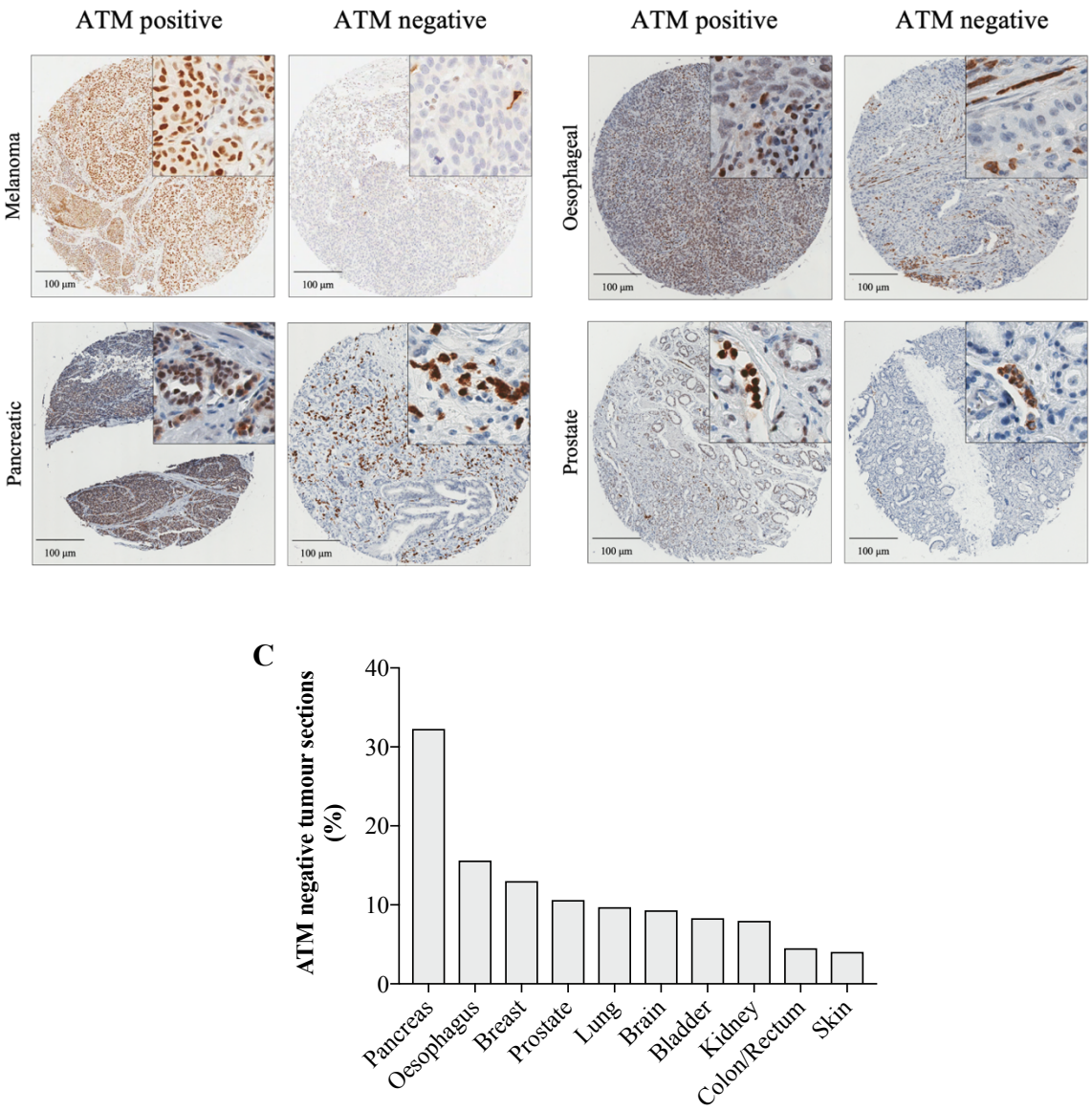


Figure 3.2 | ATM is frequently lost in human tumours

(A) Mutation frequency of ATM across different cancer subtypes, data retrieved from cBioPortal[186,187]. **(B)** Representative IHC images from different tumour specific TMAs each containing 80-208 cores, sectioned at a thickness of 4 µm. For each tumour type, representative images for sections scored as 'ATM positive' or 'ATM negative' included where positive signal is visualised by brown DAB staining of ATM (Y170) at 1:200. Sections counterstained with haematoxylin. Images of full section and magnification region at 40X using Aperio ImageScope. Scale bar = 100 µm. **(C)** Quantification of ATM-negative sections per TMA.

Representative images for each tumour type show an example of a tumour scored as ATM positive and ATM negative (Figure 3.2B). Previous data from the lab was added to include

tumour sections from the breast, colorectal, lung and melanoma TMAs. Across the tumours scored as ATM positive, tumour cell specific staining can be observed in addition to the presence of positive stromal and/or immune cell staining. In the tumours scored as ATM negative, ATM protein can only be detected in the surrounding stromal and immune cell populations. Interestingly, a noticeable sub-population of cells with high ATM expression was detected in the tumour samples. This distinct sub-population of cells can be observed to a varied extent across the different tumour types but appears to be in higher frequency in tumour sections scored as ATM negative. Loss of ATM protein expression ranged from 32.3% in the pancreatic cancer to 4% of melanoma analysed as part of this study (Figure 3.2C).

3.3 Loss of tumoural ATM may be associated with an immune phenotype

Previous data from this chapter has detected the presence of a distinctive sub-population of cells with strong ATM expression. Observations implicate this population to have cytoplasmic staining, greater prevalence in lymphoid primary (thymus) and secondary (spleen and tonsils) tissue and appear to be more prominently associated with ATM negative, rather than ATM positive, tumours (Figures 3.1 and 3.2B). Based on this, a potential biological rationale was to hypothesise that this sub-population may be of lymphoid origin.

Initial investigations questioned whether the sub-population were T lymphocytes. According to data from Figure 3.2C, the pancreatic tumour TMA was reported to have the highest incidence of ATM protein loss. A serial section of the same TMA was probed for cluster of differentiation 3 (CD3; SP7), a generic marker for T cells. Figure 3.3A shows

representative images of the same pancreatic tumour section evaluated for either ATM (upper panel) or CD3 (lower panel). The tumour was scored as ATM negative, and regions have been highlighted to depict the presence (red box) or absence (black box) of the ATM-high sub-population. In the case of CD3, the same areas of cells were both positive. Each tumour was analysed for percentage of CD3+ coverage across the section and categorised based on ATM status. ATM positive tumours had a significantly higher percentage (11.04% ± 1.42; p=0.04) of CD3 compared to ATM negative tumours (7.38 ± 0.81) (Figure 3.3B).

To evaluate further into a potential immune component of this sub-population, human lung tumour serial sections previously classified as ATM positive (squamous cell carcinoma; BBP391) and ATM negative (adenocarcinoma; BBP140) were examined for CD8 and programmed death-ligand 1 (PD-L1). Figure 3.3C confirms ATM status with tumour specific staining exclusively observed in the top panel. Tumour sections were analysed for percentage of either CD8+ or PD-L1 coverage. In the ATM positive tumour, a moderate level of CD8+ T cells (7.53%) were visualised in the tumour periphery, however the ATM negative tumour was highly positive for CD8+ T cells (48.56%) both surrounding and infiltrating the tumour. PD-L1 had minimal staining in the ATM positive tumour (0.32%) but could be visualised distinctly at the tumour periphery in the ATM negative tumour (26.73%). To expand on this data set, a serial section from the lung tumour TMA used to evaluate ATM protein loss was probed for CD8 expression. However, there did not appear to be a relationship between CD8+ T cell expression and ATM status (Figure 3.3D). Further work is required to understand the biological relevance of ATM in this subset of lymphoid cells.

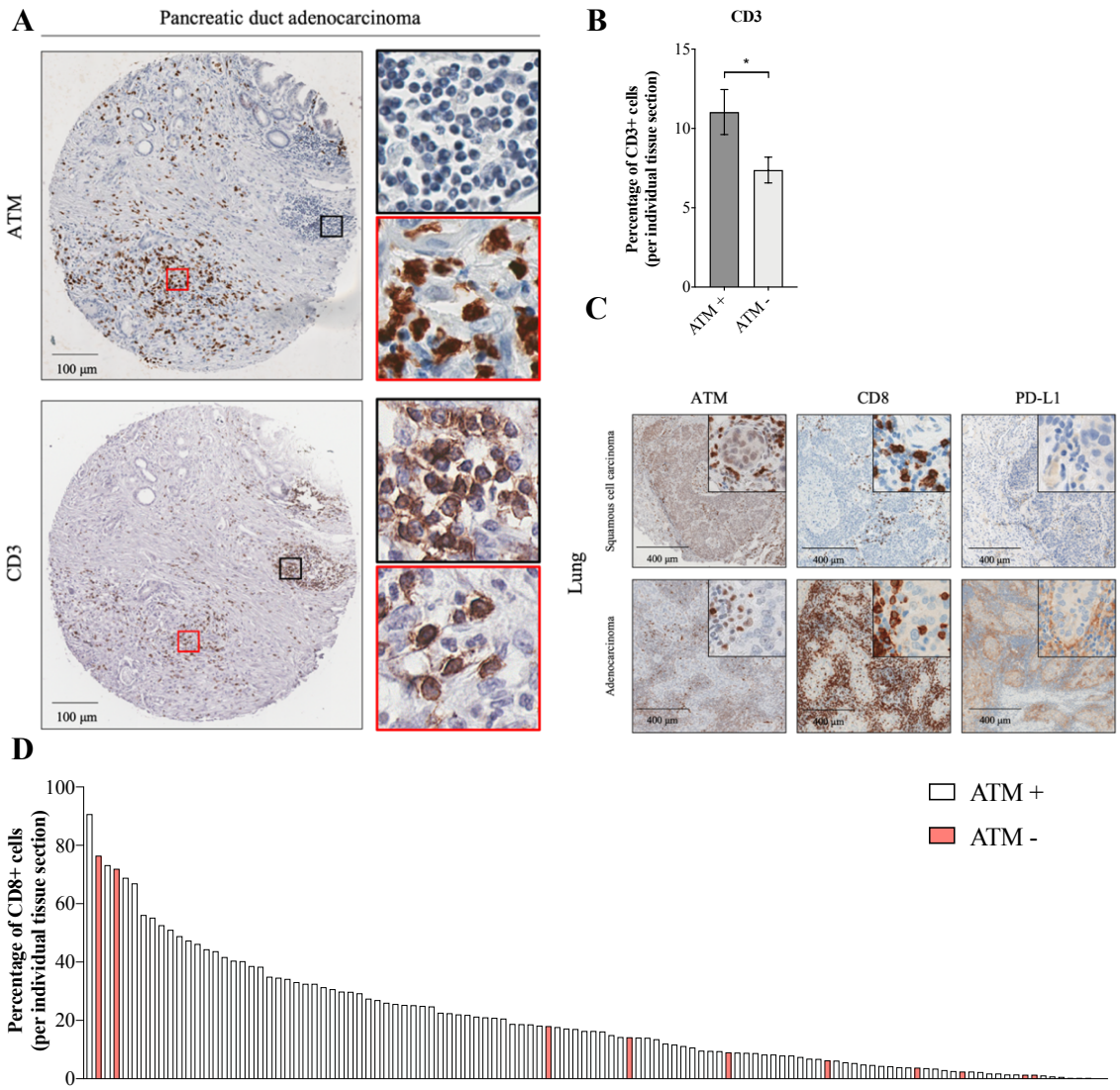


Figure 3.3 | Tumour ATM protein loss may be associated with an immune phenotype

(A) Representative images of serial sections taken from a pancreatic tumour TMA probed for ATM at 1:200 or CD3 at 1:150. Black and red boxes depict areas of positive staining and negative staining respectively and correspond to 40X magnification images. Scale bar = 100 µm **(B)** Percentage of CD3+ cells across pancreatic tumour sections scored as ATM positive (n=93) or negative (n=69). Positive cell analysis performed on QuPath and data presented as mean ± SEM. Two-tailed Student's t-test performed with statistical significance marked as * (p<0.05), ** (p<0.01) and *** (p<0.001). **(D)** Lung tumour sections (n=112) ranked for percentage CD8+. Orange bars depict ATM negative score.

3.4 Discussion

ATM is ubiquitously expressed across normal human tissue and is reported to modulate a range of functions that span both nuclear and cytoplasmic functions. The clinical manifestation of A-T corresponds to a multi-system disorder which is consistent with the widespread expression and many functions of ATM[2]. In agreement with this concept, data from this chapter confirms high expression of ATM protein across human normal tissues. Neuropathology is a characteristic feature of A-T and loss of ATM has a detrimental consequence from a clinical perspective in which the target neuronal cell population in A-T are the Purkinje cells of the cerebellum. Interestingly, IHC analysis from Figure 3.1 illustrates ATM expression is most prominent in this cell type versus other cell populations in the cerebellum[3,4,198]. Data from The Human Protein Atlas (*proteinatlas.org*) reported low expression of ATM protein in the peripheral nerve using unvalidated antibodies (mouse monoclonal MS-1198; rabbit polyclonal HPA067142). However, in this study using the validated antibody Y170, ATM protein staining could be clearly detected (Figure 3.1)[194–196]. Variability of positive signal was observed across the human eye. Interestingly, apart from the appearance of telangiectasia in the sclerae, ocular degeneration is not reported in patients with A-T despite the high exposure of ROS to the photoreceptor cells of the retina. ATM is reported to modulate the cellular response to oxidative stress and an association between this cytoplasmic function and role in this cell type would be logical[199,200]. Increasing evidence linking the role of the hypothalamic-pituitary-adrenal (HPA) axis and responses to oxidative stress have been reported. The regulation of the HPA axis is, in part, mediated by the maintenance of physiological levels of ROS and disturbances that result in excessive ROS levels cause HPA axis hyperactivation. High levels of ATM protein expression were evident in the adrenal gland however a distinct

staining pattern in the pituitary gland was seen where only cytoplasmic staining was detected in the absence of nuclear staining (Figure 3.1)[201,202].

Chronic respiratory failure is one of the leading causes of death in A-T and patients are prone to recurrent pulmonary infections. Bronchiectasis and pneumonia often precede diagnosis of pulmonary failure however the aetiology of this progressive decline has yet to be full understood[203]. Figure 3.1 illustrates positive signal for ATM expression across cell types in the lung tissue. A role for ATM in the heart has been implicated in an increased risk of ischaemic heart disease in A-T heterozygotes and experiments in $ATM^{-/-}$ mice. Both structural and functional modifications were reported in the hearts of $ATM^{-/-}$ with evidence of both hypertrophy and fibrosis associated with the lack of ATM-dependent activation of AKT. In addition, atherosclerosis was detected in ATM heterozygous mice[199,200]. Figure 3.1 indicates low levels of ATM protein expression in normal heart myocytes adjacent to highly stained lymphoid cells. Other work has shown that murine ATM is located in cardiac mitochondria, implicating a role in oxidative stress responses[204,205].

Several studies have also reported that ATM is a moderate penetrance breast cancer susceptibility gene resulting in an increased risk of breast cancer in heterozygous carriers of ATM mutations. However, the clinical significance of an association between ATM variants and breast cancer has been disputed. Particular mutations, such as ATM V2424G, are considered as high risk whilst others such as ATM D1853V, L546V and S707P are not predictive for predisposition to breast cancer. Staining for ATM expression was high in cells of the lobule and surrounding stromal areas (Figure 3.1)[130,206]. Example tissues, such as the cervix, demonstrate variability of staining intensity for ATM with positive and negative cells observed in the same region. The reproductive tissues examined in this TMA, such as the ovaries, fallopian tube and testis generally display high expression of

ATM protein. Reproductive dysfunction, often causing infertility, is classified as a feature of A-T and ATM-deficient mice are sterile. It has been proposed that gonadal abnormalities are due to exposure to endogenous damage during development. Chromosomal fragmentation and meiotic disruption result in the degeneration of oocytes and spermatocytes during embryogenesis and postnatally, respectively[207,208].

Tissues of the digestive system, such as the small intestine, are highly proliferative and exposure to radiation induces both acute and chronic effects. High ATM protein expression was observed in tissue types of the digestive tract (Figure 3.1), yet manifestations of the gastrointestinal tract and associated organs are not often reported in the context of A-T[209–211]. A distinct observation from investigating ATM protein expression in normal human tissues was the strong staining detected in tissues associated with the immune system such as the spleen, tonsil, and thymus. The potential significances of this will be discussed later.

To further support these IHC findings, alternative methods to detect ATM expression were explored including IF and RNAscope. IF has a number of potential advantages over IHC, in particular the potential for quantitation, and higher resolution detection. However, in this study, antibody staining could not be successfully optimised to determine ATM expression due to high levels of autofluorescence. Further work is required to define optimal antibody conditions to facilitate quantification. In order to determine the relationship between ATM protein and RNA expression, RNAscope was used however the formalin-fixation tissue processing procedures reduced detectable ATM RNA levels (and also control gene PPIB) in tissues below detectable levels (Supplementary Table 8.1). The detection of ATM by RNAscope in cell pellets and newly sectioned xenograft tissue implied that the RNA had become degraded over time in cut tissue sections and was not detectable in the RNAscope assay, and similar conclusions have been reported by others[212].

Since fresh-cut sections were not available for the tissues examined in this work, ATM RNA levels could not be determined by RNAscope.

Mutation frequency in ATM is reported to varying extents across several tumour types and in some cases, such as MCL, the incidence is high (>40%)[132]. However, the prevalence of ATM mutations reported do not necessarily correspond with the loss of ATM protein observed in this chapter. Possible explanations for this may be the rate at which ATM is degraded versus rates of transcription and/or translation as well as the potential for any post-translational modifications. Each tumour type that was evaluated for ATM protein loss had at least three corresponding normal tissue sections included in the multi-normal TMA however the discrepancy between reported mutation frequency and observed result could be a technical issue of threshold detection. The occurrence of a mutation does not necessarily result in a functional impairment of ATM and therefore understanding the frequency of tumoural protein loss is an important avenue to explore. Using IHC techniques could have potential utility for identifying patients with ATM tumour loss, however clinical validation would be required.

This chapter reported a range of ATM protein loss in various tumour types (Figure 3.2) which supports findings from parallel studies. Further data has shown that ATM protein loss is evident in 8% and 12% of colorectal and prostate cancers respectively[213,214]. On the contrary, analysis into pancreatic tumours showed 12.5% of the samples had lost ATM protein. However, this was reported at 24.5% in patients who had a family history of pancreatic cancer compared to 11% of patients who did not[215]. In addition, ATM loss in oesophageal cancer has been reported as 8.4% however an interesting observation identifies increased ATM protein expression in oesophageal squamous cell carcinoma and pre-malignant lesions compared to normal tissue controls[216,217]. Data investigating ATM

protein loss in NSCLC patients has been variable with reports of 9.5%, 21.8% and over 40%. Transcriptional silencing as a result of ATM promoter methylation has been proposed as a potential explanation for the discrepancies observed between ATM mutation frequency and protein loss in NSCLC. Such hypermethylation can lead to downregulation of ATM protein and subsequently functional impairment which can be documented by increased radiosensitivity seen in colorectal, glioma and breast cancer cell lines[94,138,189,197,218–220].

Evidence of high ATM protein loss has been documented as 60% of 968 cases and reduced expression in 23.1% - 76.9% in low grade (I) and higher grade (II-III) breast cancers respectively. Research into locally advanced breast cancer has also identified epigenetic silencing of ATM[134,219,221]. ATM protein expression in brain tumours has been reported to vary based on type. For example, meningioma presents with low ATM protein expression levels, higher grade brain tumours are associated with higher levels of ATM protein whilst astrocytoma has been classified as both ATM high and low expressing. In addition, 49% of glioblastoma patient samples were classified as "No or little expression" of ATM[222,223]. Contrary to this, in the context of clear cell renal cell carcinoma, higher tumour grade classification was associated with higher frequency of ATM protein loss[224]. Data implies that ATM protein expression correlates to the measured accumulation of DNA damage (ADD) in the tumour. Bladder cancer expression of ATM was evaluated based on ADD status where ~10%, ~21% or ~50% of ATM protein loss was observed in the low, medium, and high ADD groups respectively[225]. Approximately 10% and 20% of vertical and metastatic growth phase skin melanoma and 65% of uveal melanoma present with loss of ATM protein expression[226,227].

In general, the ATM expression data aligns well with the available reporting on this in human tumours. However, there is conflicting data in the literature with regard to the extent in ATM protein loss, such as noted in the lung. With the exception of the oesophageal, brain, uveal melanoma and one of the breast cancer studies, the data generated from the investigations used the same antibody clone (Y170) to evaluate ATM protein loss.

An interesting observation from this chapter regards the identification of a subset of highly ATM-positive lymphoid cells, in which the staining pattern was not confined to the nucleus. This distinct sub-population was highly abundant in normal human lymphoid tissue such as the spleen, tonsil, and thymus. Furthermore, this population appeared to be more prominent in ATM deficient tumours. Tumour DDR dysfunction has been shown to provoke activation of the host immune system through accumulation of somatic mutations that may present as neoantigens. In addition, antiviral immune signalling has been shown to occur in response to the presence of intracellular DNA fragments in the cytoplasm. In the case of the latter, pharmacological inhibition of ATM has been reported to promote mtDNA leakage into the cytoplasm. Consequently, the activation of the dsDNA sensor, cyclic guanosine monophosphate (GMP-AMP) synthase (cGAS) results in the recruitment and infiltration of lymphocytes to the TME via STING pathway activation[228–230].

A characteristic feature of A-T patients is cancer predisposition, particularly haematological malignancies. Due to the physiological generation of DSBs during V(D)J recombination and the rapid T cell population expansions, ATM has a fundamental role to safeguard against neoplastic transformation[131,231]. Interestingly, the reactivation of ATM in mice bearing T cell lymphomas resulted in tumour size reduction through apoptosis and decreased lymphoma cell proliferation. In addition, intra-S phase arrest and senescence has been observed in response to stimulation of ATM-deficient T cells[232]. Scavenging ROS

following TCR stimulation is dependent on ATM to permit T cell proliferation. In the absence of ATM, TCR-stimulated T cells undergo apoptosis, and the process of T cell development and maturation are defective. Furthermore, the pharmacological inhibition of ATM with KU-55933 in murine T cells also prevents adequate proliferation in response to TCR stimulation and cells undergo apoptosis. Interestingly, treatment with the antioxidant N-acetyl cysteine (NAC) restores the ability for ATM inhibited T cells to proliferate and reduces apoptosis[40,233,234].

In the context of ATM status, it appears that this may be associated with an immune phenotype. A stark contrast in both number and localisation of CD8+ T cells was documented between the two lung tumour sections. A greater proportion of CD8+ T cells were observed in the ATM negative section in which the majority of the cells were restricted to the tumour periphery. However infiltrating CD8+ T cells within the tumour were identified. Additionally, the detection of PD-L1 exclusive to the tumour periphery of the ATM deficient lung tumour further implicates an association between ATM tumour status and an immune exclusion phenotype. However, upon further investigation, it appears that ATM status and CD8+ recruitment and/or infiltration is not associated in this context. The exposure of U2OS cells to DNA damaging agents such as camptothecin, etoposide and IR resulted in the upregulation of both mRNA and protein PD-L1 levels that could be suppressed with the addition of ATM, ATR or CHK1 inhibition. The use of siRNA directed towards NBS1 also resulted in the same suppression of PD-L1 response[235]. Additional exploration is required to understand the biological significance of this.

Identification of the sub-population of ATM positive cells is a considerable point of interest. Using t-distributed stochastic neighbour embedding (t-SNE) analysis, ATM was found to be highly expressed in NK, NK-T cells and CD8 T cells in the lung tumour

microenvironment[236]. Firstly, NK cells are responsible for mediating T cell homeostasis through suppression of T cell activity and function. In addition, NK cell activity can result in the removal of both activated T cells and antigen-presenting (APC) cells. CD8 T cells interact with APCs and undergo extensive expansion and differentiation to perform target eradication. Finally, NK-T cells are unique in that they express both TCR and NK cell receptors, corresponding to the innate and adaptive immune systems respectively. NK-T cells have widespread roles spanning tumour surveillance and self-tolerance mechanisms. It has been proposed that activation of DDR kinases, such as ATM, could be involved in regulating NK-T cell interactions through mediating the expression of activation ligands expressed on T cells. In the context of hepatitis C virus, ATM and p53 expression are associated with an exhausted T cell state[237–241]. Additionally, ATM has been shown to upregulate the major histocompatibility complex (MHC) class I chain-related protein A (MICA) via NF-κB on activated T cells[242].

Overall, high expression of ATM protein, in nuclear and cytoplasmic regions, aligns with the devastating consequences of ATM loss in A-T patients. The extent of ATM loss in human tumours was variable across the cancer subtypes and did not correspond to reported mutational frequencies. The observation of a sub-population of cells, hypothesised to be lymphoid cells, that have high ATM expression requires further investigation.

4 ATM-dependent DNA damage responses in normal tissues

The generation of several transgenic murine models of A-T has provided a useful tool to explore the pathophysiology of the human disease and investigate potential therapeutic applications. These murine models of ATM deficiency recapitulate similar phenotypes to those observed in A-T including radiation hypersensitivity, predisposition to cancer and immune system dysfunction. A high incidence of tumour development, particularly lymphoma, is reported in ATM-deficient mice and is associated with mortality. Individuals with A-T have an increased susceptibility to cancer which has been reported in 10-40% of patients[110,243–245]. However, the development and extent of neurological defects in ATM-mutant mice is not comparable to that seen in human disease[33]. For example, the progressive ataxia and significant loss of Purkinje cells in the cerebellum seen in A-T do not present in murine models of the disease. Failure to recreate the progressive neurodegeneration of A-T in murine models has stimulated the development of alternative models for investigating A-T, such as the use of porcine and induced pluripotent stem cell (iPSC) models[29,246].

The *Atm*^{tm1Awb} mouse was engineered through targeting editing at position 5979 of the ATM coding sequence (mRNA) which has been the site of several reported human mutations[30]. These mice recapitulate the radiosensitivity, immune defects and vulnerability to tumour development as seen in A-T however abnormal neurological changes are not evident in this model[30,247]. Targeted mutations in various strains have been used including the 129S6/SvEvTac-*Atm*^{tm1Awb} mouse. In addition, 129S6 has been used as the donor strain in several congenic models with other backgrounds (B6.129S6-*Atm*^{tm1Awb}, A.129S6-

Atm^{tm1Awb} and CByJ.129S6-*Atm*^{tm1Awb})[245,248,249]. A different exon was targeted for the generation of *Atm*^{tm1Bal} which involved deletion of exon 58, consisting of the complete kinase domain. These mice demonstrate similar phenotypes to *Atm*^{tm1Awb} including heightened radiosensitivity, immunodeficiency and susceptibility to lymphoma. Unlike the *Atm*^{tm1Awb} model, loss of cerebellar neurons and neurodegeneration is evident in the *Atm*^{tm1Bal} strain. Furthermore, the aberrant activation of microglia in these mice has been associated with the generation of an inflammatory, and potentially neurotoxic, environment. However, conflicting evidence of the existence of such neurological deficits in this strain have been reported with difficulties cited over reproducibility[114,247]. Additional models include the ATM floxed (129-*Atm*$^{tm2.1Fwa}$) strain which has LoxP sites flanking exons 57-58 to offer a conditional knockout of ATM in particular tissues and the B6.129T2-*Atm*^{tm1Mfl} (Δ SRI) strain. This model generated an in-frame deletion mutation reported in cases of A-T (7636del9) which resulted in an ATM protein with a 3 amino acid deletion that lacked protein kinase activity and conferred increased radiosensitivity and susceptibility to cancer, but immune deficits were not observed[250–252]. The phenotypic variation seen in these mouse models may parallel the variable disease presentation observed in patients with A-T.

Whilst the loss of ATM can be tolerated in murine models, expression of kinase dead ATM is embryonically lethal[253]. This observation may align with the infrequency of germline ATM missense mutations in A-T (~10%) whilst over 70% of somatic mutations are missense[254,255]. Mouse models that express catalytically inactive ATM (ATM$^{KD/-}$) (transgenic: D2899A, Q2740P; knockin: D2880A) were associated with higher genomic instability than ATM-deficient mice[253,256,257]. Evidence of replication-associated DNA damage, such as increased chromatid breaks, were apparent in the ATM$^{KD/-}$ mice. Furthermore, ATM$^{KD/-}$ mice demonstrated increased sensitivity to drugs that cause

replication-associated damage, such as through formation of crosslinks or topoisomerase I inhibition compared to ATM-deficient mice. Of note, this phenomenon was not observed in response to topoisomerase II inhibition or IR. Interestingly, augmentation of immune defects was not observed with the expression of kinase dead ATM compared to total loss[253,256,257]. The notion that kinase dead ATM is more toxic than total loss of protein was further supported through the generation of a mouse model which had conditional expression of kinase dead ATM in the CNS. Purkinje cells, profoundly affected in A-T, demonstrated additional DDR impairment compared to ATM loss. However, these mice failed to show a neurological phenotype which was attributed to the level of DSB repair defects that can be tolerated by the CNS[258].

The use of ATM tamoxifen-inducible mouse models has demonstrated the recovery of ATM function. Within one month, reconstitution of ATM restored immune function, resistance to radiation, spermatogenesis, body weight and prolonged life span. In addition, ATM-dependent signalling in response to DNA damage was observed and thymoma development was delayed and in some cases prevented[207].

The studies described in this chapter aimed to explore the impact of ATM expression and activation in a murine model of ATM deficiency. These studies also aimed to investigate the different tissue-dependent responses to types of DNA-damage inducing modalities.

4.1 Expression of ATM protein in normal murine tissues

Gene expression data accessed from the Mouse Genome Informatics database (MGI) showed the detection of ATM expression across all of the tissue types included for an adult mouse (Theiler Stage 28; TS28)[259–261]. However, it appears that minimal data is available for analysing total protein expression of ATM across normal murine tissues. To expand on

this, various tissues from C57BL/6 mice were collected to determine whether total ATM protein could be detected. Tissues were sectioned at 4 μm and positive signal was visualised by brown DAB stain. A nuclear counterstain was also included. The ATM (Y170) antibody failed to react against mouse tissue and was therefore not suitable for this investigation. An alternative antibody directed against ATM (D2E2) was used which had been shown to react with murine tissues and cells via IHC and Western blot respectively (data not shown).

Visualisation of total ATM protein was observed across all murine tissues investigated (Figure 4.1). However, variable staining intensity was seen with weaker signals seen in the lungs versus the spleen, for example. Within the tissue sections, the extent of staining also varies as not all cells have been detected as ATM positive.

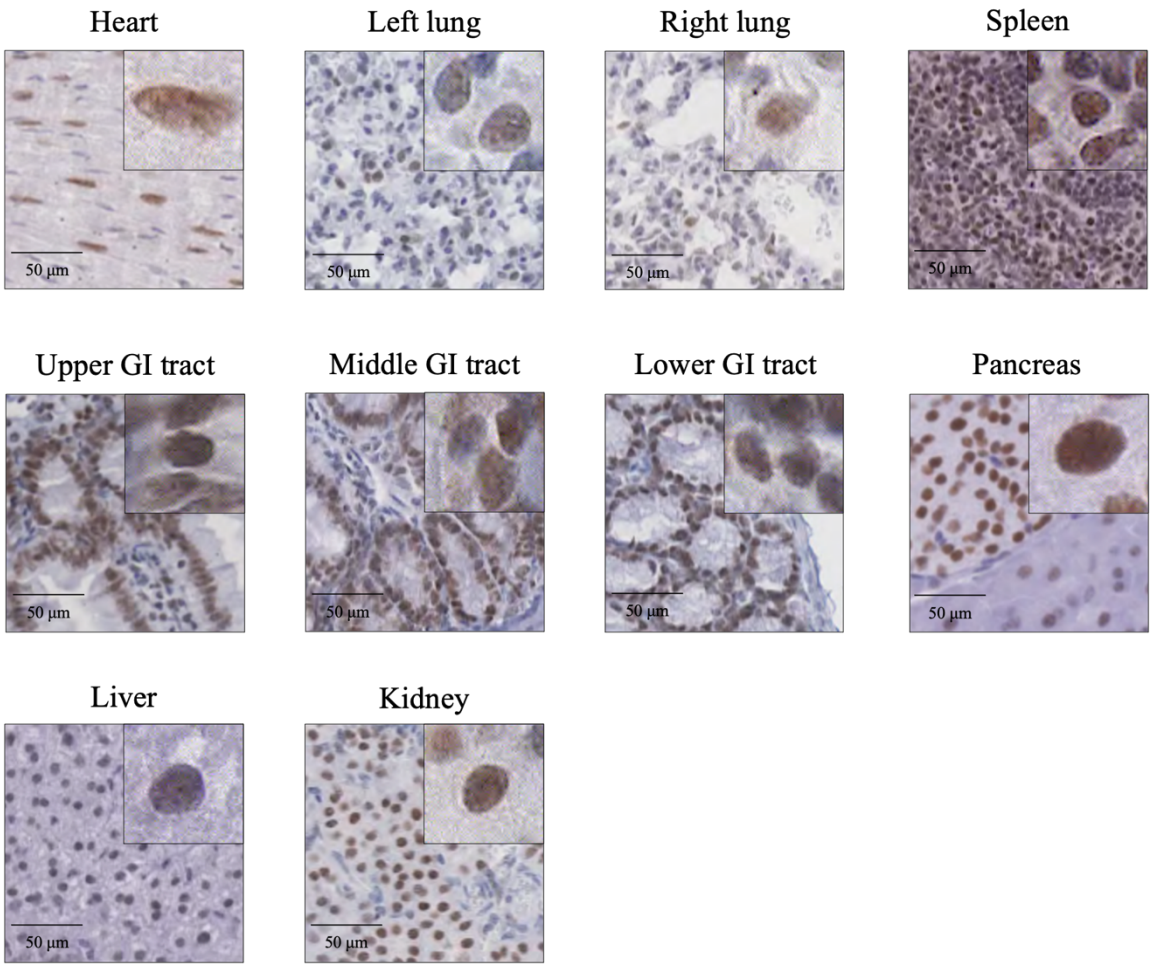


Figure 4.1 | Normal murine tissues express high total levels of ATM protein

Representative images from C57BL/6 mice tissue sections. Tissues were collected from n=3 mice and positive staining visualised by brown DAB staining corresponding to ATM (D2E2; 1:200). Sections counterstained with haematoxylin. Images shown at 10X and 40X magnification using QuPath software. Scale bar = 50 µm.

4.2 DDR following whole body irradiation

External beam radiation in the form of X-rays or gamma-rays consists of high energy photons that interact with tissues as their energy is absorbed as they pass through the body. Photons with sufficient energy collide with electrons displacing them from atoms leading to ionisation of molecules within the cell. The amount of energy absorbed by a tissue following radiation is measured in Grays (Gy; 1 Gy = 1 Joule/kilogram). IR, such as X-

rays and gamma-rays, induce genomic lesions such as DNA DSBs through two mechanisms[262,263]. Firstly, the direct interaction between radiation and the DNA molecule can cause base and sugar damage that can lead to structural disruption and DNA breaks. In addition, there are indirect effects of radiation that can be largely attributed to the ionisation of water molecules which leads to the production of free radicals. These radicals are highly reactive, possess oxidising properties and are capable of inducing DNA, protein, and lipid damage[264,265]. Since the molecular composition of the cell is approximately 70% water, it has been proposed that the majority of radiation-induced DNA damage and IR-induced toxicity are through indirect effects[266].

Evidence also suggests that radiation-induced effects on cells outside of the radiation field can occur, referred to as a bystander effect. This phenomenon in non-irradiated cells has been attributed to the consequences of immune system activation, oxidative stress and free radical generation as well as alterations in the expression of genes involved in inflammatory pathway signalling[267,268]. IR has been well-documented to induce activation of G1, S and G2 cell cycle checkpoints, and it has been found that cells in M phase are considered the most radiosensitive whereas cells in late S phase are the most radioresistant. This concept provided part of the biological rationale for the design of fractionated radiotherapy in order to capture cells in a more radiosensitive cell cycle phase. In addition, cell cycle phase is also considered a factor in determining the timing and type of cell death induced in response to IR. For example, G1 cells have prolonged survival in comparison to G2 and cell death of cells in mid-to-late S phase occurred prior to entering mitosis[269,270].

Tissues exhibit different levels of radiation sensitivity which is higher in proliferative tissues, such as the GI tract, bone marrow, and reproductive organs compared to tissues of the liver and kidney. Radiation therapy is an important treatment modality against several

cancers however the inclusion of normal tissue within the radiation field is unfortunately unavoidable, leading to dose-limiting normal tissue toxicity. Investigations have focused on the identification of targets with clinical potential to increase the radiosensitivity of tumour cells as a means of addressing the complications of normal tissue toxicity[210,271,272]. Vast tissue differences have been observed in response to radiation exposure varying from lymphocyte cell death within hours and relatively minimal changes observed in the liver and kidneys 2-weeks post-IR[273].

The heart, despite the non-proliferative characteristic of cardiomyocytes, has been shown to be radiosensitive from increased incidence of cardiovascular damage following radiation therapy for breast cancer, emphasising the consequence of normal tissue toxicity and long-term effects[274,275]. Both early- and late-stage consequences are associated with radiation exposure to the lungs presenting as pneumonitis and fibrosis respectively. In addition, acute and chronic effects as a consequence of radiation-induced toxicity of the GI tract, are common in patients receiving abdominal radiotherapy[276,277]. The spleen is not considered a particularly radiosensitive tissue, however its role in the immune system warrants care to minimise immunosuppression concerns. Interestingly, a transcriptomic study found differences in the transcriptional responses of rat spleens to low- and high-dose IR. Whilst high-dose IR, triggered increased expression of genes associated with the DDR and apoptotic signalling pathways, low-dose IR was associated with a reduction in cell cycle arrest and apoptosis and increased splenocyte proliferation[278,279]. Significant loss of endo- and exocrine functions of the pancreas have been observed as a side effect of abdominal radiotherapy and has only recently been proposed for consideration in clinical treatment planning. However, in the context of cancer, the heterogenous microenvironment characteristic of pancreatic ductal adenocarcinoma (PDAC) has been shown as a contributing factor to dampen the IR-induced anti-tumour immune response to promote

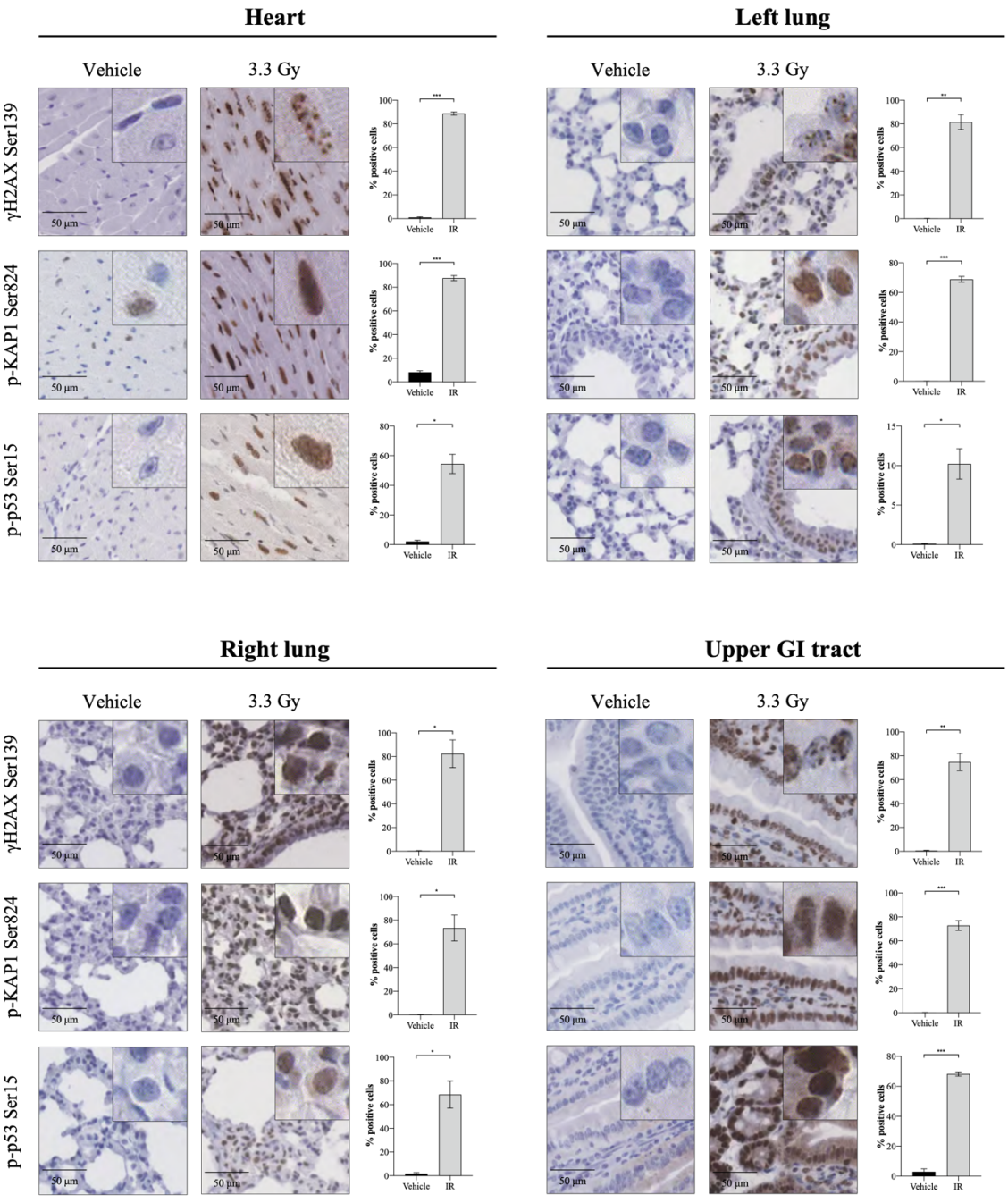
radioresistance[280,281]. The clinical manifestation of radiation-induced liver injury (RILI) can have potentially life-threatening consequences, especially in patients with additional medical complications such as cirrhosis. In the context of the kidney, radiation-induced nephropathy could take 6-18 months after exposure to IR before symptom presentation[282,283].

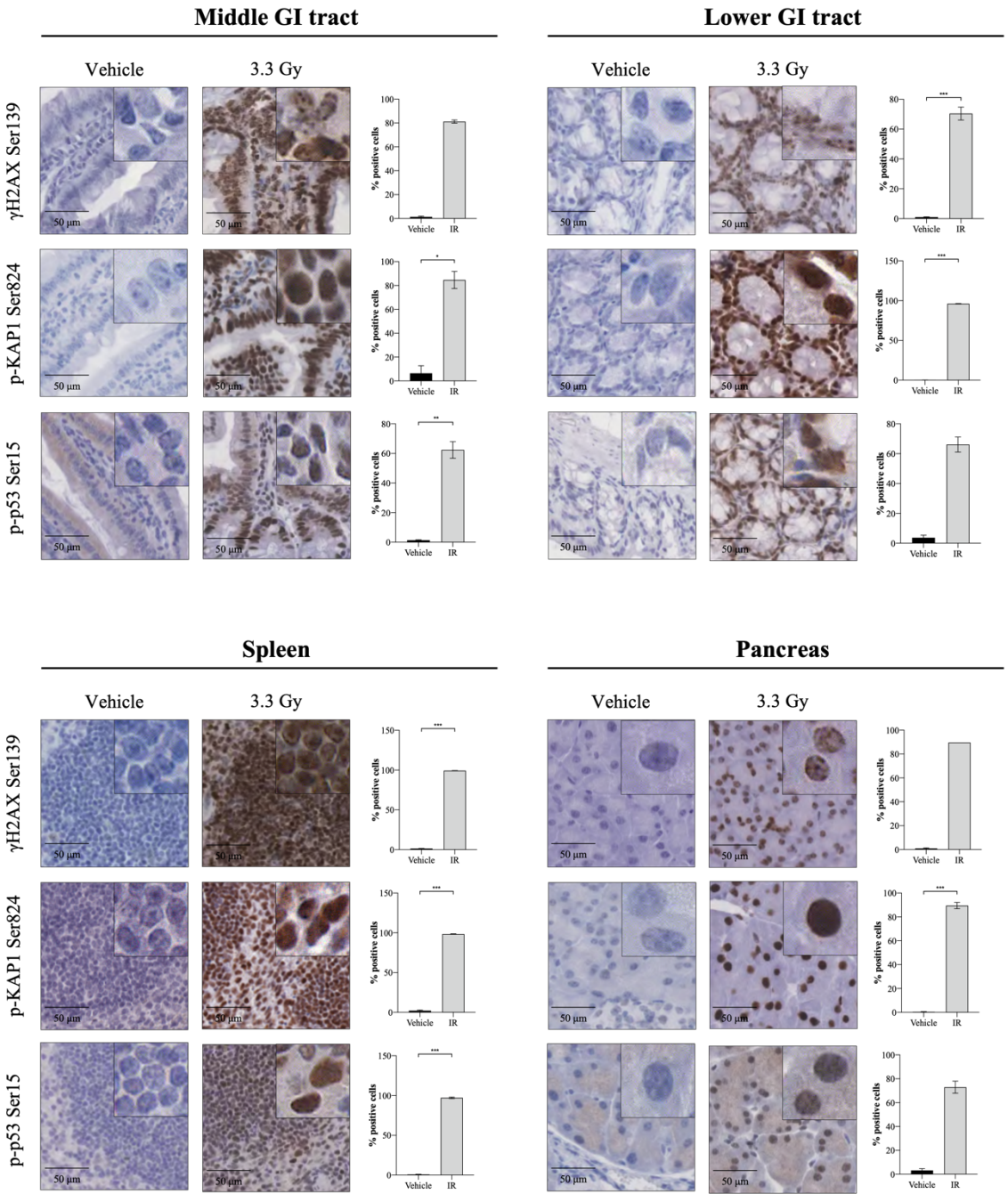
To investigate the IR-induced DDR in an *in vivo* setting, C57BL/6 mice were treated with 3.3 Gy whole-body irradiation then pulse labelled with BrdU (30 minutes) to label S phase cells, and tissues were collected 2 hours post-IR. Formalin-fixed paraffin embedded (FFPE) tissues were sectioned to a thickness of 4 μm for evaluation by IHC. Activation of the DDR in response to IR was found in all murine tissues examined (Figure 4.2). Phosphorylation of H2AX at serine 139 enabled visualisation of IR-induced sites of DNA damage which was seen as either foci or pan-nuclear staining. The distinct formation of localised γH2AX foci is indicative of sites of DNA DSBs whilst pan-nuclear γH2AX has been associated with apoptosis[284,285]. However, evidence of pan-nuclear γH2AX that is unrelated to apoptosis has been reported. Instead, activities of ATM and DNA-PK distant from the DNA damage site were proposed to mediate a pan-nuclear γH2AX response[286]. As expected, γH2AX signal was located across the entirety of tissue sections in response to IR. The percentage of cells positive for γH2AX was consistently high, evident of damage induced irrespective of cell cycle phase. Furthermore, the distribution of BrdU staining did not correspond to the tissue-wide staining of DDR markers, indicating that DNA damage was induced outside of S phase following IR (data not shown). The percentage of S phase cells in tissues was calculated and can be found in Table 4.1. IR is a potent inhibitor of cell proliferation and may have caused the stalling of replicating cells[287]. Comparison of BrdU+ staining in vehicle-treated and irradiated tissues show that a smaller percentage of cells

undergoing replication was observed in IR-treated tissues, supporting the IR-induced inhibition of DNA synthesis. However, this finding was not evident in the heart or spleen.

Consistent with detection of γH2AX in IR-treated mice, phosphorylation of KAP1 at serine 824, a marker of ATM activation in response to DNA damage, was detected across all tissues (Figure 4.2). Alike γH2AX data, this is indicative that the DDR is activated in the large majority of cells post-IR.

The tumour suppressor, p53, is phosphorylated in response to DNA damage to coordinate transient cell cycle arrest with DNA repair. ATM is a key kinase involved in p53 signalling through both direct phosphorylation at serine 15 and indirect phosphorylation through ATM-dependent activation of CHK2 which phosphorylates p53 at serine 20. This ATM-mediated phosphorylation promotes the stabilisation and accumulation of p53 through preventing ubiquitinylation by MDM2. In addition, ATM directly phosphorylates MDM2 to prevent p53 degradation[94,288]. Following IR, phosphorylation of p53 at serine 15 was visualised across most tissues (Figure 4.2). However, in comparison to quantification of γH2AX and pKAP1 positive cells, the proportion of p-p53 cells was lower in the left lung, kidney, and liver. Tissue staining of the left lung revealed p-p53 staining to be predominantly in the broncho-epithelial cells which differed from the staining pattern for phosphorylation of both H2AX and KAP1 across all cell types. In certain organs, such as the kidney, the cellular response to IR appeared heterogeneous across the tissue.


Heart
Left lung
Right lung
Upper GI tract
Vehicle
3.3 Gy
γH2AX Ser139
p-KAP1 Ser824
p-p53 Ser15
50 µm
% positive cells
Vehicle
IR


Middle GI tract
Lower GI tract
Spleen
Pancreas
Vehicle
3.3 Gy
γH2AX Ser139
p-KAP1 Ser824
p-p53 Ser15
50 µm
% positive cells
Vehicle
IR

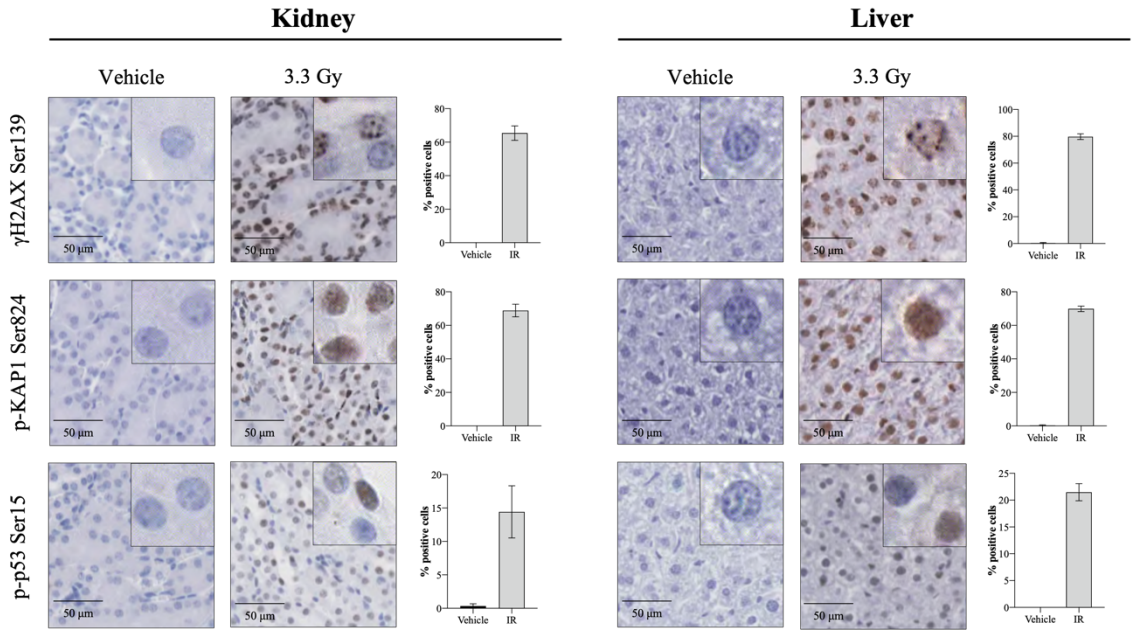


Figure 4.2 | Whole-body IR-induced DDR in murine tissues

Representative images from C57BL/6 mice tissue sections of 0 Gy or 3.3 Gy whole-body IR. Positive staining of γH2AX Ser139 (1:500), p-KAP1 Ser824 (1:2000) and p-p53 Ser15 (1:800) visualised by brown DAB staining. Data represented as mean percentage positive cells ± SEM for each marker. Statistical significance denoted by * ($p<0.01$), ** ($p<0.001$) and *** ($p<0.0001$) and performed using two-tailed Student's t-test (n=3). Statistical analysis was not performed on the liver, kidney, lower GI tract (p-p53), middle GI tract (γH2AX) and pancreas (γH2AX, p-p53) due to insufficient replicates of stained tissue. Sections counterstained with haematoxylin. Images shown at 10X and 40X magnification and quantification performed using QuPath software. Scale bar = 50 μm.

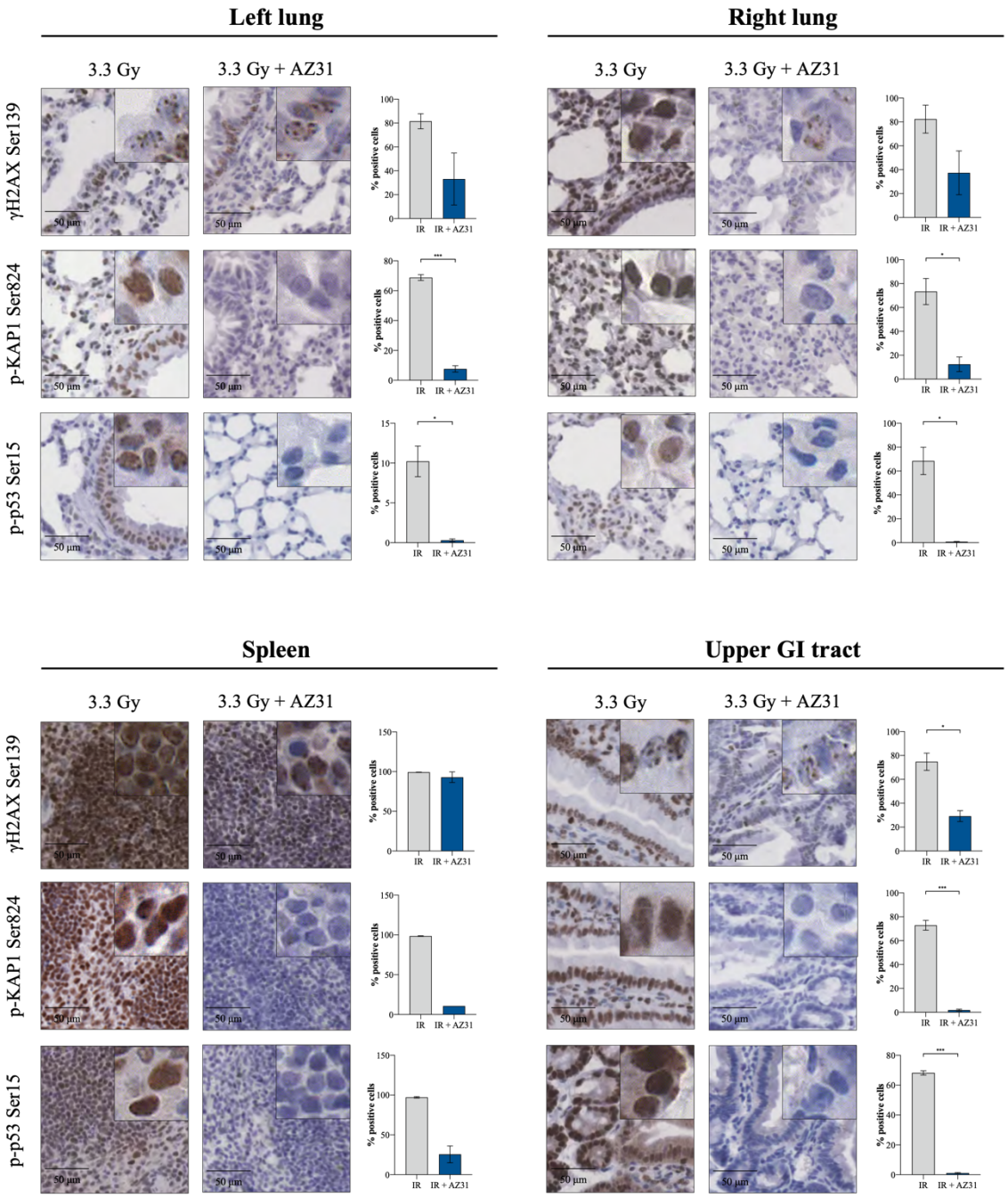
Table 4.1 | Percentage of BrdU positive cells in vehicle and IR-treated tissues

Tissue	Treatment	Percentage BrdU+ cells (± SEM)	Tissue	Treatment	Percentage BrdU+ cells (± SEM)
Heart	Vehicle	**0.5** ± 0.20	**Upper GI tract**	Vehicle	**28.5** ± 7.15
	3.3 Gy	**0.9** ± 0.62		3.3 Gy	**17.9** ±4.82
Left lung	Vehicle	**1.4** ± 0.56	**Middle GI tract**	Vehicle	**37.9** ± 10.49
	3.3 Gy	**0.7** ± 0.54		3.3 Gy	**21.7** ± 11.82
Right lung	Vehicle	**1.2** ± 0.67	**Lower GI tract**	Vehicle	**23.7** ± 0.71
	3.3 Gy	**0.9** ± 0.27		3.3 Gy	**20.1** ± 4.89
Spleen	Vehicle	**6.6** ± 0.84	**Kidney**	Vehicle	**1.4** ± 0.02
	3.3 Gy	**9.0** ± 0.71		3.3 Gy	**0.4** ± 0.07
Pancreas	Vehicle	**1.8** ± 0.13	**Liver**	Vehicle	**0.5** ± 0.02
	3.3 Gy	**0.3** ± 0.16		3.3 Gy	**0.1** ± 0.04

4.3 Treatment with the ATM kinase inhibitor AZ31 suppresses DDR signalling following whole-body IR

The development of pharmacological inhibitors of ATM kinase activity has provided insight into the many functions, and substrates of the kinase. To date, there have been over 700 downstream targets of ATM reported, spanning a range of biological pathways[289,290]. The selective ATM inhibitor, AZ31, with an IC_{50} of 1.2 nM was developed from a 3-quinoline carboxamide structure. It has been shown to inhibit ATM autophosphorylation as well as the phosphorylation of downstream targets such as KAP1 and p53. Pharmacokinetic studies of AZ31 demonstrated that the highest concentration of drug in plasma was reported at 1-hour post-administration[161,165,166,291].

The consequences of ATM inhibition in C57BL/6 mice on the DDR to IR was investigated. Pre-treatment with the ATM inhibitor, AZ31 (50 mg/kg), was incorporated into the treatment protocol. An AZ31 treatment group alone was included as part of the study but no observable staining of γH2AX, pKAP1 or p-p53 was detected (data not shown). The response of tissues to IR was dampened by the addition of AZ31 where a reduction in the phosphorylation of H2AX, KAP1 and p53 was observed (Figure 4.3). In all cases where statistical analysis was performed, AZ31 significantly reduced p-KAP1 and p-p53 levels in each tissue type. Phosphorylation of H2AX was also decreased, however not to the same extent seen for the other markers. In contrast to other tissues examined, similar staining for γH2AX was seen in cells of the spleen irrespective of the addition of AZ31.


Left lung
Right lung
Spleen
Upper GI tract
3.3 Gy
3.3 Gy + AZ31
γH2AX Ser139
p-KAP1 Ser824
p-p53 Ser15
% positive cells
IR
IR + AZ31
50 µm

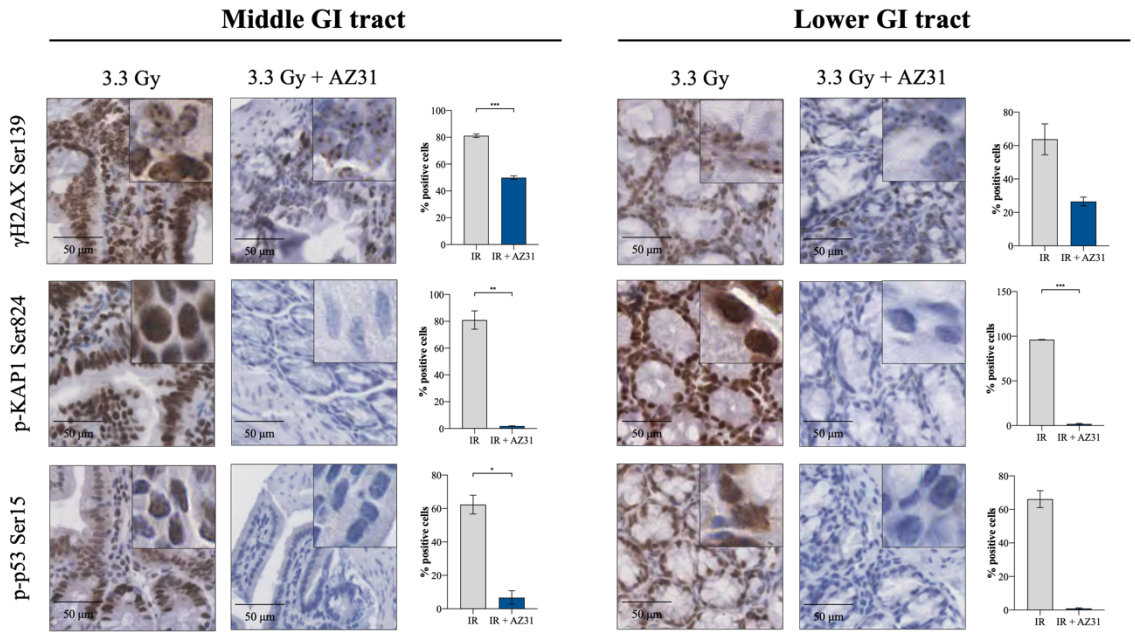


Figure 4.3 | Inhibition of IR-induced ATM signalling with AZ31

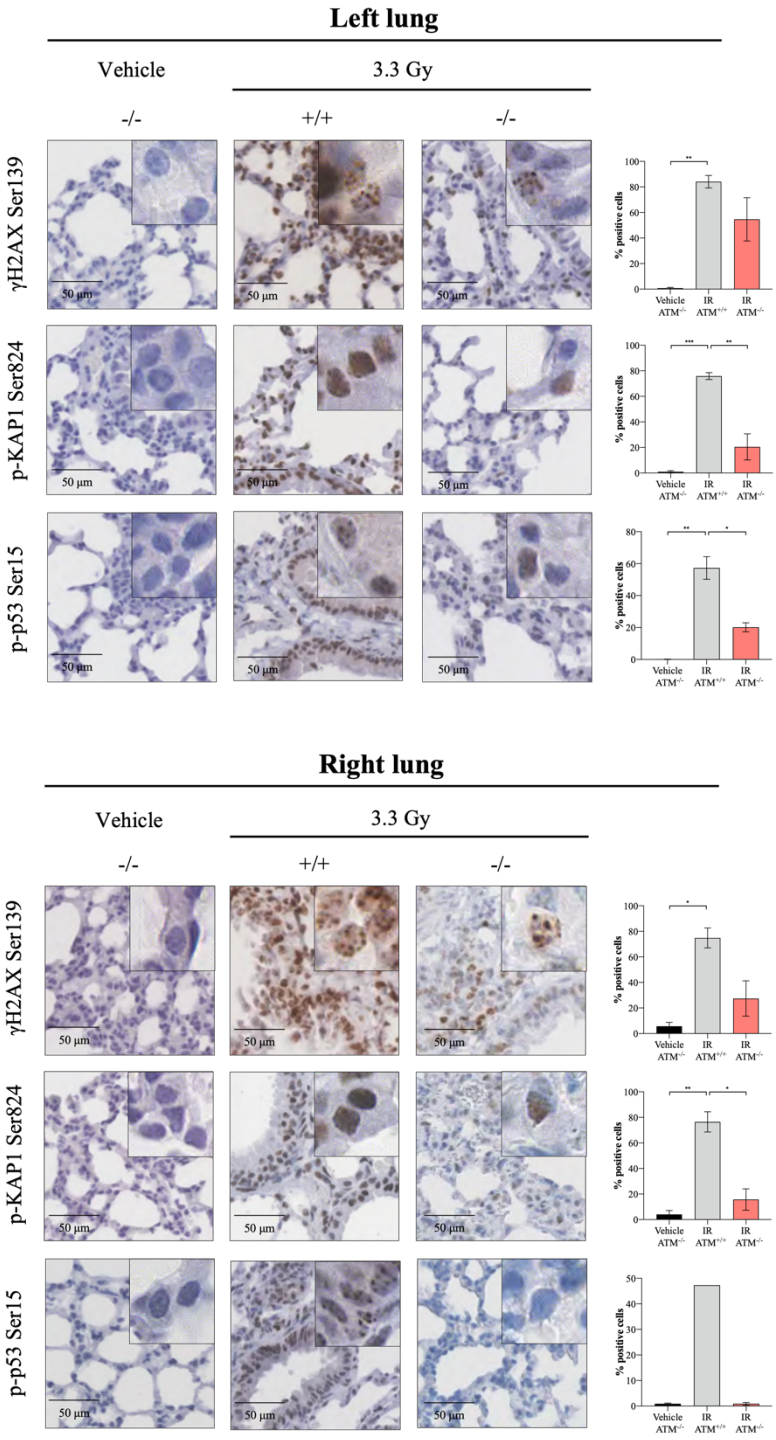
Representative images from C57BL/6 mice tissue sections of 3.3 Gy whole-body IR in the presence or absence of 50 mg/kg AZ31. Positive staining of γH2AX Ser139 (1:500), p-KAP1 Ser824 (1:2000) and p-p53 Ser15 (1:800) visualised by brown DAB staining. Data represented as mean percentage positive cells ± SEM for each marker. Statistical significance denoted by * ($p<0.01$), ** ($p<0.001$) and *** ($p<0.0001$) and performed using two-tailed Student's t-test (n=3). Statistical analysis was not performed on the spleen (p-KAP1, p-p53) and lower GI tract (p-p53) due to insufficient replicates of stained tissue. Sections counterstained with haematoxylin. Images shown at 10X and 40X magnification and quantification performed using QuPath software. Scale bar = 50 µm.

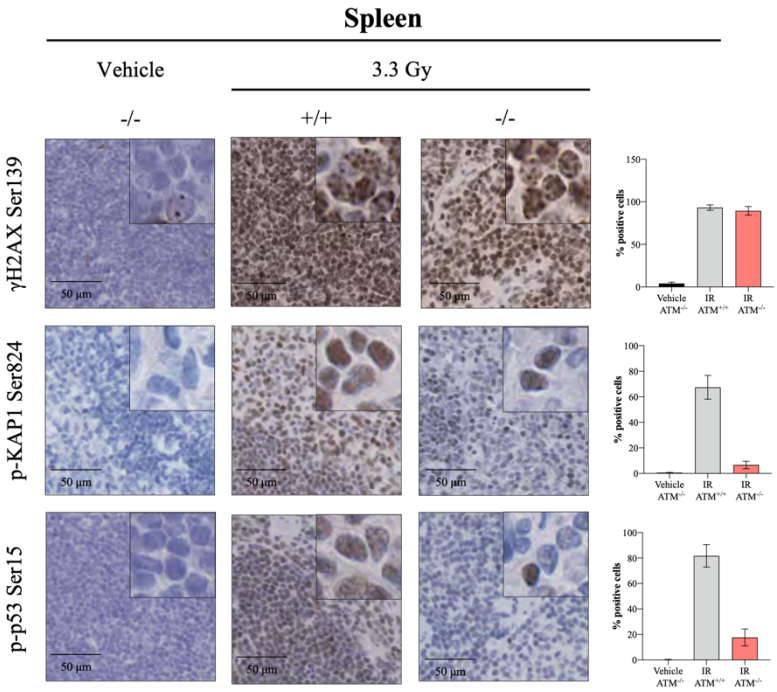
4.4 Genetic loss of functional ATM suppresses DDR signalling following whole-body IR

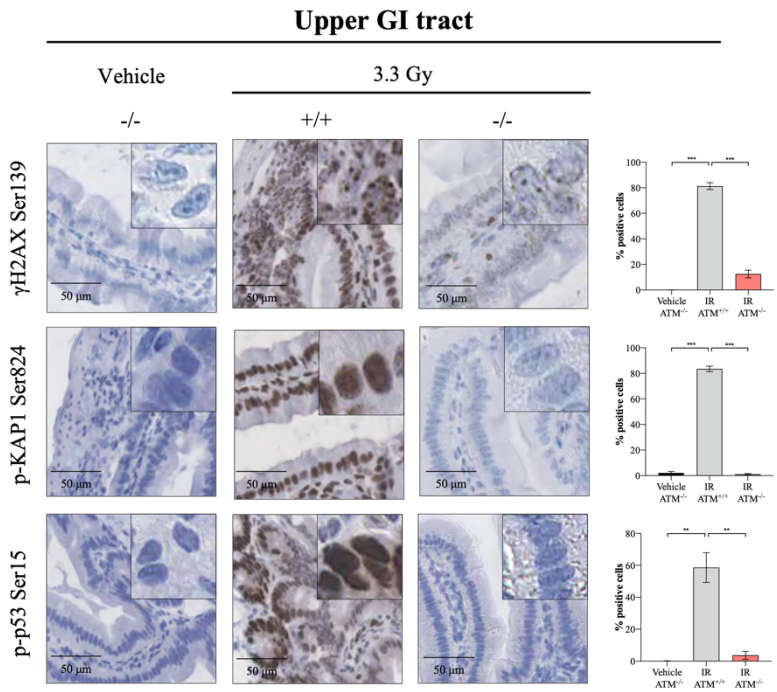
The observed differences between the loss of functional ATM compared to the expression of kinase dead ATM suggest implications for how cells in each context may respond to genotoxic modalities known to activate ATM signalling[253,255,256]. Furthermore, defective sister chromatid exchange following DNA damage has been reported in ATM inhibited cells, but is functional in ATM-deficient cells[292,293]. The use of pharmacological inhibitors

of ATM kinase may parallel that of kinase dead mutations rather than loss of ATM protein due to their targeting of function not expression.

The *Atm*^{tm1Awb} mouse was used as a model for ATM loss to investigate similarities or differences in the response to IR. For the remainder of this chapter, *Atm*^{tm1Awb} will be referred to as ATM$^{-/-}$. To confirm loss of ATM protein expression, IHC analysis was performed using ATM (D2E2). No detection of positive signal was observed in any of the tissues tested (left lung, right lung, spleen, and GI tracts; Supplementary Figure 8.1). Staining of vehicle-treated ATM$^{+/+}$ mice was performed in parallel and no differences in endogenous staining levels of γH2AX, p-KAP1 or p-p53 were observed (data not shown for ATM$^{+/+}$). Consistent with previous findings, the DDR was elicited in response to IR in the ATM$^{+/+}$ mice (Figure 4.4). Overall, the ATM$^{-/-}$ mice appeared to demonstrate a subdued staining for γH2AX, p-KAP1 and p-p53 however tissue variability was apparent. Phosphorylation of H2AX in the ATM$^{-/-}$ mice was reduced to varying extents apart from the splenic tissue in which a comparable detection of γH2AX was observed. Compared to H2AX phosphorylation, a greater reduction in the difference of both p-KAP1 and p-p53 signal between ATM$^{+/+}$ and ATM$^{-/-}$ was apparent. The inability to induce DDR involving these substrates appeared to be most prominent in the upper GI tract. Across the tissue panel investigated, a consistently lower level of DDR staining was evident however the extent of this varied.


Left lung
Vehicle
3.3 Gy
-/-
+/+
-/-
γH2AX Ser139
p-KAP1 Ser824
p-p53 Ser15
50 µm
% positive cells
Vehicle ATM-/-
IR ATM+/+
IR ATM-/-
Right lung
Vehicle
3.3 Gy
-/-
+/+
-/-
γH2AX Ser139
p-KAP1 Ser824
p-p53 Ser15
50 µm
% positive cells
Vehicle ATM-/-
IR ATM+/+
IR ATM-/-


Spleen
Vehicle
3.3 Gy
-/-
+/+
-/-
γH2AX Ser139
p-KAP1 Ser824
p-p53 Ser15
50 µm
% positive cells
Vehicle ATM-/-
IR ATM+/+
IR ATM-/-


Upper GI tract
Vehicle
3.3 Gy
-/-
+/+
-/-
γH2AX Ser139
p-KAP1 Ser824
p-p53 Ser15
50 µm
% positive cells
Vehicle ATM-/-
IR ATM+/+
IR ATM-/-

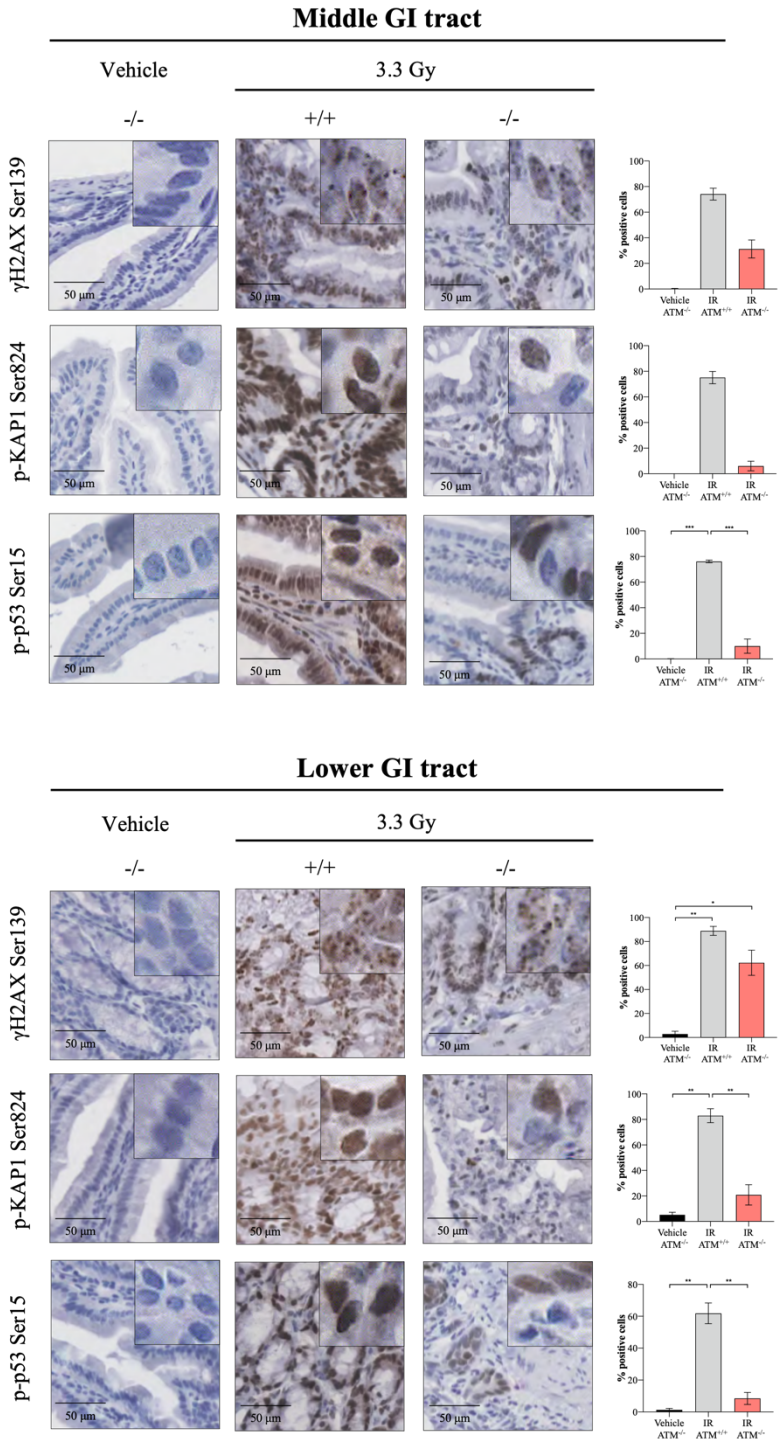


Figure 4.4 | Genetic loss of ATM suppresses IR-induced DDR signalling

Representative images from $ATM^{+/+}$ and $ATM^{-/-}$ mice tissue sections of 3.3 Gy whole-body IR. Positive staining of γH2AX Ser139 (1:500), p-KAP1 Ser824 (1:2000) and p-p53 Ser15 (1:800) visualised by brown DAB staining. Data represented as mean percentage positive cells ± SEM for each marker. Statistical significance denoted by * ($p<0.01$), ** ($p<0.001$) and *** ($p<0.0001$) and performed using two-tailed Student's t-test (n=3). Statistical analysis was not performed on the spleen due to insufficient replicates of stained tissue. Sections counterstained with haematoxylin. Images shown at 10X and 40X magnification and quantification performed using QuPath software. Scale bar = 50 µm.

4.5 DDR responses in normal tissues following irinotecan treatment

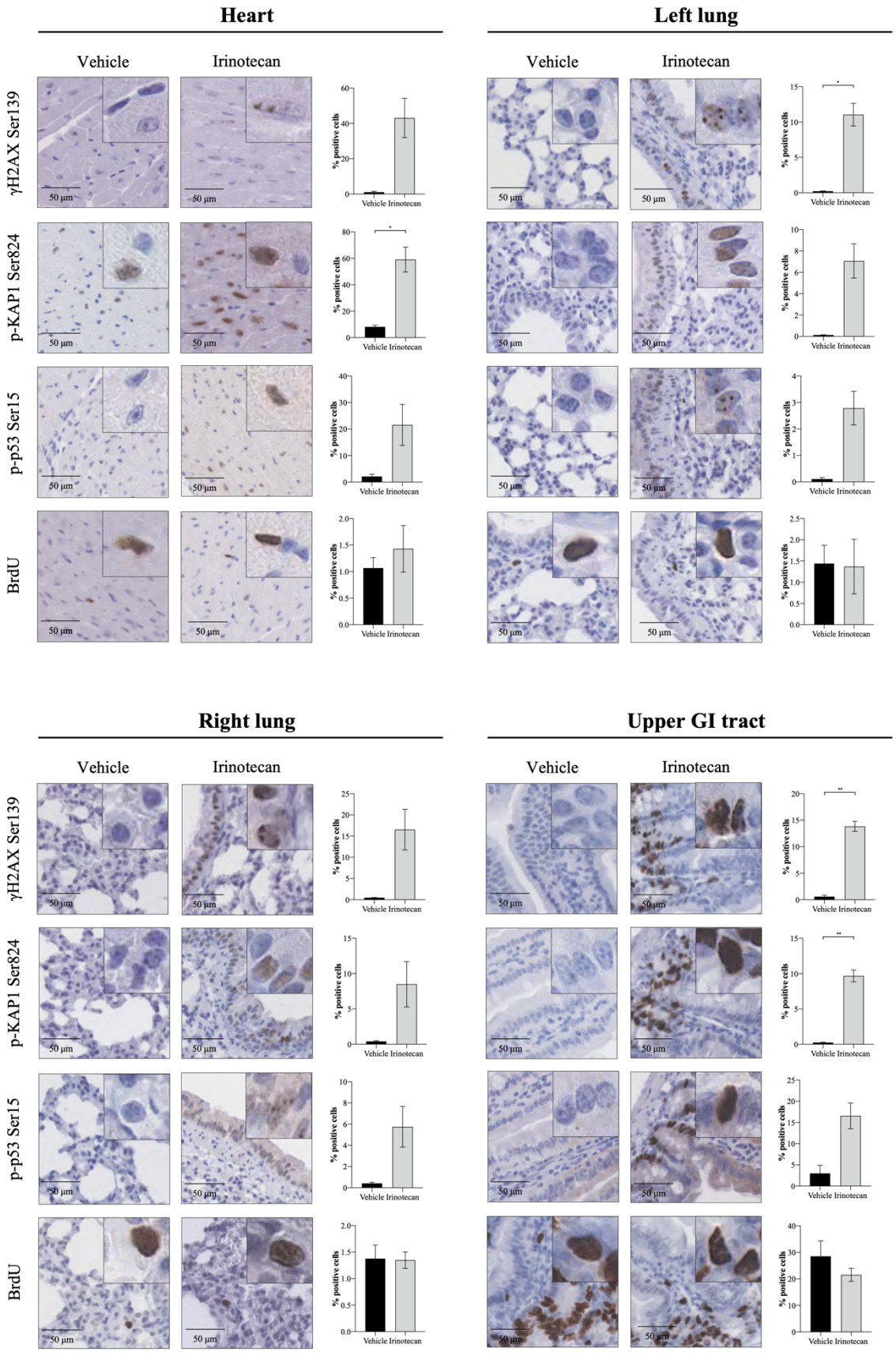
Irinotecan, also often referred to as CPT-11, is a derivative of the camptothecin family of compounds isolated from the *Camptotheca acuminata* tree. Since its discovery in 1983, irinotecan has demonstrated cytotoxic activity against several tumour types. Unlike other camptothecin analogues, irinotecan requires metabolic conversion into an active metabolite. Irinotecan undergoes carboxylesterase cleavage of the bulky bis-piperidine side chain into SN-38 (7-ethyl-10-hydroxycamptothecin). As the active metabolite of this enzymatic reaction, SN-38 is reported to have a potency of 1000-fold that of irinotecan. Metabolic inactivation and excretion of SN-38 occurs through the process of glucuronidation to form SN-38 glucuronide[294,295].

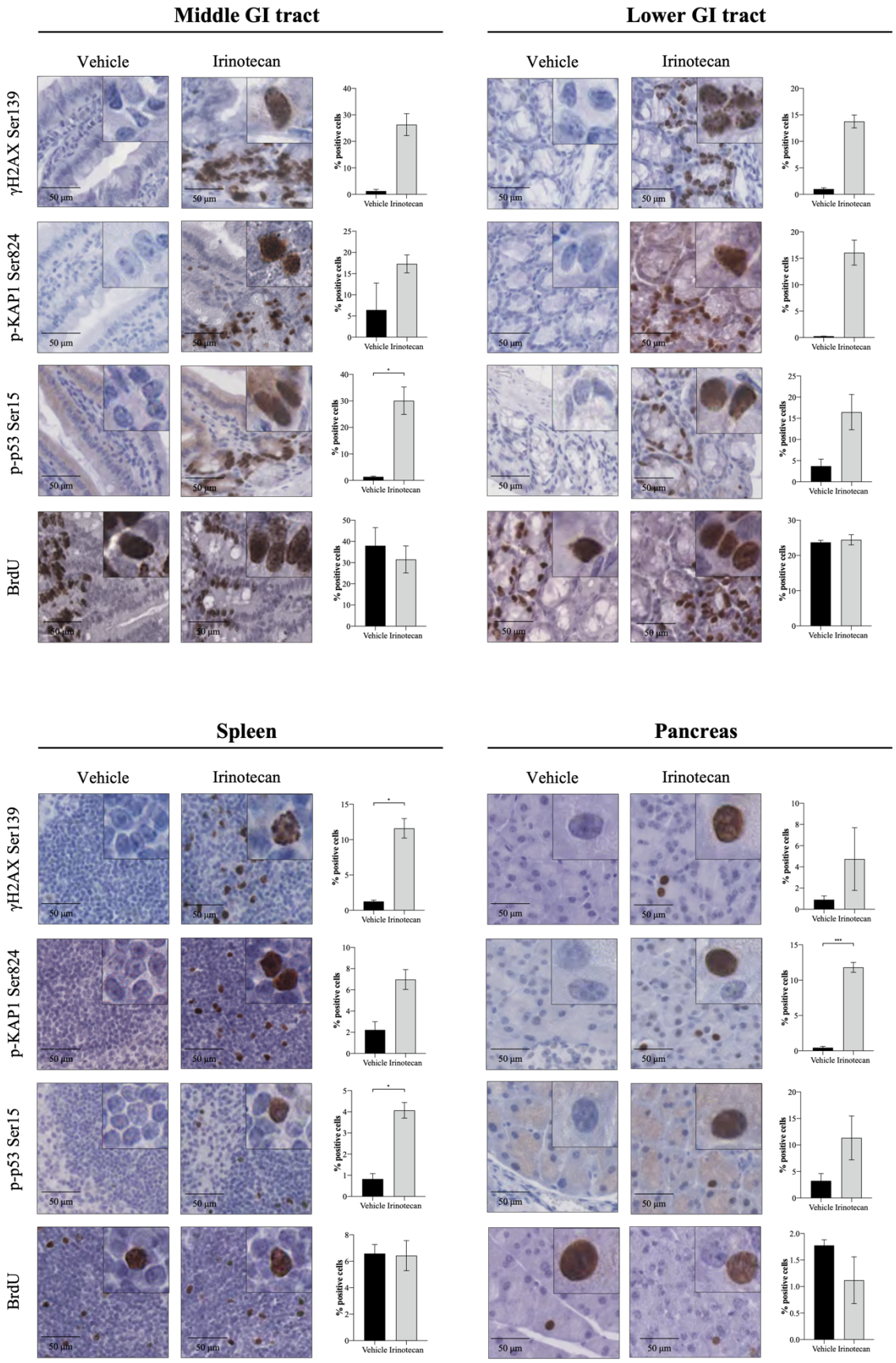
Irinotecan exerts its cytotoxicity in S phase cells through the inhibition of topoisomerase I activity. Topoisomerase I is responsible for maintaining DNA topology throughout replication and transcription by introducing ssDNA breaks. Formation of these lesions removes the torsional stress caused by supercoiled DNA. Topoisomerase IA forms a transient 5'-phosphotyrosyl bond allowing the transfer of the opposing DNA strand through the enzyme-induced break followed by strand religation. Alternatively, topoisomerase IB forms a 3'phosphotyrosyl bond and uses a controlled rotational manner[294,296]. Irinotecan can couple with these enzyme-DNA complexes to maintain a ssDNA break and prevent DNA religation. Collisions with the advancing replication fork results in DNA DSB, replication fork arrest and consequently cell death[294–296].

Administration of irinotecan has been utilised in the treatment of various cancers including lung, pancreatic, colorectal, ovarian, cervical, and gastric. Toxicities associated with the

clinical use of irinotecan include myelosuppression and diarrhoea[294,296]. Predominant distribution of irinotecan has been reported in the liver, spleen, lungs, kidneys, and heart tissues. Toxic effects have also been observed in the intestines, particularly jejunum and ileum from *in vivo* studies[297,298]. Interestingly, pharmacokinetic studies have revealed a second peak in elevated plasma levels SN-38 which has been attributed to bacterial β-glucuronidases of the gut. This results in the deconjugation of SN-38-glucuronide enabling SN-38 to be reabsorbed by the intestinal tissue[299].

The loss of ATM has been reported to confer sensitivity to camptothecin compounds through the generation of S phase dependent DNA DSBs[164]. To investigate the irinotecan-induced DDR in an *in vivo* setting, C57BL/6 mice were treated with 100 mg/kg irinotecan then pulse labelled with BrdU (30 minutes), and tissues were collected 2 hours post-administration. Sections (4 μm) from FFPE tissues were evaluated for activation of the DDR using γH2AX, p-KAP1 and p-p53 by IHC. Activation of the DDR was visualised in response to irinotecan treatment and appeared to be restricted to replicating cells, based on the staining patterns of positive cells observed (Figure 4.5). This data, consistent with literature reports of irinotecan mechanistic properties, supports the S phase targeting of cells with this compound *in vivo*[294]. However, the visualisation of DDR activation in certain non-proliferating cells was an unexpected finding. The heart is considered a low replicating tissue, yet p-KAP1 detection levels far exceeded BrdU. In addition, the broncho-epithelial cells of the lung were unstained for BrdU but positive for γH2AX foci and p-KAP1.


Heart
Left lung
Right lung
Upper GI tract
Vehicle
Irinotecan
γH2AX Ser139
p-KAP1 Ser824
p-p53 Ser15
BrdU
50 µm
% positive cells
Vehicle Irinotecan


Middle GI tract
Lower GI tract
Spleen
Pancreas
Vehicle
Irinotecan
γH2AX Ser139
p-KAP1 Ser824
p-p53 Ser15
BrdU
% positive cells
Vehicle Irinotecan
50 µm

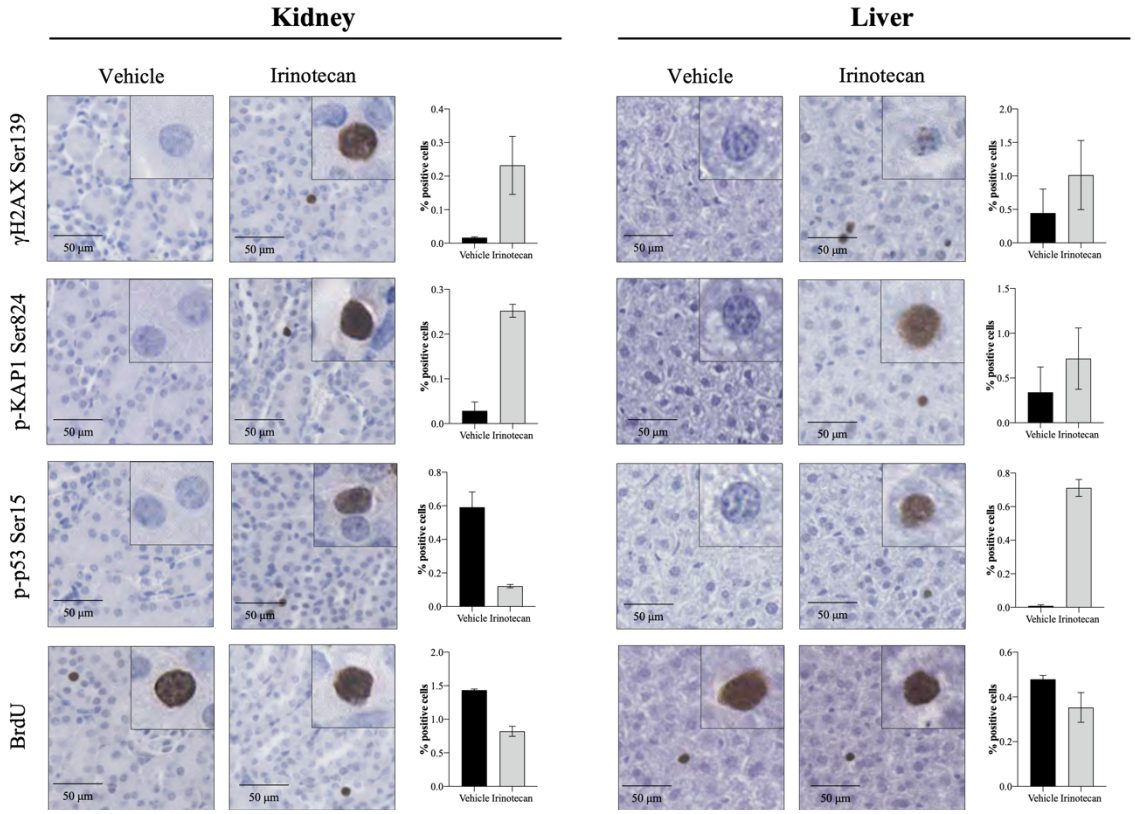


Figure 4.5 | Irinotecan-induced DDR in murine tissues

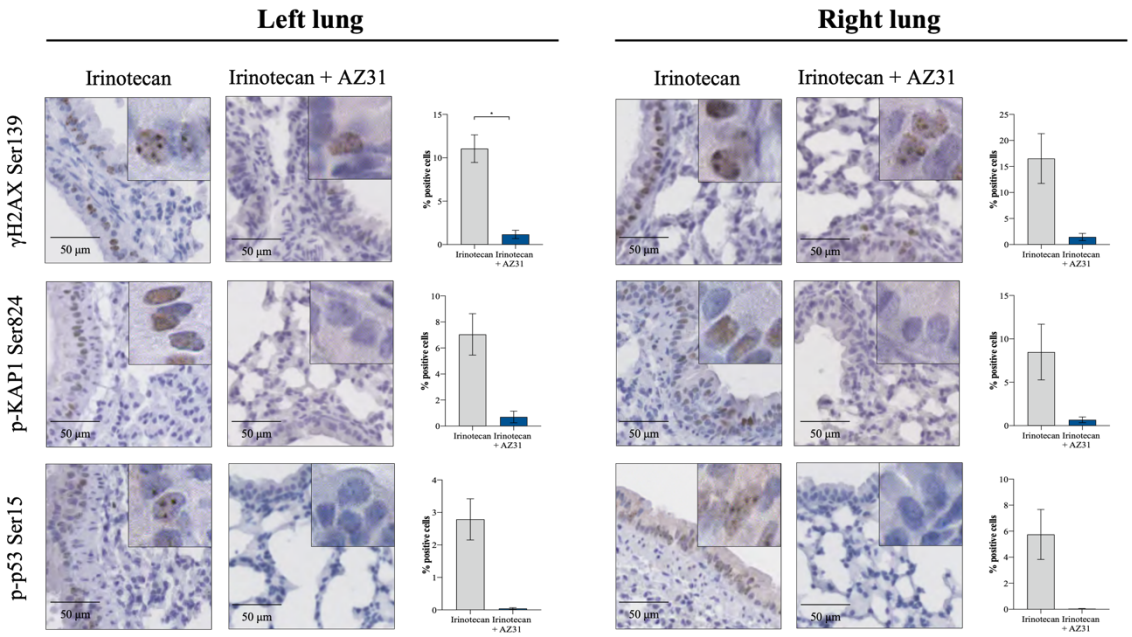
Representative images from C57BL/6 mice tissue sections of vehicle or irinotecan (100 mg/kg) treatment. Positive staining of γH2AX Ser139 (1:500), p-KAP1 Ser824 (1:2000), p-p53 Ser15 (1:800) and BrdU (1:2000) visualised by brown DAB staining. Data represented as mean percentage positive cells ± SEM for each marker. Statistical significance denoted by * ($p<0.01$), ** ($p<0.001$) and *** ($p<0.0001$) and performed using two-tailed Student's t-test (n=3). Statistical analysis was not performed on the middle GI tract (γH2AX), kidney and liver (p-p53) due to insufficient replicates of stained tissue. Sections counterstained with haematoxylin. Images shown at 10X and 40X magnification and quantification performed using QuPath software. Scale bar = 50 µm.

4.6 Treatment with the ATM kinase inhibitor AZ31 suppresses irinotecan-induced DDR signalling

Combination approaches with irinotecan and ATM inhibitors have demonstrated cytotoxic activity against tumour cells *in vitro*, even in cell lines resistant to irinotecan monotherapy. Furthermore, administration of irinotecan and the ATM inhibitor KU59403 enhanced

tumour growth delay *in vivo*[133,164,166]. An ongoing clinical trial is assessing the combination of irinotecan with the ATM inhibitor, AZD0156 (NCT02588105)[300].

In parallel to the IR response studies, the impact of AZ31 treatment on irinotecan-induced DDR responses in normal tissues was evaluated. C57BL/6 mice were pre-treated with AZ31 (50 mg/kg) followed by administration of irinotecan (100 mg/kg) for 2 hours and pulse labelled with BrdU 30 minutes before tissue collection. The addition of AZ31 demonstrates a consistent suppression of the DDR in tissues in combination with irinotecan treatment (Figure 4.6). Across the GI tract, differences were observed in the extent of DDR suppression following AZ31 and irinotecan compared to irinotecan alone. AZ31 did not have much effect on the levels of irinotecan-induced γH2AX staining in the spleen, however detection of both p-KAP1 and p-p53 was lower in the combination treatment group.



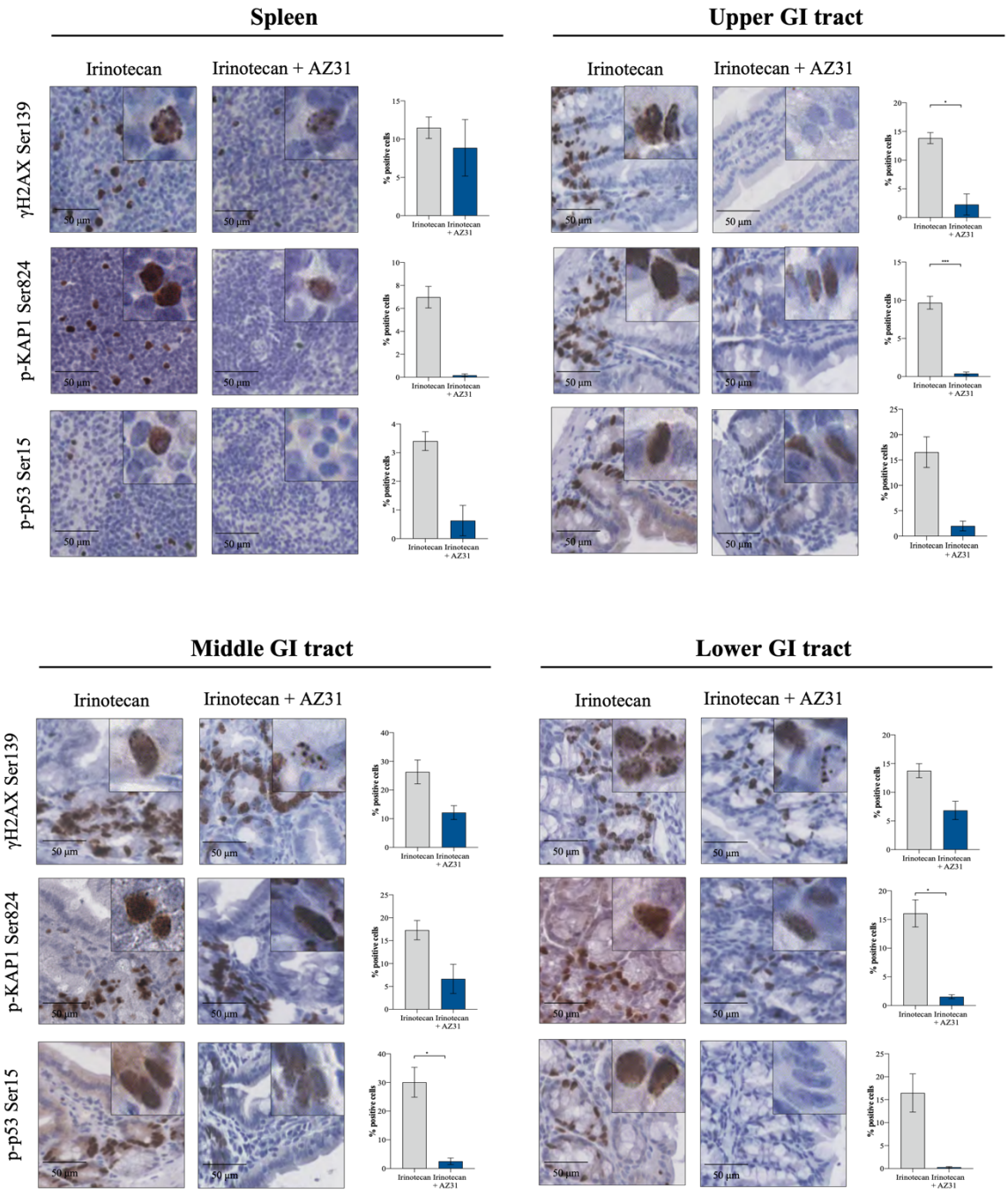


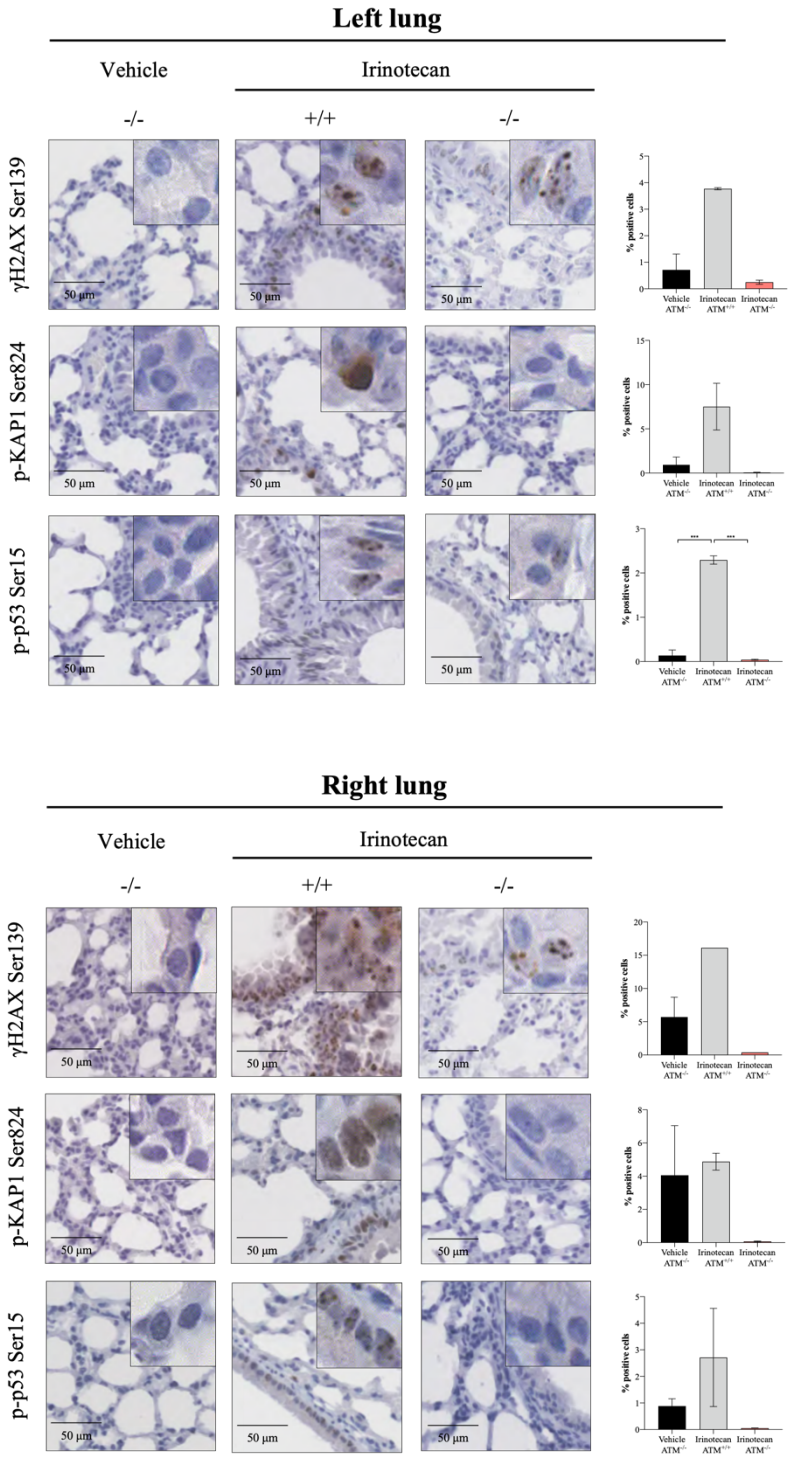
Figure 4.6 | Inhibition of irinotecan-induced ATM signalling with AZ31

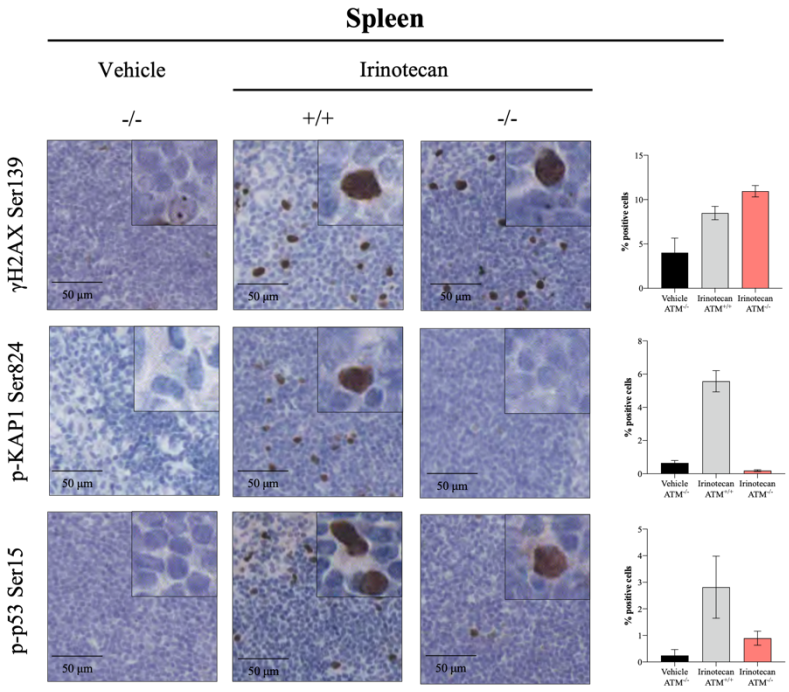
Representative images from C57BL/6 mice tissue sections of irinotecan (100 mg/kg) treatment in the presence or absence of 50 mg/kg AZ31. Positive staining of γH2AX Ser139 (1:500), p-KAP1 Ser824 (1:2000) and p-p53 Ser15 (1:800) visualised by brown DAB staining. Data represented as mean percentage positive cells ± SEM for each marker. Statistical significance denoted by * ($p<0.01$), ** ($p<0.001$) and *** ($p<0.0001$) and performed using two-tailed Student's t-test (n=3). Statistical analysis was not performed on the spleen, upper GI tract (p-p53), middle GI tract (γH2AX, p-KAP1) and lower GI tract (γH2AX) due to insufficient replicates of stained tissue. Sections counterstained with haematoxylin. Images shown at 10X and 40X magnification and quantification performed using QuPath software. Scale bar = 50 µm.

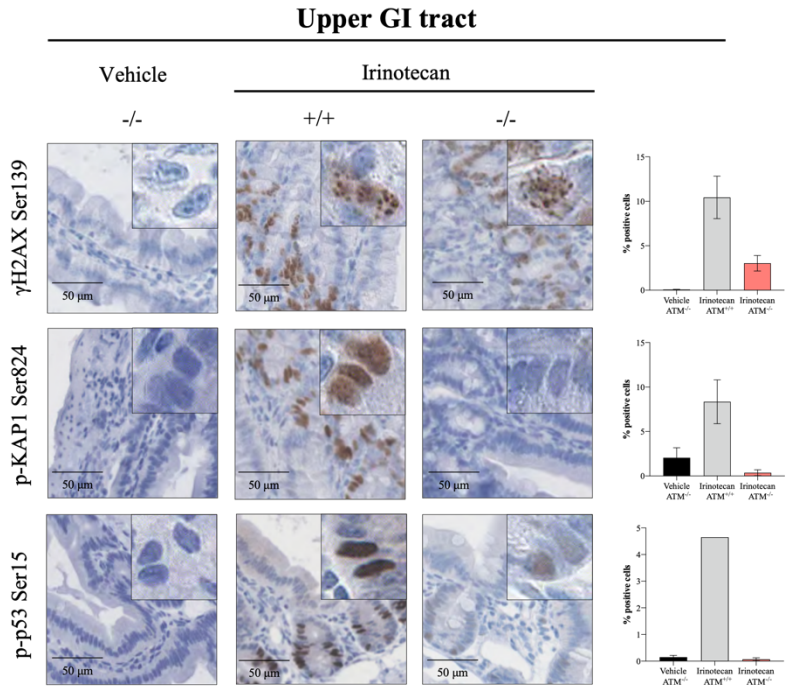
4.7 Genetic loss of ATM function suppresses DDR signalling in response to irinotecan treatment

Irinotecan, in addition to other camptothecin compounds, are reported to show enhanced efficacy against cells with HR defects. Endogenous expression of ATM has been associated with cellular sensitivity to irinotecan treatment. Whilst ATM deficiency was linked to increased chemosensitivity, high expression levels were associated with more resistance to irinotecan monotherapy[300,301].

In parallel to the IR investigations comparing the response of $ATM^{+/+}$ and $ATM^{-/-}$ mice, the study included comparisons in the response to irinotecan. Loss of ATM confers a dampened DDR which is consistently observed across the tissue types (Figure 4.7). However, the extent of this varies between normal tissues. As observed previously in this chapter, the levels of γH2AX staining in the spleen was not lower. Variations between the regions of the small intestine were observed in the $ATM^{-/-}$ mice, such as the detectable levels of p-KAP1.


Left lung
Vehicle
Irinotecan
-/-
+/+
-/-
γH2AX Ser139
p-KAP1 Ser824
p-p53 Ser15
50 µm
% positive cells
Vehicle ATM-/-
Irinotecan ATM+/+
Irinotecan ATM-/-
Right lung
Vehicle
Irinotecan
-/-
+/+
-/-
γH2AX Ser139
p-KAP1 Ser824
p-p53 Ser15
50 µm
% positive cells
Vehicle ATM-/-
Irinotecan ATM+/+
Irinotecan ATM-/-


Spleen
Vehicle
Irinotecan
-/-
+/+
-/-
γH2AX Ser139
p-KAP1 Ser824
p-p53 Ser15
50 µm
% positive cells
Vehicle ATM-/-
Irinotecan ATM+/+
Irinotecan ATM-/-


Upper GI tract
Vehicle
Irinotecan
-/-
+/+
-/-
γH2AX Ser139
p-KAP1 Ser824
p-p53 Ser15
50 µm
% positive cells
Vehicle ATM-/-
Irinotecan ATM+/+
Irinotecan ATM-/-

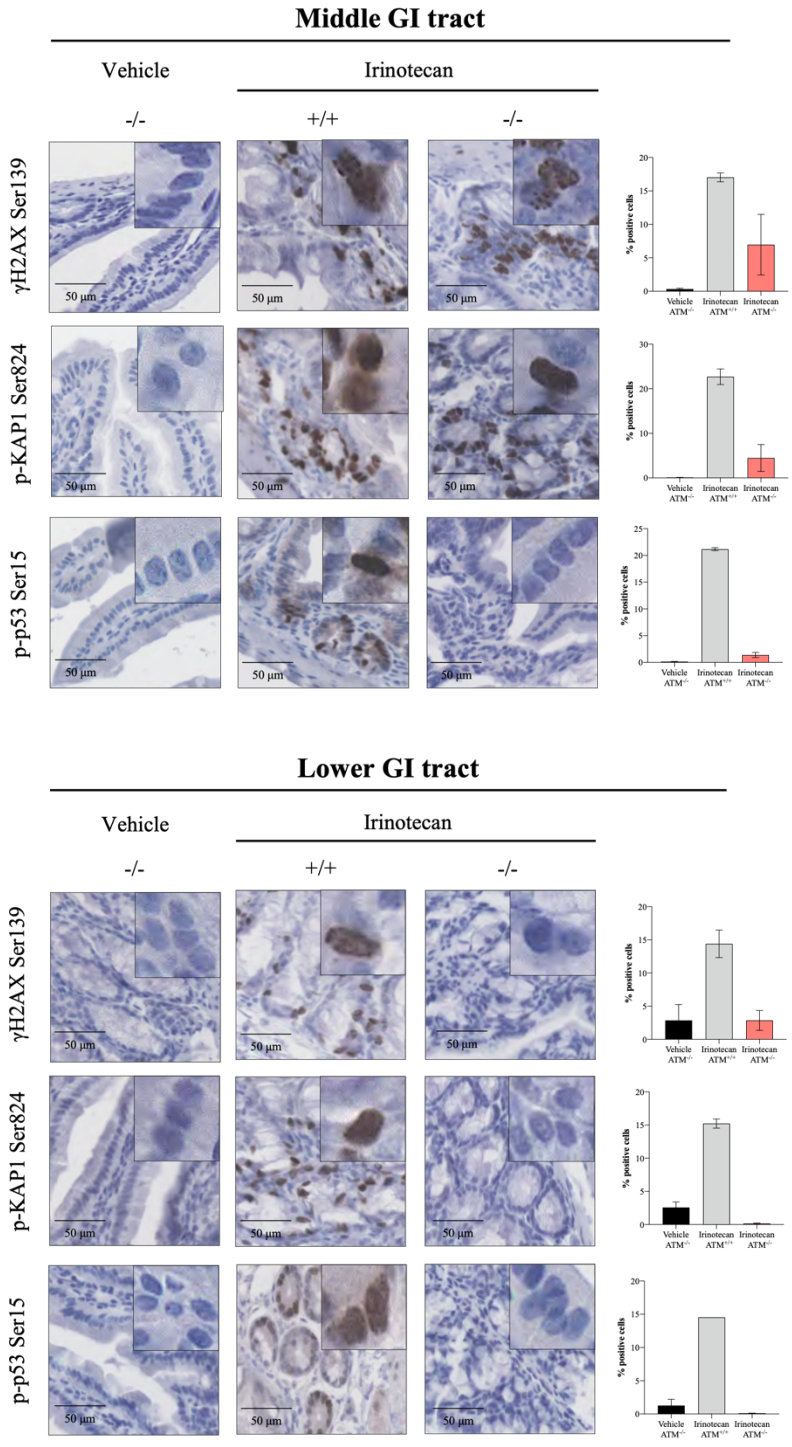


Figure 4.7 | Genetic loss of ATM suppresses irinotecan-induced DDR signalling

Representative images from $ATM^{+/+}$ and $ATM^{-/-}$ mice tissue sections of irinotecan (100 mg/kg) treatment. Positive staining of γH2AX Ser139 (1:500), p-KAP1 Ser824 (1:2000) and p-p53 Ser15 (1:800) visualised by brown DAB staining. Data represented as mean percentage positive cells ± SEM for each marker. Statistical significance denoted by * ($p<0.01$), ** ($p<0.001$) and *** ($p<0.0001$) and performed using two-tailed Student's t-test (n=3). Statistical analysis was not performed on the lungs (γH2AX), spleen, and upper, middle, and lower GI tracts due to insufficient replicates of stained tissue. Sections counterstained with haematoxylin. Images shown at 10X and 40X magnification and quantification performed using QuPath software. Scale bar = 50 µm.

4.8 ATM heterozygosity does not significantly affect DDR in response to IR or irinotecan

The effect of ATM heterozygosity on cellular functioning is uncertain. Several observations support the notion that the loss of one allele corresponds to some abnormalities. A modest increase in radiosensitivity, as well as an increased risk of breast cancer have been reported in individuals with heterozygous mutations of ATM. Modelling ATM haploinsufficiency in mice has demonstrated a modest increase in radiosensitivity and cancer susceptibility. Furthermore, whilst the DSB repair kinetics following single dose IR did not contrast that of ATM-proficient mice, increased residual DSBs were observed in response to fractionated IR compared to $ATM^{+/-}$mice[252,302,303]. In addition, a correlation between radiation sensitivity and ATM expression was reported in human tumour cells[197].

Tissues from heterozygous mice for ATM ($ATM^{+/-}$) were investigated to determine the levels of ATM protein expression that can be detected via IHC. Furthermore, the extent to which ATM signalling can be observed in response to IR and irinotecan was also investigated. Detection of ATM in heterozygote mice was variable between animals (Figure 4.8A). However, consistent with previous data in $ATM^{+/+}$ mice, detection of γH2AX, p-KAP1 and p-p53 was observed following treatment with IR or irinotecan (Figure 4.8B). Comparable levels of positive cells were reported in $ATM^{+/+}$ and $ATM^{+/-}$ mice in response to both IR and irinotecan.

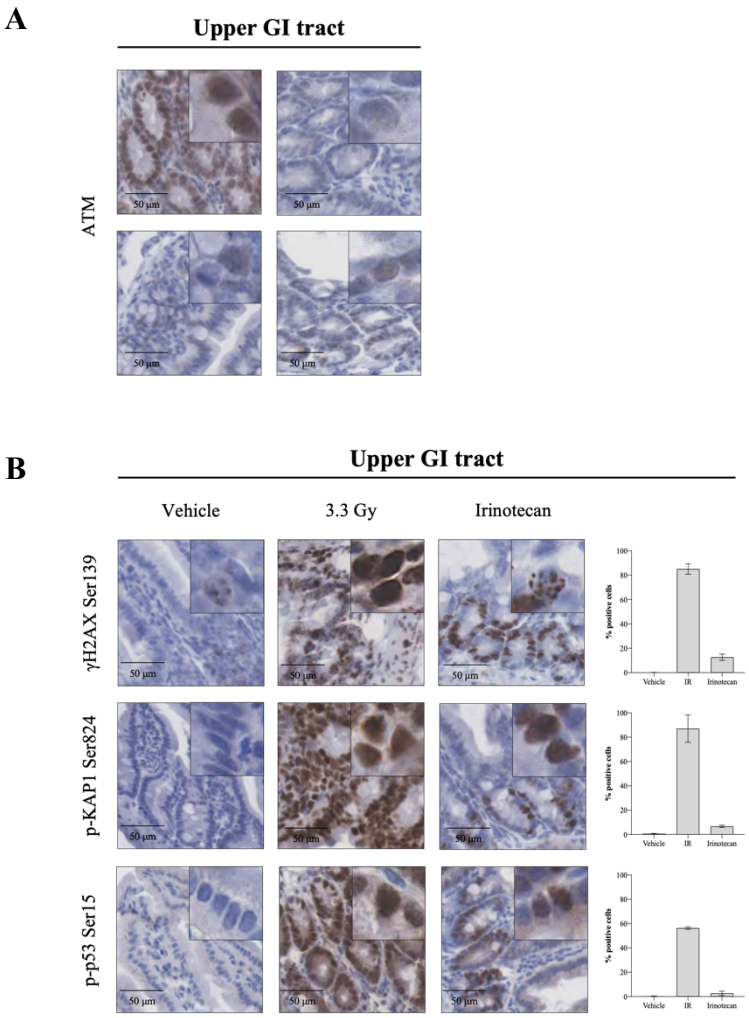


Figure 4.8 | ATM heterozygosity does not significantly affect DDR responses

(A) Representative images from $ATM^{+/-}$ mice tissue sections. Positive staining visualised by brown DAB staining corresponding to ATM (D2E2; 1:200). **(B)** Representative images from $ATM^{+/-}$ mice tissue sections of vehicle, 3.3 Gy or irinotecan (100 mg/kg) treatment. Positive staining of γH2AX Ser139 (1:500), p-KAP1 Ser824 (1:2000) and p-p53 Ser15 (1:800) visualised by brown DAB staining. Data represented as mean percentage positive cells ± SEM for each marker (n=2). **(A, B)** Sections counterstained with haematoxylin. Images shown at 10X and 40X magnification and quantification performed using QuPath software. Scale bar = 50 µm.

4.9 Discussion

Murine models have provided a useful tool to investigate the pathophysiology of A-T and provide insight into disease management and therapeutic options. In addition, the pre-clinical evaluation of the use of ATM inhibitors and synthetic lethal approaches has

supported further compound development and inclusion in clinical trials[156,157,161,304]. In this chapter, an *in vivo* system was used to model the consequences of ATM inhibition and loss on normal tissues in response to whole-body IR or irinotecan. Consistent with human expression of ATM reported in this study, expression of ATM was detected broadly across the panel of murine tissues investigated (Figure 4.1).

In response to whole-body IR (3.3 Gy) or treatment with irinotecan (100 mg/kg), the DDR in C57BL/6 mice appears functional with consistent detection of γH2AX, p-KAP1 and p-p53. Recent supporting evidence demonstrates the dose-dependent increase of γH2AX detected in normal murine tissues following IR and also observed tissue variability in the extent of H2AX phosphorylation[305]. The selected markers used in this chapter have been comprehensively shown to be targets of ATM phosphorylation[306,307]. Whilst γH2AX is indicative of sites of DNA damage, KAP1 phosphorylation (serine 824) is associated with chromatin relaxation and DNA repair at heterochromatin and p-p53 (serine 15) corresponds to transcriptional activation of cell cycle, DNA repair, and apoptosis-related genes[308–310].

Across the tissue panel, the loss or inhibition of ATM conferred broadly similar phenotypes and consistently associated with lower p-KAP1 and p-p53 levels in response to DNA damage. The extent that loss/inhibition of ATM had upon detection levels of γH2AX was variable. The detection of γH2AX in the context of ATM loss in conjunction with evidence implicating contributions of other DDR kinases indicates that γH2AX may lack selectivity for use as a biomarker of ATM activation[311–313]. Inconsistent with other tissue responses, levels of γH2AX in the spleen following IR or irinotecan were unaffected by the inhibition or loss of ATM. This retained H2AX response was an unexpected finding. Interestingly,

DNA-PK has been proposed to have a main role in the phosphorylation of H2AX following IR, specifically in the splenic tissue of C57BL/6 mice[314].

Interestingly, the role of ATM in the DDR to genotoxic agents appears to be tissue dependent. The loss of ATM corresponds to a near-ablation of p-KAP1 in some tissues yet can still be detected in others. Evidence of a suppressed, but present, DDR observed in the lung tissue of $ATM^{-/-}$ mice could be attributed to inherent tissue-specific defects. Elevated inflammatory responses within lung tissues have been reported in ATM-deficient immune cells which are highly sensitive to the induction of DNA damage and oxidative stress, both of which are consequences of IR[12].

In response to irinotecan, the loss of ATM confers lower levels of detectable γH2AX, p-KAP1 and p-p53 however the extent of this is variable, even across the regions of the GI tract. The middle GI tract, which predominantly consists of the jejunum, showed a greater level of DDR activation in response to irinotecan than the duodenum (upper) and ileum (lower). Toxicity issues of irinotecan primarily affect the small intestine, and is considered dose-limiting for clinical administration[296]. Differences in the extent that AZ31 suppresses the DDR could be attributed to drug pharmacokinetics. Tissue variations in the absorption, distribution, metabolism, and excretion of AZ31 may account for such differences. The concentration of AZ31 after 45 minutes following oral administration of 50 mg/kg has been evaluated. Highest levels were reported in the liver, followed by the small intestine and kidney, comparable levels in the colon, spleen, lung, and heart, and absence in the brain[315]. The residual DDR observed in AZ31-treated mice could also be a consequence of incomplete target inhibition. The data from this chapter revealed that the extent to which ATM inhibition or loss suppresses the DDR to IR or irinotecan is variable across normal

murine tissues, indicative that this is a biological observation rather than entirely pharmacological.

Data from this chapter have confirmed the effect of IR on normal tissues, with a robust DDR observed across entire tissues. Previous investigations have focused on normal tissue tolerance to radiation, effects of radiation on the tumour microenvironment and cytotoxic tumour effects, all of which can help inform clinical practice[273,316]. Whilst the effects of IR on normal tissues have been studied and validated, the normal tissue response to irinotecan has received less attention[273,305,317]. Analysis of markers associated with DDR activation (γH2AX, p-KAP1, p-p53) and the S phase marker, BrdU support the replication associated DNA DSB as a predominant mechanism of irinotecan toxicity. However, an interesting observation was the detection of γH2AX and pKAP1 in the broncho-epithelial cells of the lung. The lung is a relatively non-proliferative tissue, and these cells were not labelled with BrdU, indicative of an irinotecan-induced response outside of S phase. Furthermore, the detection of γH2AX foci in the broncho-epithelial cells is suggestive of irinotecan-induced non-S phase DNA damage. This finding appears to be ATM dependent as it was not observed in the context of ATM loss. Additional reports have implicated that irinotecan can exert cytotoxic effects on non-S phase cells. Here, it has been proposed that irinotecan-induced apoptosis is a consequence of transcriptionally mediated DNA damage in cells outside of S-phase[294,318]. In addition, detection levels of p-KAP1 in cardiac tissue did not correspond to BrdU staining levels in irinotecan-treated mice. The potential biological significance of these incidental findings requires further investigation.

The evaluation of ATM expression in the upper GI tracts of mice heterozygote for ATM revealed variable detection. Whilst this study could require further optimisation, the inconsistent expression of ATM seen here may reflect a potential variability in the clinical

presentation in ATM mutation carriers. However, a robust DDR was observed following IR or irinotecan treatment in the upper GI tract. In addition, these responses were comparable to those seen in $ATM^{+/+}$ mice. Furthermore, evidence of a DSB repair defect identified by the level of unrepaired DSBs has been reported following fractionated IR, but not single dose IR in $ATM^{+/-}$ mice[303]. Evaluation of ATM expression and function in additional tissues would be of interest to determine the presence of tissue-dependent effects.

Overall, this chapter has demonstrated the role of ATM in the DDR of normal tissues following exposure to IR or irinotecan. This is believed to be the first demonstration of *in vivo* induction of DNA DSBs in normal tissues by irinotecan, confirming the proposed selective action on S phase cells. Interestingly, tissue specific DNA damage responses have been observed that may provide insight into the effects of ATM activating treatments across different tissues and considerations for the use of ATM inhibitors.

5 The effect and consequences of ATM inhibition versus ATM loss

Genomic instability, promoted through the acquisition of mutations and high levels of DNA damage, is an inherent feature of tumour cells and has been proposed as an enabling characteristic contributing to the hallmarks of cancer. Such DNA damage occurs through endogenous stressors, such as hypoxia, oxidative damage, replication stress or the loss of DDR pathways[319–321]. Oncogenic stress drives the formation of DNA DSBs caused through stalled replication fork collapse. The stalling of replication forks can be induced by several factors including premature origin firing, unrepaired base lesions, depletion of deoxynucleotide pools, ribonucleotide misincorporation, the formation of aberrant DNA secondary structures or conflicts between transcription and replication processes. In addition, there are genomic regions, known as common fragile sites, that are particularly vulnerable to forming gaps or breaks in response to replication stress. These sites are considered hotspots for copy-number variation and chromosomal rearrangements in cancer[144,322,323].

Oncogene activation has been associated with increased replication stress and subsequent DNA damage in cancer. Activation of DDR pathway signalling is proposed to restrict the hyperproliferation of abnormal cells to provide a barrier against tumour development[45,324]. A key component of this defence mechanism may be through contributions of the tumour suppressor, p53. Furthermore, p53 has the highest incidence of mutations in human cancers which provides a selective pressure for mutation as a means for evading this DDR hurdle. In addition, the deregulation of several other components of the DDR network, such as ATM and BRCA1/2, have been reported in human cancer[325–327]. Defective DNA repair

pathways, whilst on one hand may promote unregulated proliferation, may also render cells susceptible to treatment modalities that would normally trigger their activation. This deficiency may also drive an increased reliance of cancer cells on compensatory DDR pathways, which may be exploited through the concept of synthetic lethality. Two genes are considered to be synthetically lethal if only the simultaneous loss of both genes, or their respective gene products, leads to cell death whilst independent inactivation of either does not impact viability. In the instance of a DDR-deficient cancer cell, pharmacological targeting of a compensatory DDR pathway may be selectively toxic to the tumour. Theoretically, non-tumour cells are able to withstand, or tolerate, such targeted therapy through the primary pathway remaining intact. The inability for a cell to repair this DNA damage, in addition to the high levels of DNA damage inherent to cancer cells, triggers cell death. As such, deficiencies in DNA repair machinery have been considered an Achilles' heel of cancer. A popular example of this is demonstrated by the excellent efficacy of PARP inhibitors against BRCA1/2 mutant cancer cells[121–124,126].

ATM plays a crucial role in the detection of DSBs and coordinating their repair with temporary cell cycle arrest through enforcement of DNA damage-induced checkpoints. The sophisticated orchestration of these processes relies on the recruitment and activation of numerous substrates that contribute to a complex signalling cascade. In addition, a cytoplasmic role of ATM involves mediating the response to genotoxic stressors, such as ROS[108]. As a key regulator of such processes, ATM has received considerable interest as a potential target for cancer therapy. Following the development of several ATM inhibitors, pre-clinical studies have explored two overall strategies for targeting ATM. Firstly, the administration of an ATM inhibitor as a monotherapy to determine synthetically lethal approaches and secondly, the combination of an ATM inhibitor with other genotoxic modalities, such as chemo- or radiotherapy. Data from these studies have

supported the continued development of ATM inhibitors aiming to transform a genetic principle into a pharmacological, and clinically viable, application[94,321,328,329]. Detailed information on the development of ATM inhibitors has been summarised in Table 1.1.

Somatic ATM mutations are a frequent occurrence in various solid and haematological malignancies where the impact on functional ATM can vary from impairment to complete loss[132,189,197]. The implications of targeting tumours that lack ATM is an attractive concept under the biological rationale that ATM-deficient tumours would exhibit heightened sensitivity to radiotherapy as well as some chemotherapeutic agents. From a clinical perspective, the intrinsic sensitisation conferred by ATM could offer potential for the delivery of targeted therapeutic approaches. The ATM inhibitors, AZD1056, AZD1390 and KU-60019 are currently undergoing clinical trials (NCT02588105, NCT03423628, NCT03215381 and NCT03571438)[156,157,161].

Interestingly, there are different phenotypes between the loss and pharmacological inhibition of ATM. Replication fork repair following IR is functional in A-T cells but aberrant in ATM-inhibited cells[293]. This has been recapitulated in murine models where the knockout of ATM is viable and can be tolerated however expression of physiological levels of kinase dead (kd) ATM causes embryonic lethality[253]. It has been proposed that the expression of ATM protein that lacks functional kinase activity can bind to sites of DNA DSBs therefore blocking alternative DNA response proteins accessing the damage site. As a result, repair is hindered leading to persistent DNA damage[253,256].

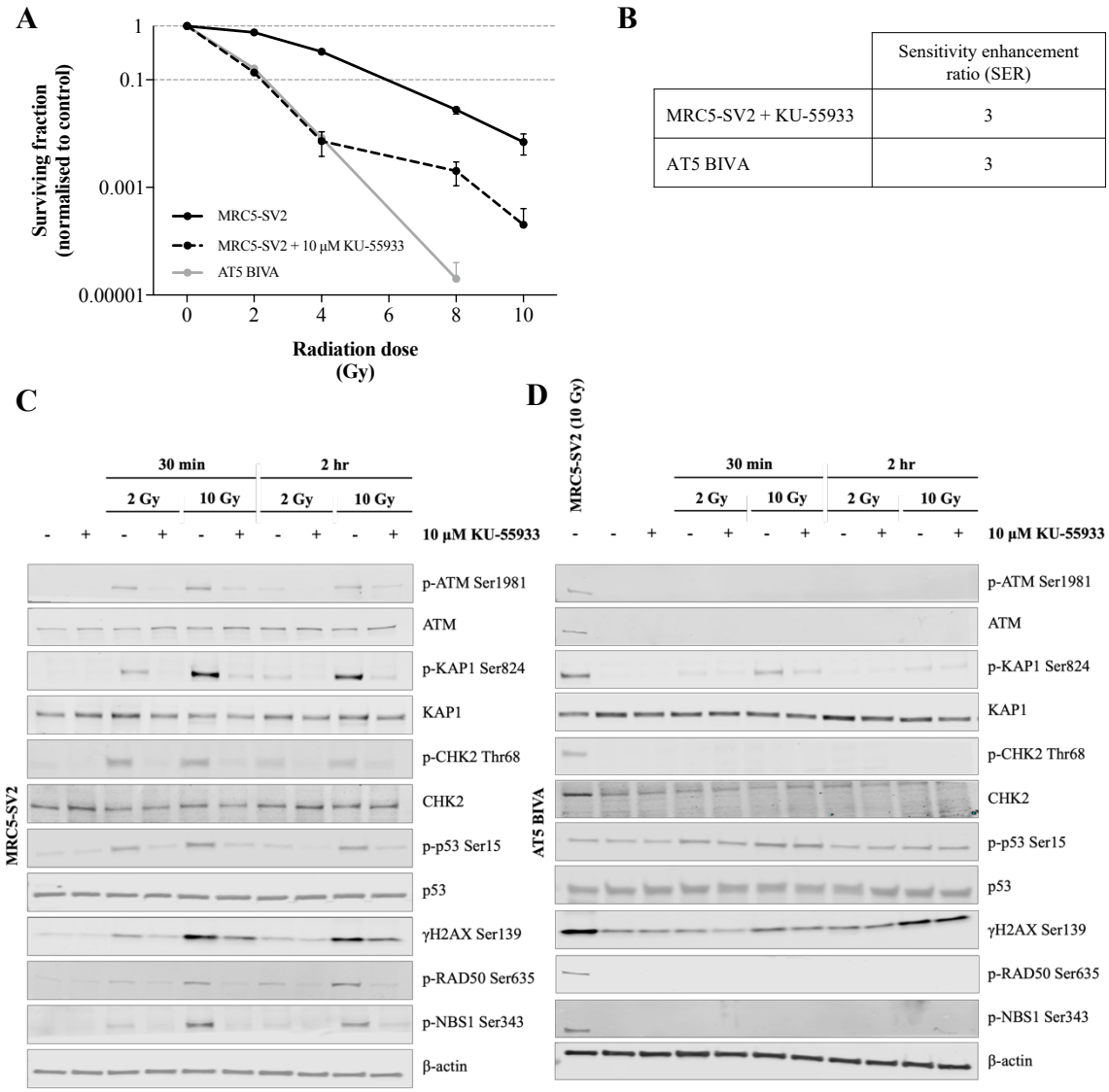
The studies described in this chapter aimed to investigate the effect and consequences of ATM inhibition versus ATM loss in the context of both non-tumour and tumour settings. This molecular investigation of ATM activation and signalling also aimed to identify potential synthetic lethality associated with the loss of functional ATM.

5.1 Sensitivity of human non-tumour lung fibroblasts to radiation and cytotoxic compounds

5.1.1 Loss of ATM confers radiosensitivity in lung fibroblasts

The inability of cells to respond to DNA DSBs renders them susceptible to genomic stress. The consequences of loss of functional ATM on increased sensitivity to IR has been well documented[330,331]. A non-tumour human lung fibroblast pair was used to investigate the effect of ATM deficiency. Whilst not an isogenic pair, AT5 BIVA cells obtained from an A-T patient provide a useful tool for modelling ATM loss in comparison to the ATM wildtype, MRC5-SV2 cell line. Immortalisation of these fibroblast lines was achieved through Simian virus 40 (SV40) transformation[332–334].

To confirm functional status of ATM activity in the fibroblast pair, the intrinsic radiation sensitivity of both cell lines was assessed. In addition, pharmacological inhibition of ATM was included. The selective ATM kinase inhibitor, KU-55933 (10 μM) has been reported to inhibit ATM at an IC_{50} of 12.9 nM from cell-free assays[160]. Assessment of surviving fractions of cells following dose-range exposure to IR was consistent with the acknowledged role of ATM in the cellular response to IR. A sensitivity enhancement ratio (SER) of 3 was observed in the context of both ATM inhibition and ATM loss (Figure 5.1A, B). Pre-treatment with 10 μM KU-55933 did not further sensitise AT5 BIVA cells (data not shown).



	Sensitivity enhancement ratio (SER)
MRC5-SV2 + KU-55933	3
AT5 BIVA	3

Figure 5.1 | ATM loss confers radiosensitisation in lung fibroblasts

(A) Clonogenic survival of MRC5-SV2 in the presence or absence of 10 µM KU-55933 versus AT5 BIVA. Data shown as mean ± SEM of two independent experiments (n=2) performed in triplicate. **(B)** SER reported at a surviving fraction of 10% compared to MRC5-SV2. **(C, D)** Western blots of MRC5-SV2 and AT5 BIVA fibroblasts exposed to 2 Gy or 10 Gy of IR. Lysates were collected at 30 minutes and 2 hours post-IR for each dose including 1 hour pre-treatment with 10 µM KU-55933 where appropriate. Representative blots (n=2) shown including loading control (β-actin). **(D)** MRC5-SV2 cells treated with 10 Gy IR included in first column used as positive control.

Confirmation of an intact cellular response in MRC5-SV2 cells following IR-induced DNA damage was shown through examination via Western blot (Figure 5.1C). Cells were

irradiated with a 'low' (2 Gy) or 'high' (10 Gy) dose and lysed at both 30 minutes and 2 hours post-IR to investigate ATM signalling. KU-55933 pre-treatments were included to block ATM-dependent kinase activation of downstream targets. The dose-dependent increase of DNA DSBs could be visualised by phosphorylation of H2AX. Evidence of ATM pathway activation in response to IR was shown by phosphorylation of ATM, KAP1, CHK2, p53, RAD50 and NBS1. These changes were less evident at 2 hours post-IR, indicative of DNA lesion repair. The pre-treatment of KU-55933 reduced target phosphorylation in each case.

In contrast, AT5 BIVA cells showed an inability to phosphorylate the majority of these ATM-dependent targets in response to IR (Figure 5.1D). Interestingly, the phosphorylation of KAP1 at serine 824 could be detected at 30 mins post-IR (10 Gy) which was diminished at the 2-hour timepoint. The diminished response might represent resolution of DNA damage and dissolution of repair complexes. The observation of high baseline p-p53, with minimal increase at 30 minutes post-IR, was noted across all conditions.

5.1.2 ATM plays a role in the response of lung fibroblasts to chemotherapeutic compounds

Alongside the profound radiosensitisation effect seen with ATM deficiency, the disruption of ATM function could also lead to increased sensitivity to chemotherapeutic drugs. Selective inhibitors of ATM have been reported to render cancer cells sensitive to classic DSB-inducing compounds. For instance, the loss of ATM kinase activity in both p53-functional and p53-deficient cells increased chemosensitivity to topoisomerase I (camptothecin, topotecan) and II (doxorubicin, epirubicin and etoposide) poisons[160,164,335]. Furthermore, the combination of irinotecan with the ATM inhibitor, AZ31, demonstrated efficacy against tumours previously reported as irinotecan-resistant[166]. In addition, studies

have shown loss of ATM function in PTEN-deficient breast cancer cells and in p53-deficient cells enhances sensitivity to cisplatin and antimetabolites (5-fluorouracil and gemcitabine) respectively[335,336].

To evaluate the non-tumour consequences of ATM loss versus inhibition, the sensitivity of lung fibroblasts to several clinically approved chemotherapeutic drugs was assessed. Cell viability was analysed following cell treatment with a dilution series of paclitaxel, etoposide, gemcitabine, cisplatin, irinotecan, or SN-38. Information regarding the mechanisms of action and clinical applications of the chemotherapeutic drugs tested is listed in Table 5.1.

Table 5.1 | Overview of chemotherapeutic drugs

Drug	Mechanism of action	Cell cycle phase	Clinical applications	References
Paclitaxel	Stabilisation of GDP-bound tubulin and promotes microtubule polymerisation and aggregation	G1, G2/M	Ovarian, NSCLC, breast, and Kaposi sarcoma	[337–339]

Etoposide	Topoisomerase II inhibitor; binds to intermediate enzyme-DNA complex to prevent DNA re-ligation	S, G2	Lymphoma, testicular, lung and sarcoma	340–342
Gemcitabine	Deoxycytidine analogue; incorporates into DNA causing the premature termination of replication as well as fork stalling	S	Bladder, ovarian, breast, pancreatic and NSCLC	343–346
Cisplatin	Forms both intra- and inter-strand crosslinks to interfere with DNA replication	Not cell cycle specific	Head and neck, bladder, ovarian, testicular, cervical, lung, breast and oesophageal	347,348

Irinotecan	Topoisomerase I inhibitor; prevents DNA strand relegation through binding to the enzyme-DNA complex to induce replication arrest, SSBs and subsequent DSB formation	S	Colorectal	[294–296]
SN-38	Active metabolite of irinotecan	S	N/A	[294,296,349]

Investigations into the role of ATM for determining sensitivities to chemotherapeutic drugs revealed that the impact of ATM inhibition may not always correspond to that of ATM loss (Figure 5.2A). Inhibition of topoisomerase I and II, with irinotecan and etoposide respectively, in combination with ATM inhibition appears to moderately sensitise MRC5-SV2 cells at the lower doses used. In comparison, the loss of ATM, as illustrated by AT5 BIVA cells, demonstrates significantly increased sensitivity to both of these agents. Interestingly, the most noticeable sensitisation was observed in AT5 BIVA cells following treatment with SN-38. IC_{50} values in Table 5.2 reflect the profound sensitivity to SN-38 seen in the context of ATM loss (50-fold) but not ATM inhibition (1.6-fold). However, the consequences of ATM loss and ATM inhibition appear consistent in response to paclitaxel treatment (Figure 5.2A, Table 5.2). A modest effect of ATM loss was observed with gemcitabine and cisplatin treatment, with the latter at higher doses.

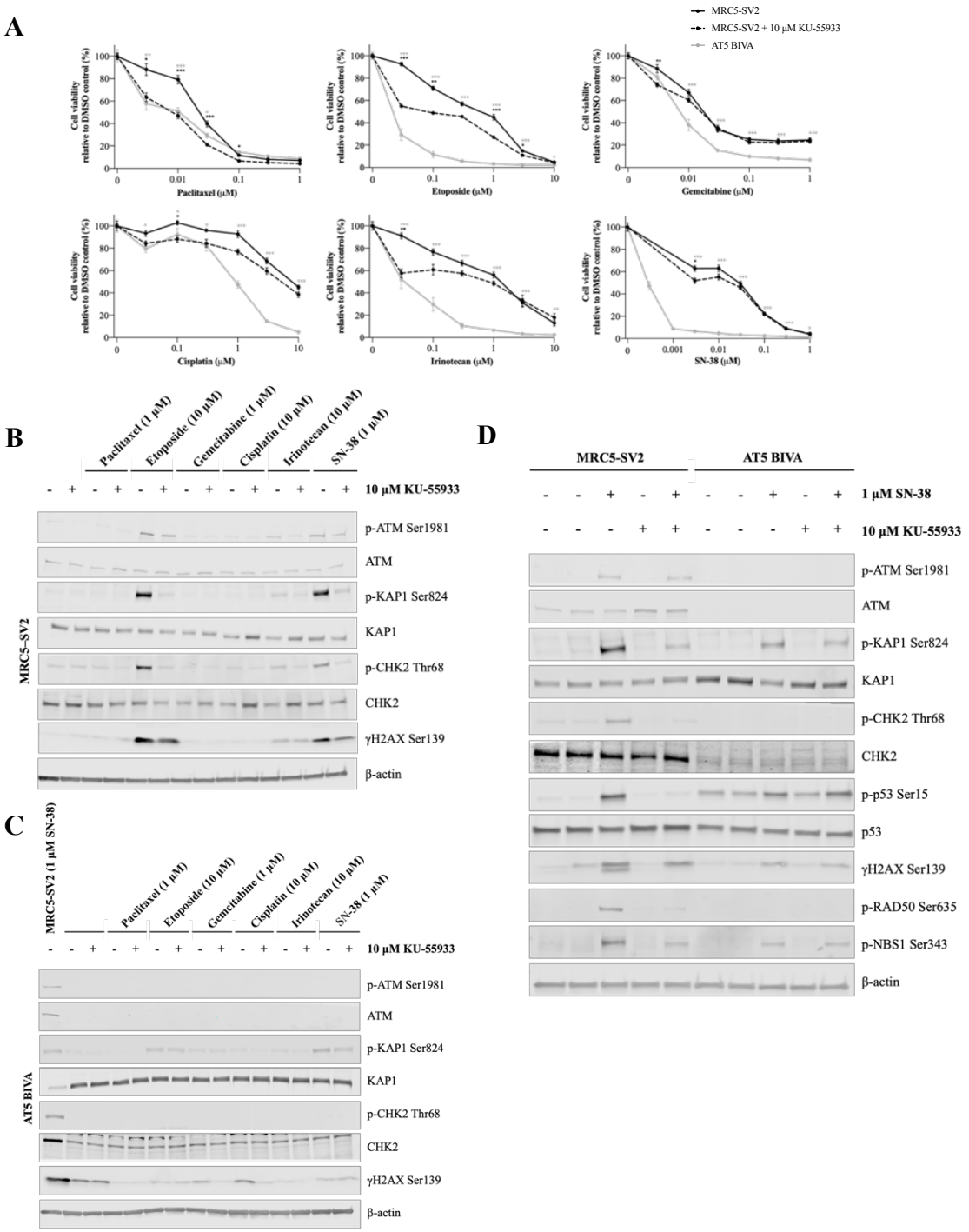


Figure 5.2 | ATM has a role in the fibroblast response to chemotherapeutic drugs

(A) Cell viability of MRC5-SV2 in the presence or absence of 10 µM KU-55933 versus AT5 BIVA following exposure to a dilution series of paclitaxel, etoposide, gemcitabine, cisplatin, irinotecan, or SN-38. Data shown as mean ± SEM of at least four independent experiments (n=4) performed in triplicate. Statistical significance denoted by * ($p<0.01$), ** ($p<0.001$) and *** ($p<0.0001$). **(B, C)** Western blot of MRC5-SV2 and AT5 BIVA fibroblasts treated with chemotherapeutic drugs in the presence or absence of 10 µM KU-55933. **(D)** Western blot of MRC5-SV2 and AT5 BIVA fibroblasts exposed to 1 µM SN-38 including a pre-treatment with 10 µM KU-55933 where indicated. **(B, C, D)** Representative blots (MRC5-SV2, n=2; AT5 BIVA, n=1; fibroblasts, n=2) shown including β-actin loading control.

Table 5.2 | Sensitivity of ATM wildtype, ATM inhibited and ATM mutant lung fibroblasts to paclitaxel, etoposide, gemcitabine, cisplatin, irinotecan, and SN-38

	Paclitaxel mean IC_{50} (nM) (+/- SEM range)	**Etoposide mean IC_{50} (µM)** (+/- SEM range)	**Gemcitabine mean IC_{50} (nM)** (+/- SEM range)	**Cisplatin mean IC_{50} (µM)** (+/- SEM range)	**Irinotecan mean IC_{50} (µM)** (+/- SEM range)	**SN-38 mean IC_{50} (nM)** (+/- SEM range)
MRC5-SV2	**18.34** (15.10 – 21.58)	**0.44** (0.33 – 0.55)	**10.62** (8.81 – 12.44)	**6.24** (5.97 – 6.51)	**0.82** (0.66 – 0.98)	**16.67** (13.84 – 19.49)
MRC5-SV2 + 10 µM KU-55933	**7.40** (5.15 – 9.65)	**0.11** (0.09 – 0.12)	**8.96** (7.98 – 9.94)	**3.89** (3.57 – 4.21)	**0.39** (0.24 – 0.54)	**10.71** (9.09 – 12.32)
AT5 BIVA	**7.86** (4.98 – 10.74)	**0.03** (0.02 – 0.04)	**7.5** (5.49 – 9.50)	**0.77** (0.59 – 0.94)	**0.06** (0.03 – 0.08)	**0.33** (0.28 – 0.38)

The extent that these chemotherapeutic drugs can activate the canonical ATM DDR signalling pathway in lung fibroblasts was investigated. Cells were pre-treated with 10 µM KU-55933 for 1 hour prior to treatment with 1 µM paclitaxel, 10 µM etoposide, 1 µM gemcitabine, 10 µM cisplatin, 10 µM irinotecan or 1 µM SN-38 for one hour. Activation of the ATM pathway could only be visualised by phosphorylation of ATM, KAP1, CHK2 and H2AX in response to exposure to the topoisomerase I (irinotecan, SN-38) and II

(etoposide) poisons (Figure 5.2B). A modest response of irinotecan, in comparison to etoposide and SN-38, was noted. As expected in the context of ATM loss, phosphorylation of ATM and CHK2 was not detected (Figure 5.2C). Evidence for ATM-independent phosphorylation of KAP1 was observed in AT5 BIVA cells treated with either etoposide or SN-38. In addition, elevated levels of p-KAP1 serine 824 may also be detectable following gemcitabine and irinotecan. Phosphorylation of H2AX was observed in AT5 BIVA cells following etoposide and SN-38 treatment as well as gemcitabine, cisplatin, and irinotecan however in the instance of the latter three conditions, an off-target effect of KU-55933 is seen. Furthermore, high baseline γH2AX serine 139 levels were detected in AT5 BIVA control conditions.

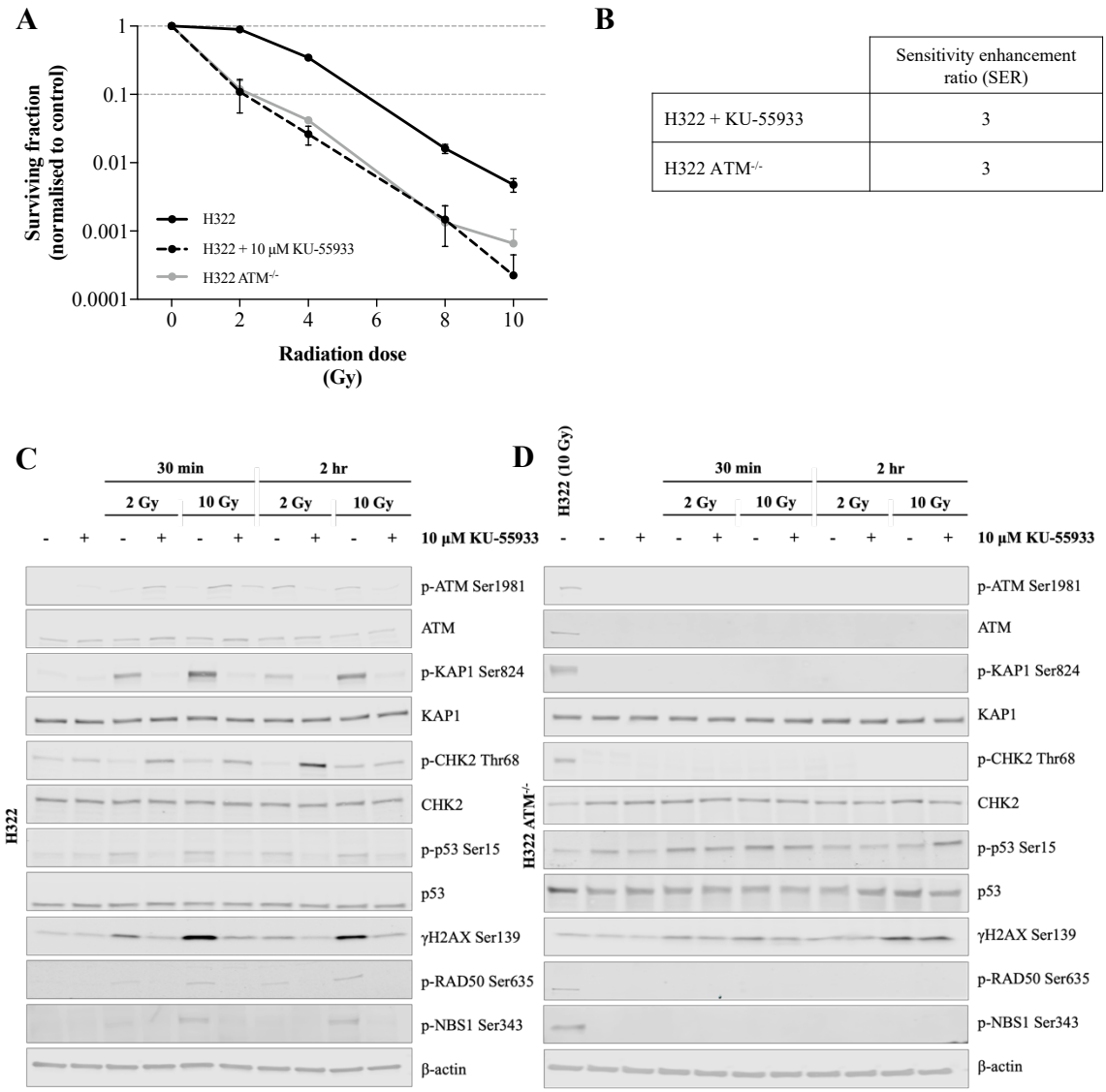
The profound response observed with loss of ATM in lung fibroblasts on the sensitivity to SN-38 was not recapitulated with the use of pharmacological inhibition. Furthermore, the detection of pKAP1 serine 824, a substrate considered ATM-dependent, in AT5 BIVA fibroblasts sparked additional interest. To explore the DNA damage signalling pathway in more detail, activation of additional targets was investigated in response to SN-38. Using the same experimental design as before, fibroblasts were pre-treated with 10 μM KU-55933 followed by 1 μM SN-38 (Figure 5.2D). An ATM-dependent response was observed in the MRC5-SV2 fibroblasts where the SN-38-induced phosphorylation of ATM, KAP1, CHK2, p53, RAD50 and NBS1 which was dampened by addition of the ATM inhibitor. Consistent with previous findings, p-KAP1 serine 824 was detected in AT5 BIVA cells in response to SN-38. Furthermore, phosphorylation of the MRN component, NBS1, was also observed. In addition, the overall response in AT5 BIVA fibroblasts appears limited in comparison to the wildtype, MRC5-SV2. There was no evidence of ATM, CHK2 orRAD50 phosphorylation in the AT5 BIVA cells. Observed levels of baseline pp53 were higher in AT5 BIVA than MRC5-SV2.

5.2 Sensitivity of human lung isogenic tumour cells to radiation and cytotoxic compounds

5.2.1 Loss of ATM confers radiosensitivity in lung tumours

The notion of targeting loss of ATM with radiotherapy stemmed from the observation of a profound cellular and clinical radiosensitivity phenotype[38,131]. To compare tumour cell responses to the previous fibroblast data, the isogenic H322 lung cell pair for ATM loss was used. Confirmation for the loss of functional ATM can be observed through investigating intrinsic radiation sensitivity. Pharmacological inhibition of ATM with 10 μM KU-55933 was also included in parallel. Consistent with the acknowledged role of ATM, both inhibition and loss corresponded to a SER of 3 (Figure 5.3A, B). In addition, the H322 $ATM^{-/-}$ did not exhibit increased sensitivity with the addition of KU-55933 (data not shown).

Assessment of the cellular response to IR was performed using Western blot (Figure 5.3B). Activation of the DDR was evident from the ATM-dependent phosphorylation of ATM, KAP1, CHK2, p53, H2AX, RAD50 and NBS1 in H322 cells. A greater response was observed in response to 10 Gy in comparison to 2 Gy. In contrast, H322 $ATM^{-/-}$ were unable to phosphorylate the majority of these targets. Exceptions to this include the IR-induced H2AX phosphorylation as well as high baseline protein levels of p-p53 serine 15, with modest increase in IR conditions.



	Sensitivity enhancement ratio (SER)
H322 + KU-55933	3
H322 ATM$^{-/-}$	3

Figure 5.3 | ATM loss confers radiosensitisation in isogenic lung tumour pair

(A) Clonogenic survival of H322 in the presence or absence of 10 μM KU-55933 versus H322 ATM$^{-/-}$. Data shown as mean ± SEM of two independent experiments (n=2) performed in triplicate. **(B)** SER reported at a surviving fraction of 10% compared to H322. **(C, D)** Western blots of H322 and H322 ATM$^{-/-}$ exposed to 2 Gy or 10 Gy of IR. Lysates were collected at 30 minutes and 2 hours post-IR for each dose including 1 hour pre-treatment with 10 μM KU-55933 where appropriate. Representative blots (n=2) shown including loading control (β-actin). **(D)** H322 cells treated with 10 Gy IR included in first column as positive control.

5.2.2 ATM plays a role in the response of lung tumour cells to chemotherapeutic compounds

Combining chemotherapeutic drug treatments with DNA repair inhibitors has received considerable scientific interest. The panel of chemotherapeutic drugs in 5.1.2 were used against the H322 isogenic cell line pair to explore the effects of ATM inhibition and loss on chemosensitivity in a tumour cell context. Of the six agents tested, increased sensitivity could only be observed in response to etoposide and irinotecan treatment, which was also seen in the fibroblast data. Comparison of IC_{50} values showed varying effects of the loss of ATM function in response to the chemotherapeutic drugs (Table 5.3). In contrast to the profound sensitivity with ATM deficiency in fibroblasts to SN-38, no difference in SN-38 sensitivity was observed between the wildtype, ATM-inhibited and ATM-deficient tumour cells (Figure 5.4). Furthermore, neither the inhibition or loss of ATM in H322 cells sensitised to paclitaxel, gemcitabine, or cisplatin.

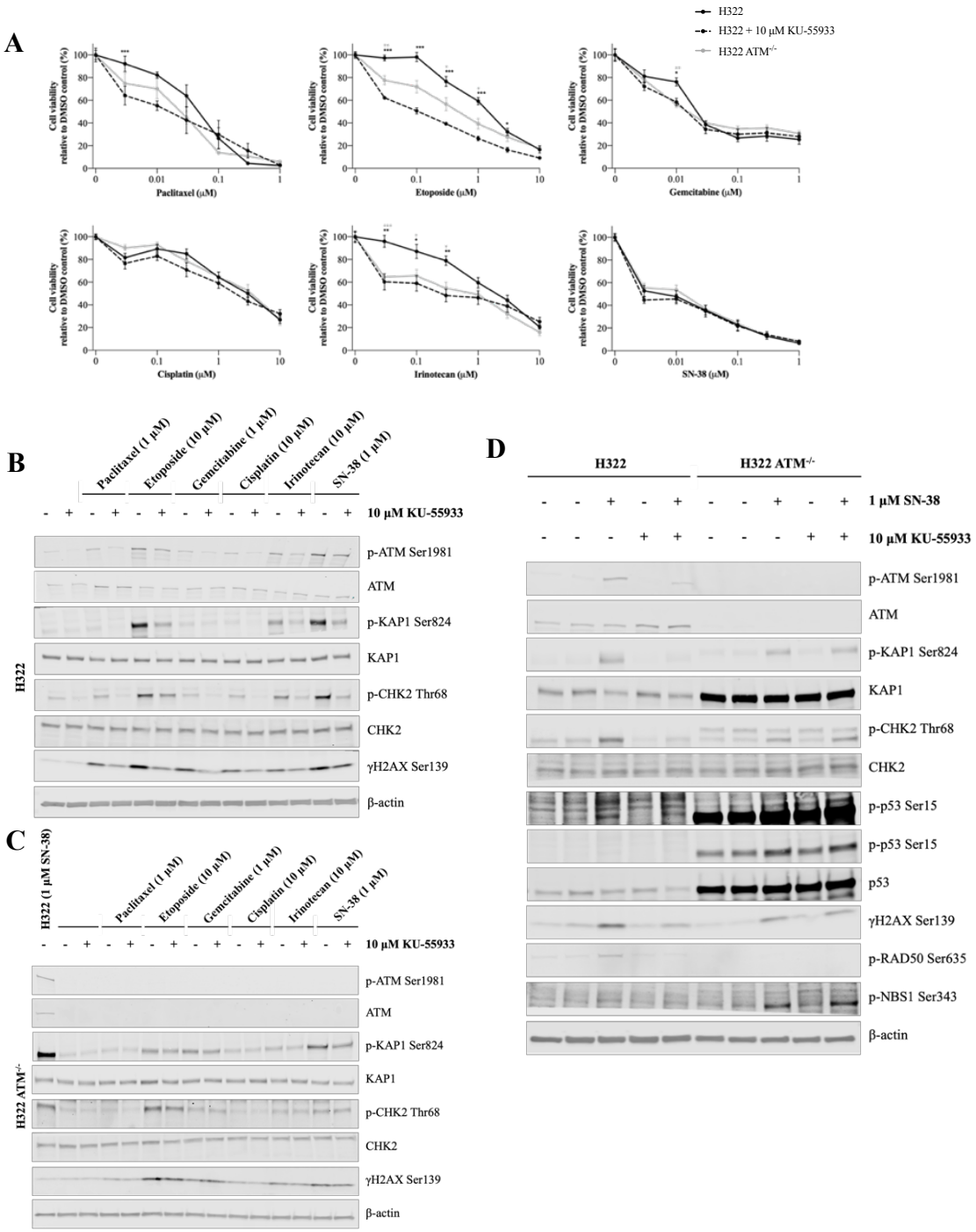


Figure 5.4 | ATM has a role in the tumour response to chemotherapeutic drugs

(A) Cell viability of H322 in the presence or absence of 10 µM KU-55933 versus H322 ATM$^{-/-}$ following exposure to a dilution series of paclitaxel, etoposide, gemcitabine, cisplatin, irinotecan, or SN-38. Data shown as mean ± SEM of at least four independent experiments (n=4) performed in triplicate. Statistical significance denoted by * ($p<0.01$), ** ($p<0.001$) and *** ($p<0.0001$). **(B, C)** Western blot of H322 and H322 ATM$^{-/-}$ tumour cells treated with chemotherapeutic drugs in the presence or absence of 10 µM KU-55933. **(C)** H322 cells treated with 1 µM SN-38 included in first column as positive control. **(D)** Western blot of H322 and H322 ATM$^{-/-}$ tumour cells exposed to 1 µM SN-38 including a pre-treatment with 10 µM KU-55933 where indicated. **(B, C, D)** Representative blots (H322, n=2; H322 ATM$^{-/-}$, n=2; tumour, n=1) shown including β-actin loading control.

Table 5.3 | Sensitivity of ATM wildtype, ATM inhibited and ATM deficient lung tumour cells to paclitaxel, etoposide, gemcitabine, cisplatin, irinotecan, and SN-38

	Paclitaxel mean IC_{50} (nM) (+/- SEM range)	**Etoposide mean IC_{50} (µM)** (+/- SEM range)	**Gemcitabine mean IC_{50} (nM)** (+/- SEM range)	**Cisplatin mean IC_{50} (µM)** (+/- SEM range)	**Irinotecan mean IC_{50} (µM)** (+/- SEM range)	**SN-38 mean IC_{50} (nM)** (+/- SEM range)
H322	**50.39** (20.02 – 80.76)	**1.09** (0.90 – 1.28)	**21.43** (17.59 – 25.27)	**1.84** (1.53 – 2.14)	**1.20** (1.12 – 1.27)	**11.45** (0.49 – 22.42)
H322 + 10 µM KU-55933	**26.46** (5.15 – 47.77)	**0.10** (0.08 – 0.12)	**9.81** (7.80 – 11.82)	**0.96** (0.72 – 1.20)	**0.24** (0.05 – 0.42)	**8.63** (3.63 – 13.63)
H322 $ATM^{-/-}$	**23.19** (14.72 – 31.67)	**0.37** (0.19 – 0.55)	**9.83** (8.45 – 11.22)	**1.81** (1.31 – 2.31)	**0.53** (0.18 – 0.89)	**12.11** (4.37 – 19.84)

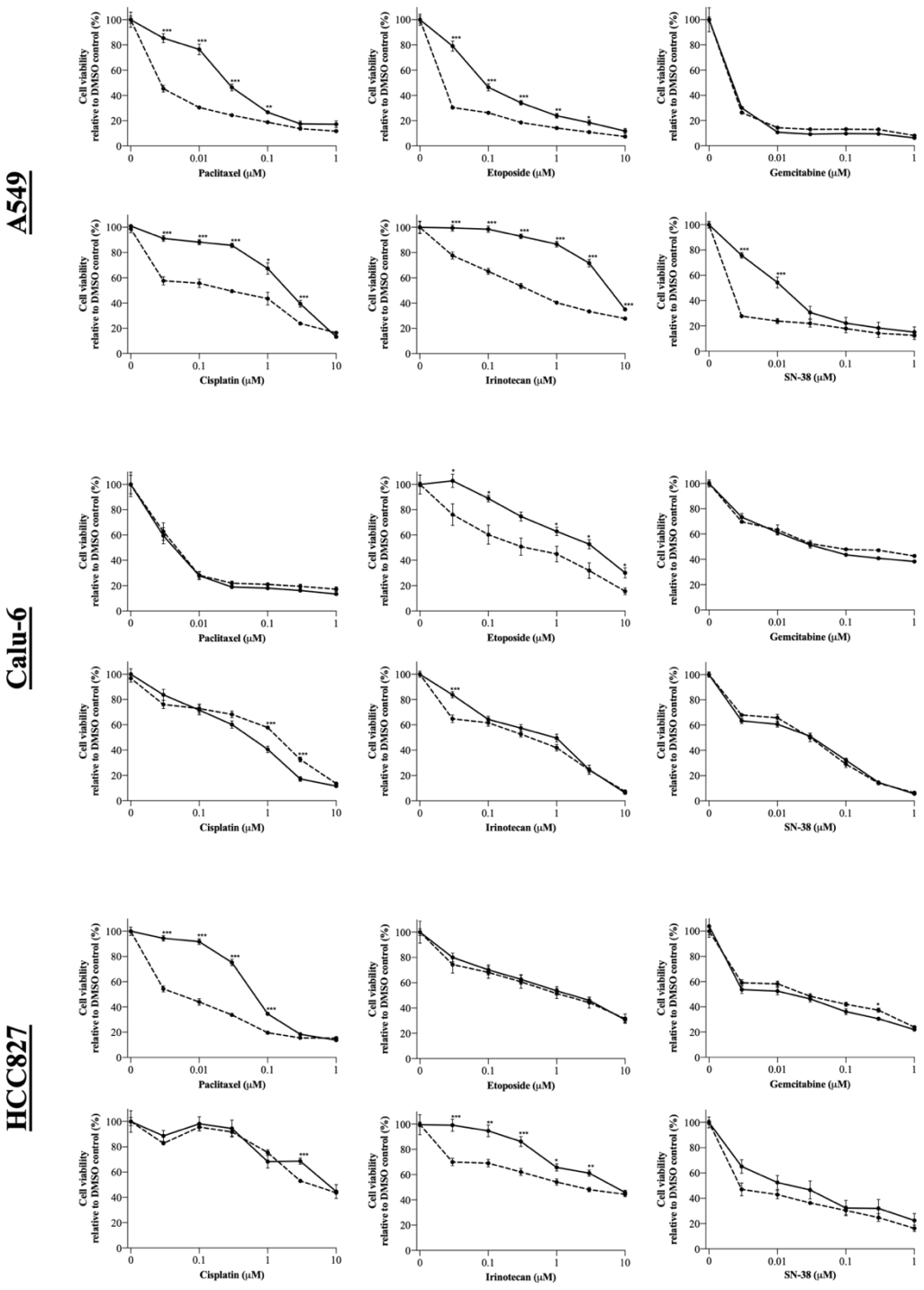
In parallel to the fibroblast data, H322 and H322 $ATM^{-/-}$ were tested for activation of components of the DDR pathway in response to treatment with chemotherapeutic drugs. The cellular response of H322 cells was comparable to the MRC5-SV2 fibroblasts in which ATM-dependent activation of DDR targets was observed in topoisomerase I and II-treated cells (Figure 5.4B). Consistent with the evidence of ATM-independent phosphorylation seen in AT5 BIVA fibroblasts, H322 $ATM^{-/-}$ tumour cells had increased levels of p-KAP1

serine 824 and p-CHK2 threonine 68 induced by etoposide, gemcitabine, and SN-38 (Figure 5.4C).

The ability of H322 ATM$^{-/-}$ to elicit a DDR to SN-38 was explored further. Cells were pre-treated with 10 μM KU-55933 before incubation with 1 μM SN-38. DDR responses in H322 ATM wildtype cells were similar to that of MRC5-SV2 in terms of phosphorylation activity of ATM, KAP1, CHK2, p53, H2AX and NBS1 in an ATM dependent manner, indicated by dampened responses in the presence of KU-55933 (Figure 5.4D). Despite loss of functional ATM, H322 ATM$^{-/-}$ cells were shown to phosphorylate KAP1, CHK2 and NBS1 in response to SN-38 treatment. Total levels of KAP1 and p53 are noticeably higher in the ATM-deficient tumour cells compared to the wildtype counterpart. In addition, levels of baseline p-p53 are high across all conditions.

5.2.3 Loss of ATM function in tumour cells is associated with sensitivity to certain chemotherapeutic drugs

The functional loss of ATM in H322 cells conferred increased sensitivity to the topoisomerase poisons etoposide and irinotecan (Figure 5.4A). This investigation was expanded to include additional lung tumour cell lines that are wildtype for ATM (A549, Calu-6, HCC827) or harbour known functionally inactivating ATM homozygous mutations (H1395, H23). In addition, the ATM wildtype colon adenocarcinoma cell line, HT-29, was included. Cell viability was analysed following treatment with a dilution series of paclitaxel, etoposide, gemcitabine, cisplatin, irinotecan or SN-38 in the presence or absence of 10 μM KU-55933.


A549
Calu-6
HCC827
Cell viability relative to DMSO control (%)
Paclitaxel (μM)
Etoposide (μM)
Gemcitabine (μM)
Cisplatin (μM)
Irinotecan (μM)
SN-38 (μM)
0 μM KU-55933
10 μM KU-55933

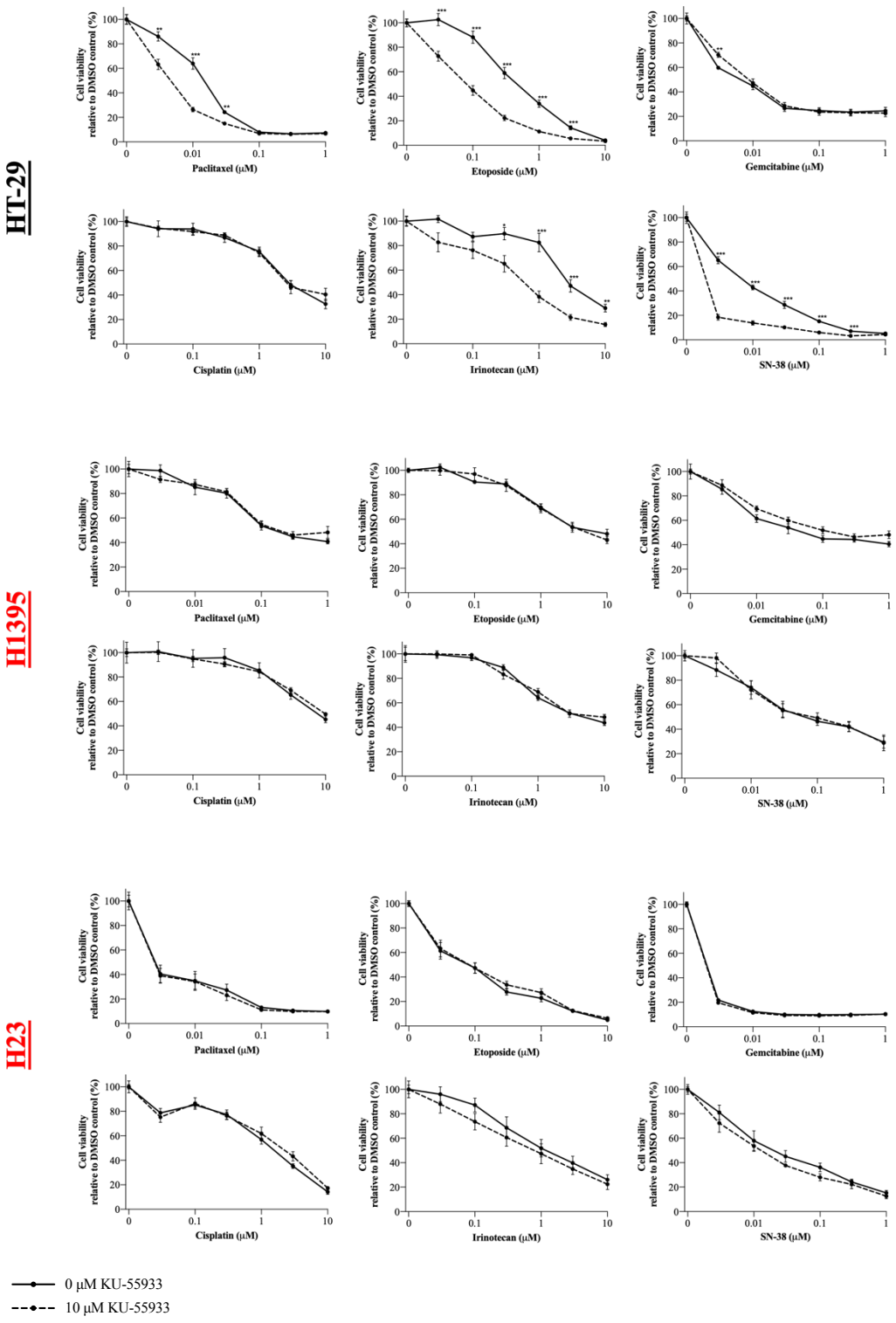


Figure 5.5 | Loss of ATM in tumour cell lines confers differential sensitivities to chemotherapeutic agents

(A) Cell viability of A549, Calu-6, HCC827, HT-29, H1395 and H23 in the presence (dashed line) or absence of KU-55933 (solid line) following exposure to a dilution series of paclitaxel, etoposide, gemcitabine, cisplatin, irinotecan, or SN-38. Data shown as mean ± SEM of at least three independent experiments (n=3) performed in triplicate. Statistical significance denoted by * ($p<0.01$), ** ($p<0.001$) and *** ($p<0.0001$). Cell lines with confirmed ATM mutation stated in red.

Inhibition of ATM showed an inconsistent effect against the different chemotherapeutic drugs of the cell lines tested (Figure 5.5). A549 cells, wildtype for ATM and p53, were significantly sensitised to five of the compounds tested with the addition of 10 μM KU-55933. The exception was gemcitabine, in which A549 cells were inherently sensitive to the concentrations tested. In comparison, Calu-6 cells appear relatively resistant to ATM inhibitor-induced chemosensitivity. Furthermore, the addition of 10 μM KU-55933 significantly increased cell viability of Calu-6 cells at 1 and 3 μM doses of cisplatin. ATM inhibition conferred sensitivity of HCC827 cells to paclitaxel and irinotecan, but not SN-38. HT-29 cells showed increased sensitivity to paclitaxel and the topoisomerase poisons when treated with 10 μM KU-55933. Viability of the ATM mutant cells (H23, H1395) was not affected by the addition of the ATM inhibitor. In comparison to H1395, H23 cells, which also harbour a p53 mutation, demonstrated a greater reduction in cellular viability in the presence of paclitaxel, etoposide, gemcitabine, SN-38, and a modest difference with irinotecan. H23 cells were very sensitive to the toxic effects of gemcitabine treatment.

5.3 Role of ATM independent phosphorylation of KAP1

5.3.1 Loss of ATM confers delayed induction of DDR in tumour cells but not fibroblasts

KAP1 is a well-recognised substrate of ATM and is its phosphorylation at serine 824 in response to DNA damage is generally considered to be mediated by ATM[153,350–352]. The unexpected observation of KAP1 in ATM-deficient cell lines sparked interest into the potential reasons for this. In response to DNA DSBs, ATM is rapidly activated to contribute to the transduction of a signalling cascade in a timely manner[68,353]. Previous data from this chapter has shown evidence of KAP1 phosphorylation in response to SN-38

treatment for 1 hour. To investigate the kinetics of substrate activation following SN-38 exposure, cells were analysed for phosphorylation of various target proteins via Western blot following various incubation times with SN-38. Consistent with reports of rapid ATM activation, the ATM-proficient cells (MRC5-SV2 and H322) demonstrate a response to DNA damage can be visualised after 10-15 minutes for most markers (Figures 5.6A, C).

Phosphorylation of RAD50 in MRC5-SV2 was not detected until 30 minutes post-treatment with SN-38. ATM-deficient fibroblasts displayed a comparable induction kinetics of p-KAP1 following 15 minutes of SN-38 exposure (Figure 5.6B). In support of previous data, p-NBS1 at serine 343 was detected but with slightly delayed kinetics compared to MRC5-SV2. The phosphorylation of RAD50 in AT5 BIVA cells, which had not been detected previously in this chapter, was observed from 3 hours. In comparison, H322 $ATM^{-/-}$ demonstrated a slower induction of the DNA damage response respective to H322 (Figure 5.6D).

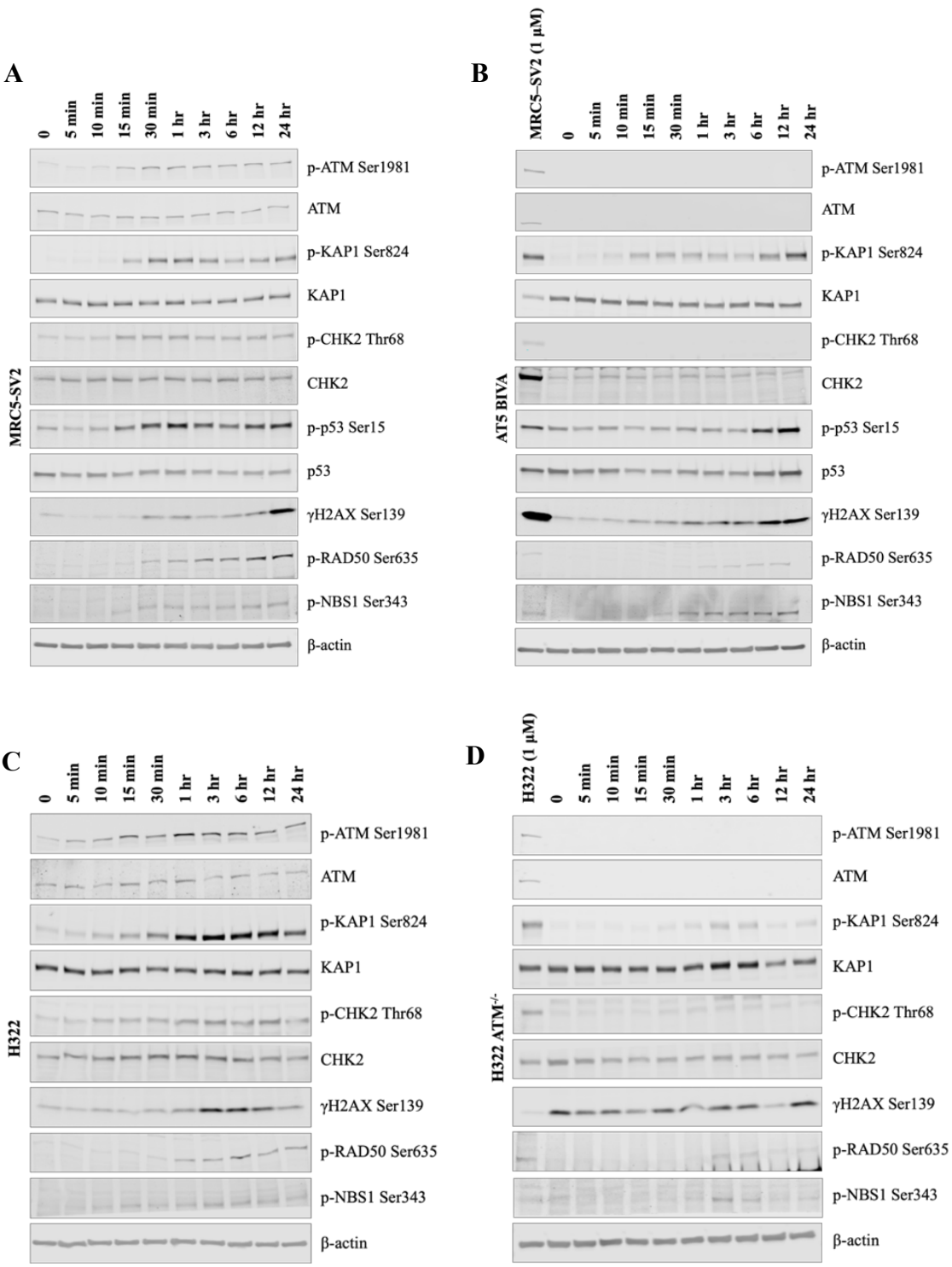


Figure 5.6 | Induction of ATM pathway activation in response to SN-38

(A-D) Western blot of **(A)** MRC5-SV2 and **(B)** AT5 BIVA **(C)** H322 and **(D)** H322 ATM$^{-/-}$ cells treated with 1 μM SN-38 for various timepoints. Representative blots (MRC5-SV2, n=2; AT5 BIVA, n=2; H322, n=1; H322 ATM$^{-/-}$, n=1) shown including β-actin loading control. **(B, D)** MRC5-SV2 or H322 cells treated with 1 μM SN-38 included in first column as positive control.

5.3.2 SN-38 targeting is predominantly restricted to S phase cells

Diverse functions of KAP1 have been reported including chromatin relaxation in response to DDR activation, transcriptional regulation as well as associated functions in cytokine production and virus replication. Furthermore, inducible knockout can be tolerated in adult mice whilst homozygous Kap1 mutations are embryonically lethal[354–356]. A role for ATM-KAP1 signalling has been associated with DSB repair within heterochromatin. Interestingly, the loss of KAP1 relieves the requirement for ATM involvement in repair whilst DSB repair defects are reported in cells expressing mutant KAP1 that cannot be targeted by ATM phosphorylation[90,153,357].

As the active metabolite of irinotecan, SN-38 exerts its cytotoxic effects in S phase cells through inhibition of topoisomerase I activity[294]. To visualise the S phase targeting by SN-38 and determine if this corresponded with phosphorylation of KAP1, cells were treated with SN-38 and labelled with EdU and p-KAP1 serine 824 antibody. Pre-treatment of 10 μM KU-55933 was incorporated to evaluate the dependency on ATM signalling. Consistent with previous data of this chapter, MRC5-SV2 fibroblasts display ATM-dependent phosphorylation of KAP1 indicated by the dramatic reduction in p-KAP1 positive cells in the presence of KU-55933 compared to SN-38 alone (Figure 5.7A). In comparison, the phosphorylation of KAP1 in AT5 BIVA cells was not altered by the addition of KU-55933. The majority of SN-38-induced p-KAP1 was reported in EdU positive cells and was comparable between the fibroblast pair (MRC5-SV2, 65%; AT5 BIVA, 67%). The proportion of p-KAP1+/EdU+ double positive cells was increased in the ATM-deficient fibroblasts in the presence of KU-55933 (89%). Comparable results were observed in the tumour cell pair, with the exception that ATM inhibition had less of an effect at diminishing SN-38-induced p-KAP1 in H322 cells. In response to SN-38

exposure, ATM-proficient cell lines show a greater activation of KAP1 compared to their ATM-deficient counterparts. Overall, whilst the majority of cells positive for p-KAP1 are EdU positive, SN-38 induced p-KAP1 appears to not be entirely exclusive to EdU positive cells.

The ability for the fibroblast and tumour pairs to form colonies following SN-38 treatment was assessed. Cells were incubated with a dilution series of SN-38 for either 1 hour or 24 hours including a pre-treatment with 10 μM KU-55933 condition. Both inhibition and loss of ATM resulted in fewer colonies forming following 1 hour exposure to SN-38, consistent between both cell line pairs (Figure 5.7B). This data, in conjunction with knowledge of topoisomerase I inhibition, implicates the S phase specific killing of cells during this window. However, cells were unable to form colonies following 24-hour exposure to SN-38, irrespective of ATM function.

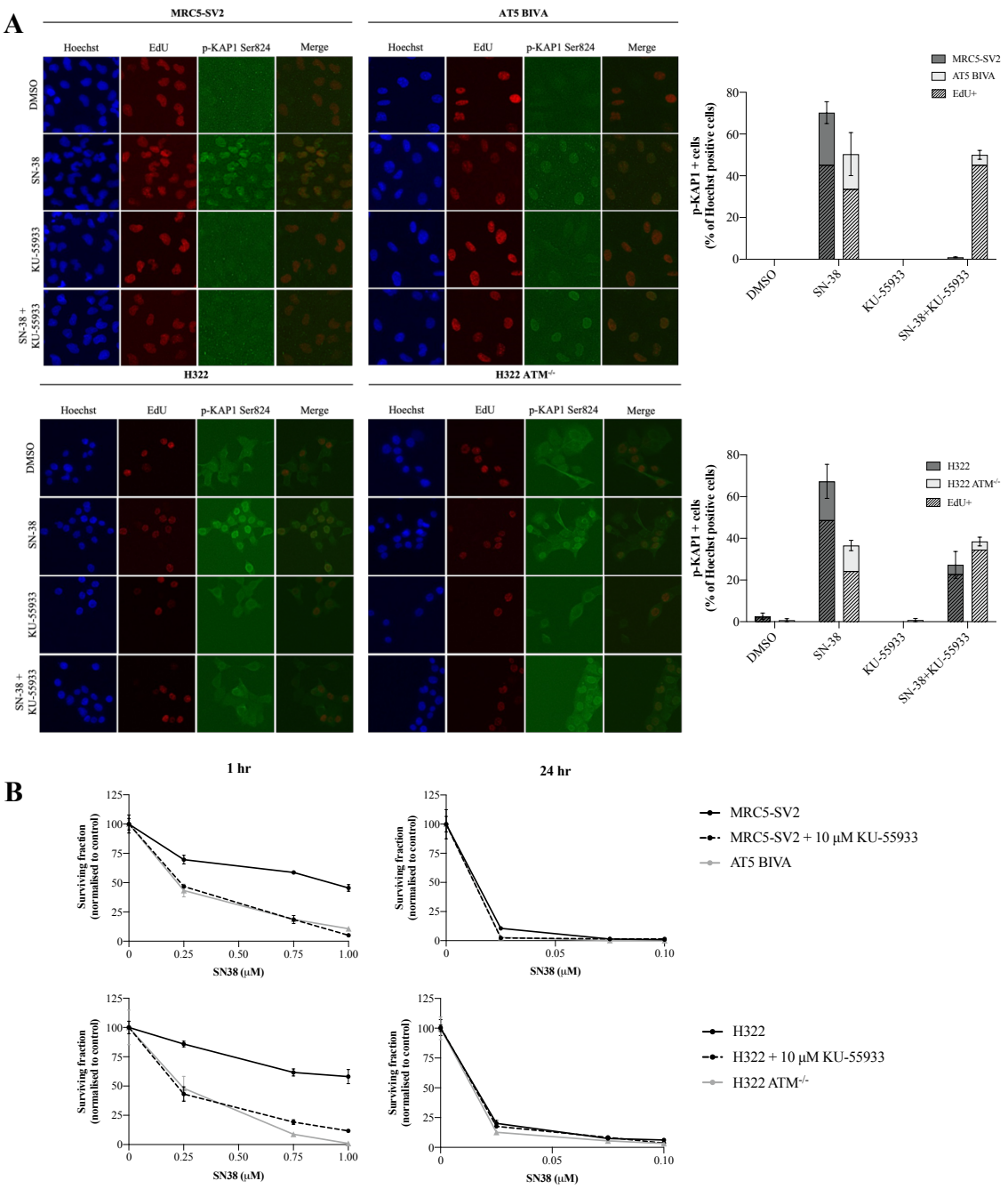


Figure 5.7 | SN-38 targeting of S phase cells

(A) Representative IF images of MRC5-SV2, AT5 BIVA, H322 and H322 ATM$^{-/-}$ following SN-38 treatment in the presence or absence of 10 μM KU-55933. IF staining for Hoechst (blue), EdU (red) and p-KAP1 (Ser824; green) with merged imaged. Quantification of cells scored as positive for p-KAP1 as a percentage of Hoechst positive cells. Proportion of double positive (p-KAP1+, EdU+) cells represented by dashed lines in bar. Data represented as mean ± SEM (n=1). **(B)** Clonogenic survival of fibroblast (top) and tumour (bottom) cell pairs after 1 hour or 24 hours of SN-38 treatment. Data shown as mean ± SEM of two independent experiments (n=2) performed in triplicate.

5.3.3 Contributions of DNA-PK to compensate for loss of ATM

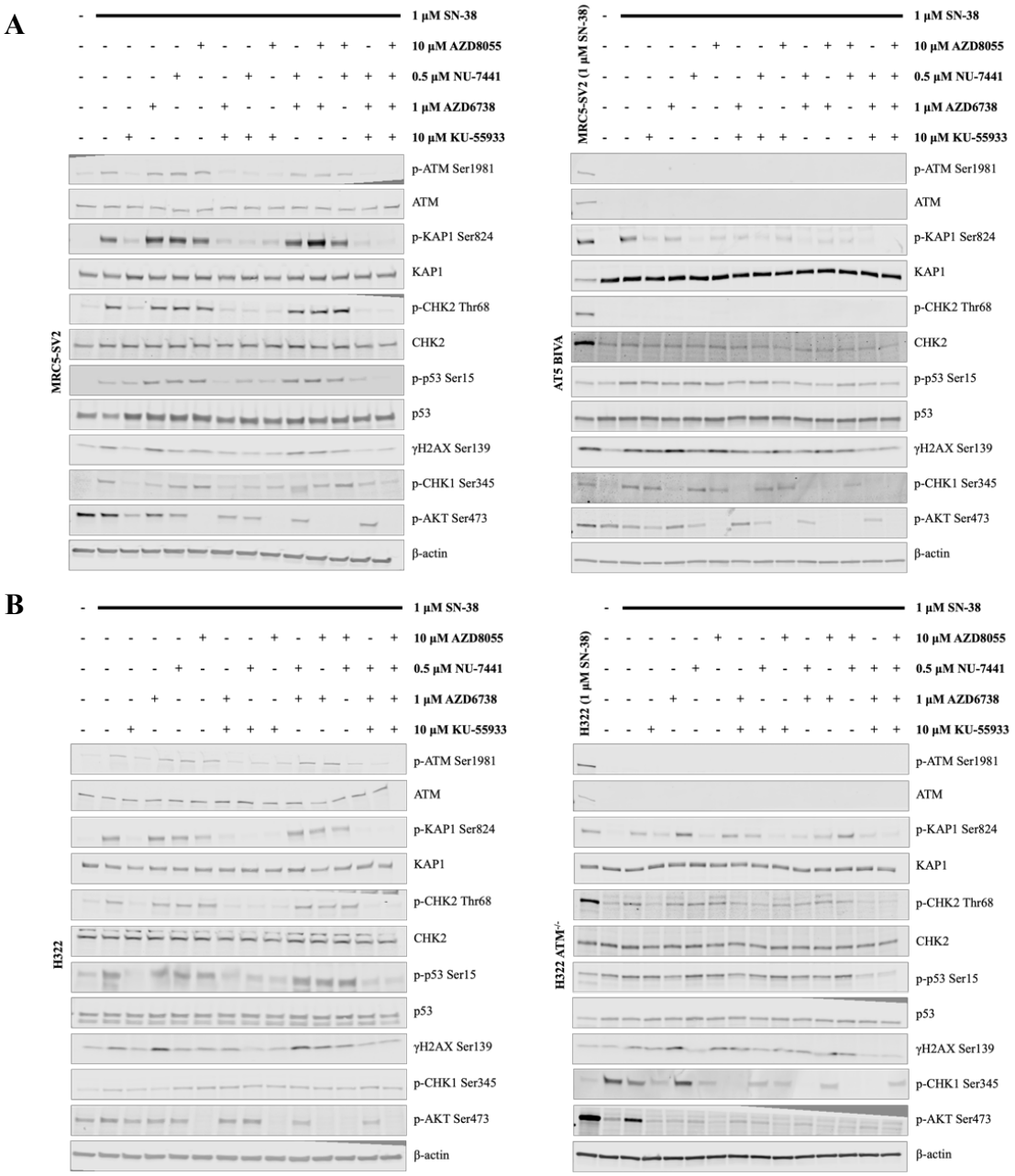
The three apical DDR kinases, ATM, ATR, and DNA-PK (PRKDC) have been well-documented for their roles in efficiently responding to DNA damage. Whilst established roles in responding to specific lesions have been reported, these DDR proteins share several substrates and the ability to crosstalk in the complex coordination of DNA repair. In addition, the notion that these kinases may compensate for the loss of another and understanding the interplay between them is of interest and may provide insight into the use of DDR protein targeting in cancer therapy[38,115,358]. ATM, ATR and DNAPK all belong to the PIKK family of protein kinases in addition to mTOR, SMG1 and TRAAP. All PIKK members have been implicated in the DDR and, with the exception of TRAAP, possess kinase activity[36,139,359].

Western blot analysis was used to investigate the potential contributions of PIKK members to the ATM-independent phosphorylation of KAP1 previously observed. The fibroblast and tumour cell line pair were pre-treated in the absence or presence of various combinations of ATM (10 μM KU-55933), ATR (1 μM AZD6738), DNA-PK (0.5 μM NU-7441) and mTOR (10 μM AZD8055) inhibitors prior to treatment with 1 μM SN-38. The selective ATR, DNA-PK and mTOR inhibitors have been reported to inhibit their targets at an IC_{50} of 1 nM, 14 nM and 0.8 nM respectively[360–362]. Additional markers were included to demonstrate target inhibition such as p-CHK1 Ser345 and p-AKT Ser473. Technical issues with p-DNA-PK Ser2056 antibody hindered use in this study however previous data has demonstrated 0.5 μM NU-7441 is specific and sufficient to radiosensitise[363].

Consistent with previous findings, the DDR induced in ATM-proficient fibroblast and tumour cells in response to SN-38 treatment is dependent on ATM signalling, as evident

through the diminished phosphorylation in the presence of KU-55933 (Figure 5.8A, B). Interestingly, a potential minor contribution of mTOR activity is observed, which may be cell specific and would require further investigation. ATM-independent phosphorylation of KAP1 is observed in the AT5 BIVA cells in which pre-treatment with 0.5 μM NU-7441 diminishes this response (Figure 5.8A). A minimal reduction in γH2AX was observed after DNA-PK inhibition as well as PI3K inhibitor combinations however no changes were evident in the phosphorylation levels of p53, with only a minor effect of inhibitor combinations. In parallel, inhibition of DNA-PK also reduced p-KAP1 detection in H322 $ATM^{-/-}$ cells whilst ATR inhibition increased phosphorylation of KAP1 but decreased p-p53 (Figure 5.8B).

To determine the sensitivity of the cell line pairs to single agent PIKK family inhibitors, cell viability was analysed using resazurin-based assay following exposure to dilution series of each inhibitor. PARP inhibition has been demonstrated to confer synthetic lethality with tumours that harbour deficiencies in HR[364]. To evaluate the impact of ATM loss on sensitivity to PARP inhibitors, BMN673 was included in this study. Variations in sensitivities of the cell lines against the different compound inhibitors was observed (Figure 5.8C). Firstly, inhibition of ATM with KU-55933 was tolerated across the concentrations tested. Loss of ATM in fibroblasts corresponded to increased sensitivity to ATR, DNA-PK, mTOR, and PARP inhibition. In comparison, H322 $ATM^{-/-}$ showed a modest sensitivity compared to H322. Additional experiments are required to complete the panel for the sensitivity of the H322 isogenic pair to mTOR inhibition.


A
1 μM SN-38
10 μM AZD8055
0.5 μM NU-7441
1 μM AZD6738
10 μM KU-55933
MRC5-SV2
MRC5-SV2 (1 μM SN-38)
AT5 BIVA
p-ATM Ser1981
ATM
p-KAP1 Ser824
KAP1
p-CHK2 Thr68
CHK2
p-p53 Ser15
p53
γH2AX Ser139
p-CHK1 Ser345
p-AKT Ser473
β-actin
B
H322
H322 (1 μM SN-38)
H322 ATM-/-

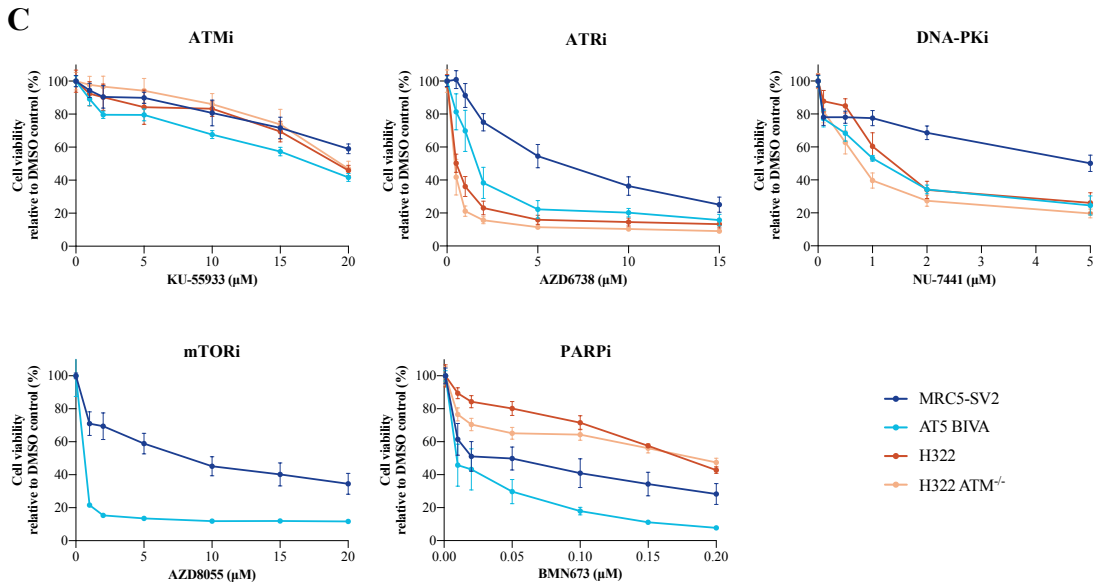


Figure 5.8 | Compensation of ATM loss by DNA-PK in response to SN-38

(A-B) Western blot of the **(A)** fibroblast and **(B)** tumour cell line pairs following treatment with 1 μM SN-38 and combinations of PI3K inhibitors. Representative blots (n=1) shown including β-actin loading control. MRC5-SV2 or H322 cells treated with 1 μM SN-38 included in first column as positive control. **(C)** Cell viability of MRC5-SV2, AT5 BIVA, H322 and H322 ATM$^{-/-}$ following exposure to DDR inhibitors. Data shown as mean ± SEM of at least three independent experiments (n=3) performed in triplicate.

5.4 Screening-based identification of compounds that confer synthetic lethality with loss of ATM

A screening approach was used with the aim of identifying compounds that are synthetically lethal with the loss of ATM. The paired fibroblast (MRC5-SV2, AT5 BIVA) and tumour (H322, H322$^{-/-}$) cell lines were treated with the kinase chemogenomic set (KCGS) library consisting of 187 kinases that covered 215 targets at three concentrations (0.1, 1 and 10 μM)[178,179]. Cell viability was assessed using a resazurin-based assay after a 3-day incubation with the library (Figure 5.9A). Comparisons of ATM-proficient and ATM-deficient cells for the fibroblast and tumour pairs revealed compounds that achieved the greatest sensitivity or resistance with ATM loss (Figure 5.9B). Assessment of the top-

ranked compounds revealed partial overlap at the concentrations used in the screen (Figure 5.9C). Table 5.4 highlights the top ten ranked compounds highlighted for conferring greatest sensitivity with ATM loss in fibroblasts. Targets of each compound are listed with the original target specified in red text, as listed according to the KCGS dataset. Identification of the insulin-like growth factor (IGF) 1 receptor (IGF1R) inhibitor (GSK1838705) as a top hit for inhibiting viability in ATM-deficient fibroblasts has been included for publication[365]. Additional compound hits included ATR, CHK1, epidermal growth factor receptor (EGFR) and several CDKs.

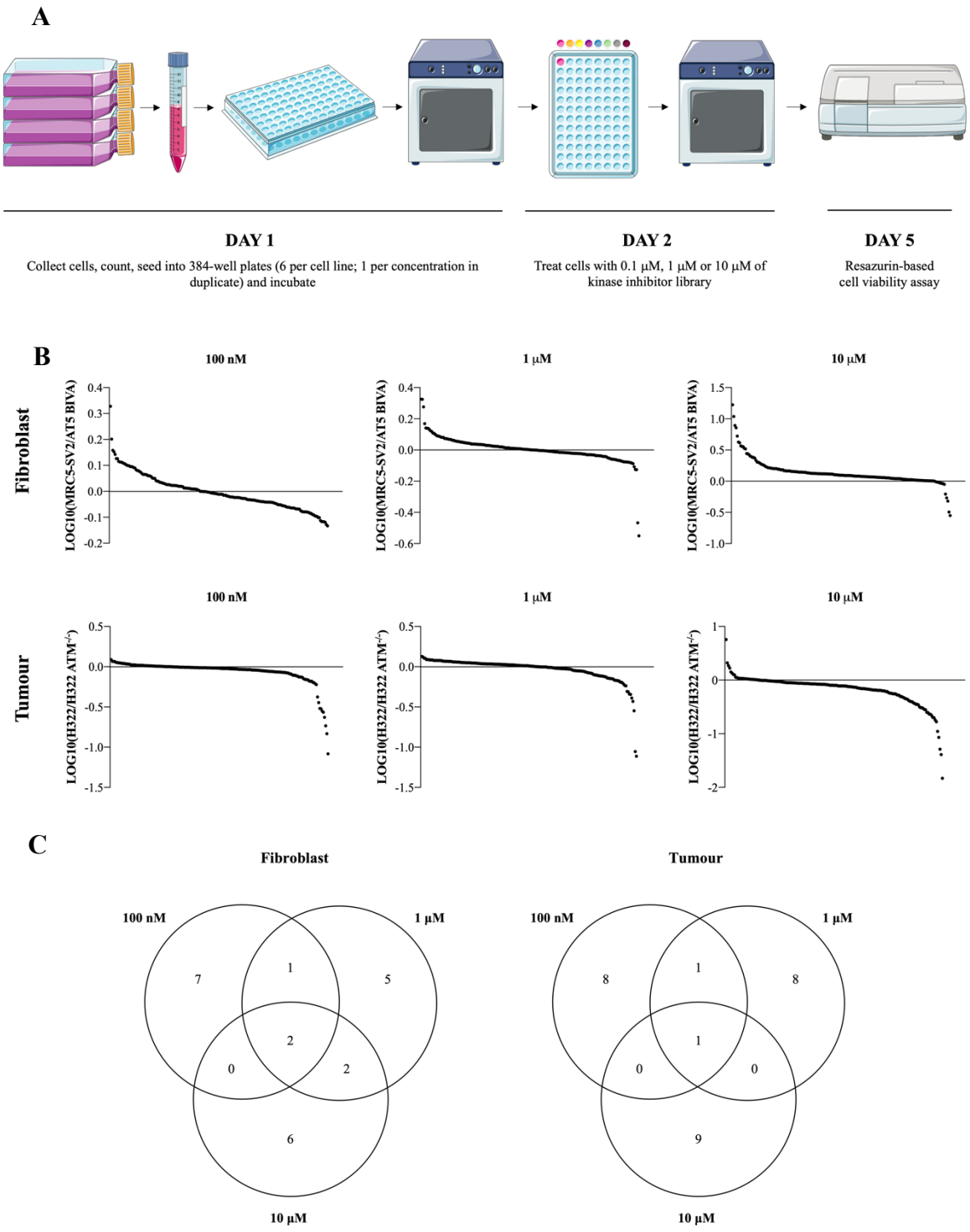


Figure 5.9 | Kinase screen reveals compounds that confer synthetic lethality with loss of ATM

(A) Schematic of the kinase screen. Figure produced using Servier Medical Art provided by Servier, licensed under a Creative Commons Attribution 3.0 Unported License[366]. **(B)** Fibroblasts (MRC5-SV2, AT5 BIVA) and tumour cells (H322 and H322 ATM$^{-/-}$) treated with 187 compounds at 0.1, 1 and 10 µM. Cell viability was measured using resazurin-based assay. Graphs represent compounds screened at each concentration and ranked by ratio of $\log_{10}$ATM-proficient cell/ATM-deficient cell. **(C)** Venn diagram depicting common top-ranked (10) hits for each concentration.

Table 5.4 | Screening hits from lung fibroblast cell pair

	0.1 µM		1 µM		10 µM	
	Compound	**Target**	**Compound**	**Target**	**Compound**	**Target**
1	GW525701	EPHB6	GSK1838705	ALK, CLK2, CLK1, FER, FES, IGF1R, IRR, MYLK	GW440135	KIT, MAP2K5, KDR, PDGFRA
2	GSK1838705	ALK, CLK2, CLK1, FER, FES, IGF1R, IRR, MYLK	GW525701	EPHB6	ERK5-IN-1	MAPK7
3	CCT251921	CDK8, CDK19	PFE-PKIS 40	PIK3CG, PIK3CA, PIK3C2G, PIK3CD, PIK3CB, PIK3C2B, MTOR, PI4KB	GW525701	EPHB6

4	PFE-PKIS 40	PIK3CG, PIK3CA, PIK3C2G, PIK3CD, PIK3CB, PIK3C2B, MTOR, PI4KB	GW440135	KIT, MAP2K5, KDR, PDGFRA	DDR1-in-1	DDR1
5	TPKI-26	PLK1, PLK2, PLK3	GW810372X	GSK3B, CLK2, HIPK1	GSK1392956A	INSR, IGF1R, PTK2B
6	BI00133844	EGFR, ERBB2, EPHA6, LYN, BLK, RET, MEK5, EPHB4, LCK, SRC, HCK, ERBB4	JNK-IN-7	JNK1, JNK2, JNK3, IRAK1, YSK4, ERK3, RIOK2, PIP5K2C, CDKL5, ICK, DRAK1	BI00601000	MAPK14

7	BIRZ0518XX	PRKCQ, PRKCE, PRKCD	SB-725317	CDK2, GSK3B	PFE-PKIS 40	PIK3CG, PIK3CA, PIK3C2G, PIK3CD, PIK3CB, PIK3C2B, MTOR, PI4KB
8	GSK583	RIPK2	D2202-1	DDR1, NTRK3, NTRK2, NTRK1	PFE-PKIS 12	CASK
9	GW855857	ACVR1B, TGFBR1, PRKD1, PRKD2, PRKD3	CCT244747	CHEK1, PRKAA1, RPS6KA1, RPS6KA3	GSK1398477	PDGFRB
10	VE-822	ATR, ATM	GSK223675	TGFBR1, ACVR1B, PRKD1	D2202-1	DDR1, NTRK3, NTRK2, NTRK1

Table 5.5 highlights the top ten ranked compounds highlighted for conferring greatest sensitivity with ATM loss in the lung tumour cell pair. Targets of each compound are listed

with the original target specified in red text, as listed according to the KCGS dataset. Top hits include several CDK members as well as CHK2.

Table 5.5 | Screening hits from lung tumour cell pair

	0.1 µM		1 µM		10 µM	
	Compound	**Target**	**Compound**	**Target**	**Compound**	**Target**
1	PFE-PKIS 32	CDK4, TTK	PFE-PKIS 44	CDK4	BI00601000	MAPK14
2	GW572399X	CDK2	GW280670X	CDK2	NVP-2	CDK9, TAOK3, HIPK4, CDK13, IRAK1, DYRK1A
3	NVS-PAK1-1	PAK1	PFE-PKIS 32	CDK4, TTK	GW440135	KIT, MAP2K5, KDR, PDGFRA
4	GSK481	RIPK1	GSK2373690	PIK3CB, PIK3CG	PFE-PKIS 12	CASK
5	BIRB0876BS	DDR1, MAPK14	BIRZ0518XX	PRKCQ, PRKCE, PRKCD	CCT241533	CHEK2, MARK3, PHK

6	TPKI-100	MAPK10	XMD8-87	FRK, PTK6, TNK2	GW440146	MAP2K5, BLK
7	SB-517081	KIT	SB-517081	KIT	DDR1-in-1	DDR
8	GW868318	MAPK14, MAPK11	GSK2336394	PIK3CB	GSK2328680	PIK3CB
9	SB-708998	MYLK2	HTH-01-015	NUAK1	GW300660X	CDK1, CDK2, CLK2, MELK
10	HG-10-102-01	LRRK2	BI00614644	MAPKAPK2, MAPKAPK5, PIM3	PFE-PKIS 32	CDK4, TTK

Compounds were identified that were top-ranked for conferring sensitivity in ATM-deficient fibroblast and tumour cells. These include GW440135, DDR1-in-1, BI00601000, PFE-PKIS-12. Interestingly, the compounds BIRB0876BS and GW440146 were reported in the top ten compounds for synthetic lethality with ATM loss in tumour cells however the ATM wildtype cells were more sensitive of the fibroblast pair. On the other hand, several compounds had a synthetic lethality with AT5 BIVA cells but not H322 ATM$^{-/-}$. These include GW525701, GW810372X and CCT244747. In addition, treatment with GSK237701A, GSK461364, BI2536 and TPKI-24 conferred resistance with ATM loss. Concentration-dependent effects were seen in which compounds were reported as

conferring sensitivity or resistance of ATM-deficient cells depending on dose. Examples include TPKI-26, BIRZ0578XX, JNK-IN-7, GSK1398477 and VE-821. Further work is required to validate screening hits and understand the implications of this work.

Discussion

Functional loss of ATM represents an attractive target for developing therapeutic approaches against cancer. The inability of cells to respond to DNA DSBs renders them susceptible to modalities that induce genotoxic insults. The cellular radiosensitivity identified in A-T prompted investigations into targeting ATM therapeutically[94]. However, only a fraction of IR-induced breaks are reported to be dependent on ATM. This DSB repair process also involves the nuclease Artemis, several mediator proteins including H2AX, MDC1, RNF8, RNF168 and 53BP1 as well as c-NHEJ components. In contrast, approximately 75-80% of IR-induced DSBs are repaired using an ATM-independent process that relies on c-NHEJ proteins and is performed with faster kinetics[131,367]. The allocation of repair mechanisms correlates with the subtle repair defect characteristic of A-T cells. Whilst the rate of DSB re-joining is comparable to ATM-proficient cells, A-T cells have a greater proportion of breaks that failed to re-join[149]. The ATM-dependent repair of DSBs is proposed to signify regions of heterochromatin. ATM phosphorylation of KAP1 promotes chromatin relaxation to facilitate the access of DNA repair factors[3,153].

Data from this chapter demonstrated an equivalent SER of non-tumour lung fibroblasts and lung tumour cells to IR in the context of ATM inhibition or loss. In addition, ATM inhibition has been shown to enhance radiation sensitivity to the same extent in normal fibroblasts and glioma cells[162]. This raises concerns of the normal tissue toxicity that could be associated with the clinical utility of ATM inhibitors. Whilst single-agent ATM inhibition has been reported to be well-tolerated, the combination with radiotherapy

requires consideration for the potential toxicity on normal tissues, especially in the instance of highly proliferative tissues. Furthermore, sufficient radiosensitisation has been observed following transient inhibition of ATM indicating that prolonged inhibition may not be required and potentially alleviate clinical side effects[94,158,163,292,368].

Conventional cancer therapies induce DNA damage to exhibit potent effects on tumour cells. Targeted inhibition of the DDR can augment the cytotoxic activity of radio- or chemotherapies. Various inhibitors against DDR proteins, such as ATM and ATR, have been developed which have conferred increased sensitivity to various agents[94,369]. Endogenous levels of p-CHK2 observed in H322 cells suggest there may be a potential impact of ATM inhibition alone in these cells. However, this data showed that exposure to various concentrations of KU-55933 was well tolerated in these cells. Conversely, H322 cells demonstrate sensitivity to inhibition of ATR with the compound AZD6738. A potential reason for this observation could be the constitutive activation of ATR in these cells as a result of a compromised S phase and expression of oncogenes that promote replication stress[370–372]. Inhibition of mTOR conferred substantial sensitivity to ATM-deficient fibroblasts, which may be attributed to its roles in the cellular stress response[373]. Further investigation is required to determine whether mTOR inhibition confers sensitivity in ATM-deficient tumours. The effect of ATM loss on the sensitivity to PARP inhibition was greater in fibroblasts than in the H322 tumour pair, in which the tumour cells were relatively tolerant to concentrations of BMN673. The inhibition of PARP has been associated with heightened sensitivity of cells that exhibit HR defects. Recent data has shown that whilst DDR signalling was impacted by the loss of ATM, HR function remained intact. Loss of ATM in prostate cancer cells conferred substantial sensitivity to ATR inhibition however this effect was not observed with PARP inhibition[374]. Furthermore, cells with defective HR have been reported to exhibit increased sensitivity to

cross-linking agents such as cisplatin. However, our data demonstrated that pharmacological inhibition of ATM failed to enhance the sensitivity of the HT-29 colorectal line and the lung tumour cell lines tested, with the exception of A549. Additional data has also shown that ATM inhibition did not confer increased sensitivity to cisplatin in cervical, endometrial, or ovarian cancer cells[375]

Cellular viability, as measured through a resazurin-based proliferation assay, demonstrated that the loss, but not inhibition of ATM in human lung fibroblasts was associated with increased sensitivity to SN-38. MRC5-SV2 cells have previously been reported as relatively resistant to CPT treatment which has been attributed to the amount of CPT-induced cleavable complexes formed. Inhibition of DNA polymerases revealed the importance of collisions between cleavable complexes and the replication machinery in fuelling the toxicity of this agent in S phase cells[376]. In the instance of the lung tumour isogenic cell pair, neither loss nor inhibition sensitised cells to SN-38 (Figure 5.4A). H322 cells have previously been reported as particularly resistance to irinotecan-induced toxicity which has been partially attributed to the lower carboxylesterase activity and slower uptake compared to other lung tumour cell lines. Furthermore, of the cell lines that were studied, H322 displayed the highest protein expression of topoisomerase I but lowest level of topoisomerase II, although this was not considered a determinant of irinotecan sensitivity[377,378]. Unfortunately, clinical resistance to irinotecan therapy is often reported and ascribed to several mechanisms including increased drug efflux, inefficient conversion to the active metabolite SN-38, overexpression of uridine glucuronyl transferases (UGT) to inactivate SN-38, as well as structural changes to the target enzyme[294].

Interestingly, clonogenic survival analysis revealed that following 1 hour incubation with SN-38, both the inhibition and loss of ATM resulted in fewer colonies in the fibroblast and

tumour cells (Figure 5.7B). SN-38 inhibits the action of topoisomerase I and the temporary exposure of this compound to the cells suggests S phase targeting of cells. Whilst a greater proportion of ATM-proficient cells were able to form colonies following this 1-hour incubation, these cells were unable to form colonies following 24-hour incubation. The extended exposure of cells to SN-38 removes the intrinsic advantage of targeting the loss of ATM that is seen following transient treatment.

The transient formation of topoisomerase I-DNA covalent complexes and subsequent generation of SSBs helps to relax DNA supercoiling. Proteolytic removal of the enzyme-DNA complex is essential to prevent collision with either replication or transcription machinery. Failure to remove the torsional stress from supercoils or the complex can result in transcriptional arrest or the generation of DSBs[379,380]. ATM deficiency results in the accumulation of topoisomerase I-DNA covalent complexes, DNA breaks and delays in the recovery of transcription[381]. The loss of ATM indirectly causes further accumulation of topoisomerase I-DNA covalent complexes induced through the increase in cellular ROS[382]. Inhibition of topoisomerase I has also been implicated in transcriptional modifications. Following 4-hour treatment with CPT, transcript levels of *Hsp70* and *c-myc* were reduced whilst an increase was seen in mRNA abundance of *c-fos*. The activation and repression of gene transcription may have consequences on drug sensitivity. For examples, the authors proposed that *c-myc* repression may prevent S phase entry which could confer decreased sensitivity to topoisomerase I inhibition[383]. Furthermore, global gene expression is repressed in mouse neurons following exposure to topoisomerase I inhibitors[381]. In addition, ATM has been reported to be activated in response to the formation of R loops due to paused RNA polymerase at DNA lesions, CPT-induced enzyme-DNA complexes in quiescent cells in the absence of DSBs, as well as persistent SSBs[384–386]. Recent studies have also proposed that the target of irinotecan may extend beyond topoisomerase I. SN-

38 has been reported to interact with MDM2 and directly bind Bcl-xL to promote induction of p53-dependent apoptosis[296,387].

Comparison of IC_{50} values of fibroblast and tumour cells to etoposide reveals similar results for inhibition, but not loss of ATM. However, the addition of 10 μM KU-55933 decreased IC_{50} by 10-fold in H322 and 4-fold in MRC5-SV2 cells compared to etoposide treatment alone (Tables 5.2, 5.3). Furthermore, the loss of ATM in fibroblasts decreased IC_{50} of etoposide by 14.6-fold but 2.9-fold in the tumour cells. A greater reduction in IC_{50} values of irinotecan was observed following the loss of ATM in the fibroblast pair (14-fold) compared to the tumours (2.3-fold). Inhibition of ATM sensitised fibroblasts by approximately 2-fold and 5-fold respectively for MRC5-SV2 and H322 cells. Whilst neither the inhibition nor loss of ATM conferred additional sensitivity of tumour cells to SN-38 treatment, a profound response was observed in the fibroblasts. Loss of ATM decreased IC_{50} value by 50-fold however this was not recapitulated in the context of ATM inhibition.

The data in this chapter also included additional sensitivities against a panel of lung cancer cell lines, and one colorectal cancer cell line. Consistent with the absence of an effect of ATM inhibition on H322 lung tumour, the other lung cancer tumour lines were also not sensitised to SN-38. However, an exception to this was the increased sensitivity observed in A549 cells following the addition of the ATM inhibitor, KU-55933. Enhanced sensitivity to SN-38 of colorectal cell lines have been reported in combination with AZ31 administration, as also replicated in this chapter with HT-29 cells and KU-55933[166]. However further research into the effect on ATM inhibition on SN-38 in other tumour types is required as this may have clinical implications. For example, it may be that lung cancer derived from lung cells have a different response to SN-38 than other tissues.

However, the effect of ATM inhibition in A549 cells was not specific for a particular class of chemotherapy which could suggest an effect through p53. Additional tumour cells wildtype for p53 would be required to address this question.

Phosphoproteomic analysis has revealed that the loss of ATM and consequences on substrate phosphorylation can be partially compensated for by ATR and DNA-PK. In this context, the majority of ATM-dependent substrates could not be activated following DNA damage in a compensatory manner[388]. Data from this chapter supports this notion that the ATM-independent phosphorylation of typically ATM-dependent substrates can occur following the formation of genotoxic lesions however activation of the intact pathway in its entirety is not observed. In response to SN-38 treatment, ATM-independent activation of target proteins appears to be a selective mechanism.

An important question to address is whether the remaining functional DDR proteins are acquiring a novel function or are instead undergoing an exacerbation of a pre-existing, but minor, role in cellular response to ATM loss. Data from this chapter has shown a marked reduction, rather than ablation, of target phosphorylation in ATM-proficient cells in the presence of 10 μM KU-55933. Residual activation of proteins in response to DDR may be a consequence of inadequate inhibition of ATM or the potential contributions of additional DDR proteins. Activation of a subset of protein targets in the absence of ATM indicates that the observations from this chapter are not a result of residual ATM activity in the deficient § .

Both ATM and ATR share substrate specificity for their kinase activity and several examples of these substrates have been shown to be targets of both kinases. Together, ATM and ATR are considered to be responsible for governing the cellular response to genotoxic stress. Additionally, the loss of ATM protein has been shown to result in the increased

sensitivity to ATR inhibition enforced through a checkpoint defect. Here, cells were able to arrest in G2 but failed to arrest adequately in S phase following SN-38 treatment[94,389]. Furthermore, VE-822 is a potent inhibitor of ATR kinase and was reported as a top-ten hit from the screen performed in this chapter to confer sensitivity with loss of ATM in fibroblasts. Several studies have also reported a greater sensitivity to ATR inhibition in the context of ATM mutation/loss[390]. Interestingly, this observation is not recapitulated in the context of ATM depletion through RNA interference (siATM). Treatment of AZD6738 in ATM-deficient PDAC xenografts demonstrated tumour growth delay whilst the combination with gemcitabine caused tumour regression[391–393]. ATM and DNA-PK are both involved in the cellular response to DNA damage and their recruitment to DSB sites to perform respective roles in DDR signalling pathways[394]. The process of V(D)J recombination required activity of complementary and distinct functions of ATM and DNA-PK[395]. Investigations into the contributions of ATM and DNA-PK in murine lymphocytes during DSB repair reveal dependency on DNA-PK for p53 activation and DNA repair regulation in the absence of ATM. From these findings, it was proposed that in ATM-proficient cells, DNA-PK is largely responsible as a component of NHEJ whilst in the absence of ATM, DNA-PK can perform a compensatory function[396]. Interestingly, DNA-PK-deficient cells have been found to lack sensitivity to ATR inhibition whilst overexpression of DNA-PK increased sensitivity to VE-821. In contrary to loss of DNA-PK, DNA-PK inhibition with NU-7441 sensitised cells to ATR inhibition[397].

Recent investigations into the PIKK-dependent compensation for the loss of ATM has demonstrated activity of both ATR and DNA-PK. In line with data from this chapter, not all ATM substrates could be activated via the remaining DDR proteins. A study revealed that in A-T cells, the majority of contributions were predominantly ATR-dependent that were performed with slow kinetics. On the other hand, the proportion of targets activated

by DNA-PK compensation were performed rapidly[388,398]. The data from this chapter has demonstrated evidence for the ATM-independent phosphorylation of KAP1. In addition, p-NBS1 was observed as well as p-CHK2 in the ATM-deficient tumour cells in response to SN-38 but not IR. The observation of ATM-independent activation of substrates in tumour cells selective to certain chemotherapeutic drugs implicates the importance of context. Together, this data confirms the activation of various DDR proteins traditionally considered ATM-dependent.

KAP1 was originally identified as a transcriptional co-repressor. To date, several functions have been attributed to the physiological role of KAP1 spanning both transcription and non-transcription related[355,399]. Transcriptional regulation has been proposed as a role of DNA-PK through the phosphorylation of KAP1 at serine 824. Activation of KAP1 in this context has been shown to be required by RNA polymerase II[142]. As mentioned previously, inhibition of topoisomerase I has been associated with effects on transcription. The combination of SN-38 and DNA-PK inhibition has been reported to cause increased sensitivity to the topoisomerase I poison[400]. In addition, synthetic lethality of DNA-PK inhibition has been demonstrated in mouse models with ATM-deficient lymphomas[142]. Attenuation of the G2 checkpoint following DNA-PK inhibition in ATM-deficient cells has also been documented[56,401,402]. Interestingly, a genetic screen has identified that in ATM-deficient cells, the suppression of genes associated with NHEJ, such as LIG4 and XRCC4, resulted in increased resistance to the toxic effects of topotecan. However, resistance to topotecan was not observed in *Prkdc*-deficient mice treated with an ATM inhibitor[300].

Data from this chapter proposes a compensatory role of DNA-PK in the context of ATM loss in response to S phase damage, which may have implications in targeting ATM-

deficient tumours. Whilst DNA-PK may be able to tolerate normal levels of endogenous damage to the cell in the absence of ATM, increasing replication stress in these cells through inhibition of WEE1 or hydroxyurea (HU) treatment in combination with a DNA-PK inhibitor may be intolerable. Targeting ATM-deficient tumours with irinotecan is a promising concept however data shown in this chapter demonstrates the effect in tumour cells may be modest. Therefore, based on the potential compensation of DNA-PK in ATM-deficient cells, the addition of a DNA-PK inhibitor in combination with irinotecan, or another S phase agent, may selectively target tumours lacking ATM.

Overall, the differences displayed within this chapter between ATM kinase inhibition and ATM loss indicate that the consequences of these result in different phenotypes. The disconnect between loss and inhibition presents as variation in pathway signalling and the sensitivity to certain chemotherapeutic drugs. A parallel example to the differences between the loss and inhibition of ATM has been reported in the context of PARP. Inhibition of PARP confers greater sensitivity to alkylating agents and delay in SSB repair compared to PARP depletion[403]. The variability of responses of the different cell lines to chemotherapeutic drugs provides an insight into the complexities of targeting tumours in the context of ATM inhibition or loss.

6 General Discussion and Conclusion

The clinical presentation of A-T corresponds to a multi-system disorder which parallels the wide-spanning nuclear and cytoplasmic roles documented of ATM[2]. Since the cloning and sequencing of the ATM gene in 1995, there has been huge advancement and insight into the various functions of ATM and the consequences of disruption[404]. However, fundamental questions remain unanswered regarding the aspects of the clinical manifestation and progression of A-T as well as fully elucidating the contributions of ATM to the cellular response following DNA damage. ATM protein is ubiquitously expressed in normal human tissue and functions via the canonical DDR pathway to mediate the repair of DNA DSB with coordination of cell cycle arrest. Functional loss of ATM, a common occurrence in several tumour types, is a promising target for developing therapeutic approaches against cancer. ATM loss is associated with increased genomic instability, a characteristic of tumour cells, and the inability of cells to mount an appropriate DDR in the presence of DNA DSBs renders them susceptible to DNA damaging agents[319,321]. Targeting ATM loss in tumours with radiotherapy is a rational approach because of the profound cellular and clinical radiosensitivity phenotypes observed but this would not be as practicable in disseminated metastatic cancer, where radiotherapy does not usually play a significant role in treatment[38,131].

The central aim of this report revolved around the concept of synthetic lethality to selectively target ATM-deficient tumours. To support this aim, the expression of ATM protein in normal human tissues was first evaluated in addition to identifying the extent of loss of ATM protein in human tumours. Furthermore, to understand the *in vivo* consequences of targeting ATM loss on normal tissues following DNA DSB induction

necessitated the use of murine models. In addition, this investigation aimed to identify synthetic lethal approaches in the context of ATM inhibition or ATM loss.

High expression of ATM protein across all normal tissues examined aligns with the detrimental consequences of ATM loss across multiple systems that is seen in A-T patients. Furthermore, ATM protein expression was detected in both the nuclear and cytoplasmic regions of cells providing additional support for distinct roles of ATM function in these cellular components. The extent of loss of ATM protein expression observed in human tumours was variable across cancer subtypes and did not correspond with reported mutation frequencies[132]. An interesting finding was the observation of sub-populations of cells (likely lymphoid cells) that had high expression of ATM protein, predominantly in tissues associated with the immune system such as the spleen, tonsil, and thymus, as well as tumours that lacked detectable ATM protein expression. The identification and functional role of ATM in these cells remains unanswered. Further investigation is required to understand the biological significance of this. In addition, there may be clinical implications of the use of ATM inhibitors which may impact this sub-population.

Investigations into the consequences of ATM inhibition and loss on normal tissues in response to whole-body IR and irinotecan treatment were modelled *in vivo*. To our knowledge, this is the first demonstration of an ATM-dependent DNA DSB DDR in response to irinotecan treatment in normal tissues. Across all tissues investigated, the pharmacological inhibition or genetic loss of ATM conferred broadly similar phenotypes which were consistently associated with lower p-KAP1 and p-p53 levels in response to DNA damage. However, the extent of γH2AX staining was variable following the inhibition/loss of ATM and suggested that there may be tissue-dependent differences in DDR signalling to γH2AX following induction of DNA DSB that are independent of ATM.

Although irinotecan induces a DNA damage dependent DDR predominantly in replicating/S phase cells, our data also identified a robust DDR in irinotecan-treated animals in certain non-S phase tissue compartments, which was nonetheless dependent on functional ATM signalling, exemplified by the broncho-epithelial cells of the lung. Further investigation into the implications of this unexpected finding is needed.

The accumulated data from this study stresses that the consequences and targeting of ATM inhibition/loss in tumours is not straightforward. With a particular focus on topoisomerase I inhibition, differences were observed in the sensitivity of non-tumour cells between ATM inhibition and ATM loss. However, in proliferation assays, this was not recapitulated in the isogenic non-small cell tumour cell lines or in non-small cell tumour cell lines in combination with KU-55933, a pharmacological inhibitor of ATM kinase. Nonetheless, both the inhibition and loss of ATM conferred comparable sensitivity to SN-38 in a non-tumour and tumour setting but only following short-term exposure to SN-38 in clonogenic assays. These studies highlight the potential complexities of targeting ATM-deficiency in tumours.

Inhibiting the IGF-IGF1R axis has been identified as an approach to target the loss of ATM[365]. This finding was part of a collaborative project, and the screening hit was successfully validated by additional investigations. Other targets identified in the screen were ATR, which has been previously reported, and CDK and mTOR, which are novel targets reported in this work and warrant further investigation[374]. Additional target validation was provided through the use of the selective inhibitors AZD6738 (ATR) and AZD8055 (mTOR) in the context of ATM loss. Importantly, drug candidates are available for each of these targets to explore this further in the clinic.

Targeting ATM loss in the context of irinotecan has presented with complexities surrounding tumour sensitivities and the potential compensation for ATM loss in the signalling response to replication-associated DNA damage. In human tumours, the presence of ATM mutations is likely to coincide with additional somatic mutations. The relationship between ATM loss and sensitivity to topoisomerase I inhibition is unlikely to be straightforward. Whilst ATM loss has been reported to confer sensitivity to CPT family compounds in tumour cells, this sensitivity was not observed in the lung tumour cell lines investigated in the present work, except under conditions of brief exposure (1 hr) in clonogenic assays[164,300]. A more detailed understanding of the consequences of topoisomerase I inhibition as well as ATM inhibition/loss on tumour cells is required. The compensatory DDR signalling in response to SN-38 identified in our work highlighted the potential of combining agents that induce replicative stress with DNA-PK inhibition to selectively target tumours that lack functional ATM.

Overall, the identification of loss of ATM protein expression in tumours presents the potential for informing a targeted therapy approach. The occurrence of ATM mutations, especially heterozygous mutations, does not necessarily result in the functional impairment of ATM dependent signalling. Therefore, identifying loss of protein is an important additional avenue to explore and may be of more direct functional relevance than detecting mutations. The differences between ATM loss and inhibition, as well as differences between non-tumour and tumour cells, indicate phenotypic variability. Investigations underlying the relationship with ATM function and topoisomerase I inhibition requires further attention.

In conclusion, our work has identified high levels of loss of ATM protein expression in some tumour types. Although selective sensitivity of ATM-deficient tumour cells to SN-

38/irinotecan is not straightforward and is associated with the activation of compensatory DDR signalling pathways following S phase damage, our screening data has identified additional targets (CDK, mTOR) that could be evaluated in ATM-deficient tumours in the clinic and further validated in pre-clinical models. Taken together, our data suggests that normal tissue may respond in a biologically diverse way to anti-cancer therapies and in a distinct manner from tumours. This may be an important factor for taking into account when considering the biological and toxicological consequences of single drug, and drug combinations, in the clinic in a way which may not be apparent from current toxicology testing.

7 References

1. McGrath-Morrow, S. A. *et al.* Multidisciplinary management of ataxia telangiectasia: Current perspectives. *J. Multidiscip. Healthc.* **14**, 1637–1643 (2021).

2. Rothblum-Oviatt, C. *et al.* Ataxia telangiectasia: A review. *Orphanet J. Rare Dis.* **11**, 1–21 (2016).

3. McKinnon, P. J. ATM and the Molecular Pathogenesis of Ataxia Telangiectasia. *Annu. Rev. Pathol. Mech. Dis.* **7**, 303–321 (2012).

4. Bottini, A. R., Gatti, R. A., Wirenfeldt, M. & Vinters, H. Heterotopic Purkinje cells in ataxia-telangiectasia. *Neuropathology* **32**, 23–29 (2011).

5. Shiloh, Y., Andegeko, Y. & Tsarfaty, I. In search of drug treatment for genetic defects in the DNA damage response: The example of ataxia-telangiectasia. *Semin. Cancer Biol.* **14**, 295–305 (2004).

6. Iourov, I. Y., Vorsanova, S. G., Liehr, T., Kolotii, A. D. & Yurov, Y. B. Increased chromosome instability dramatically disrupts neural genome integrity and mediates cerebellar degeneration in the ataxia-telangiectasia brain. *Hum. Mol. Genet.* **18**, 2656–2669 (2009).

7. Amirifar, P., Ranjouri, M. R., Yazdani, R., Abolhassani, H. & Aghamohammadi, A. Ataxia-telangiectasia: A review of clinical features and molecular pathology. *Pediatr. Allergy Immunol.* **30**, 277–288 (2019).

8. Driessen, G. J. *et al.* Antibody deficiency in patients with ataxia telangiectasia is caused by disturbed B- and T-cell homeostasis and reduced immune repertoire

diversity. *J. Allergy Clin. Immunol.* **131**, 1367–1375 (2013).

9. Schubert, R., Reichenbach, J. & Zielen, S. Deficiencies in CD4+ and CD8+ T cell subsets in ataxia telangiectasia. *Clin. Exp. Immunol.* **129**, 125–132 (2002).

10. van Os, N. J. H. *et al.* Ataxia-telangiectasia: recommendations for multidisciplinary treatment. *Dev. Med. Child Neurol.* **59**, 680–689 (2017).

11. McGrath-Morrow, S. A. *et al.* Inflammation and transcriptional responses of peripheral blood mononuclear cells in classic ataxia telangiectasia. *PLoS One* **13**, 1–16 (2018).

12. Saunders, R. A. *et al.* Elevated inflammatory responses and targeted therapeutic intervention in a preclinical mouse model of ataxia-telangiectasia lung disease. *Sci. Rep.* **11**, 1–15 (2021).

13. Yeo, A. J. *et al.* Increased susceptibility of airway epithelial cells from ataxia-telangiectasia to S. pneumoniae infection due to oxidative damage and impaired innate immunity. *Sci. Rep.* **9**, 1–10 (2019).

14. Gumy-Pause, F., Wacker, P. & Sappino, A. P. ATM gene and lymphoid malignancies. *Leukemia* **18**, 238–242 (2004).

15. Taylor, A. M. R., Metcalfe, J. A., Thick, J. & Mak, Y. F. Leukemia and Lymphoma in Ataxia Telangiectasia. *Blood* **87**, 423–38 (1996).

16. Bakhtiar, S. *et al.* The incidence and type of cancer in patients with ataxia-telangiectasia via a retrospective single-centre study. *Br. J. Haematol.* **194**, 879–887 (2021).

17. Nazaryan-Petersen, L., Bjerregaard, V. A., Nielsen, F. C., Tommerup, N. & Tümer, Z. Chromothripsis and DNA repair disorders. *J. Clin. Med.* **9**, 1–9 (2020).

18. Reiman, A. *et al.* Lymphoid tumours and breast cancer in ataxia telangiectasia; Substantial protective effect of residual ATM kinase activity against childhood tumours. *Br. J. Cancer* **105**, 586–591 (2011).

19. Lavin, M. F. Radiosensitivity and oxidative signalling in ataxia telangiectasia: An update. *Radiother. Oncol.* **47**, 113–123 (1998).

20. Pollard, J. M. & Gatti, R. A. Clinical Radiation Sensitivity with DNA Repair Disorders: An overview. *Int. J. Radiat. Oncol. - Biol. - Phys.* **74**, 1323–1331 (2009).

21. Ahmed, O., Felimban, Y. & Almehdar, A. T cell ALL in a child with Ataxia telangiectasia; diagnosis and management challenges. *Hematology* **26**, 348–354 (2021).

22. Tamminga, R. Y. J., Dolsma, W. V., Leeuw, J. A. & Kampinga, H. H. Chemo- and radiosensitivity testing in a patient with ataxia telangiectasia and Hodgkin disease. *Pediatr. Hematol. Oncol.* **19**, 163–171 (2002).

23. Hart, R. M., Kimler, B. F., Evans, R. G. & Park, C. H. Radiotherapeutic management of medulloblastoma in a pediatric patient with ataxia telangiectasia. *Int. J. Radiat. Oncol. - Biol. - Phys.* **13**, 1237–1240 (1987).

24. Nissenkorn, A. *et al.* Endocrine abnormalities in ataxia telangiectasia: Findings from a national cohort. *Pediatr. Res.* **79**, 889–894 (2016).

25. Natale, V. A. I. *et al.* Growth in ataxia telangiectasia. *Orphanet J. Rare Dis.* **16**, 1–14 (2021).

26. Schubert, R., Reichenbach, J. & Zielen, S. Growth factor deficiency in patients with ataxia telangiectasia. *Clin. Exp. Immunol.* **140**, 517–519 (2005).

27. Hu, H., Nahas, S. & Gatti, R. A. Assaying Radiosensitivity of Ataxia-Telangiectasia. in *ATM Kinase* 1–11 (2017).

28. Savitsky, K. *et al.* A single ataxia telangiectasia gene with a product similar to PI-3 kinase. *Science (80-.).* **268**, 1749–1753 (1995).

29. Lee, P. *et al.* SMRT compounds abrogate cellular phenotypes of ataxia telangiectasia in neural derivatives of patient-specific hiPSCs. *Nat. Commun.* **4**, 1–8 (2013).

30. Barlow, C. *et al.* Atm Deficient Mice: A Paradigm of Ataxia Telangiectasia. *Cell* **86**, 159–171 (1996).

31. Gilad, S. *et al.* Predominance of null mutations in ataxia-telangiectasia. *Hum. Mol. Genet.* **5**, 433–439 (1996).

32. Lavin, M. F. *et al.* Functional consequences of sequence alterations in the ATM gene. *DNA Repair (Amst).* **3**, 1197–1205 (2004).

33. Rogatcheva, M. B. *et al.* Characterization of the porcine ATM gene: towards the generation of a novel non-murine animal model for Ataxia-Telangiectasia. *Gene* **405**, 27–35 (2007).

34. Lakin, N. D. *et al.* Analysis of the ATM protein in wild-type and ataxia telangiectasia cells. *Oncogene* **13**, 2707–2716 (1996).

35. Sandoval, N. *et al.* Characterization of ATM gene mutations in 66 ataxia

telangiectasia families. *Hum. Mol. Genet.* **8**, 69–79 (1999).

36. Lovejoy, C. A. & Cortez, D. Common mechanisms of PIKK regulation. *DNA Repair (Amst).* **8**, 1004–1008 (2009).

37. Perry, J. & Kleckner, N. The ATRs, ATMs, and TORs Are Giant HEAT Repeat Proteins. *Cell* **112**, 151–155 (2003).

38. Blackford, A. N. & Jackson, S. P. ATM, ATR, and DNA-PK: The Trinity at the Heart of the DNA Damage Response. *Mol. Cell* **66**, 801–817 (2017).

39. Guo, Z., Kozlov, S., Lavin, M. F., Person, M. D. & Paull, T. T. ATM activation by oxidative stress. *Science (80-.).* **330**, 517–521 (2010).

40. Lee, J. H. & Paull, T. T. Mitochondria at the crossroads of ATM-mediated stress signaling and regulation of reactive oxygen species. *Redox Biol.* **32**, 101511 (2020).

41. Tubbs, A. & Nussenzweig, A. Endogenous DNA Damage as a Source of Genomic Instability in Cancer. *Cell* **168**, 644–656 (2017).

42. Caron, P., van der Linden, J. & Attikum, H. V. Bon voyage: A transcriptional journey around DNA breaks. *DNA Repair (Amst).* **82**, 102686 (2019).

43. Schipler, A. & Iliakis, G. DNA double-strand-break complexity levels and their possible contributions to the probability for error-prone processing and repair pathway choice. *Nucleic Acids Res.* **41**, 7589–7605 (2013).

44. Hakem, R. DNA-damage repair; the good, the bad, and the ugly. *EMBO J.* **27**, 589–605 (2008).

45. O'Connor, M. J. Targeting the DNA Damage Response in Cancer. *Mol. Cell* **60**,

547–560 (2015).

46. Pearl, L. H., Schierz, A. C., Ward, S. E., Al-Lazikani, B. & Pearl, F. M. G. Therapeutic opportunities within the DNA damage response. *Nat. Rev. Cancer* **15**, 166–180 (2015).

47. O'Driscoll, M. & Jeggo, P. A. The role of double-strand break repair - insights from human genetics. *Nat. Rev. Genet.* **7**, 45–54 (2006).

48. Mills, K. D., Ferguson, D. O. & Alt, F. W. The role of DNA breaks in genomic instability and tumorigenesis. *Immunol. Rev.* **194**, 77–95 (2003).

49. Jung, D. & Alt, F. W. Unraveling V(D)J recombination; insights into gene regulation. *Cell* **116**, 299–311 (2004).

50. Vítor, A. C., Huertas, P., Legube, G. & de Almeida, S. F. Studying DNA Double-Strand Break Repair: An Ever-Growing Toolbox. *Front. Mol. Biosci.* **7**, 1–16 (2020).

51. Her, J. & Bunting, S. F. How cells ensure correct repair of DNA double-strand breaks. *J. Biol. Chem.* **293**, 10502–10511 (2018).

52. Brandsma, I. & Gent, D. C. Pathway choice in DNA double strand break repair: Observations of a balancing act. *Genome Integr.* **3**, 1–10 (2012).

53. Mahaney, B. L., Meek, K. & Lees-Miller, S. P. Repair of ionizing radiation-induced DNA double strand breaks by non-homologous end-joining. *Biochem. J.* **417**, 639–650 (2009).

54. Griffith, A. J., Blier, P. R., Mimori, T. & Hardin, J. A. Ku polypeptides synthesized

in vitro assemble into complexes which recognize ends of double-stranded DNA. *J. Biol. Chem.* **267**, 331–338 (1992).

55. Mari, P. O. *et al.* Dynamic assembly of end-joining complexes requires interaction between Ku70/80 and XRCC4. *Proc. Natl. Acad. Sci. U. S. A.* **103**, 18597–18602 (2006).

56. Yue, X., Bai, C., Xie, D., Ma, T. & Zhou, P. K. DNA-PKcs: A Multi-Faceted Player in DNA Damage Response. *Front. Genet.* **11**, (2020).

57. DeFazio, L. G., Stansel, R. M., Griffith, J. D. & Chu, G. Synapsis of DNA ends by DNA-dependent protein kinase. *EMBO J.* **21**, 3192–3200 (2002).

58. Davis, A. J. & Chen, D. J. DNA double strand break repair via non-homologous end-joining. *Transl. Cancer Res.* **2**, 130–143 (2013).

59. Ackerson, S. M., Romney, C., Schuck, P. L. & Stewart, J. A. To Join or Not to Join: Decision Points Along the Pathway to Double-Strand Break Repair vs. Chromosome End Protection. *Front. Cell Dev. Biol.* **9**, 1–19 (2021).

60. Phipps, J. & Dubrana, K. DNA Repair in Space and Time: Safeguarding the Genome with the Cohesin Complex. *Genes (Basel).* **13**, 198 (2022).

61. Chiruvella, K. K., Liang, Z. & Wilson, T. E. Repair of double-strand breaks by end joining. *Cold Spring Harb. Perspect. Biol.* **5**, 1–21 (2013).

62. Caracciolo, D., Riillo, C., Di Martino, M. T., Tagliaferri, P. & Tassone, P. Alternative Non-Homologous End-Joining: Error-Prone DNA Repair as Cancer's Achilles' Heel. *Cancers (Basel).* **13**, 1392 (2021).

63. Velic, D. *et al.* DNA Damage Signalling and Repair Inhibitors: The Long-Sought-After Achilles' Heel of Cancer. *Biomolecules* **5**, 3204–3259 (2015).

64. Helleday, T., Lo, J., van Gent, D. C. & Engelward, B. P. DNA double-strand break repair: from mechanistic understanding to cancer treatment. *DNA Repair (Amst).* **6**, 923–935 (2007).

65. Krejci, L., Altmannova, V., Spirek, M. & Zhao, X. Homologous recombination and its regulation. *Nucleic Acids Res.* **40**, 5795–5818 (2012).

66. Zhao, F., Kim, W., Kloeber, J. A. & Lou, Z. DNA end resection and its role in DNA replication and DSB repair choice in mammalian cells. *Exp. Mol. Med.* **52**, 1705–1714 (2020).

67. Lee, J.-H. & Paull, T. T. ATM activation by DNA double-strand breaks through the Mre11-Rad50-Nbs1 complex. *Science (80-.).* **308**, 551–554 (2005).

68. Bakkenist, C. J. & Kastan, M. B. DNA damage activates ATM through intermolecular autophosphorylation and dimer dissociation. *Nature* **421**, 499–506 (2003).

69. Du, F. *et al.* Dimer monomer transition and dimer re-formation play important role for ATM cellular function during DNA repair. *Biochem. Biophys. Res. Commun.* **452**, 1034–1039 (2014).

70. So, S., Davis, A. J. & Chen, D. J. Autophosphorylation at serine 1981 stabilizes ATM at DNA damage sites. *J. Cell Biol.* **187**, 977–990 (2009).

71. Daniel, J. A. *et al.* Multiple autophosphorylation sites are dispensible for murine ATM activation in vivo. *J. Cell Biol.* **183**, 777–783 (2008).

72. Kozlov, S., Gueven, N., Keating, K., Ramsay, J. & Lavin, M. F. ATP activates ataxia-telangiectasia mutated (ATM) in vitro. Importance of autophosphorylation. *J. Biol. Chem.* **278**, 9309–9317 (2003).

73. Pellegrini, M. *et al.* Autophosphorylation at serine 1987 is dispensible for murine Atm activation in vivo. *Nature* **443**, 222–225 (2006).

74. Uziel, T. *et al.* Requirement of the MRN complex for ATM activation by DNA damage. *EMBO J.* **22**, 5612–5621 (2003).

75. Mailand, N. *et al.* RNF8 Ubiquitylates Histones at DNA Double-Strand Breaks and Promotes Assembly of Repair Proteins. *Cell* **131**, 887–900 (2007).

76. Huen, M. S. Y. *et al.* RNF8 transduces the DNA-damage signal via histone ubiquitylation and checkpoint protein assembly. *Cell* **131**, 901–914 (2007).

77. Doil, C. *et al.* RNF168 binds and amplifies ubiquitin conjugates on damaged chromosomes to allow accumulation of repair proteins. *Cell* **136**, 435–446 (2009).

78. Maréchal, A. & Zou, L. DNA damage sensing by the ATM and ATR kinases. *Cold Spring Harb. Perspect. Biol.* **5**, 1–17 (2013).

79. Shibata, A. & Jeggo, P. A. ATM's role in the repair of DNA double-strand breaks. *Genes (Basel).* **12**, 1370 (2021).

80. Stucki, M. *et al.* MDC1 Directly Binds Phosphorylated Histone H2AX to Regulate Cellular Responses to DNA Double-Strand Breaks. *Cell* **123**, 1213–1226 (2005).

81. Löbrich, M. *et al.* γH2AX foci analysis for monitoring DNA double-strand break repair. *Cell Cycle* **9**, 662–669 (2010).

82. Lou, Z. *et al.* MDC1 Maintains Genomic Stability by Participating in the Amplification of ATM-Dependent DNA Damage Signals. *Mol. Cell* **21**, 187–200 (2006).

83. Kijas, A. W. *et al.* ATM-dependent phosphorylation of MRE11 controls extent of resection during homology directed repair by signalling through Exonuclease 1. *Nucleic Acids Res.* **43**, 8352–8367 (2015).

84. Lavin, M. F., Kozlov, S., Gatei, M. & Kijas, A. W. ATM-dependent phosphorylation of all three members of the MRN complex: From sensor to adaptor. *Biomolecules* **5**, 2877–2902 (2015).

85. Tarsounas, M., Davies, A. A. & West, S. C. RAD51 localization and activation following DNA damage. *Philos. Trans. R. Soc. B Biol. Sci.* **359**, 87–93 (2004).

86. West, S. C. Molecular views of recombination proteins and their control. *Nat. Rev. Mol. Cell Biol.* **4**, 435–445 (2003).

87. Li, X. & Heyer, W. D. Homologous recombination in DNA repair and DNA damage tolerance. *Cell Res.* **18**, 99–113 (2008).

88. Wyatt, H. D. M., Sarbajna, S., Matos, J. & West, S. C. Coordinated actions of SLX1-SLX4 and MUS81-EME1 for holliday junction resolution in human cells. *Mol. Cell* **52**, 234–247 (2013).

89. Sarbajna, S., Davies, D. & West, S. C. Roles of SLX1-SLX4, MUS81-EME1, and GEN1 in avoiding genome instability and mitotic catastrophe. *Genes Dev.* **28**, 1124–1136 (2014).

90. Beucher, A. *et al.* ATM and Artemis promote homologous recombination of

radiation-induced DNA double-strand breaks in G2. *EMBO J.* **28**, 3413–3427 (2009).

91. Shaltiel, I. A., Krenning, L., Bruinsma, W. & Medema, R. H. The same, only different - DNA damage checkpoints and their reversal throughout the cell cycle. *J. Cell Sci.* **128**, 607–620 (2015).

92. Kaina, B. DNA damage-triggered apoptosis: critical role of DNA repair, double-strand breaks, cell proliferation and signaling. *Biochem. Pharmacol.* **66**, 1547–1554 (2003).

93. Oren, M. Decision making by p53: Life, death and cancer. *Cell Death Differ.* **10**, 431–442 (2003).

94. Weber, A. M. & Ryan, A. J. ATM and ATR as therapeutic targets in cancer. *Pharmacol. Ther.* **149**, 124–138 (2015).

95. Maya, R. *et al.* ATM-dependent phosphorylation of Mdm2 on serine 395: role in p53 activation by DNA damage. *Genes Dev.* **15**, 1067–1077 (2001).

96. Bartek, J. & Lukas, J. Pathways governing G1/S transition and their response to DNA damage. *FEBS Lett.* **490**, 117–122 (2001).

97. Cheng, Q. Mechanisms of p53 stabilization. *Cell Cycle* **9**, 472–478 (2010).

98. Iyer, D. R. & Rhind, N. The intra-S checkpoint responses to DNA damage. *Genes (Basel).* **8**, (2017).

99. Willis, N. & Rhind, N. Regulation of DNA replication by the S-phase DNA damage checkpoint. *Cell Div.* **4**, 1–10 (2009).

100. Liu, Y. *et al.* The intra-S phase checkpoint directly regulates replication elongation to preserve the integrity of stalled replisomes. *Proc. Natl. Acad. Sci. U. S. A.* **118**, 1–11 (2021).

101. Stark, G. R. & Taylor, W. R. Analyzing the G2/M Checkpoint. *Methods Mol. Biol.* **280**, 51–82 (2004).

102. de Gooijer, M. C. *et al.* The G2 checkpoint—a node-based molecular switch. *FEBS Open Bio* **7**, 439–455 (2017).

103. Schmidt, M. *et al.* Regulation of G2/M transition by inhibition of WEE1 and PKMYT1 Kinases. *Molecules* **22**, 1–17 (2017).

104. Phaniendra, A., Jestadi, D. B. & Periyasamy, L. Free Radicals: Properties, Sources, Targets, and Their Implication in Various Diseases. *Indian J. Clin. Biochem.* **30**, 11–26 (2015).

105. Birben, E., Sahiner, U. M., Sackesen, C., Erzurum, S. & Kalayci, O. Oxidative stress and antioxidant defense. *World Allergy Organ. J.* **5**, 9–19 (2012).

106. Lee, J. H. & Paull, T. T. Cellular functions of the protein kinase ATM and their relevance to human disease. *Nat. Rev. Mol. Cell Biol.* **22**, 796–814 (2021).

107. Zhang, Y. *et al.* Mitochondrial redox sensing by the kinase ATM maintains cellular antioxidant capacity. *Sci. Signal.* **11**, 1–24 (2018).

108. Paull, T. T. Mechanisms of ATM activation. *Annu. Rev. Biochem.* **84**, 711–738 (2015).

109. Olcina, M. M., Grand, R. J. A. & Hammond, E. M. ATM activation in hypoxia -

causes and consequences. *Mol. Cell. Oncol.* **1**, 1–8 (2014).

110. Weyemia, U. *et al.* NADPH oxidase 4 is a critical mediator in Ataxia telangiectasia disease. *Proc. Natl. Acad. Sci. U. S. A.* **112**, 2121–2126 (2015).

111. Lee, J. *et al.* ATM directs DNA damage responses and proteostasis via genetically separable pathways. *Sci. Signal.* **11**, 5598 (2018).

112. Kim, M.-H., Kim, A., Yu, J. H., Lim, J. W. & Kim, H. Glutamine deprivation induces interleukin-8 expression in ataxia telangiectasia fibroblasts. *Inflamm. Res.* **63**, 347–356 (2014).

113. Maciejczyk, M. *et al.* Antioxidant defense, redox homeostasis, and oxidative damage in children with ataxia telangiectasia and nijmegen breakage syndrome. *Front. Immunol.* **10**, 1–11 (2019).

114. Song, X., Ma, F. & Herrup, K. Accumulation of cytoplasmic DNA due to ATM deficiency activates the microglial viral response system with neurotoxic consequences. *J. Neurosci.* **39**, 6378–6394 (2021).

115. Jackson, S. P. & Bartek, J. The DNA-damage response in human biology and disease. *Nature* **461**, 1071–1078 (2009).

116. Tiwari, V. & Wilson, D. M. DNA Damage and Associated DNA Repair Defects in Disease and Premature Aging. *Am. J. Hum. Genet.* **105**, 237–257 (2019).

117. Bouwman, P. & Jonkers, J. The effects of deregulated DNA damage signalling on cancer chemotherapy response and resistance. *Nat. Rev. Cancer* **12**, 587–598 (2012).

118. Huang, R. & Zhou, P. K. DNA damage repair: historical perspectives, mechanistic pathways and clinical translation for targeted cancer therapy. *Signal Transduct. Target. Ther.* **6**, 254 (2021).

119. Brandsma, I., Fleuren, E. D. G., Williamson, C. T. & Lord, C. J. Directing the use of DDR kinase inhibitors in cancer treatment. *Expert Opin. Investig. Drugs* **26**, 1341–1355 (2017).

120. Hu, Y. & Guo, M. Synthetic lethality strategies: Beyond BRCA1/2 mutations in pancreatic cancer. *Cancer Sci.* **111**, 3111–3121 (2020).

121. Huang, A., Garraway, L. A., Ashworth, A. & Weber, B. Synthetic lethality as an engine for cancer drug target discovery. *Nat. Rev. Drug Discov.* **19**, 23–38 (2020).

122. Topatana, W. *et al.* Advances in synthetic lethality for cancer therapy: cellular mechanism and clinical translation. *J. Hematol. Oncol.* **13**, 1–22 (2020).

123. Bryant, H. E. *et al.* Specific killing of BRCA2-deficient tumours with inhibitors of poly(ADP-ribose) polymerase. *Nature* **434**, 913–917 (2005).

124. Farmer, H. *et al.* Targeting the DNA repair defect in BRCA mutant cells as a therapeutic strategy. *Nature* **434**, 917–921 (2005).

125. Li, L. Y., Guan, Y. Di, Chen, X. S., Yang, J. M. & Cheng, Y. DNA Repair Pathways in Cancer Therapy and Resistance. *Front. Pharmacol.* **11**, 1–13 (2021).

126. Pilié, P. G., Gay, C. M., Byers, L. A., O'Connor, M. J. & Yap, T. A. PARP Inhibitors: Extending Benefit Beyond BRCA-Mutant Cancers. *Clin. Cancer Res.* **25**, 3759–3771 (2019).

127. Mc Gee, M. M. Targeting the Mitotic Catastrophe Signaling Pathway in Cancer. *Mediators Inflamm.* **2015**, 146282 (2015).

128. Visconti, R., Della Monica, R. & Grieco, D. Cell cycle checkpoint in cancer: A therapeutically targetable double-edged sword. *J. Exp. Clin. Cancer Res.* **35**, 1–8 (2016).

129. Ahmed, M. & Rahman, N. ATM and breast cancer susceptibility. *Oncogene* **25**, 5906–5911 (2006).

130. Moslemi, M. *et al.* The association between ATM variants and risk of breast cancer: a systematic review and meta-analysis. *BMC Cancer* **21**, (2021).

131. Lavin, M. F. Ataxia-telangiectasia: from a rare disorder to a paradigm for cell signalling and cancer. *Nat. Rev. Mol. Cell Biol.* **9**, 759–769 (2008).

132. Choi, M., Kipps, T. & Kurzrock, R. ATM mutations in cancer: Therapeutic implications. *Mol. Cancer Ther.* **15**, 1781–1791 (2016).

133. Gachechiladze, M., Skarda, J., Bouchalova, K., Soltermann, A. & Joerger, M. Predictive and Prognostic Value of DNA Damage Response Associated Kinases in Solid Tumors. *Front. Oncol.* **10**, 1–10 (2020).

134. Bueno, R. C. *et al.* ATM down-regulation is associated with poor prognosis in sporadic breast carcinomas. *Ann. Oncol.* **25**, 69–75 (2014).

135. Lee, H. E. *et al.* DNA damage response-related proteins in gastric cancer: ATM, Chk2 and p53 expression and their prognostic value. *Pathobiology* **81**, 25–35 (2013).

136. Randon, G. *et al.* Prognostic impact of ATM mutations in patients with metastatic colorectal cancer. *Sci. Rep.* **9**, 1–7 (2019).

137. Stucci, L. S. *et al.* The atm gene in breast cancer: Its relevance in clinical practice. *Genes (Basel).* **12**, 727 (2021).

138. Villaruz, L. C. *et al.* ATM protein is deficient in over 40% of lung adenocarcinomas. *Oncotarget* **7**, 57714–57725 (2016).

139. Shaik, A. & Kirubakaran, S. Evolution of PIKK family kinase inhibitors: A new age cancer therapeutics. *Front. Biosci.* **25**, 1510–1537 (2020).

140. Angira, D., Shaik, A. & Thiruvenkatam, V. Structural and strategic landscape of PIKK protein family and their inhibitors: an overview. *Front. Biosci.* **25**, 1538–1567 (2020).

141. Calonge, T. M., Eshaghi, M., Liu, J., Ronai, Z. & O'Connell, M. J. Transformation/transcription domain-associated protein (TRRAP)-mediated regulation of wee1. *Genetics* **185**, 81–93 (2010).

142. Mohiuddin, I. S. & Kang, M. H. DNA-PK as an Emerging Therapeutic Target in Cancer. *Front. Oncol.* **6**, 1–8 (2019).

143. Collis, S. J., DeWeese, T. L., Jeggo, P. A. & Parker, A. R. The life and death of DNA-PK. *Oncogene* **24**, 949–961 (2005).

144. Zeman, M. K. & Cimprich, K. A. Causes and Consequences of Replication Stress. *Nat. Cell Biol.* **16**, 2–9 (2014).

145. Saldivar, J. C., Cortez, D. & Cimprich, K. A. The essential kinase ATR: Ensuring

faithful duplication of a challenging genome. *Nat. Rev. Mol. Cell Biol.* **18**, 622–636 (2017).

146. Painter, R. B. Radioresistant DNA synthesis: an intrinsic feature of ataxia telangiectasia. *Mutat. Res. Mol. Mech. Mutagen.* **84**, 183–190 (1981).

147. Kastan, M. B. *et al.* A mammalian cell cycle checkpoint pathway utilizing p53 and GADD45 is defective in ataxia-telangiectasia. *Cell* **71**, 587–597 (1992).

148. Gilad, S. *et al.* Genotype-Phenotype Relationships in Ataxia-Telangiectasia and Variants. *Am. J. Hum. Genet.* **62**, 551–561 (1998).

149. Cornforth, M. N. & Bedford, J. S. On the Nature of a Defect in Cells from Individuals with Ataxia-Telangiectasia. *Science (80-.).* **227**, 1589–1591 (1985).

150. Foray, N. *et al.* Hypersensitivity of ataxia telangiectasia fibroblasts to ionizing radiation is associated with a repair deficiency of DNA double-strand breaks. *Int. J. Radiat. Biol.* **72**, 271–283 (1997).

151. Goodarzi, A. A., Jeggo, P. & Lobrich, M. The influence of heterochromatin on DNA double strand break repair: Getting the strong, silent type to relax. *DNA Repair (Amst).* **9**, 1273–1282 (2010).

152. Ziv, Y. *et al.* Chromatin relaxation in response to DNA double-strand breaks is modulated by a novel ATM-and KAP-1 dependent pathway. *Nat. Cell Biol.* **8**, 870–876 (2006).

153. Goodarzi, A. A. *et al.* ATM Signaling Facilitates Repair of DNA Double-Strand Breaks Associated with Heterochromatin. *Mol. Cell* **31**, 167–177 (2008).

154. Woodbine, L., Brunton, H., Goodarzi, A. A., Shibata, A. & Jeggo, P. A. Endogenously induced DNA double strand breaks arise in heterochromatic DNA regions and require ataxia telangiectasia mutated and Artemis for their repair. *Nucleic Acids Res.* **39**, 6986–6997 (2011).

155. Sharma, N. K. *et al.* Intrinsic mitochondrial DNA repair defects in Ataxia Telangiectasia. *DNA Repair (Amst).* **13**, 22–31 (2014).

156. Riches, L. C. *et al.* Pharmacology of the ATM Inhibitor AZD0156: Potentiation of Irradiation and Olaparib Responses Preclinically. *Mol. Cancer Ther.* **19**, 13–25 (2020).

157. Durant, S. T. *et al.* The brain-penetrant clinical ATM inhibitor AZD1390 radiosensitizes and improves survival of preclinical brain tumor models. *Sci. Adv.* **4**, 1–16 (2018).

158. Rainey, M., Charlton, M., Stanton, R. & Kastan, M. Transient inhibition of ATM kinase is sufficient to enhance cellular sensitivity to Ionizing Radiation. *Cancer Res.* **68**, 7466–7474 (2008).

159. Guo, K., Shelat, A. A., Guy, R. K. & Kastan, M. B. Development of a cell-based, high-throughput screening assay for ATM kinase inhibitors. *J. Biomol. Screen.* **19**, 538–546 (2014).

160. Hickson, I. *et al.* Identification and characterization of a novel and specific inhibitor of the ataxia-telangiectasia mutated kinase ATM. *Cancer Res.* **64**, 9152–9159 (2004).

161. Huang, C., Filippone, N. R., Reiner, T. & Roberts, S. Sensors and Inhibitors for the

Detection of Ataxia Telangiectasia Mutated (ATM) Protein Kinase. *Mol. Pharm.* **18**, 2470–2481 (2021).

162. Golding, S. E. *et al.* Improved ATM kinase inhibitor KU-60019 radiosensitizes glioma cells, compromises insulin, AKT and ERK prosurvival signaling, and inhibits migration and invasion. *Mol. Cancer Ther.* **8**, 2894–2902 (2009).

163. Golding, S. E. *et al.* Dynamic inhibition of ATM kinase provides a strategy for glioblastoma multiforme radiosensitization and growth control. *Cell Cycle* **11**, 1167–1173 (2012).

164. Batey, M. A. *et al.* Preclinical evaluation of a novel ATM inhibitor, KU59403, in vitro and in vivo in p53 functional and dysfunctional models of human cancer. *Mol. Cancer Ther.* **12**, 959–967 (2013).

165. Degorce, S. L. *et al.* Discovery of Novel 3-Quinoline Carboxamides as Potent, Selective, and Orally Bioavailable Inhibitors of Ataxia Telangiectasia Mutated (ATM) Kinase. *J. Med. Chem.* **59**, 6281–6292 (2016).

166. Greene, J. *et al.* The novel ATM inhibitor (AZ31) enhances antitumor activity in patient derived xenografts that are resistant to irinotecan monotherapy. *Oncotarget* **8**, 110904–110913 (2017).

167. Karlin, J. *et al.* Orally bioavailable and blood-brain-barrier penetrating ATM inhibitor (AZ32) radiosensitises intracranial gliomas in mice. *Mol. Cancer Ther.* **17**, 1637–1647 (2019).

168. Ball, L. G. & Xiao, W. Molecular basis of ataxia telangiectasia and related diseases. *Acta Pharmacol. Sin.* **26**, 897–907 (2005).

169. Alderton, G. K. *et al.* Seckel syndrome exhibits cellular features demonstrating defects in the ATR-signalling pathway. *Hum. Mol. Genet.* **13**, 3127–3138 (2004).

170. Brown, E. J. & Baltimore, D. ATR disruption leads to chromosomal fragmentation and early embryonic lethality. *Genes Dev.* **14**, 397–402 (2000).

171. van der Burg, M., van Dongen, J. J. M. & van Gent, D. C. DNA-PKcs deficiency in human: long predicted, finally found. *Curr. Opin. Allergy Clin. Immunol.* **9**, 503–509 (2009).

172. McBride, K. A. *et al.* Li-Fraumeni syndrome: Cancer risk assessment and clinical management. *Nat. Rev. Clin. Oncol.* **11**, 260–271 (2014).

173. Frebourg, T. *et al.* Guidelines for the Li–Fraumeni and heritable TP53-related cancer syndromes. *Eur. J. Hum. Genet.* **28**, 1379–1386 (2020).

174. Smida, M. *et al.* MEK inhibitors block growth of lung tumours with mutations in ataxia-telangiectasia mutated. *Nat. Commun.* **7**, 1–13 (2016).

175. Bialkowska, A. B., Ghaleb, A. M., Nandan, M. O. & Yang, V. W. Improved swiss-rolling technique for intestinal tissue preparation for immunohistochemical and immunofluorescent analyses. *J. Vis. Exp.* **2016**, 1–8 (2016).

176. Maughan, T. *et al.* Addition of cetuximab to oxaliplatin-based first-line combination chemotherapy for treatment of advanced colorectal cancer: results of the randomised phase 3 MRC COIN trial. *Lancet* **377**, 2103–2114 (2011).

177. Corrie, P. G. *et al.* Adjuvant bevacizumab for melanoma patients at high risk of recurrence: Survival analysis of the AVAST-M trial. *Ann. Oncol.* **29**, 1843–1852 (2018).

178. Drewry, D. H. *et al.* Progress towards a public chemogenomic set for protein kinases and a call for contributions. *PLoS One* **12**, 1–20 (2017).

179. Wells, C. I. *et al.* The kinase chemogenomic set (KCGS): An open science resource for kinase vulnerability identification. *Int. J. Mol. Sci.* **22**, 1–18 (2021).

180. Zhang, J. H., Chung, T. D. & Oldenburg, K. R. A Simple Statistical Parameter for Use in Evaluation and Validation of High Throughput Screening Assays. *J. Biomol. Screen.* **4**, 67–73 (1999).

181. Gately, D. P., Hittle, J. C., Chan, G. K. T. & Yen, T. J. Characterization of ATM Expression, Localization, and Associated DNA-dependent Protein Kinase Activity. *Mol. Biol. Cell* **9**, 2361–74 (1998).

182. Stagni, V., Ferri, A., Cirotti, C. & Barilà, D. ATM Kinase-Dependent Regulation of Autophagy: A Key Player in Senescence? *Front. Cell Dev. Biol.* **8**, 1–6 (2021).

183. So, E. Y. & Ouchi, T. Translational initiation regulated by ATM in dendritic cells development. *Cell Death Dis.* **5**, 1–11 (2014).

184. Gueven, N. *et al.* Regulation of the Atm promoter In Vivo. *Genes, Chromosom. Cancer* **45**, 61–71 (2006).

185. Boultwood, J. Ataxia telangiectasia gene mutations in leukaemia and lymphoma. *J. Clin. Pathol.* **54**, 512–516 (2001).

186. Cerami, E. *et al.* The cBio Cancer Genomics Portal: An Open Platform for Exploring Multidimensional Cancer Genomics Data. *Cancer Discov.* **2**, 401–4 (2012).

187. Gao, J. *et al.* Integrative Analysis of Complex Cancer Genomics and Clinical Profiles Using the cBioPortal Complementary Data Sources and Analysis Options. *Sci. Signal.* **6**, 1–20 (2014).

188. Puiggros, A., Blanco, G. & Espinet, B. Genetic abnormalities in chronic lymphocytic leukemia: Where we are and where we go. *Biomed Res. Int.* **2014**, (2014).

189. Jette, N. R. *et al.* ATM-deficient cancers provide new opportunities for precision oncology. *Cancers (Basel).* **12**, 1–13 (2020).

190. Lane, D. P. p53, guardian of the genome. *Nature* **358**, 15–16 (1992).

191. Lee, C. S. *et al.* Enhancing the landscape of colorectal cancer using targeted deep sequencing. *Sci. Rep.* **11**, 1–26 (2021).

192. Weigelt, B. *et al.* The landscape of somatic genetic alterations in breast cancers from atm germline mutation carriers. *J. Natl. Cancer Inst.* **110**, 1030–1034 (2018).

193. Mareckova, A. *et al.* ATM and TP53 mutations show mutual exclusivity but distinct clinical impact in mantle cell lymphoma patients. *Leuk. Lymphoma* **60**, 1420–1428 (2019).

194. Uhlén, M. *et al.* Tissue-based map of the human proteome. *Science (80-.).* **347**, (2015).

195. Uhlén, M. *et al.* A human protein atlas for normal and cancer tissues based on antibody proteomics. *Mol. Cell. Proteomics* **4**, 1920–1932 (2005).

196. Uhlen, M. *et al.* A pathology atlas of the human cancer transcriptome. *Science (80-*

.). **357**, (2017).

197. Weber, A. M. *et al.* Phenotypic consequences of somatic mutations in the ataxiatelangiectasia mutated gene in non-small cell lung cancer. *Oncotarget* **7**, 60807–60822 (2016).

198. Yang, Y. & Herrup, K. Loss of neuronal cell cycle control in ataxia-telangiectasia: A unified disease mechanism. *J. Neurosci.* **25**, 2522–2529 (2005).

199. Leemput, J. *et al.* ATM localization and gene expression in the adult mouse eye. *Mol. Vis.* **15**, 393–416 (2009).

200. Raz-Prag, D. *et al.* A Role for Vascular Deficiency in Retinal Pathology in a Mouse Model of Ataxia-Telangiectasia. *Am. J. Pathol.* **179**, 1533–1541 (2011).

201. Schiavone, S., Jaquet, V., Trabace, L. & Krause, K. H. Severe life stress and oxidative stress in the brain: From animal models to human pathology. *Antioxidants Redox Signal.* **18**, 1475–1490 (2013).

202. Trifunovic, S. *et al.* The Function of the Hypothalamic–Pituitary–Adrenal Axis During Experimental Autoimmune Encephalomyelitis: Involvement of Oxidative Stress Mediators. *Front. Neurosci.* **15**, 1–14 (2021).

203. Schroeder, S. A. & Zielen, S. Infections of the respiratory system in patients with ataxia-telangiectasia. *Pediatr. Pulmonol.* **49**, 389–399 (2013).

204. Foster, C. R., Zha, Q., Daniel, L. L., Singh, M. & Singh, K. Lack of ATM induces structural and functional changes in the heart: Role in β-adrenergic receptor-stimulated apoptosis. *Exp. Physiol.* **97**, 506–515 (2012).

205. Blignaut, M., Loos, B., Botchway, S. W., Parker, A. W. & Huisamen, B. Ataxia-Telangiectasia Mutated is located in cardiac mitochondria and impacts oxidative phosphorylation. *Sci. Rep.* **9**, 1–11 (2019).

206. Pizzamiglio, L., Focchi, E. & Antonucci, F. ATM Protein Kinase: Old and New Implications in Neuronal Pathways and Brain Circuitry. *Cells* **9**, 1–24 (2020).

207. Di Siena, S. *et al.* Atm reactivation reverses ataxia telangiectasia phenotypes in vivo. *Cell Death Dis.* **9**, 1–13 (2018).

208. Barlow, C. *et al.* Atm deficiency results in severe meiotic disruption as early as leptonema of prophase I. *Development* **125**, 4007–17 (1998).

209. Kim, J. H., Jenrow, K. A. & Brown, S. L. Mechanisms of radiation-induced normal tissue toxicity and implications for future clinical trials. *Radiat. Oncol. J.* **32**, 103–115 (2014).

210. Barnett, G. C. *et al.* Normal tissue reactions to radiotherapy: Towards tailoring treatment dose by genotype. *Nat. Rev. Cancer* **9**, 134–142 (2009).

211. Krauthammer, A. *et al.* Long-term nutritional and gastrointestinal aspects in patients with ataxia telangiectasia. *Nutrition* **46**, 48–52 (2018).

212. Baena-Del Valle, J. A. *et al.* Rapid loss of RNA Detection by In Situ Hybridization in Stored Tissue Blocks and Preservation by Cold Storage of Unstained Slides. *Am. J. Clin. Pathol.* **148**, 398–415 (2017).

213. Sundar, R. *et al.* Ataxia Telangiectasia Mutated Protein Loss and Benefit From Oxaliplatin-based Chemotherapy in Colorectal Cancer. *Clin. Colorectal Cancer* **17**, 280–284 (2018).

214. Kaur, H. B. *et al.* Genomic and Clinical-Pathologic Characterization of ATM-deficient Prostate Cancer. *Clin. Cancer Res.* **26**, 4869–4881 (2020).

215. Kim, H. *et al.* Having pancreatic cancer with tumoral loss of ATM and normal TP53 protein expression is associated with a poorer prognosis. *Clin. Cancer Res.* **20**, 1865–1872 (2014).

216. Sarbia, M., Ott, N., Pühringer-Oppermann, F. & Brücher, B. L. D. M. The predictive value of molecular markers (p53, EGFR, ATM, CHK2) in multimodally treated squamous cell carcinoma of the oesophagus. *Br. J. Cancer* **97**, 1404–1408 (2007).

217. Jiang, Y. *et al.* Ataxia-telangiectasia mutated expression is associated with tobacco smoke exposure in esophageal cancer tissues and benzo[a]pyrene diol epoxide in cell lines. *Int. J. Cancer* **120**, 91–95 (2007).

218. Petersen, L. F. *et al.* Loss of tumour-specific ATM protein expression is an independent prognostic factor in early resected NSCLC. *Oncotarget* **8**, 38326–38336 (2017).

219. Vo, Q. N. *et al.* The ATM gene is a target for epigenetic silencing in locally advanced breast cancer. *Oncogene* **23**, 9432–9437 (2004).

220. Flanagan, J. M. *et al.* Gene-body hypermethylation of ATM in peripheral blood DNA of bilateral breast cancer patients. *Hum. Mol. Genet.* **18**, 1332–1342 (2009).

221. Cuatrecasas, M. *et al.* ATM gene expression is associated with differentiation and angiogenesis in infiltrating breast carcinomas. *Histol. Histopathol.* **21**, 149–156 (2006).

222. Estiar, M. A. & Mehdipour, P. ATM in breast and brain tumors: a comprehensive

review. *Cancer Biol. Med.* **15**, 210–227 (2018).

223. Seol, H. J. *et al.* Prognostic implications of the DNA damage response pathway in glioblastoma. *Oncol. Rep.* **26**, 423–430 (2011).

224. Ren, W., Xue, B., Chen, M., Liu, L. & Zu, X. Low Expression of ATM Indicates a Poor Prognosis in Clear Cell Renal Cell Carcinoma. *Clin. Genitourin. Cancer* **17**, 433–439 (2019).

225. Schepeler, T. *et al.* A high resolution genomic portrait of bladder cancer: correlation between genomic aberrations and the DNA damage response. *Oncogene* **32**, 3577–3586 (2013).

226. Moschos, S. J. *et al.* Suppressing the high-level expression and function of ATM in advanced-stage melanomas does not sensitize the cells to ionizing radiation. *Cancer Biol. Ther.* **8**, 1815–1825 (2009).

227. Jha, J. *et al.* Prognostic relevance of ATM protein in uveal melanoma and its association with clinicopathological factors. *Int. J. Clin. Oncol.* **24**, 1526–1535 (2019).

228. Sun, W. *et al.* Targeting DNA Damage Repair for Immune Checkpoint Inhibition: Mechanisms and Potential Clinical Applications. *Front. Oncol.* **11**, 1–12 (2021).

229. Qing, T. *et al.* Diverse immune response of DNA damage repair-deficient tumors. *Cell Reports Med.* **2**, 100276 (2021).

230. Hu, M. *et al.* ATM inhibition enhances cancer immunotherapy by promoting mtDNA leakage and cGAS/STING activation. *J. Clin. Invest.* **131**, 1–15 (2021).

231. Matei, I. R., Guidos, C. J. & Danska, J. S. ATM-dependent DNA damage surveillance in T-cell development and leukemogenesis: The DSB connection. *Immunol. Rev.* **209**, 142–158 (2006).

232. Riabinska, A. *et al.* ATM activity in T cells is critical for immune surveillance of lymphoma in vivo. *Leukemia* **34**, 771–786 (2020).

233. Bagley, J., Singh, G. & Iacomini, J. Regulation of Oxidative Stress Responses by Ataxia-Telangiectasia Mutated Is Required for T Cell Proliferation. *J. Immunol.* **178**, 4757–4763 (2007).

234. Vacchio, M. S., Olaru, A., Livak, F. & Hodes, R. J. ATM deficiency impairs thymocyte maturation because of defective resolution of T cell receptor α locus coding end breaks. *Proc. Natl. Acad. Sci. U. S. A.* **104**, 6323–6328 (2007).

235. Sato, H. *et al.* DNA double-strand break repair pathway regulates PD-L1 expression in cancer cells. *Nat. Commun.* **8**, (2017).

236. Lambrechts, D. *et al.* Phenotype molding of stromal cells in the lung tumor microenvironment. *Nat. Med.* **24**, 1277–1289 (2018).

237. Zingoni, A., Ardolino, M., Santoni, A. & Cerboni, C. NKG2D and DNAM-1 activating receptors and their ligands in NK-T cell interactions: Role in the NK cell-mediated negative regulation of T cell responses. *Front. Immunol.* **3**, 1–7 (2012).

238. Zhang, N. & Bevan, M. J. CD8+ T Cells: Foot Soldiers of the Immune System. *Immunity* **35**, 161–168 (2011).

239. Tupin, E., Kinjo, Y. & Kronenberg, M. The unique role of natural killer T cells in the response to microorganisms. *Nat. Rev. Microbiol.* **5**, 405–417 (2007).

240. Chan, C. J., Smyth, M. J. & Martinet, L. Molecular mechanisms of natural killer cell activation in response to cellular stress. *Cell Death Differ.* **21**, 5–14 (2014).

241. Barili, V. *et al.* Targeting p53 and histone methyltransferases restores exhausted CD8+ T cells in HCV infection. *Nat. Commun.* **11**, (2020).

242. Cerboni, C. *et al.* Antigen-activated human T lymphocytes express cell-surface NKG2D ligands via an ATM/ATR-dependent mechanism and become susceptible to autologous NK-cell lysis. *Blood* **110**, 606–615 (2007).

243. Cao, J. *et al.* Identifying ataxia-telangiectasia in cancer patients: Novel insights from an interesting case and review of literature. *Clin. Case Reports* **9**, 995–1009 (2020).

244. Campbell, A. *et al.* A novel mouse model for ataxia-telangiectasia with a N-terminal mutation displays a behavioral defect and a low incidence of lymphoma but no increased oxidative burden. *Hum. Mol. Genet.* **24**, 6331–6349 (2015).

245. Genik, P. C. *et al.* Strain background determines lymphoma incidence in Atm knockout mice. *Neoplasia (United States)* **16**, 129–136 (2014).

246. Beraldi, R. *et al.* A novel porcine model of ataxia telangiectasia reproduces neurological features and motor deficits of human disease. *Hum. Mol. Genet.* **24**, 6473–6484 (2015).

247. Li, J., Chen, J., Vinters, H. V., Gatti, R. A. & Herrup, K. Stable brain ATM message and residual kinase-active ATM protein in ataxia-telangiectasia. *J. Neurosci.* **31**, 7568–7577 (2011).

248. Shibamoto, M. *et al.* Activation of DNA damage response and cellular senescence in cardiac fibroblasts limit cardiac fibrosis after myocardial infarction. *Int. Heart J.*

60, 944–957 (2019).

249. Ahuja, A. K. *et al.* The effects of Atm haploinsufficiency on mutation rate in the mouse germ line and somatic tissue. *Mutagenesis* **23**, 367–370 (2008).

250. Perkhofer, L. *et al.* ATM deficiency generating genomic instability sensitizes pancreatic ductal adenocarcinoma cells to therapy-induced DNA damage. *Cancer Res.* **77**, 5576–5590 (2017).

251. Spring, K. *et al.* Atm knock-in mice harboring an in-frame deletion corresponding to the human ATM 7636de19 common mutation exhibit a variant phenotype. *Cancer Res.* **61**, 4561–4568 (2001).

252. Spring, K. *et al.* Mice heterozygous for mutation in Atm, the gene involved in ataxia-telangiectasia, have heightened susceptibility to cancer. *Nat. Genet.* **32**, 185–190 (2002).

253. Yamamoto, K. *et al.* Kinase-dead ATM protein causes genomic instability and early embryonic lethality in mice. *J. Cell Biol.* **198**, 305–313 (2012).

254. Putti, S., Giovinazzo, A., Merolle, M., Falchetti, M. L. & Pellegrini, M. Atm kinase dead: From ataxia telangiectasia syndrome to cancer. *Cancers (Basel).* **13**, 1–14 (2021).

255. Daniel, J. A. *et al.* Loss of ATM kinase activity leads to embryonic lethality in mice. *J. Cell Biol.* **198**, 295–304 (2012).

256. Menolfi, D. & Zha, S. ATM, ATR and DNA-PKcs kinases-the lessons from the mouse models: Inhibition ≠ deletion. *Cell Biosci.* **10**, 1–15 (2020).

257. Yamamoto, K. *et al.* Kinase-dead ATM protein is highly oncogenic and can be preferentially targeted by topo-isomerase I inhibitors. *Elife* **5**, 1–25 (2016).

258. Tal, E. *et al.* Inactive Atm abrogates DSB repair in mouse cerebellum more than does Atm loss, without causing a neurological phenotype. *DNA Repair (Amst).* **72**, 10–17 (2018).

259. Bult, C. J. *et al.* Mouse Genome Database (MGD) 2019. *Nucleic Acids Res.* **47**, D801–D806 (2019).

260. Smith, C. M. *et al.* The mouse Gene Expression Database (GXD): 2019 update. *Nucleic Acids Res.* **47**, D774–D779 (2019).

261. Krupke, D. M. *et al.* The Mouse Tumour Biology Database (MTB): A Comprehensive Resource for Mouse Models of Human Cancer. *Cancer Res.* **77**, e67–e70 (2017).

262. Bolus, N. E. Basic review of radiation biology and terminology. *J. Nucl. Med. Technol.* **45**, 259–264 (2017).

263. Yamada, Y. Principles of Radiotherapy. in *Synopsis of Clinical Oncology* 66–71 (2010).

264. Reisz, J. A., Bansal, N., Qian, J., Zhao, W. & Furdui, C. M. Effects of ionizing radiation on biological molecules - mechanisms of damage and emerging methods of detection. *Antioxidants Redox Signal.* **21**, 260–292 (2014).

265. Borrego-Soto, G., Ortiz-López, R. & Rojas-Martínez, A. Ionizing radiation-induced DNA injury and damage detection in patients with breast cancer. *Genet. Mol. Biol.* **38**, 420–432 (2015).

266. Desouky, O., Ding, N. & Zhou, G. Targeted and non-targeted effects of ionising radiation. *J. Radiat. Res. Appl. Sci.* **8**, 247–254 (2015).

267. Morgan, W. F. & Sowa, M. B. Effects of ionizing radiation in nonirradiated cells. *Proc. Natl. Acad. Sci. U. S. A.* **102**, 14127–14128 (2005).

268. Najafi, M., Fardid, R., Hadidi, G. & Fardid, M. The Mechanisms of Radiation-Induced Bystander Effect. *J. Biomed. Phys. Eng.* **4**, 163–172 (2014).

269. Syljuåsen, R. G. Cell Cycle Effects in Radiation Oncology. in *Radiation Oncology* 1–8 (2019).

270. Sia, J., Szmyd, R., Hau, E. & Gee, H. E. Molecular Mechanisms of Radiation-Induced Cancer Cell Death: A Primer. *Front. Cell Dev. Biol.* **8**, 1–8 (2020).

271. Jiang, Y. *et al.* Olaparib increases the therapeutic index of hemithoracic irradiation compared with hemithoracic irradiation alone in a mouse lung cancer model. *Br. J. Cancer* **124**, 1809–1819 (2021).

272. Carlos-Reyes, A., Muñiz-Lino, M. A., Romero-Garcia, S., López-Camarillo, C. & Hernández-de la Cruz, O. N. Biological Adaptations of Tumor Cells to Radiation Therapy. *Front. Oncol.* **11**, 1–21 (2021).

273. McBride, W. H. & Schaue, D. Radiation-induced tissue damage and response. *J. Pathol.* **250**, 647–655 (2020).

274. Darby, S. C. *et al.* Radiation-Related Heart Disease: Current Knowledge and Future Prospects. *Int. J. Oncol. - Biol. - Phys.* **76**, 656–665 (2010).

275. Menezes, K. M., Wang, H., Hada, M. & Saganti, P. B. Radiation Matters of the

Heart: A Mini Review. *Front. Cardiovasc. Med.* **5**, 1–10 (2018).

276. Arroyo-Hernández, M. *et al.* Radiation-induced lung injury: current evidence. *BMC Pulm. Med.* **21**, 1–12 (2021).

277. Olcina, M. M. & Giaccia, A. J. Reducing radiation-induced gastrointestinal toxicity -The role of the PHD/HIF axis. *J. Clin. Invest.* **126**, 3708–3715 (2016).

278. Liu, J. *et al.* Radiation-related lymphopenia is associated with spleen irradiation dose during radiotherapy in patients with hepatocellular carcinoma. *Radiat. Oncol.* **12**, 1–7 (2017).

279. Puukila, S. *et al.* Transcriptomic Response in the Spleen after Whole-Body Low-Dose X-Ray Irradiation. *Radiat. Res.* **196**, 66–73 (2021).

280. Gemici, C. *et al.* Volumetric decrease of pancreas after abdominal irradiation, it is time to consider pancreas as an organ at risk for radiotherapy planning. *Radiat. Oncol.* **13**, 1–7 (2018).

281. Oweida, A. J. *et al.* Response to radiotherapy in pancreatic ductal adenocarcinoma is enhanced by inhibition of myeloid-derived suppressor cells using STAT3 anti-sense oligonucleotide. *Cancer Immunol. Immunother.* **70**, 989–1000 (2021).

282. Zhu, W., Zhang, X., Yu, M., Lin, B. & Yu, C. Radiation-induced liver injury and hepatocyte senescence. *Cell Death Discov.* **7**, (2021).

283. Klaus, R., Niyazi, M. & Lange-Sperandio, B. Radiation-induced kidney toxicity: molecular and cellular pathogenesis. *Radiat. Oncol.* **16**, 1–11 (2021).

284. Lee, Y., Wang, Q., Shuryak, I., Brenner, D. J. & Turner, H. C. Development of a

high-throughput γ-H2AX assay based on imaging flow cytometry. *Radiat. Oncol.* **14**, 1–10 (2019).

285. Ding, D. *et al.* Induction and inhibition of the pan-nuclear gamma-H2AX response in resting human peripheral blood lymphocytes after X-ray irradiation. *Cell Death Discov.* **2**, (2016).

286. Meyer, B. *et al.* Clustered DNA damage induces pan-nuclear H2AX phosphorylation mediated by ATM and DNA-PK. *Nucleic Acids Res.* **41**, 6109–6118 (2013).

287. Iliakis, G., Wang, Y., Guan, J. & Wang, H. DNA damage checkpoint control in cells exposed to ionizing radiation. *Oncogene* **22**, 5834–5847 (2003).

288. Williams, A. B. & Schumacher, B. p53 in the DNA-damage-repair process. *Cold Spring Harb. Perspect. Med.* **6**, 1–15 (2016).

289. Kastan, M. B. & Lim, D.-K. The many substrates and functions of ATM. *Nat. Rev. Mol. Cell Biol.* **1**, 179–186 (2000).

290. Matsuoka, S. *et al.* ATM and ATR substrate analysis reveals extensive protein networks responsive to DNA damage. *Science (80-.).* **316**, 1160–1166 (2007).

291. Hickson, I., Pike, K. G. & Durant, S. T. Targeting ATM for Cancer Therapy: Prospects for Drugging ATM. in *Targeting the DNA Damage Response for Anti-Cancer Therapy* 185–208 (2018).

292. Choi, S., Gamper, A. M., White, J. S. & Bakkenist, C. J. Inhibition of ATM kinase activity does not phenocopy ATM protein disruption: Implications for the clinical utility of ATM kinase inhibitors. *Cell Cycle* **9**, 4052–4057 (2010).

293. White, J. S., Choi, S. & Bakkenist, C. J. Transient ATM Kinase Inhibition Disrupts DNA Damage-Induced Sister Chromatid Exchange. *Sci. Signal.* **3**, 1–11 (2010).

294. Xu, Y. & Villalona-Calero, M. A. Irinotecan: Mechanisms of tumor resistance and novel strategies for modulating its activity. *Ann. Oncol.* **13**, 1841–1851 (2002).

295. Fujita, K. I., Kubota, Y., Ishida, H. & Sasaki, Y. Irinotecan, a key chemotherapeutic drug for metastatic colorectal cancer. *World J. Gastroenterol.* **21**, 12234–12248 (2015).

296. Kciuk, M., Marciniak, B. & Kontek, R. Irinotecan—still an important player in cancer chemotherapy: A comprehensive overview. *Int. J. Mol. Sci.* **21**, 1–21 (2020).

297. Yao, Y. *et al.* Dissecting target toxic tissue and tissue specific responses of irinotecan in rats using metabolomics approach. *Front. Pharmacol.* **8**, 1–11 (2017).

298. Hatfield, M. J. *et al.* Organ-specific carboxylesterase profiling identifies the small intestine and kidney as major contributors of activation of the anticancer prodrug CPT-11. *Biochem. Pharmacol.* **81**, 24–31 (2012).

299. de Man, F. M., Goey, A. K. L., van Schaik, R. H. N., Mathijssen, R. H. J. & Bins, S. Individualization of Irinotecan Treatment: A Review of Pharmacokinetics, Pharmacodynamics, and Pharmacogenetics. *Clin. Pharmacokinet.* **57**, 1229–1254 (2018).

300. Balmus, G. *et al.* ATM orchestrates the DNA-damage response to counter toxic non-homologous end-joining at broken replication forks. *Nat. Commun.* **10**, 1–18 (2019).

301. Subhash, V. V. *et al.* ATM expression predicts veliparib and irinotecan sensitivity in gastric cancer by mediating p53-independent regulation of cell cycle and

apoptosis. *Mol. Cancer Ther.* **15**, 3087–3096 (2016).

302. Barlow, C., Eckhaus, M. A., Schaffer, A. A. & Wynshaw-Boris, A. Atm haploinsufficiency results in increased sensitivity to sublethal doses of ionizing radiation in mice. *Nat. Genet.* **21**, 359–360 (1999).

303. Rübe, C. E. *et al.* Accumulation of DNA Double-Strand Breaks in Normal Tissues After Fractionated Irradiation. *Int. J. Radiat. Oncol. - Biol. - Phys.* **76**, 1206–1213 (2010).

304. Lavin, M. F. The appropriateness of the mouse model for ataxia-telangiectasia: Neurological defects but no neurodegeneration. *DNA Repair (Amst).* **12**, 612–619 (2013).

305. Lee, S.-G., Kim, N., Park, I. B., Park, J. H. & Myung, K. Tissue-specific DNA damage response in Mouse Whole-body irradiation. *Mol. Cell. Toxicol.* **18**, 131–139 (2022).

306. Cremona, C. A. & Behrens, A. ATM signalling and cancer. *Br. Dent. J.* **217**, 3351–3360 (2014).

307. Phan, L. M. & Rezaeian, A. H. Atm: Main features, signaling pathways, and its diverse roles in DNA damage response, tumor suppression, and cancer development. *Genes (Basel).* **12**, 1–11 (2021).

308. Matthaios, D. *et al.* γ-H2AX expression detected by immunohistochemistry correlates with prognosis in early operable non-small cell lung cancer. *Onco. Targets. Ther.* **5**, 309–314 (2012).

309. White, D. E., Ivanov, A. V, Corsinotti, A., Peng, H. & Lee, S. C. The ATM substrate

KAP1 controls DNA repair in heterochromatin: Regulation by HP1 proteins and Serine 473/824 phosphorylation. *Mol. Cancer Res.* **10**, 401–414 (2016).

310. Lakin, N. D. & Jackson, S. P. Regulation of p53 in response to DNA damage. *Oncogene* **18**, 7644–7655 (1999).

311. Stiff, T. *et al.* ATM and DNA-PK Function Redundantly to Phosphorylate H2AX after Exposure to Ionizing Radiation. *Cancer Res.* **64**, 2390–2396 (2004).

312. Stope, M. B. Phosphorylation of histone H2A.X as a DNA-associated biomarker (Review). *World Acad. Sci. J.* **3**, 1–5 (2021).

313. Mah, L. J., El-Osta, A. & Karagiannis, T. C. γh2AX: A sensitive molecular marker of DNA damage and repair. *Leukemia* **24**, 679–686 (2010).

314. Koike, M., Sugasawa, J., Yasuda, M. & Koike, A. Tissue-specific DNA-PK-dependent H2AX phosphorylation and gamma-H2AX elimination after X-irradiation in vivo. *Biochem. Biophys. Res. Commun.* **376**, 52–55 (2008).

315. Kiesel, B. F. *et al.* LC-MS/MS assay for the simultaneous quantitation of the ATM inhibitor AZ31 and the ATR inhibitor AZD6738 in mouse plasma. *J. Pharm. Biomed. Anal.* **138**, 158–165 (2017).

316. Koontz, B. F., Verhaegen, F. & Ruysscher, D. D. E. Tumour and normal tissue radiobiology in mouse models : how close are mice to mini-humans ? *Br. J. Radiol.* **90**, 20160441 (2017).

317. Komarova, E. A., Christov, K., Faerman, A. I. & Gudkov, A. V. Different impact of p53 and p21 on the radiation response of mouse tissues. *Oncogene* **19**, 3791–3798 (2000).

318. Morris, E. J. & Geller, H. M. Induction of neuronal apoptosis by camptothecin, an inhibitor of DNA topoisomerase-I: Evidence for cell cycle-independent toxicity. *J. Cell Biol.* **134**, 757–770 (1996).

319. Negrini, S., Gorgoulis, V. G. & Halazonetis, T. D. Genomic instability - an evolving hallmark of cancer. *Nat. Rev. Mol. Cell Biol.* **11**, 220–228 (2010).

320. Hanahan, D. & Weinberg, R. A. Hallmarks of Cancer: The Next Generation. *Cell* **144**, 646–674 (2011).

321. Helleday, T., Petermann, E., Lundin, C., Hodgson, B. & Sharma, R. A. DNA repair pathways as targets for cancer therapy. *Nat. Rev. Cancer* **8**, 193–204 (2008).

322. Li, S. & Wu, X. Common fragile sites: protection and repair. *Cell Biosci.* **10**, 1–9 (2020).

323. Simpson, B. S., Pye, H. & Whitaker, H. C. The oncological relevance of fragile sites in cancer. *Commun. Biol.* **4**, 1–4 (2021).

324. Bartkova, J. *et al.* DNA damage response as a candidate anti-cancer barrier in early human tumorigenesis. *Nature* **434**, 864–870 (2005).

325. Gorgoulis, V. G. *et al.* Activation of the DNA damage checkpoint and genomic instability in human precancerous lesions. *Nature* **434**, 907–913 (2005).

326. Halazonetis, T. D., Gorgoulis, V. G. & Bartek, J. An oncogene-induced DNA damage model for cancer development. *Science (80-.).* **319**, 1352–5 (2008).

327. Pilié, P. G., Tang, C., Mills, G. B. & Yap, T. A. State-of-the-art strategies for targeting the DNA damage response in cancer. *Nat. Rev. Clin. Oncol.* **16**, 81–104

(2019).

328. Lavin, M. F. & Yeo, A. J. Clinical potential of ATM inhibitors. *Mutat. Res.* **821**, 111695 (2020).

329. Jin, M. H. & Oh, D.-Y. ATM in DNA repair in cancer. *Pharmacol. Ther.* **203**, 107391 (2019).

330. Taylor, A. M. R. *et al.* Ataxia telangiectasia: a human mutation with abnormal radiation sensitivity. *Nature* **258**, 427–429 (1975).

331. Hammond, E. M. & Muschel, R. J. Radiation and ATM inhibition: The heart of the matter. *J. Clin. Invest.* **124**, 3289–3291 (2014).

332. Ahuja, D., Sáenz-Robles, M. T. & Pipas, J. M. SV40 large T antigen targets multiple cellular pathways to elicit cellular transformation. *Oncogene* **24**, 7729–7745 (2005).

333. Morelli, C., Barbisan, F., Iaccheri, L. & Tognon, M. SV40-immortalized human fibroblasts as a source of SV40 infectious virions. *Mol. Med.* **10**, 112–116 (2004).

334. Murnane, J. P., Fuller, L. F. & Painter, R. B. Establishment and characterization of a permanent pSV ori--transformed ataxia-telangiectasia cell line. *Exp. Cell Res.* **158**, 119–126 (1985).

335. Fedier, A. *et al.* Loss of atm sensitises p53-deficient cells to topoisomerase poisons and antimetabolites. *Ann. Oncol.* **14**, 938–945 (2003).

336. Li, K. *et al.* ATM inhibition induces synthetic lethality and enhances sensitivity of PTEN-deficient breast cancer cells to cisplatin. *Exp. Cell Res.* **366**, 24–33 (2018).

337. Zhu, L. & Chen, L. Progress in research on paclitaxel and tumor immunotherapy.

Cell. Mol. Biol. Lett. **24**, 1–11 (2019).

338. Zhang, D., Yang, R., Wang, S. & Dong, Z. Paclitaxel: New uses for an old drug. *Drug Des. Devel. Ther.* **8**, 279–284 (2014).

339. Wang, T. H., Wang, H. S. & Soong, Y. K. Paclitaxel-induced cell death. *Cancer* **88**, 2619–2628 (2000).

340. Montecucco, A., Zanetta, F. & Biamonti, G. Molecular mechanisms of etoposide. *Exp. Clin. Sci.* **14**, 95–108 (2015).

341. Lee, J. H. & Berger, J. M. Cell cycle-dependent control and roles of DNA topoisomerase II. *Genes (Basel).* **10**, (2019).

342. Kwok, K. K., Vincent, E. C. & Gibson, J. N. *Antineoplastic Drugs*. *Pharmacology and Therapeutics for Dentistry: Seventh Edition* (Elsevier, 2017). doi:10.1016/B978-0-323-39307-2.00036-9.

343. De Sousa Cavalcante, L. & Monteiro, G. Gemcitabine: Metabolism and molecular mechanisms of action, sensitivity and chemoresistance in pancreatic cancer. *Eur. J. Pharmacol.* **741**, 8–16 (2014).

344. Karnitz, L. M. *et al.* Gemcitabine-induced activation of checkpoint signaling pathways that affect tumor cell survival. *Mol. Pharmacol.* **68**, 1636–1644 (2005).

345. Barton-Burke, M. Gemcitabine: A pharmacologic and clinical overview. *Cancer Nurs.* **22**, 176–183 (1999).

346. Gálvez-Peralta, M. *et al.* Overcoming S-phase checkpoint-mediated resistance: Sequence-dependent synergy of gemcitabine and 7-ethyl-10-hydroxycamptothecin

(SN-38) in human carcinoma cell lines. *Mol. Pharmacol.* **74**, 724–735 (2008).

347. Dasari, S. & Bernard Tchounwou, P. Cisplatin in cancer therapy: Molecular mechanisms of action. *Eur. J. Pharmacol.* **740**, 364–378 (2014).

348. Aldossary, S. A. Review on pharmacology of cisplatin: Clinical use, toxicity and mechanism of resistance of cisplatin. *Biomed. Pharmacol. J.* **12**, 7–15 (2019).

349. Voigt, W. *et al.* Topoisomerase-I inhibitor SN-38 can induce DNA damage and chromosomal aberrations independent from DNA synthesis. *Anticancer Res.* **18**, 3499–3505 (1998).

350. Garvin, A. J. & Morris, J. R. SUMO, a small, but powerful, regulator of double-strand break repair. *Philos. Trans. R. Soc. London, Ser. B, Biol. Sci.* **372**, 1–12 (2017).

351. Li, X. *et al.* Role for KAP1 serine 824 phosphorylation and sumoylation/desumoylation switch in regulating KAP1-mediated transcriptional repression. *J. Biol. Chem.* **282**, 36177–36189 (2007).

352. Frohns, F. *et al.* Differences in the Response to DNA Double-Strand Breaks between Rod Photoreceptors of Rodents, Pigs, and Humans. *Cells* **9**, 1–16 (2020).

353. Lee, J.-H. & Paull, T. T. Activation and regulation of ATM kinase activity in response to DNA double-strand breaks. *Oncogene* **26**, 7741–7748 (2007).

354. Iyengar, S. & Farnham, P. J. KAP1 protein: An enigmatic master regulator of the genome. *J. Biol. Chem.* **286**, 26267–26276 (2011).

355. Cheng, C.-T. KAPtain in charge of multiple missions: Emerging roles of KAP1.

World J. Biol. Chem. **5**, 308 (2014).

356. Rousseaux, M. W. C. *et al.* Depleting Trim28 in adult mice is well tolerated and reduces levels of α-synuclein and tau. *Elife* **7**, 1–16 (2018).

357. Shibata, A. *et al.* Factors determining DNA double-strand break repair pathway choice in G2 phase. *EMBO J.* **30**, 1079–1092 (2011).

358. Fedak, E. A., Adler, F. R., Abegglen, L. M. & Schiffman, J. D. ATM and ATR Activation Through Crosstalk Between DNA Damage Response Pathways. *Bull. Math. Biol.* **83**, 1–30 (2021).

359. Imseng, S., Aylett, C. H. & Maier, T. Architecture and activation of phosphatidylinositol 3-kinase related kinases. *Curr. Opin. Struct. Biol.* **49**, 177–189 (2018).

360. Vendetti, F. P. *et al.* The orally active and bioavailable ATR kinase inhibitor AZD6738 potentiates the anti-tumor effects of cisplatin to resolve ATM-deficient non-small cell lung cancer in vivo. *Oncotarget* **6**, 44289–44305 (2015).

361. Leahy, J. J. J. *et al.* Identification of a highly potent and selective DNA-dependent protein kinase (DNA-PK) inhibitor (NU7441) by screening of chromenone libraries. *Bioorganic Med. Chem. Lett.* **14**, 6083–6087 (2004).

362. Chresta, C. M. *et al.* AZD8055 is a potent, selective, and orally bioavailable ATP-competitive mammalian target of rapamycin kinase inhibitor with in vitro and in vivo antitumor activity. *Cancer Res.* **70**, 288–298 (2010).

363. Willoughby, C. E. *et al.* Selective DNA-PKcs inhibition extends the therapeutic index of localized radiotherapy and chemotherapy. *J. Clin. Invest.* **130**, 258–271

(2020).

364. Keung, M. Y. T., Wu, Y. & Vadgama, J. V. PARP inhibitors as a therapeutic agent for homologous recombination deficiency in breast cancers. *J. Clin. Med.* **8**, 435 (2019).

365. Rieunier, G. *et al.* Targeting IGF perturbs global replication through ribonucleotide reductase dysfunction. *Cancer Res.* **81**, 2128–2141 (2021).

366. Servier Medical Art. smart.servier.com.

367. Qi, Y. *et al.* Mechanistic modelling of slow and fast NHEJ DNA repair pathways following radiation for g0/g1 normal tissue cells. *Cancers (Basel).* **13**, 2202 (2021).

368. Moding, E. *et al.* Atm deletion with dual recombinase technology preferentially radiosensitizes tumor endothelium. *J. Clin. Invest.* **124**, 3325–3338 (2014).

369. Curtin, N. J. Inhibiting the DNA damage response as a therapeutic manoeuvre in cancer. *Br. J. Pharmacol.* **169**, 1745–1765 (2013).

370. Szydzik, J. *et al.* ATR inhibition enables complete tumour regression in ALK-driven NB mouse models. *Nat. Commun.* **12**, 1–18 (2021).

371. Kim, D., Liu, Y., Oberly, S., Freire, R. & Smolka, M. B. ATR-mediated proteome remodeling is a major determinant of homologous recombination capacity in cancer cells. *Nucleic Acids Res.* **46**, 8311–8325 (2018).

372. Barnieh, F. M., Loadman, P. M. & Falconer, R. A. Progress towards a clinically-successful ATR inhibitor for cancer therapy. *Curr. Res. Pharmacol. Drug Discov.* **2**, 100017 (2021).

373. Aramburu, J., Ortells, M. C., Tejedor, S., Buxadé, M. & López-Rodríguez, C. Transcriptional regulation of the stress response by mTOR. *Sci. Signal.* **7**, 1–12 (2014).

374. Rafiei, S. *et al.* ATM Loss Confers Greater Sensitivity to ATR Inhibition than PARP Inhibition in Prostate Cancer. *Cancer Res.* **80**, 2094–2100 (2020).

375. Teng, P. N. *et al.* Pharmacologic inhibition of ATR and ATM offers clinically important distinctions to enhancing platinum or radiation response in ovarian, endometrial, and cervical cancer cells. *Gynecol. Oncol.* **136**, 554–561 (2015).

376. Ryan, A. J., Squires, S., Strutt, H. L., Evans, A. & Johnson, R. T. Different fates of camptothecin-induced replication fork-associated double-strand DNA breaks in mammalian cells. *Carcinogenesis* **15**, 823–828 (1994).

377. Beck, H., Capranico, G. & Beck, H. Multidrug Sensitivity Phenotype of Human Lung Cancer Cells Associated with Topoisomerase II Expression. *Cancer Res.* **52**, 1666–1674 (1992).

378. Van Ark-Otte, J. *et al.* Determinants of CPT-11 and SN-38 activities in human lung cancer cells. *Br. J. Cancer* **77**, 2171–2176 (1998).

379. Wang, J. C. Cellular roles of DNA topoisomerases: A molecular perspective. *Nat. Rev. Mol. Cell Biol.* **3**, 430–440 (2002).

380. Pommier, Y., Sun, Y., Huang, S. Y. N. & Nitiss, J. L. Roles of eukaryotic topoisomerases in transcription, replication and genomic stability. *Nat. Rev. Mol. Cell Biol.* **17**, 703–721 (2016).

381. Corti, A. *et al.* DNA damage and transcriptional regulation in iPSC-derived neurons

from Ataxia Telangiectasia patients. *Sci. Rep.* **9**, 1–13 (2019).

382. Alagoz, M., Chiang, S. C., Sharma, A. & El-Khamisy, S. F. ATM Deficiency Results in Accumulation of DNA-Topoisomerase I Covalent Intermediates in Neural Cells. *PLoS One* **8**, e58239 (2013).

383. Collins, I., Weber, A. & Levens, D. Transcriptional Consequences of Topoisomerase Inhibition. *Mol. Cell. Biol.* **21**, 8437–8451 (2001).

384. Tresini, M. *et al.* The core spliceosome as target and effector of non-canonical ATM signaling. *Nature* **523**, 53–58 (2015).

385. Katyal, S. *et al.* Aberrant Topoisomerase-1-DNA Lesions are Pathogenic in Neurodegenerative Genome Instability Syndromes. *Nat. Neurosci.* **17**, 813–821 (2014).

386. Khoronenkova, S. V. & Dianov, G. L. ATM prevents DSB formation by coordinating SSB repair and cell cycle progression. *Proc. Natl. Acad. Sci. U. S. A.* **112**, 3997–4002 (2015).

387. Lee, B. *et al.* A novel mechanism of irinotecan targeting MDM2 and Bcl-xL. *Biochem. Biophys. Res. Commun.* **514**, 518–523 (2019).

388. Schlam-Babayov, S., Ziv, Y. & Shiloh, Y. It takes three to the DNA damage response tango. *Mol. Cell. Oncol.* **8**, 1881395 (2021).

389. Ditano, J. P., Donahue, K. L., Tafe, L. J., McCleery, C. F. & Eastman, A. Sensitivity of cells to ATR and CHK1 inhibitors requires hyperactivation of CDK2 rather than endogenous replication stress or ATM dysfunction. *Sci. Rep.* **11**, 1–16 (2021).

390. Kantidze, O. L., Velichko, A. K., Luzhin, A. V., Petrova, N. V. & Razin, S. V. Synthetically Lethal Interactions of ATM, ATR, and DNA-PKcs. *Trends in Cancer* **4**, 755–768 (2018).

391. Italiano, A. ATR inhibition as an attractive therapeutic resource against cancer. *Cancer Discov.* **11**, 14–16 (2021).

392. Mei, L., Zhang, J., He, K. & Zhang, J. Ataxia telangiectasia and Rad3-related inhibitors and cancer therapy: Where we stand. *J. Hematol. Oncol.* **12**, 1–8 (2019).

393. Dunlop, C. R. *et al.* Complete loss of ATM function augments replication catastrophe induced by ATR inhibition and gemcitabine in pancreatic cancer models. *Br. J. Cancer* **123**, 1424–1436 (2020).

394. Caron, P. *et al.* Non-redundant Functions of ATM and DNA-PKcs in Response to DNA Double-Strand Breaks. *Cell Rep.* **13**, 1598–1609 (2015).

395. Gapud, E. J. & Sleckman, B. P. Unique and redundant functions of ATM and DNA-PKcs during V(D)J recombination. *Cell Cycle* **10**, 1928–1935 (2011).

396. Callén, E. *et al.* Essential Role for DNA-PKcs in DNA Double-Strand Break Repair and Apoptosis in ATM-Deficient Lymphocytes. *Mol. Cell* **34**, 285–297 (2009).

397. Middleton, F. K. *et al.* Common cancer-associated imbalances in the DNA damage response confer sensitivity to single agent ATR inhibition. *Oncotarget* **6**, 32396–32409 (2015).

398. Schlam-Babayov, S. *et al.* Phosphoproteomics reveals novel modes of function and inter-relationships among PIKKs in response to genotoxic stress. *EMBO J.* **40**, e104400 (2021).

399. Bacon, C. W. *et al.* KAP1 Is a Chromatin Reader that Couples Steps of RNA Polymerase II Transcription to Sustain Oncogenic Programs. *Mol. Cell* **78**, 1133-1151.e14 (2020).

400. Davidson, D., Amrein, L., Panasci, L. & Aloyz, R. Small molecules, inhibitors of DNA-PK, targeting DNA repair, and beyond. *Front. Pharmacol.* **4**, 1–7 (2013).

401. Arlander, S. J. H., Greene, B. T., Innes, C. L. & Paules, R. S. DNA protein kinase-dependent G2 checkpoint revealed following knockdown of ataxia-telangiectasia mutated in human mammary epithelial cells. *Cancer Res.* **68**, 89–97 (2008).

402. Shang, Z. F. *et al.* Inactivation of DNA-dependent protein kinase leads to spindle disruption and mitotic catastrophe with attenuated checkpoint protein 2 phosphorylation in response to DNA damage. *Cancer Res.* **70**, 3657–3666 (2010).

403. Murai, J. *et al.* Differential trapping of PARP1 and PARP2 by clinical PARP inhibitors. *Cancer Res.* **72**, 5588–5599 (2013).

404. Savitsky, K. *et al.* The complete sequence of the coding region of the ATM gene reveals similarity to cell cycle regulators in different species. *Hum. Mol. Genet.* **4**, 2025–2032 (1995).

8 Supplementary

Table 8.1 | Sample comparison for RNAscope technology

Sample	Probe	Average count/cell ± SEM
HeLa cell pellet	PPIB	30.1 ± 2.27
	ATM	3.6 ± 0.39
Lung tissue section	PPIB	<1
	ATM	<1
Calu-6 xenograft	PPIB	18.1 ± 0.99
	ATM	1.1 ± 0.18

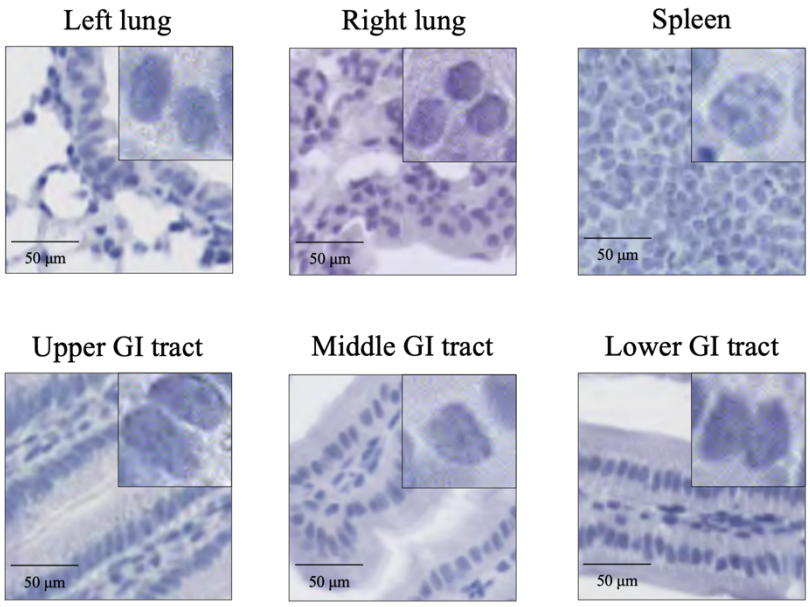


Figure 8.1 | ATM protein is not detected in normal murine tissues from ATM$^{-/-}$ mice

Representative images from ATM$^{-/-}$ mice tissue sections. Tissues were collected from n=3 mice and show an absence of positive DAB staining. Incubated with ATM (D2E2) primary antibody at 1:200. Sections counterstained with haematoxylin. Images shown at 10X and 40X magnification using QuPath software. Scale bar = 50 µm.